Investigation of Residual Stresses in X65 Narrow-Gap Pipe Girth Welds

A thesis submitted for the degree of
Doctor of Philosophy

By
Yao Ren

Department of Mechanical, Aerospace and Civil Engineering
College of Engineering, Design and Physical Sciences
Brunel University London, Uxbridge
United Kingdom
March 2018

Abstract

This research investigated the residual stresses in narrow-gap API 5L X65 pipe girth welds in as-welded and after post weld heat treatment (PWHT) conditions. The PWHT included global furnace and local practices. Non-destructive neutron diffraction (ND) strain scanning was carried out on selected pipe spools and strain-free reference samples for the determination of the lattice spacing before and after PWHT. The as-welded and post-heat treatment residual stresses measured in the pipe spools were examined and compared. Experimental work also included full residual stress mapping in the weldment and through-thickness measurement at weld centre and close to the external and internal pipe surfaces. The measured profiles were compared with the recommendations given in British flaw assessment procedure BS 7910 "*Guide to methods for assessing the acceptability of flaws in metallic structures*" and the UK nuclear industry's R6 procedure. The design, preparation and experimental neutron diffraction measurement procedures for the determination of the strain-free lattice parameter in various configurations of reference samples and in the required directions were discussed. The variability of the lattice spacing in the reference samples was found depended on the specimen manufacture methods and thermal process.

Welding residual stresses were also simulated using finite element analysis (FEA) modelling approach. The simulated thermal cycles and transient strains at specific locations were compared with the experimental readings. The residual stress profiles derived from finite element model were compared with the measurements from neutron diffraction. It was found, the measured and simulated, as-welded - residual stress profiles showed good consistency in terms of stress distribution and magnitude to reasonable extent. Measurement results also indicated that local PWHT was effective in reducing the residual stresses in the pipes to a level similar to that achieved by a global approach.

Declaration

I hereby declare no portion of the work referred to in the dissertation has been submitted in support of an application for another degree or qualification of this or any other university or other institute of learning.

Acknowledgement

The work presented in this thesis would not have been possible without the support of several people. I take this opportunity to extend my sincere gratitude and appreciation to all them.

I would like to express my special appreciation and thanks to my supervisors Dr. Bing Wang of Brunel University London and Dr. Yin Jin Janin of TWI Ltd., whose enthusiastic and supportive supervision, invaluable guidance and encouragements from the preliminary to the concluding level enabled me to develop an understanding of the subject.

Special thanks to Dr. Anna Paradowska who offer me the opportunity to use the resources and equipment at the Australian Nuclear Science and Technology Organization (ANSTO) where the neutron diffraction stress measurement was carried out. Her useful advice and comments on the measurement side of this research are really appreciated.

I am grateful to many individuals for the scientific collaboration, valuable advices and assistance in this research, especially Dr. Simon Smith, Dr. Isabel Hadley, Dr. Museok Kwak and Dr. Elvin Eren. I also wish to thank Mr. Runlin Chen and Mr. David Drew for all the help when the experiment was performed at Subsea Seven.

This research was jointly supported by Brunel University London and TWI. I offer my regards and blessings to all of those who supported me in any respect during the completion of the project.

Last but not the least, I would like to thank to all my friends and family members, without whose unconditional love and support, I would never have been able to attempt this work.

Contents

Nomenclature

Abbreviations

ANSTO	Australia Nuclear Science and Technology Organisation
ECA	Engineering Critical Assessment
FEA	Finite Element Analysis
HAZ	Heat Affected Zone
ND	Neutron Diffraction
RS	Residual Stress
SG	Strain Gauge
TC	Thermocouple
TWI	The Welding Institute
XRD	X-Ray Diffraction

Symbols

D	Pipe outside diameter, mm
t	Pipe wall thickness, mm
D/t	Pipe standard dimension ratio
P_{AW}	Pipe spool in as-welded condition
P_{HT}	Pipe spool after post weld heat treatment
σ_y^+	The higher value of the yield strength (at room temperature) of the weld or parent material, MPa
σ_y^*	The lower value of the yield strength (at room temperature) of the weld or parent material, MPa
$\sigma_R^{L,O}$	Longitudinal (hoop) thought-thickness residual stress at pipe outer surface, MPa
$\sigma_R^{L,B}$	Longitudinal (hoop) thought-thickness residual stress at the bore (inner surface), MPa

σ_R^T	Transverse (axial) residual stress through the pipe wall thickness, MPa
r_0	Radius of the yield zone, mm

List of Tables

List of Figures

1 Introduction

1.1 Background

A weld joint consists of three metallurgical different regions, namely weld metal, heat affected zone (HAZ) and parent metal. Residual stresses are introduced during welding as a result of parent metal restraint on the shrinkage of hot weld metal during cooling - due to thermal expansion and contraction - and/or simultaneous microstructural phase transformation [1].

In a weldment, residual stresses can possibly be as high as the material's yield strength or even higher at room temperature. In industrial production, one of the reasons for the preference narrow-gap multi-pass welding, apart from the advantages of higher productivity rates and reduced weld volume compare to conventional grooves, is the relatively lower heat input during welding, resulting in a smaller heat affected zone. Lower heat input also introduces lower levels of residual stresses [2].

Many experimental and simulation investigations have been carried out for determining the residual stress distribution and magnitude in pipes, both at the surface and through wall thickness [3-6]. Destructive and non-destructive residual stress measurement techniques have been employed [7, 8] with the latter being more commonly used. Among the non-destructive techniques, neutron diffraction has a number of distinct merits. A neutron beam wave length is comparable to atomic spacing [9]. This technique has the advantage of penetrating subsurface and deeply inside the bulk of material up to several centimetres, and it provides a three-dimensional residual stress state. The technique has been successfully utilized to investigate residual stresses in pipe girth welds [10-12].

Post weld heat treatment (PWHT) is applied after welding, aiming at reducing residual stresses in thick-walled components and thus improving the structural integrity performance [13]. It is an optional procedure in fabrication practice, and the need for this is largely dependent on the grade of the material, component thickness and the criticality of application. PWHT is commonly conducted in an enclosed furnace for a few hours to remove the hydrogen, improve fracture toughness and relax residual stresses in components when possible. However, in the circumstances that conventional furnace PWHT is not feasible, local PWHT can be considered as

an alternative for the application of which equipment availability, geometry of the structure, fabrication requirements and working environment should be all taken into consideration [14].

In terms of relief of residual stresses, the PWHT holding temperature has been demonstrated to be more critical than the holding time. Information on the effectiveness of PWHT has been incorporated into industrial standards and codes such as BS 7910 [15], which assumes that in wide grove welds, different levels of stress relief occur in both transverse and longitudinal directions following a conventional furnace PWHT. BS7910 also provides information on the effect of PWHT temperature. However, the guidance provided is not intended to be relevant to narrow-gap welds. In addition, the information regarding the degree of stress relief after local PWHT is still limited; although some practical work with regard to local PWHT has been carried out experimentally and analytically to investigate the effective heating band width for stress relaxation [16-19] and through-thickness temperature gradient criteria [20-22].

In this work, stresses in narrow-gap girth welds in pipe spools were measured, both in the as-welded condition and after global and local PWHT. Residual stress distributions were identified non-destructively by neutron diffraction and compared with the recommendations given in two engineering critical assessment procedures; BS 7910 and R6 [23]. Welding residual stresses were simulated using finite element analysis (FEA).

1.2 Objectives

The objectives of this research are:

- To quantify residual stresses in pipe girth welds fabricated using industrial-established welding procedures and compare the extent of stress relief in welds using global (in furnace) and local post weld heat treatment.
- To investigate the effect of using various reference samples for the determination of strain-free lattice parameters hence the residual stresses in pipe welds using neutron diffraction technique.
- To evaluate the stress states in narrow-gap girth welds using engineering critical assessment procedures for as-welded and after PWHT conditions.

- To simulate welding residual stresses in narrow-gap multi-pass weld employing finite element analysis (FEA) approach and understand the importance of welding data (temperature, strain and material properties) to the accuracy of stress prediction.

1.3 Outline of the thesis

The work carried out in this PhD project is presented in detail in nine chapters:

Chapter 1 introduces the research background, objectives and thesis outline.

Chapter 2 reviews previous studies related to residual stress evaluation including measurement technique and finite element method, stress relieve using various PWHT approaches.

Chapter 3 describes experimental procedure to fabricate pipe girth weld and carry out global and local PWHT for stress relief purpose. The characterization of the material properties is also included in this chapter.

Chapter 4 details the methodology using neutron diffraction technique for the measurement of residual stresses. Recommendations given in various flaw assessment procedures are also reviewed.

Chapter 5 investigates the strain-free lattice parameters measured from various designed reference samples and analyses the accuracy and impact of using certain lattice spacing for the subsequent determination of residual stresses.

Chapter 6 evaluates the residual stress in narrow-gap welds in both as-welded and after PWHT conditions. The measured profiles are compared with current engineering critical assessment (ECA) procedures.

Chapter 7 compares the thermal cycles, strain histories as well as final residual stresses obtained from FEA model with the results from welding process and neutron diffraction measurement.

Chapter 8 examines the impact of the work and the associated findings including the limitations and merits.

Chapter 9 summarises the overall conclusions of the research and makes recommendations for future work.

Reference

[1] E. J. Hearn, "Contact stress, residual stress and stress concentrations," in *Mechanics of Materials-2An Introduction to the Mechanics of Elastic and Plasyic Deformation of Solids and Structural Materials*, Third Edit., 1997, pp. 381–442.

[2] A. M. Paradowska, J. W. H. Price, R. Ibrahim, and T. R. Finlayson, "The effect of heat input on residual stress distribution of steel welds measured by neutron diffraction," *J. Achiev. Mater. Manuf. Eng.*, vol. 17, no. 1–2, pp. 385–388, 2006.

[3] R. F. D. Scaramangas, A. and Porter Goff, "Residual stress and deformation in welded pipe joints.," in *Joints in Structural Steelwork, Proc. Int. Conf.*, 1981.

[4] E. F. Rybicki, E. Merrick, J. Wert, and P. A. McGuire, "The Effect of Pipe Thickness on Residual Stresses due to Girth Welds," *J. Press. Vessel Technol.*, vol. 104, no. 3, pp. 204–209, 1982.

[5] R. H. Leggatt, "Residual stressesat girth welds in pipes," *Weld. Energy-Related Proj.*, pp. 429–440, 1984.

[6] P. Dong, "On the Mechanics of Residual Stresses in Girth Welds," *J. Press. Vessel Technol.*, vol. 129, no. 3, p. 345, 2007.

[7] A. M. Paradowska, J. W. H. Price, T. R. Finlayson, R. B. Rogge, R. L. Donaberger, and R. Ibrahim, "Comparison of Neutron Diffraction Measurements of Residual Stress of Steel Butt Welds With Current Fitness-for-Purpose Assessments," *J. Press. Vessel Technol.*, vol. 132, no. 5, p. 51503, Oct. 2010.

[8] N. S. Rossini, M. Dassisti, K. Y. Benyounis, and A. G. Olabi, "Methods of measuring residual stresses in components," *Mater. Des.*, vol. 35, pp. 572–588, Mar. 2012.

[9] P. Withers and H. Bhadeshia, "Residual stress. Part 1–measurement techniques," *Mater. Sci. Technol.*, vol. 17, no. April, pp. 355–365, 2001.

[10] B. Chen *et al.*, "In situ neutron diffraction measurement of residual stress relaxation in a welded steel pipe during heat treatment," *Mater. Sci. Eng. A*, vol. 590, pp. 374–383, Jan. 2014.

[11] R. D. Haigh *et al.*, "Neutron diffraction residual stress measurements on girth-welded 304 stainless steel pipes with weld metal deposited up to half and full pipe wall thickness," *Int. J. Press. Vessel. Pip.*, vol. 101, pp. 1–11, Jan. 2013.

[12] T. Neeraj, T. Gnäupel-Herold, H. J. Prask, and R. Ayer, "Residual stresses in girth welds of carbon steel pipes: neutron diffraction analysis," *Sci. Technol. Weld. Join.*, vol. 16, no. 3, pp. 249–253, Apr. 2011.

[13] B. L. Josefson, "Stress redistribution during Annealing of a Multipass Butt-Welded Pipe," *ASME J Press. Vessel Technol.*, vol. 105, pp. 165–170, May 1983.

[14] D. N. Crofft, *Heat Treatment Of Welded Steel Structures*. 1996.

[15] "BSI, 'BS7910:2013 Guide to methods for assessing the acceptability of flaws in metallic structures,' 2013," 2013.

[16] W. Soete and R. Vancrombrugge, "An industrial method for the determination of initial stresses," *Proc SESA*, vol. 8, no. 1, pp. 17–28, 1950.

[17] R. T. Rose, "Stress in Cylindrical Vessels due to Local Heating Stress Relief of Circumferential Welds," *Br. Weld. J.*, pp. 19–21, 1960.

[18] J. I. Bluhm, "Fracture Mechanics, SAE Technical Paper 630101," Jan. 1963.

[19] H. MURAKAWA, H. LU, and J. WANG, “Mechanical Behavior in Local Postweld Heat Treatment (Report II) : Determination of Critical Heated Band during Local PWHT(Mechanics, Strength & Structure Design),” *Trans. JW RI*, vol. 27, pp. 89–95, 1998.
[20] E. G. Shifrin and M. I. Rich, “Effect of Heat Source Width in Local Heat Treatment of Piping,” *Weld. J.*, vol. 53, no. 12, pp. 792–799, Dec. 1973.
[21] C. Bloch, J. Hill, and D. Connell, “Proper PWHT Can Stop Stress-Induced Corrosion,” *Weld. J.*, vol. 76, no. 5, pp. 31–41, 1997.
[22] H. LU, J. WANG, and H. MURAKAWA, “Mechanical Behavior in Local Postweld Heat Treatment (Report III) : Criteria for heated band width based on through-thickness temperature distribution(Mechanics, Strength & Structure Design),” *Trans. JW RI*, vol. 27, pp. 89–95, 1998.
[23] I. Milne, R. Ainsworth, A. Dowling, and A. Stewart, “Assessment of the integrity of structures containing defects,” *Int. J. Press. Vessel. Pip.*, vol. 32, no. 1–4, pp. 3–104, Jan. 1988.

2 Literature review

2.1 Residual stress due to welding

Residual stresses present in a component are in a self-equilibrium state in absence of any external loadings. They arise from any misfits either between different regions or different phases within a material. These misfits might be a result of three principle mechanisms: mechanical process, chemical reaction and/or heat treatment which lock in the stresses within the component.

Residual stresses within a component are three-dimensional. In terms of length scale, residual stresses can be long range over macroscopic dimensions (Type I); intergranular over a dimension of 3 to10 times grain size (Type II) or even over atomic scale and balanced within a grain (Type III) [1].

Due to the difference in thermal expansion coefficient of three regions (weld metal, HAZ (heat affected zone and parent metal) in a weldment, residual stresses are introduced when the contraction of weld metal is restrained by the surrounding parent metal during cooling and potential structural phase transformation [2]. Therefore, in a single-pass weld residual stresses are predominantly tensile and are balanced by compressive stresses far from the weld.

A typical sketch of the distribution of the longitudinal (along welding direction) and transverse (transverse to welding direction) residual stresses are illustrated in Figure 2.1 [3].

The factors affecting residual stresses [4] in weld joints and structures include:

- Residual stresses present in materials before welding which result from manufacturing process,
- Material properties (mechanical, metallurgical and thermal properties),
- The geometry of the parts to be jointed,
- External restraint applied to the parts,
- Welding procedures including welding preparation, welding condition pass sequence etc.,
- Residual stress obtained or relieved by manufacturing operations, thermal treatment and/or mechanical loading.

Both the sharp temperature gradient and volumetric changes accompanying transformation of the metal during cooling can also contribute to high residual stresses [5].

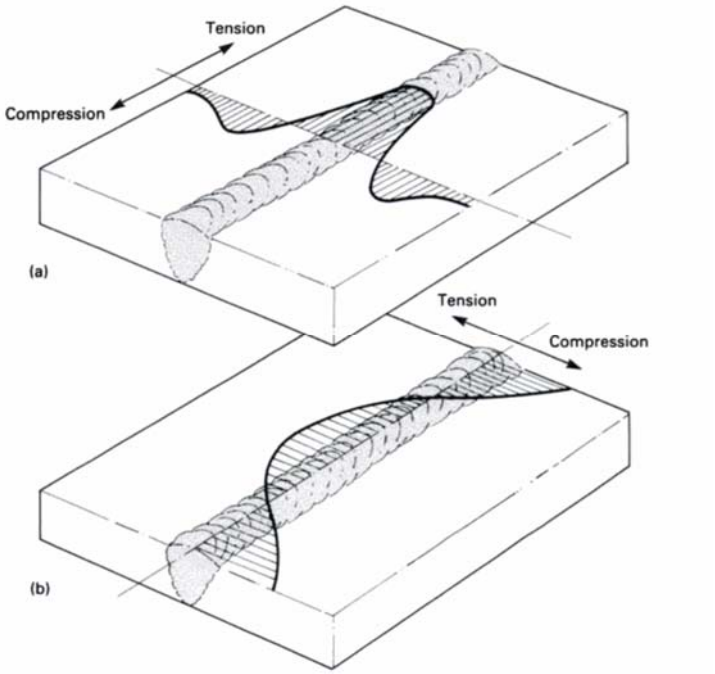

Figure 2.1 Typical distribution of (a) longitudinal and (b) transverse residual stresses in a welded joint [3]

Modification of residual stresses after welding can be achieved through various methods (Table 2-1) either subsequent manufacturing operations or service life of the welded structure [4]. The application of post weld heat treatment (PWHT) is beneficial in relieving residual stresses especially when structural integrity is of concern.

Table 2-1 Methods for modification of residual stresses after welding

Manufacturing operations	Processes during service life
• Local weld repairs • Temporary fixture relaxation • Subsequent welding operations • Surface treatment: peening and case hardening • Machining operations: material removal • Distortion correction: plastic deformation, flame straightening • Mechanical loading or treatment • Thermal treatment: PWHT in a furnace or via local methods	• Normal or exceptional service loads • Creep at operating temperature • Irradiation • Contact stresses • In-service repairs • Loss of materials due to corrosion or erosion

2.2 Residual Stresses in Pipe Girth Weld

Welding residual stresses in pipe girth welds are generally categorized as axial stress which is longitudinal to pipe length, hoop stress which is parallel to the circumferential weld and radial stresses which is along the radius.

Early work on residual stresses in butt circumferential welded pipe was conducted on thin-walled ($\frac{7}{16}$ inch thick and 30 inch in diameter) pipes [6]. It was found, at weld centreline, tensile hoop stresses existed on both inner and outer surfaces. In contrast, axial residual stresses were in compressive on outer surface and tensile on inner surface. It was because the circumferential tendon force lead to shrinkage in the welding direction, axial stresses at weld centre became compressive on outer surface and tensile on inner surface after solidification [7]. The magnitude of residual stress decreased as the distance from the weld increased.

The effect of pipe wall thickness on the distribution of residual stresses was also investigated in the pipe in 1000mm diameter [7]. Axial residual stress at weld centre had linear distribution through the pipe wall in thickness of 9.1mm. while when pipe thickness increased to 15mm and 19.5 mm, axial residual stress presented a nonlinear trend from inner surface outwards. Further research [8] employed an analytical model to predict parameters affecting residual stress and its through-thickness distribution, which was the net linear heat input per pass per unit wall thickness and geometry ratio (cylinder radius to wall thickness).

Leggatt [9], [10] carried out detailed residual stresses measurement on a pipe surface and through the pipe wall thickness. The magnitude and distribution of hoop and axial residual stresses on inner and outer surface are presented in Figure 2.2. Hoop bending during weld fabrication induced tensile hoops stresses concentrated highly in weld bead and adjacent material. Although the axial residual stresses, caused by bending force, were predominantly tensile on outer surface and compressive on inner surface, were compressive at weld centreline on outer surface. This finding encouraged Leggatt to a further investigate the through-thickness variation of longitudinal stress.

Stress distribution at weld centre were determined using layering method which was typically non-linear (Figure 2.3). The measured residual stresses were compressive

on outer surface but reached a peak tensile value of 200MPa beneath 10mm from component surface and zero on inner surface. These results confirmed previous publications [6], [10] that stress trend at inner surface were from tensile for pipe thinner than 16mm to compressive for pipes thicker than 25mm. Similar results of axial residual stress variation were obtained [11] by measuring 16mm thick pipe of 914mm diameter.

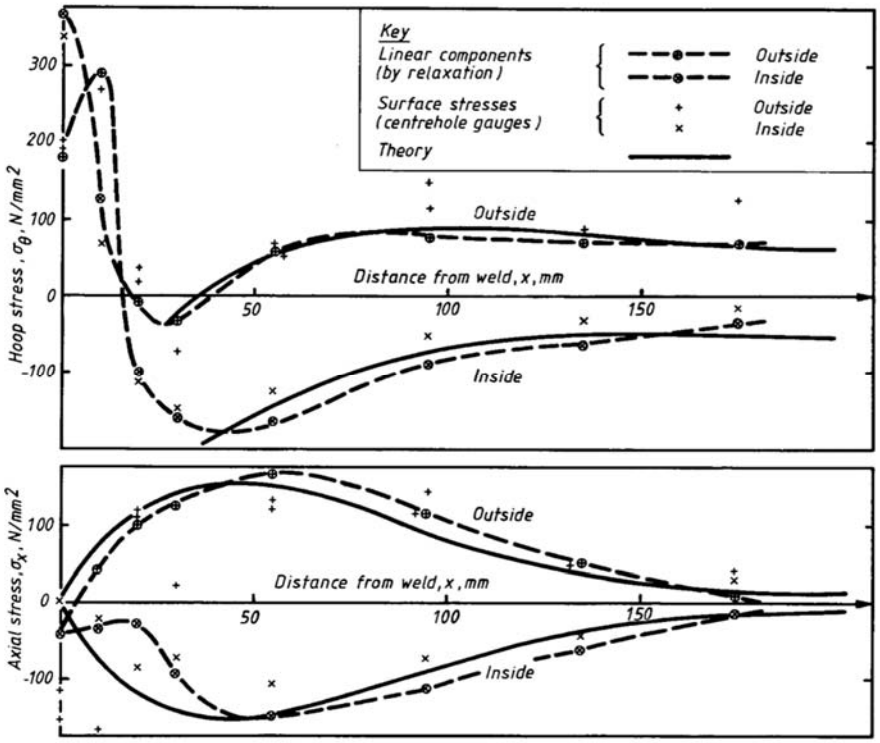

Figure 2.2 Axial variation of hoop and axial stresses [9]

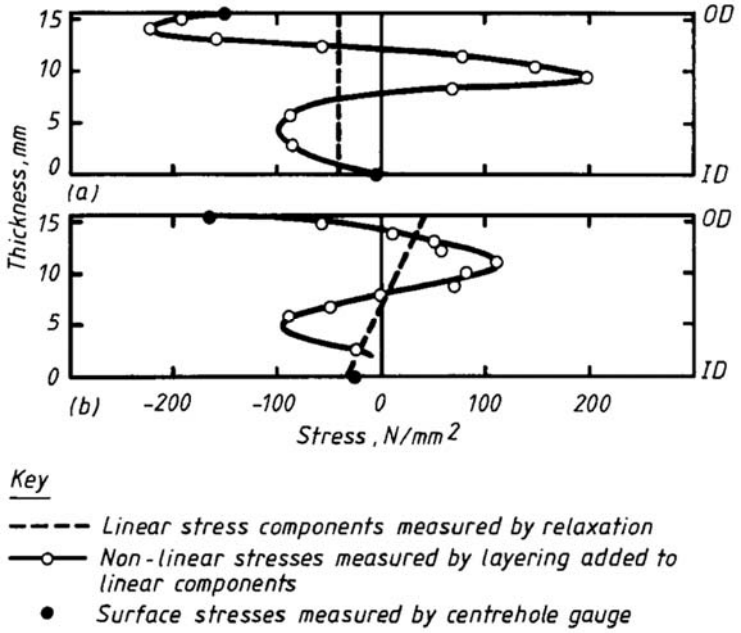

Figure 2.3 Through thickness variation of axial stresses (a) on weld centreline, (b) edge of weld [9]

Welding residual stress field was found to be approximately rotationally symmetric [12] in multi-pass welded pipe (Figure 2.4) both circumferentially and longitudinally. This result was obtained using strain gages attached in three equally spaced azimuthal positions on the outer surface of the pipes. This experimentally determined stress redistribution [12], [13] has also been validated by numerical simulation.

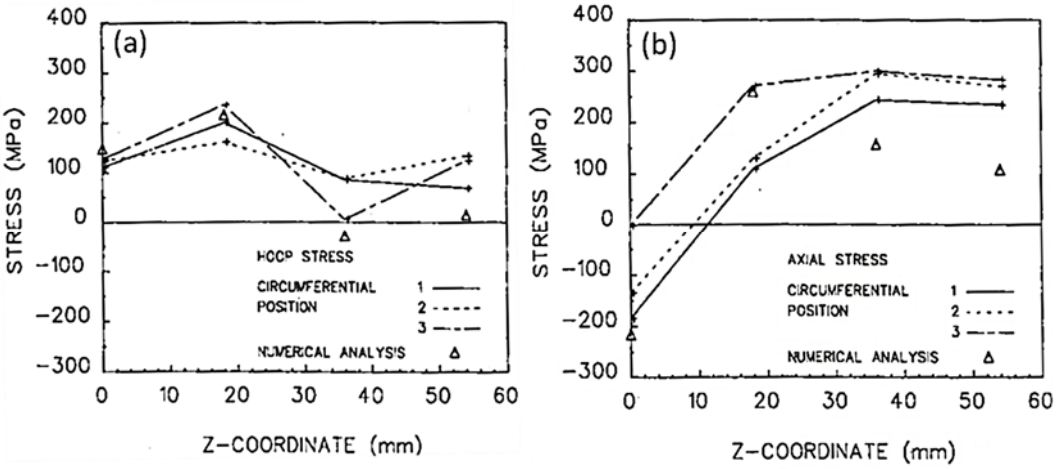

Figure 2.4 Experimentally determined residual (a) hoop and (b) axial stresses at outer surface of the pipe after welding [12]

Specific experiments to evaluate transient and residual stresses in a single pass butt-welded pipe were carried out [14]. Jonsson and Josefson adopted low heat input with well-controlled welding parameters to produce a high cooling rate, which thought to be promoting a non-rotationally symmetric stress field. Strain gauges were attached at different angular positions near weld centreline on the pipe outer surface. Welding residual stresses were also measured using hole-drilling at weld centreline and other two axial positions 17mm and 30mm from weld centreline. It was observed residual hoop stresses were reasonably rotationally symmetric while axial residual stresses varied obviously in circumferential direction after cooling.

The effect of groove shape on welding stress state was examined and compared using single-U and narrow-gap grooves for multi-pass butt-welding thick-walled pipes [15]. The residual stress measured on the outer surface of narrow-gap-grooved pipe was higher than that on the pipe with single-U shape groove. It was also found that the residual state was no longer exhibited a rotational symmetricity at the weld centre.

2.3 Welding residual stress simulation

2.3.1 Two-dimensional modelling

In order to simulate welding process and predict the resulted residual stresses, two-dimensional (2D) models can be employed, in which the components are assumed to be in a rotational axisymmetric condition [16]. The greatest advantage of 2D model is reduced requirement for computational power and time as only the plane perpendicular to the direction of weld is modelled. However, it was believed a 2D model can be over simplified by limiting the analysis on one section of the whole geometry [17], [18]. Therefore, it was recommended that experimental data should be used to validate results predicted by numerical simulation.

Residual stresses predicted from finite element analysis models have shown to be in good agreement with laboratory measurement. This approach thereafter was applied to explore the factors that affect residual stresses such as number of welding passes [19], pipe wall thickness [20]–[22], the shape of groove [23] and solid state phase transformation [24]–[26].

Rotational symmetry model [23] using load-step approach was implemented to simulate the temperature history and residual stress field on welding grooves of different shapes (narrow-gap vs. single-U). The results, especially for narrow-gap groove, were validated using authors' previous experimental measurement. However, as phase transformation was not taken into account, the increase in yield strength could not be evaluated through hardening behaviour or volumetric expansion.

FEA analysis is often performed sequentially, in two or more analysis steps; i.e. temperature field determined from transient heat transfer analysis is adopted as the load in following thermal stress analysis. ABAQUS code has been available for decades to simulate the welding process, with which an uncoupled sequential axisymmetric model was used to predict welding residual stresses in multi-pass butt-welded modified 9Cr-1Mo steel pipe when considering solid-state phase transformation [24].

2.3.2 Three-dimensional modelling

As 2D simulation is not capable to capture the considerable effect of weld start/stop and weld track modelling, it is unable to reproduce the travelling arc along circumferential welds thus, the rapid change of residual stresses that cannot be observed in the overlapping region. This overestimates the hoop residual stresses in circumferential welds [27], [28]. To obtain accurate results, three-dimensional (3D) modelling can be employed instead. The selection of software has little impact on the outcome of the simulation [29].

The first 3D FE modelling by Mazumder (1988) was to apply transient, moving heat source heat transfer analysis for the gas metal arc (GMA) welding process [30]. The results obtained were accepted to be used for determining the heating and cooling rate, weld pool shape and HAZ. Shortcoming of the trial were for one thing the weld was only 25.4mm long which could not represent the practical welds, for the other thing modelling was restricted by very coarse FE meshes [16].

Other factors such as pipe dimensions and phase transformation can affect welding residual stresses distribution and magnitude. 3D analysis was performed by varying them internal radius to wall thickness ratio (r/t) at 10, 20, 50 and 100 [31]. It concluded that residual stresses were obviously influenced by pipe diameter in thin-walled pipe weld which r/t was larger than 10. For high strength carbon steel pipes, it was predicted solid state phase transformation had small effect on axial residual stress but it could reduce the hoop stresses in the weld and HAZ [32]. Another analysis proved that hoop stresses in thin-walled cylinders were sensitive to angular location from the weld start position [33].

2.3.3 Affecting factors for welding simulations

Martensitic phase transformation is a key factor affecting residual stresses during welding. Rapid heating material above the upper critical temperature creates face-centred cubic (FCC) and the subsequent rapid cooling below martensite transformation line transforms FCC into body centred (BCC) tetragonal structure which results in an increase in volume and material's tensile strength. Deng and Murakawa [24] found both the distribution and the magnitude of residual stresses in

material were significantly affected by volumetric change due to phase transformation.

The effect of phase transformation on welding residual stresses has been studied for various ferritic steels [24]–[26], [34], [35], but it has not been investigated in this work.

Many other experiments were carried out to examine the effect of various parameters (i.e. pipe thickness and number of weld pass, net line energy Q, ratio of pipe inner radius to thickness r/t, weld metal yield stress and inter pass temperature) on welding residual stress [19], [22]. Conclusions were drawn from a series simulation:

(1) with an increase in pipe wall thickness, the tensile axial residual stresses through pipe thickness displayed a compression-tension-compression-tension variation from the inner surface outwards;
(2) Hoop stresses remain tensile but reduce in magnitude as the wall thickness become greater.
(3) The tensile axial stress at inner wall decreased with increasing r/t ratio and the hoop stresses at weld centreline could vary significantly depending on yield strength.

2.4 Residual Stress Measurement Techniques

2.4.1 Destructive methods

2.4.1.1 Sectioning

Sectioning method is known as one of the many available destructive technique for residual stress measurement. The principle of this method involves measuring the deformation of the removed material from component to determine the residual stresses. This technique relies on the fact that residual stresses in material will be relaxed and redistributed upon machining (i.e. slitting, cutting and etc.) and a new equilibrium stress state will be achieved [36]. Change in strain can be measured using either electrical or mechanical strain gages.

Sectioning technique was first introduced as a method to determine longitudinal residual stresses in bars, in which the measurement of the change in length was made as the bar was slitting into strips[37]. Follow this idea, sectioning was not only

applied to determine longitudinal residual stresses but also those transverse to specimen thickness [38], [39]. The steps of the whole process are shown in Figure2.5. Prior to any cutting, strain gauges were attached, and initial readings of the strain were obtained. The elements were cut longitudinally from the component (sectioning) and measurements were taken by mechanical extensometer. Before any further cutting for through thickness strain measurement, more strain gauge points were attached along the side of elements and after that, the elements were sawing to strips across the thickness (slicing). Additional reading of strain before and after slicing were obtained from the readings.

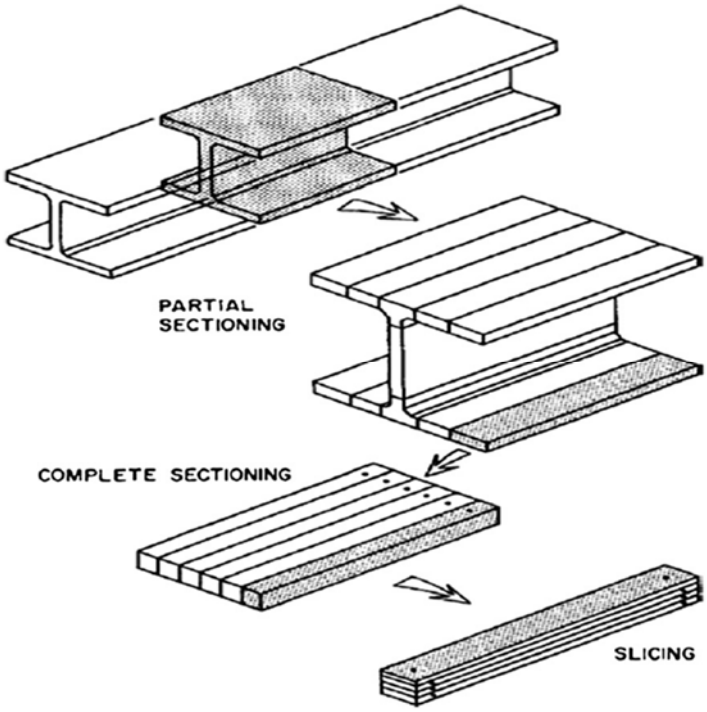

Figure 2.5 Steps in sectioning method

The sectioning method is simple but only sufficiently accurate to measure the longitudinal residual stresses in component. Potential errors can be generated due to the change in temperature during cutting. It is recommended to avoid temperature fluctuation.

2.4.1.2 Contour method

The contour method [40] was developed based on the Buechner's superposition principle [41] initially introduced in early 2000s [42], [43]. The method is capable to determine the residual stresses by simply cutting a component into two pieces and measure the displacements that are normal to the new-cut surfaces. The

displacements resulted from the relief of the residual stress induced by the cutting process. The measured date can be used to calculate the residual stresses and coupled with finite element models. It is possible to provide a 2D map of stress variation across the cutting surfaces.

The principle of the contour method can be easily illustrated in 2D [43]. Simply as seen in 2D Figure 2.6, the original residual stress state A is in the specimen. Once cut in two pieces, the relived stresses on the cut-out surfaces will result in a surface contour change in B. The free surface in C is then forced back to its original configuration. And the original residual stresses are calculated by superimposing the stress states in B and C.

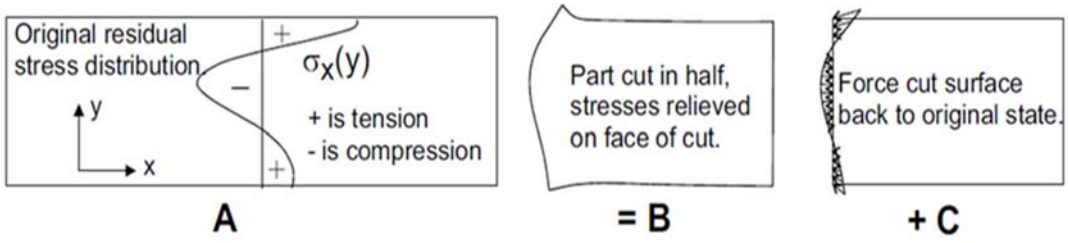

Figure 2.6 Superposition principle used to calculate original residual stress from measurement of surface contour after cutting a part into two [43].

This principle assumes that all material deformation is linear elastic and no additional stresses were introduced during cutting. Although the stress state in B is unknown and the stresses of the whole body cannot be precisely determined, the stress in free surface must be zero. Therefore, the stresses along the cut surfaces can be accurately determined after forcing back the deformed surface. There are four steps involves: (1) specimen cutting, (2) contour measuring, (3) data reduction and (4) stress analysis [36], [44].

Unlike conventional residual stress measurement techniques only provide 1D variation of the residual stress state, contour method is highly precise in generating a full 2D map of residual stress map though it is destructive in nature. It has been further extended to measure multiple residual stress components by making multiple cuts [45] and more recent application was carried out on determining the residual stresses in cylinders[46], [47] .

2.4.1.3 Other destructive methods

Other common used destructive methods include excision, splitting, layer removal and slitting. The application of all these techniques is based on the principle of stress relaxation, only some of them are specialised in assessing the residual stresses in specific geometries.

Excision is able to quantitively determine the residual stress with a few simple steps. It involves attaching one or more strain gauges on the surface of the component to be measured, and then excising the material fragment with attached strain gauge(s). With this process, residual stresses in material will be relieved, leaving the fragment stress-free, and strain gauge(s) will measure corresponding strains. Excision is typically applied on thin plate because it is straightforward to cut the fragment that around the strain gauge(s). Thicker excision also can be achieved however full excising on material is not convenient due to the undercutting process requires excavating the material [36], [48].

The application of splitting method [49] is illustrated in Figure 2.7. Specimen may present in opening or closing behaviour after a deep cut sawn into the material. The relaxation induced deformation indicates the sign and approximate magnitude of the relieved residual stresses. This method is generally used for residual stresses assessment in thin-walled tube. Different cutting arrangement can be used to evaluate either longitudinal or circumferential residual stresses [50]. Both of these two arrangement are typical examples of Stoney's Method [51], and is also known as the curvature method, which measures the deflection or curvature of the thin-walled workpiece aroused by the addition or removal of the material containing residual stresses [48].

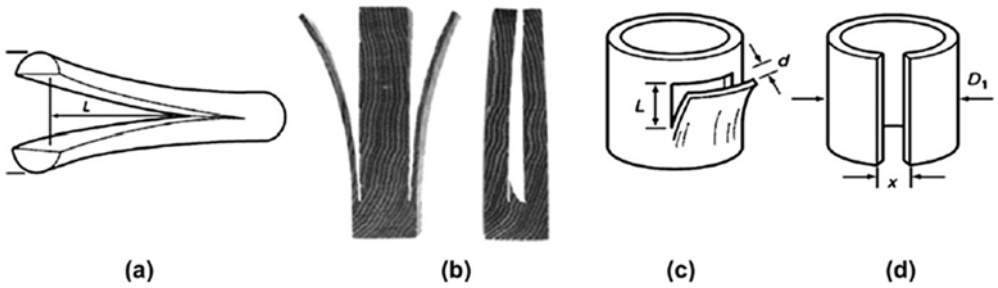

Figure 2.7 The splitting method: (a) for rod[49]**, (b) for wood, (c) for axial in tubes, (d) for circumferential stresses in tubes [50].**

Layer removal method is a generalization of Stoney's method [48]. Measurement of the deformation is accomplished by removing a sequence of layers of material, which can be applied on both flat plate and cylindrical specimens (Figure 2.8). Residual stresses in the specimen should vary through thickness but remain uniform parallel to the surface. Strain gauges are attached on the surface of the specimen whereas the layers of the material are removed from the opposite surface [52].

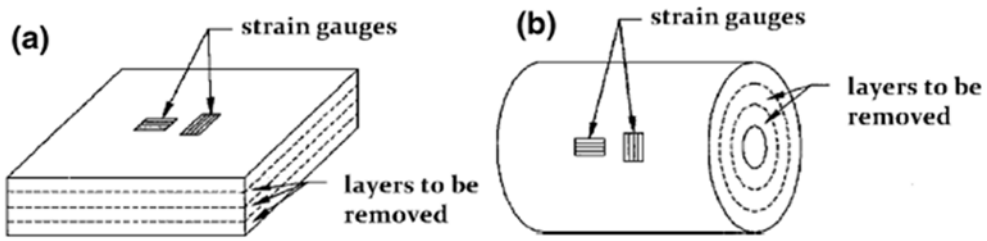

Figure 2.8 Layer removal method, (a) flat plate, (b) cylinder.

In the application of cylindrical specimen, it is also called Sachs technique. Strain gauges are attached either outside or inside surface to measure the deformation as the layers are removed from the opposite surface. Although this method is typically applied to metal specimen, it is not suitable for evaluating residual stresses in weld because the strain gauge are only able to measure global relief of residual stresses not those local to a specific region, i.e. weld metal [53] .

Slitting method is quite similar to the hole drilling method except a slit is used. It is also alternatively named as crack compliance method, the sawcut method or the slotting method. Figure 2.9 illustrates the attachment of the strain gauges which is either on the front or the back of the specimen surface. With the increase in slit depth, the relieved strain can be read from attached strain gauges.

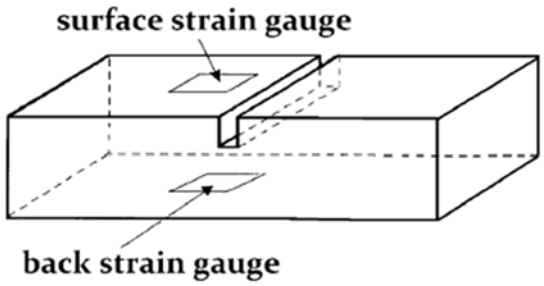

Figure 2.9 Slitting method

Unlike hole-drilling method which is able to measure three in-plane residual stresses, slitting can only assess the residual stresses normal to the cutting plane but the

residual stress profile across thickness can be obtained. The majority of plasticity errors in slitting measurements was caused by the plasticity near the cut tip. The errors, correlated to stress intense factor, were strongly dependent on the amount of constraint provided by the part width [54].

2.4.2 Semi-destructive

2.4.2.1 Hole-drilling

Hole drilling method is the most widely used technique for residual stress measurement. This semi-destructive technique has the advantages of good accuracy and reliability when evaluating residual stresses and only generates little localised damage on specimen which is repairable and tolerable [36]. The steps of this method are: (1) drilling a small hole on the specimen where the material is stressed, (2) measuring the relieved strain in the adjacent material around the hole and (3) calculating the corresponding residual stresses [1], [55].

The hole drilling method is based on the principles that inherent stresses in component can be determined by disturbing their stress equilibrium through some mechanical device and measuring the resulting deformations[56]. It was firstly introduced in 1930s by Mather who applied a mechanical extensometer and a circular hole drilling through a stressed plate. In 1950s, mechanical extensometer was replaced by strain gauge which greatly improved the accuracy and reliability of strain measurement and allowed small hole to use [57]. The hole-drilling strain-gauge method was later established as ASTM E837 standard. Detailed principles of test procedure were introduced in extensive literature [58], [59].

Hole-drilling method, determines the macro surface residual stresses, in comparison with other measure techniques is applicable to almost the material only if the material is machinable. However the residual stresses should not be exceed the 60% to 70% of the yield strength [36]. Residual stress in depth of the specimen can be deduced by incrementally deepening the hole whereas reliable results are hardly obtained when depth is much larger than the hole diameter [1]. Machining induced stresses by high-speed hole-drilling was proved to be lower than other hole-drilling methods which provide a higher accuracy for stress measurement, whilst the drill will be worn fast when it is working on the material with high hardness leading to further errors. With the assistance of electrical discharge machining (EDM) process,

there is no constraint on mechanical properties of the ferrous material and the drilled hole is highly precise.

Hole-drilling technique has been used in many investigations. Leggatt [9], [10] applied central hole-drilling on pipe girth weld to determine the surface residual stress distribution and magnitude. Olabi and Hashimi [60], [61] investigated the effect of post weld heat treatment on residual stress relaxation on steel components with this method. And this measurement technique was also applied on tubular cluster [62]. With the use of multi strain gauges, high quality data can be collected for residual stress evaluation [63].

2.4.2.2 Ring-core method

Ring-core method is another common method for surface residual stress measurement [58], [64], [65]. The principle of the technique involves drilling an annular groove on the specimen surface thereby leaving a core of the material in the centre of the groove. The internal diameter of the ring is generally from 15-150mm and the depth of the ring-core range between 25%-150% of its internal diameter [58]. The deformation of the core can be measured by strain gauge and the stresses relaxed during machining thereafter can be calculated from stress-strain relationship. Figure 2.10 shows the difference of strain gage installation between hole-drilling and ring-core methods.

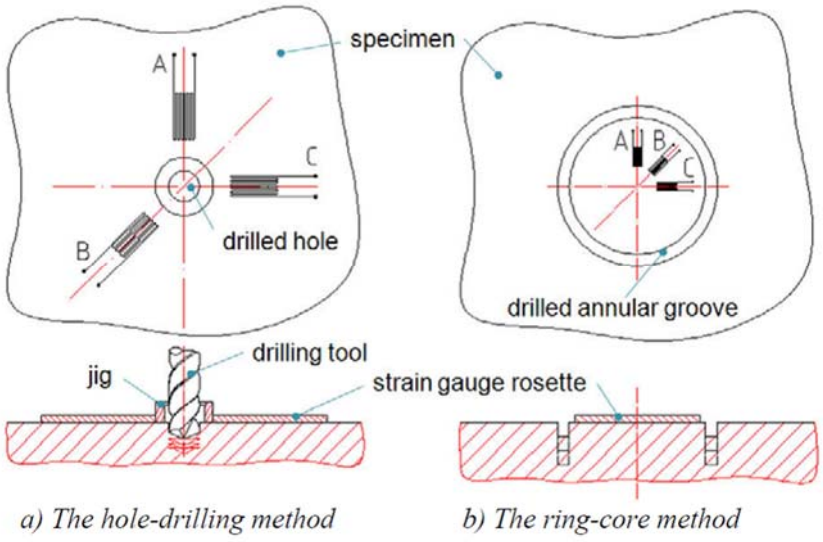

Figure 2.10 Difference between hole-drilling and ring-core methods [65].

Ring-core method was first introduced by Milbredt in 1951 to substitute hole-drilling technique [58]. Gunnert [66] proposed technique to measure relaxed stresses by using a mechanical extensometer. In order to solve the problem of disconnecting and reconnecting the strain gauge wires for ring drilling process, cutting methods haves been improved with air-abrasion method, electro-discharge (EDM) and spark erosion machining.

Comparing with hole-drilling method, ring-core method comes with many advantages [65]. Firstly, it is possible to measure residual stresses to greater depth. Secondly, it is insensitive to errors due to the eccentricity with the central placed strain gage rosette. Moreover, residual stresses as high as yield strength can be measured. And also, the influence of residual stress and the temperature changes during drilling are smaller than that of hole-drilling technique.

2.4.2.3 Deep-hole method

Deep-hole drilling [67] is a semi-destructive residual stress measurement technique developed as a combination of both hole-drilling and ring-core methods [36]. It determines the residual stress by measuring the change of diameter of a reference hole that drilled through depth of the thick component before and after the residual stress relaxation, during which a column of the material containing the hole is removed from the component [67].

The steps of the conventional DHD including: (1) gluing bushes at both front and back surfaces of the component prior to any drilling, (2) gun-drilling a hole through the depth of the specimen, (3) measuring the initial diameter of the hole accurately at several depth and angles with an air probe, (4) trepanning a column which containing the hole coaxially to relieve residual stresses by electric-discharge machining (EDM) [68], [69] during which axial strain is measured with the assistance of LVDT (linear variable differential transformer) [70], [71], and (5) finally re-measure the changes in diameter and column height to determine the initial residual stresses state. Figure 2.11 lists the steps in the strain measurement process with DHD method.

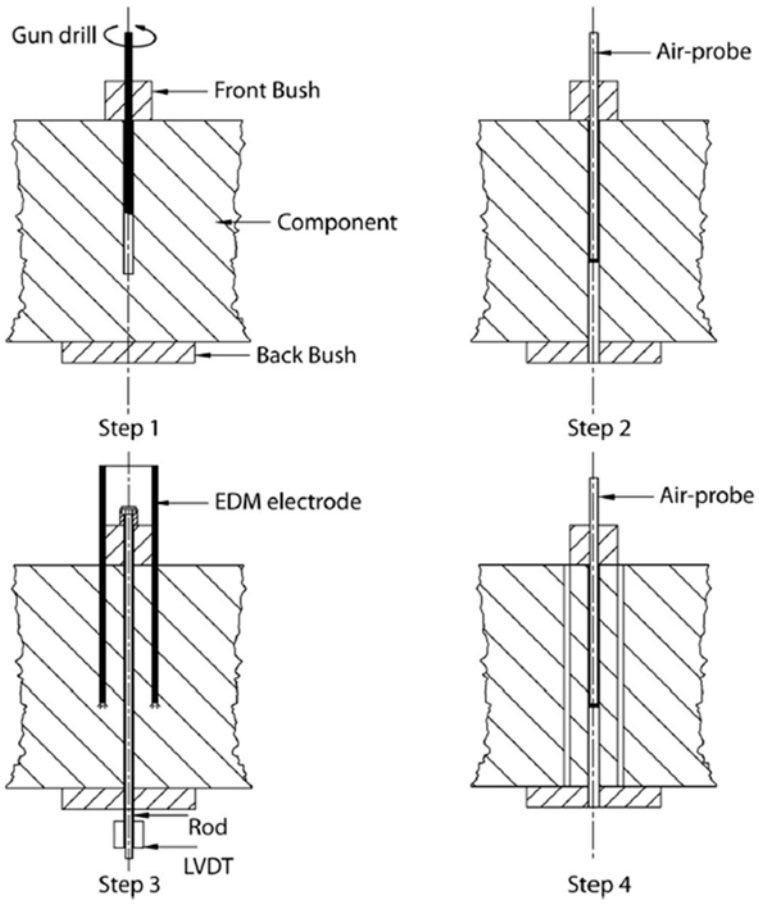

Figure 2.11 Schematic of DHD method and steps in the measurement process

2.4.3 Non-destructive techniques

2.4.3.1 X-ray diffraction

In homogeneous polycrystalline materials, the stress value can be determined from the interatomic strain assuming that stress is proportional to the measured strain [72]. X-ray diffraction (XRD) techniques exploit the fact that when a material is under stress, applied or residual, the resultant elastic strains cause a change in spacing of the atomic planes in the crystal structure. XRD is capable of direct measurement this interplanar atomic spacing, and from this reading the total stress on the metal can be determined [73], [74].

There are basically three techniques for residual stress measurement using X-ray diffraction method. They are the single exposure or one-angle technique (SET); the double exposure or two-angle techniques (DET) and $sin^2\psi$ or multi-angle technique. The exposure angle is defined as the angle between the incident X-ray beam and the specimen surface normal [72]. Angle ψ is the angle between the normal of the

surface and the indent and diffracted beam bisector, which is also the angle between the normal to the diffracting lattice planes and the sample surface [75]. Diffraction occurs at an angle 2θ, defined by Bragg's Law: $n\lambda = 2d \sin\theta$, where n is an integer denoting the order of diffraction, λ is the x-ray wave length, d is the lattice spacing of crystal planes, and θ is the diffraction angle (Figure 2.12).

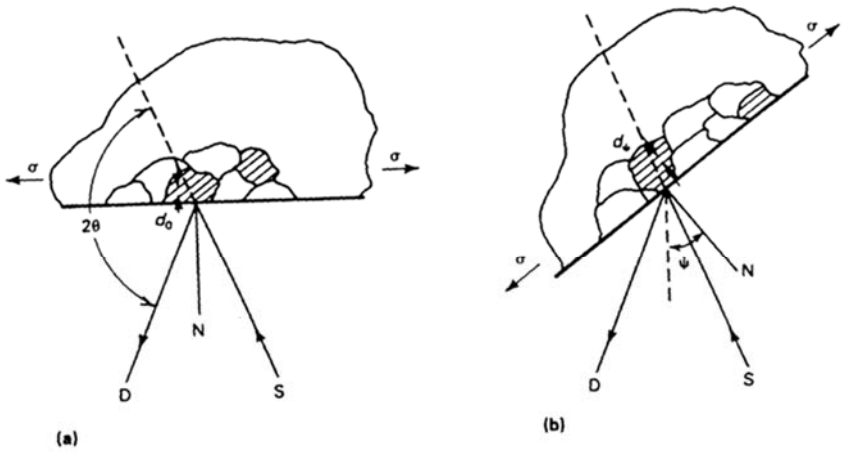

(a)ψ = 0. (b) ψ = ψ (sample rotated through some known angle ψ). D, x-ray detector: S, x-ray source; N, normal to the surface.

Figure 2.12 Principles of x-ray diffraction stress measurement

The stress measurement by XRD is based on the theory of elasticity for deformation in arbitrary direction in which penetrated thin layer of the material surface is assumed under plane-stress condition. The stress distribution is described by principle stresses σ_{11} and σ_{22} in the plane of the surface, shown in Figure 2.13 below [76]. There is no stress acting perpendicular to the free surface, a strain ε_{33} component perpendicular to the surface, exists as a result of the Poisson's ratio contractions caused by the two principle stresses [76]. The strain $\varepsilon_{\phi\psi}$ is given by:

$$\boldsymbol{\varepsilon_{\phi\psi} = \left(\frac{1+\nu}{E}\right)\sigma_\phi sin^2\psi - \left(\frac{\nu}{E}\right)(\sigma_{11} + \sigma_{22})} \quad (2.1)$$

Where E, ν are elastic constant, ϕ and ψ are azimuthal and polar angles in the spherical coordinate system, σ_ϕ are measured stress component in the ϕ-direction [77]. In terms of changes in linear dimensions of the crystal lattice this equation can be expressed as:

$$\boldsymbol{\varepsilon_{\phi\psi} = \frac{\Delta d}{d_0} = \frac{d_{\phi\psi} - d_0}{d_0}} \quad (2.2)$$

Where $d_{\phi\psi}$, d_0, are interplanar distances for analyses and free of stress material, respectively. The lattice spacing for any orientation then is:

$$d_{\phi\psi=}\left(\frac{1+\nu}{E}\right)\sigma_{\phi}sin^{2}\psi-\left(\frac{\nu}{E}\right)d_{0}(\sigma_{11}+\sigma_{22})+d_{0} \quad (2.3)$$

This is the fundamental relationship between lattice spacing and the biaxial stresses in the surface of the sample. The lattice spacing $d_{\phi\psi}$ is a linear function of $\sin^2\psi$. The stress can be determined by measuring the lattice spacing with at least two ψ angles.

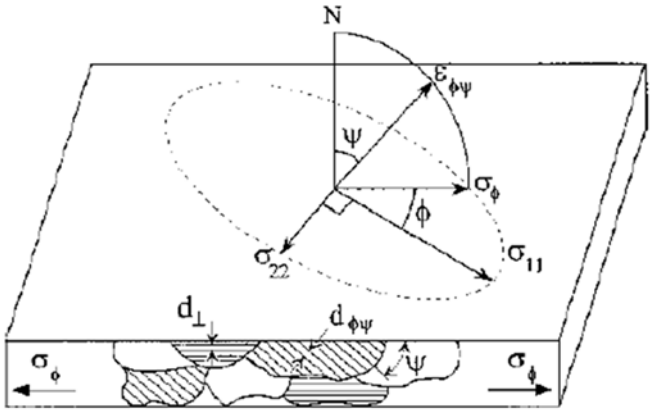

Figure 2.13 Plane-stress elastic model [76]

XRD technique for residual stress measurement was believed to be rapid, economical, accurate and high-resolution on thick-plate weldments [78]. However, due to the capability of penetration and the effect of the thickness on the stress measurement results are not negligible in weldments, X-ray is only allowed to evaluated the stress generated in material surface layer [79]. This non-destructive method can be combined with layer removal technique to achieve stress profile through the thickness of the sample, but then the method becomes destructive [80].

Synchrotron X-ray diffraction has become a promising method for analysing the tri-axial residual stress state [81]. Unlike conventional lab x-rays, this hard source provides beams of high energy X-ray millions of times more intense and penetration depth up to hundreds of time greater [82]. Investigators preferred to apply synchrotron X-ray rather than neutron diffraction in stress state determination on aluminium alloy because of smaller gauge volume and rapid data acquisition [83]. Nevertheless, there are also some drawbacks. Lower diffraction angle of synchrotron X-ray means that gauge volume is elongated which is excellent lateral to the beam but well suited for plate geometries with large in-plane stress. With a small gauge volume, synchrotron X-ray tends to produce speckled diffraction patterns due to the insufficient grain diffraction [83].

2.4.3.2 Neutron diffraction

The principle of measuring residual stress in components is similar to that of X-ray diffraction, in which residual strains are determined directly by the changes in lattice place spacing [84] from their stress-free condition. However, unlike X-ray is only able to measure surfaces stresses, neutron diffraction has the advantage of penetrating inside bulk material up to several centimetres [1],[36].

There are two neutron diffraction techniques have been developed for residual stress measurement: conventional method employs monochromatic beam and time-of-flight approach which utilises pulsed beam source. Monochromatic beam can provide the best performance when a small region of the whole diffraction profile is required. Figure 2.14 illustrates the detection of lattice strain by diffraction.

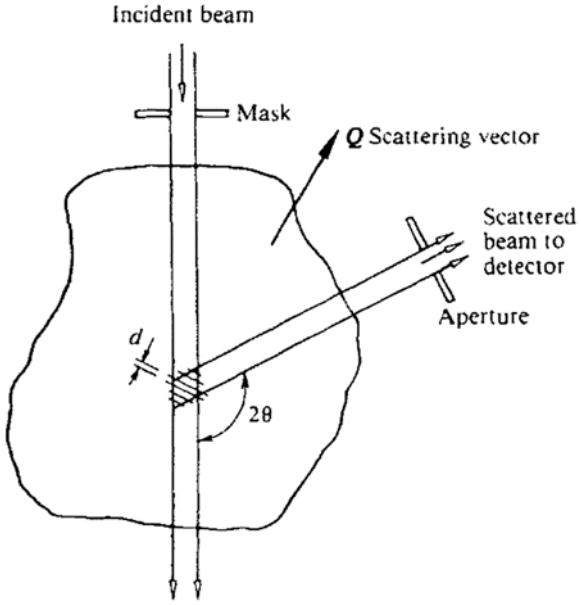

Figure 2.14 Principles of the diffraction technique showing Bragg reflection from crystal [85]

In a polycrystalline material, only those grains lattice plane which allows Bragg reflection will contribute to the scattering. Bragg reflection occurs when the normal to deflecting planes bisects the incident and scattered neutron beam and then parallel to the change in neutron wave vector **Q** [84]–[86]**.**

Once neutron beam with a wavelength λ is incident on a crystalline material, a diffraction pattern with peaks is produced. If d is the lattice spacing in the direction of Q and 2θ is the scattering angle then Bragg's law gives the position of the peak value,

$$2d \sin\theta = \lambda \tag{2.4}$$

A small change in the lattice parameters Δd will result in $\Delta\theta$ in the angular position of the Bragg reflection, the lattice strain ε, in the direction of the scattering vector is

$$\varepsilon = \frac{\Delta d}{d} = -\Delta\theta \cdot \cot\theta \tag{2.5}$$

This is the 2θ-scan method, λ is fixed and θ is measured. In the λ-scan method, θ is kept constant and λ is measured [87]. For instance time-of-flight approach, the scattering angle is usually in 2θ=90° [86] and strain can be determined from an analysis of individual peaks. The corresponding strain instrument, conventional angular and time-of-flight, are shown in Figure 2.15 [88].

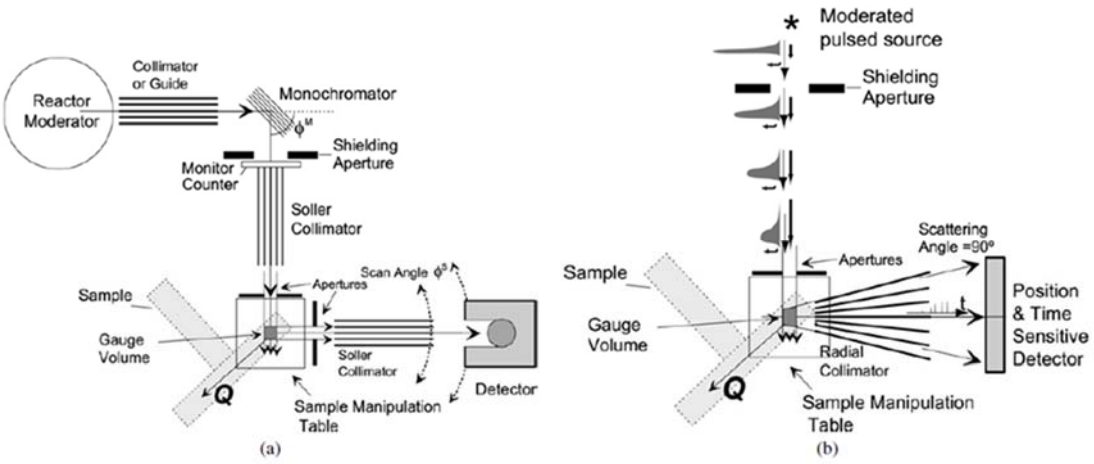

Figure 2.15 (1) conventional monochromatic two theta scanning as practised at a constant flux source (2) time-of-flight instrument as might be found at a pulsed spallation source. In both cases the strain is measured in the direction of the Q vector [88]

Residual stress field in welding structures such as pipe girth weld [86], [89], [90], T-type and double V butt joint [91], [92] in plates has been investigated. It was found that two neutron-diffraction configuration modes can significantly increase the available beam penetration path length in ferritic steel weld plate. These configurations use the wavelengths of 2.39 and 1.55 Å corresponding to the diffraction peaks of (110) and (211), respectively.

2.4.3.3 Diffraction techniques in crystalline material

Diffraction techniques using X-ray or neutrons have been widely applied as they are non-destructive. Measurement methods and subsequent data-processing may depend on the selected crystal phase and/or orientation in either polycrystalline material or single crystals. For example, within a macroscopic sampling volume, the interplanar

lattice spacing can be generally interpreted as a representative atomic plane or an averaged value of measured lattice pacing at a given measurement location [16].

Metallic polycrystalline solids consist of a collection of many small crystalline or grains with different crystallographic orientations [94]. The nucleation and growth of the gains are greatly affected by the various stages of the solidification and manufacturing processes, for instance the rolling direction.

With regard to a crystalline solid, a single crystal is a large grain or an object which contains uninterrupted order and repeated arrangement of the atoms [94]. Because the entire sample is continuous with no grain boundaries, single crystals can be artificially produced to form a regular geometric with flat faces, to obtain absolute value of lattice spacing using non-destructive methods.

The 'powder method' also can be adopted for the analysis of the crystal structures in polycrystalline materials. When diffractive beams with fixed wave length strike on a sample, they will be simultaneously reflected at the atoms planes that oriented at the appropriate Bragg's angle. The scattered beams produce cones of the beams and their projections on a detector are called Debye-Scherrer circles [18]. A typical diffraction pattern contains several Bragg peaks. The intensities of diffracted peaks interpret on the positions and types of atoms within the unit cell. Interplanar lattice spacing therefore can be obtained.

In comparison, scattered beams originating from a single crystal produce diffraction spots instead of Debye-Scherrer circles. Each spot corresponds to a unique lattice plane (hkl).

However, powder diffraction may require larger sample volumes than that of single crystal, therefore highly absorbing isotope in the sample might result in very little scattering observed in the materials [96].

Early investigation of using single crystal neutron diffraction as a supplement to X-ray diffraction for the studies of crystal structure was in 1950s [97]. X-ray single crystal diffraction has the advantage of inherent enhanced resolution, but a major limitation of this diffraction technique is its insensitivity to hydrogen atoms [96],

[98]. While using neutron source materials contain hydrogen can be measured with ensured scattering strength.

2.5 Post Weld Heat Treatment – PWHT

2.5.1 Overview

PWHT, either in the form of a global or a local approach, has been widely applied on the welded structure for many years. Figure 2.16 exhibits the effect of the PWHT on the magnitude and distribution of hoop, axial and radial residual stresses through the thickness of a girth weld at weld centreline [12], in which the residual stress magnitude in all three directions were reduced significantly (Figure 2.16b).

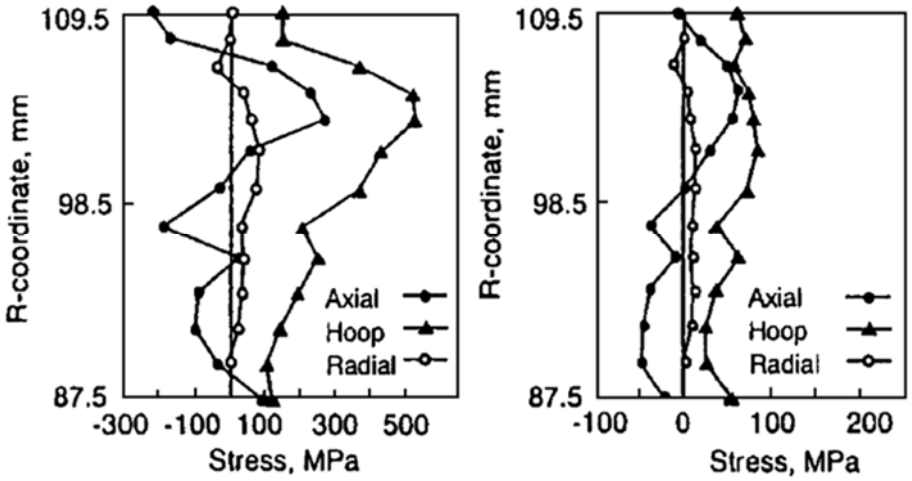

Figure 2.16.Through wall thickness distributions of residual stresses in pipe girth weld centreline; (a) as-welded, (b) after PWHT [12]

Once a welded component is heat treated at elevated temperature with sufficient time, the structure is no longer capable to support the initial residual stress with reduced yield strength; then the residual stress would be relieved by plastic or creep deformation [99].

The extent of residual stress relaxation is dependent on time and temperature, of which temperature has a stronger effect than time does. The control of cooling is necessary because a slow and uniform cooling will effectively avoid reintroducing residual stresses. The parameters affecting the efficiency of the PWHT includes [5]:

- The heating rate to the desired temperature;
- The maximum required temperature;

- The time during which the maximum temperature is maintained;
- The cooling rate from the maximum temperature to room temperature.

The advantages of PWHT included: 1) it removes the existing hydrogen from weldment, which prevents embrittlement after cooling; 2) it also comes with tempering effect during which the material toughness, ductility and corrosion resistance will be improved; 3) the relief of the residual stresses can be achieved by plastic and creep deformation. Therefore, PWHT is also called stress-relief heat treatment [100].

There can also be detrimental effects if the heat treatment is not appropriately performed. If the maximum temperature exceeds the critical value, it will result in the deterioration of the material tensile and creep strengths. High-temperature precipitations within microstructures will also embrittle the material and reduce the material toughness. The carbide-forming alloy elements within material can enhance the material strength at PWHT temperature but require higher temperature to achieve stress relief [5].

PWHT carried out in a furnace is a more preferred option since not only more even the distributed temperature can be achieved but also the control of the heating cycle is not difficult. The peak residual stresses in weldments have been reported to be reduced to a level of 30% of material yield strength when heat treated in the furnace at approximately 600°C for a period of time and followed by furnace cooling [60], [101].

Numerical modelling can be used to predict or estimate the degree of residual stress relaxation induced by PWHT process, but this is not included in the scope of this project.

2.5.2 Published works on Local PWHT

There are some circumstances under which it is infeasible or unnecessary to perform PWHT in a permanent furnace. For instance, when it is difficult to fit a large-scale component entirely into a furnace facility under field services. It is also recommended to perform local PWHT when a small region of the component, such as in pipelines, is required to be heat treated [102].

For welded components, local PWHT is carried out on a weldment which includes the weld metal, heat affected zone and adjacent volume of base material, under the expectation that the same outcome can be achieved as that heating in a furnace does. Locally heat-treating a pipe cluster with heating pads up to 600°C for 1 hour and cooling back to room temperature was conducted previously [62]. The results showed the tensile residual stress was reduced about by 40% of material tensile strength and in hoop direction, tensile stresses were either reduced or change to compressive.

The requirements for local heat treatment are similar to that for furnace PWHT. The thermal gradient away from the hot zone should not be too steep for a specific distance to ensure no additional thermal stresses are induced. The soaking temperatures must be strictly controlled and monitored, for which a lower limit temperature (the minimum PWHT temperature below lower critical temperature) should be used to guarantee that the heating area experiences a stress relaxation with an appropriate tempering. The upper soaking temperature limit, based upon the knowledge of the equilibrium diagram, is not allowed to exceed the lower critical (A_{C1}) line. At higher temperature, ferrite phase that is in body centred cubic crystal structure (BCC) will be austenized, giving a face centred cubic (FCC) structure. Undesired phase and microstructure transformation can result in volumetric change in the component which often show in the form of distortion.

A 360-degree band heating, namely circumferencial, is generally performed on tubes or pipes after welding. Ieminologies used in this application of heating include soak band (SB), heated band (HB) and gradient control band (GCB), as seen in Figure 2.17. Nomenclatures are after the Figure.

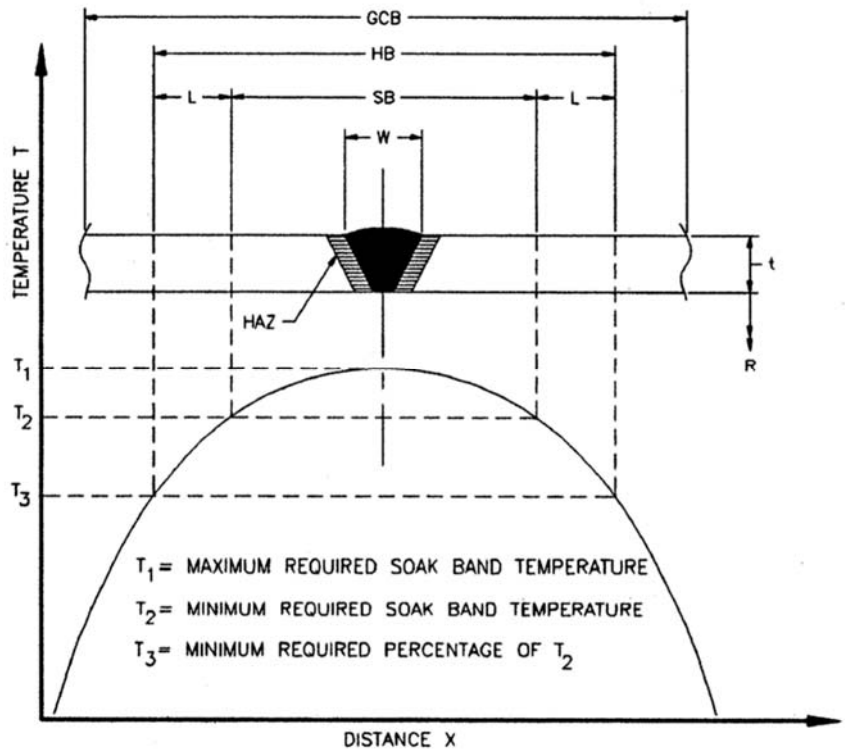

Figure2.17 Local circumferential heating diagram

W = Widest width of weld

HAZ = Heat affected zone

SB = Sock band

L = Minimum distance over which the temperature may drop to a percentage of that at the edge odf the soak band

HB = Heated band (width of heat source)

GCB = Gradient control band (minimum width of insulation and/or gradient heat source)

t = Nominal thickness

R = Inside radius

The definations of the the SB, the HB and the GCB are descibed as follows and their recommended standard widths in UK and American practices are summarsied in Table 2-2.

(1) Soak Band

The soak band is an area consists of the weld, the HAZ and a part of adjacent parent material. It should be heated within specific temperature range to achieve desired

results. The recommended minimum SB width for local PWHT based on ASME Section III, section VIII and AWS D10.10 is the thickness of the weld or 2 inches (50mm); whichever is less, on either side of the weld at its greatest width. In comparison, BS EN 13445 and PD 5500 recommends minimum SB equals to the total width of the weld and HAZs. Another option is ASME B31.1 and B31.3 define that the SB width is proportionally increased with the pipe wall thickness.

(2) Heated Band

When heating a pipe, the HB width should be wide enough to ensure the through-thickness temperature of SB meet the requirement and control the induced thermal stresses. For the determination of the width of HB, there are two criteria. One is based on induced stress, and the other is the through-thickness temperature gradient.

For induced stress criterion, early works was done in 1960s [6], [103] by limiting the induced thermal stress (via temperature distribution control) during local PWHT to a level less than material yield strength at PWHT temperature. Therefore, no secondary residual stresses would be introduced after a localized heating. Rose [103] made an assumption of axial symmetrical temperature distribution for local heat treatment on vessels and he pointed out that the parameters which determined the heat flow were: 1) rate of heat input, 2) the width of the HB and 3) the specific distance which satisfied temperature requirement and heating time. Though the assumption has not been validated by additional studies, it was practically accepted that the total heat input should be proportional to the width of the HB. Heating time should be determined by the required temperature for stress relief and it does not vary due to the change of the HB width.

Burdekin [6] extended the experiments to obtain detailed analysis of local stress relaxation in cylinders. It was found a wider HB (16 inch vs. 4 inch) achieved greater magnitude of stress relief. The width of the HB was believed to be related to the geometry parameter $\sqrt{Rt}$ (R is the cylinder radius, t is the shell thickness) and it is recommended $5\sqrt{Rt}$ might be adequate. The total HB width of $5\sqrt{Rt}$ is recommended in standards BS EN 13445 and PD5500. In contrast, it is suggested to be $W + 5\sqrt{Rt}$ ($2.5\sqrt{Rt}$ on either side of a weld) in BS 2633 and $SB + 4\sqrt{Rt}$ ($2\sqrt{Rt}$ on either side of the soak band) in AWS D10.10.

For the through-thickness temperature gradient criterion, a detailed experiment on local heat treatment of pipe component was carried out to determine the impact of heat source width [104]. It was found that increasing the heat source width when applying local heating method would decrease the radial thermal gradient in thick-walled pipe. This gradient remained unaffected by energy density. It was also discovered applying a minimum width of five times the wall could be effectively relieve the stresses in first hour.

The use of HB as wide as five times the pipe wall thickness was suggested insufficient to create minimal thermal gradient in desired local area where is susceptible to localized corrosion after PWHT. This is because uniform relief of residual stresses could not be guaranteed [105]. The use of Hills Number H_i, ratio of heat source area to heat loss area, was proposed to achieve the required thermal gradient when determining the width for HB. As recommended in AWS10.10, the minimum HB width is

$$HB=H_i\,[(OD^2-ID^2)/2+(ID)(SB)]/OD \quad (2.6)$$

where OD is the pipe outer diameter, ID pipe inner diameter.

The value of H_i is dependent on the size and position of the pipe as well as the number of the circumferential control zone. For instance, a pipe size up to 6NPS (nominal pipe size, OD in 6.625 inch), H_i=5 could be used for one circumferential control zone in horizontal position. H_i=3 could be used for pipes with at least two circumferential control zones and larger than 6NPS.

(3) Gradient Control Band

Gradient control band (GCB) is the minimum insulation area implemented on the heat source, which is as a function of controlling the axial temperature gradient and heat loss. The width of GCB is recommended $10\sqrt{Rt}$ in BS EN 13445 and PD 5500. It also can be calculated as a sum of HB and $4\sqrt{Rt}$, provided in AWS D10.10.

(4) Axial Temperature Gradient

A feasible axial temperature gradient will reduce the possibility of inducing additional stresses during PWHTT. BS 2633 requires that material at a distance of $2.5\sqrt{Rt}$ on either side of the weld centreline (the edge of the SB) be at a temperature

greater than one-half of heat treatment temperature. AWS D10.10 specifies that the maximum axial temperature gradient requires the maximum temperature drop from the edge of the HB is one-half the temperature at the edge of the SB.

Table 2-2 Comparison of the recommended widths of SB, HB and GCB in UK and American practices

Standards	Soak band (SB)	Heated band (HB)	Gradient control band (GCB)
BS EN 13445	W + 2HAZs	$5\sqrt{Rt}$	$10\sqrt{Rt}$
PD 5500	W + 2HAZs	$5\sqrt{Rt}$	$10\sqrt{Rt}$
BS 2633	-	$W + 5\sqrt{Rt}$	-
ASME III	W + min[100mm,2t]	Temperature is gradually diminished to avoid harmful thermal gradient	-
ASME VIII	W + min[100mm,2t]	Temperature is gradually diminished to avoid harmful thermal gradient	-
ASME B31.1	$3t_{max}$	-	-
ASME B31.3	$3t_{max}$	-	-
AWS D10.10	W + min[100mm,2t]	Maximum [HB1, HB2, SB+50mm] HB1 =SB + $4\sqrt{Rt}$ HB2 = Hi[$\frac{OD^2-ID^2}{2}$ + (ID)(SB)]/OD (H_i=3 or 5)	HB + $4\sqrt{Rt}$

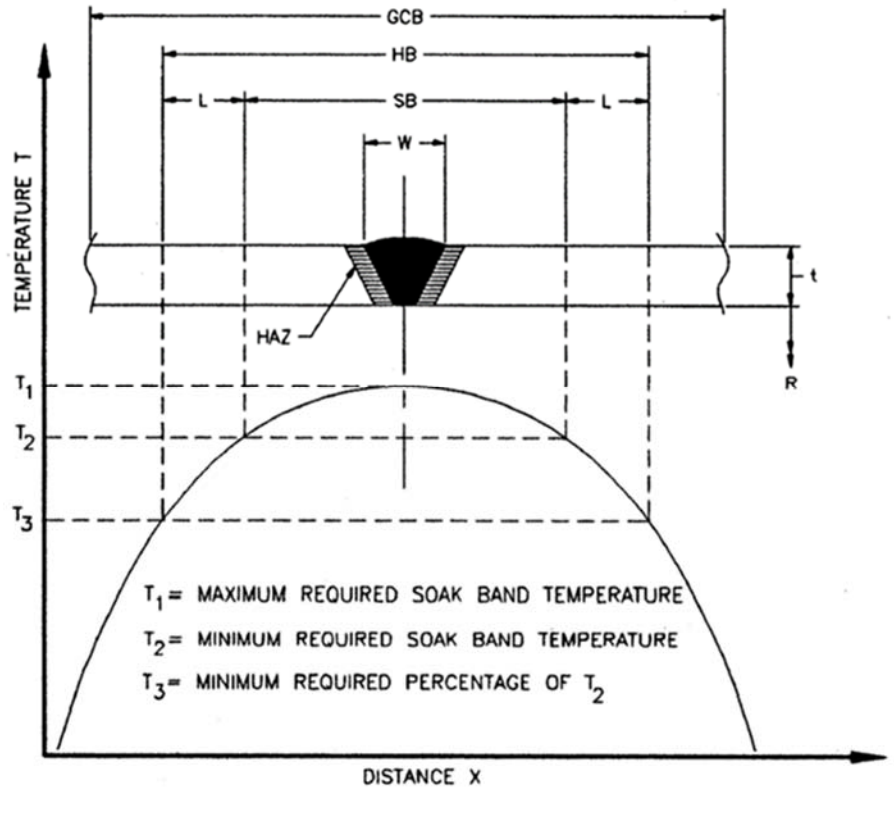

Other essential PWHT conditions include heating rate, hold time, holding temptation and cooling rate. Fast heating and cooling rate are unwanted because steep thermal

gradient will be produced which will result in additional residual stresses. In addition, material should be heated at an appropriate holding temperature for some time to allow stress to relieve. Table 2-3 summarises the recommended PWHT parameters in UK and American standards.

Table 2-3 Recommended PWHT parameters in UK and American standards

<table>
<tr><th></th><th>Holding temperature (°C)</th><th>Heating rate (°C/h)</th><th>Cooling rate (°C/h)</th><th>Holding time</th></tr>
<tr><td>BSEN 13445</td><td>530-580(±40)</td><td colspan="2" rowspan="2">≤ 220
above 400°C</td><td>2t min</td></tr>
<tr><td>PD 5500</td><td>550-620</td><td>30 min</td></tr>
<tr><td>BS 2633</td><td>580-620</td><td>≤ 220
above 400°C</td><td>≥ 275
above 400°C</td><td>2.5t min (minimum 30min)</td></tr>
<tr><td>ASME III</td><td>595-675</td><td colspan="2">≤ 220°C/hr divided by the maximum thickness in inches above 425°C</td><td>2t min</td></tr>
<tr><td>ASME VIII</td><td>Minimum 595</td><td>≤ 222°C/hr divided by the maximum thickness in inches above 425°C</td><td>≤ 280°C/hr divided by the maximum thickness in inches above 425°C</td><td>1 hr/25mm (minimum 15min)</td></tr>
<tr><td>ASME B31.1</td><td>595-650</td><td colspan="2">≤ 315°C/hr divided by $^1/_2$ the maximum thickness of the material in inches at weld above 315°C</td><td rowspan="2">1h/25mm (Minimum 15min)</td></tr>
<tr><td>ASME B31.3</td><td>595-650</td><td colspan="2">≤ 335°C/hr divided by $^1/_2$ the maximum thickness of the material in inches at weld above 315°C</td></tr>
<tr><td>AWS D10.10</td><td>-</td><td>≤ 444°C/hr divided by the thickness in inches</td><td>≤ 278°C/hr divided by the thickness in inches</td><td>-</td></tr>
</table>

2.5.3 Local heating methods

Heating methods can be classified as either direct or indirect [106]. A furnace-based heat treatment transferred the energy to material indirectly using the heat produced from fuel or electrical energy. Heating the workpiece by flame, induction coil and electrical resistance are known as direct methods.

2.5.3.1 Direct heat source

Local heating can be performed using multi heat sources. In a previous investigation [107], a local low-temperature heating method was conducted on welded plate to evaluate the reduction of the residual stresses. As shown in Figure 2.18, local heating

was accomplished by moving source with two gas torches, symmetrically positioned at the side of weld with a specific distance. Compressive residual stresses were induced with implemented additional cooling system. Similar heating process was carried out using multiple beams on electron beam welded sheets [108]. Numerical calculation and experiment data were in good agreement for stress evaluation.

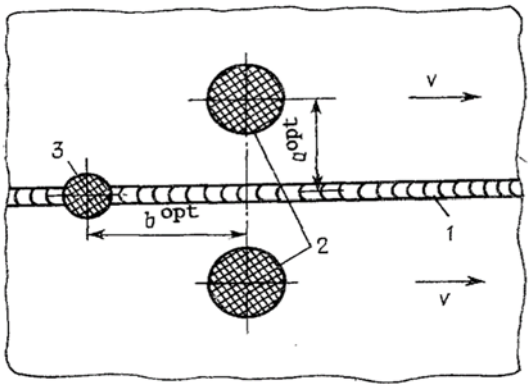

Figure 2.18 Diagram showing local pre-heating of welded seams of the plates: (1) welded seam; (2) heating zone; (3) cooling zone[107]

Though local PWHT can be applied directly after welding without setting up additional equipment[108], [109], heating the weldment locally with flames (torches) is not recommended [111] because it is highly dependent on operator's skill. This means there is a high risk associated with flame heating.

When applying local PWHT on circular welded joints, induction heating or electric resistance heating are generally used in practices [112]. For oil processing and petrochemical pipelines, flexible electric resistance heating is more preferred [111]. Welded joints in large pressure vessels are recommended to use induction heating to achieve local PWHT [113].

2.5.3.2 Induction heating

Induction heating is achieved through coils, carrying alternating current, of which the magnetic field induced by eddy current is used to heat the workpiece (Figure 2.19). As heat loss is presented as a basic electrical formula: $P=i^2R$ where i is the current and R is the resistance, copper is considered as the ideal material for coil due to its excellent low electric resistance [114]. The applications of induction heating have been broadened from localized joining and surface-hardening[115], [116] to heat treating on different materials [117] such as modifying residual stress of girth welded stainless pipe[118].

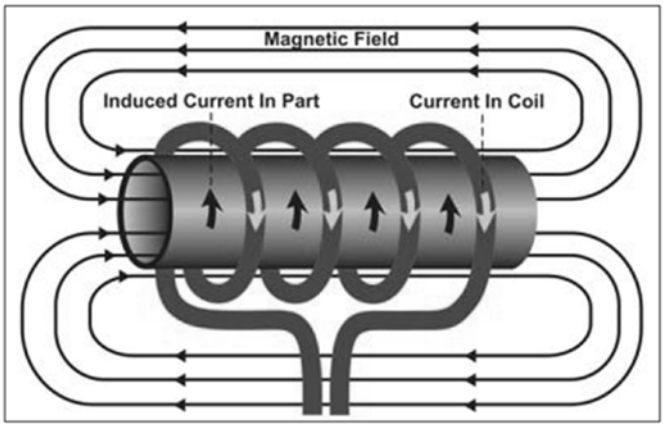

Figure 2.19 the principle of induction heating process

The principles for using induction heating approach have been introduced elsewhere[114], [116]: 1) the coil turns range should be adjusted for controlling the heat input with given voltage and frequency, ensuring the energy input is neither excessive or insufficient. 2) Generally, high current frequency is not desired as the magnetic field decreases rapidly if only pipe the surface is heated. Then the centre part requires to be heated with accumulated time; however, under this circumstance the skin will be overheated. 3) Pipes must be ferromagnetic; otherwise magnetic field will be uniformly distributed between the coil space rather than concentrating on wall thickness. Energy therefore is unnecessarily wasted. 4) Carbon, low alloys and other ferrite steels cannot be heated over 760°C, beyond which they become non-ferromagnetic [119].

2.5.3.3 Electric resistance heating

Another way of applying local post PWHT is using electric resistance. When an electrical current is passed through high resistance conductors, heating effect occurs as a function of I^2R, where I =current and R=resistance. It is the current that directly connects to the heating element which transfers the thermal radiated towards the heated part. Unlike the traditional heating furnaces [120], the equipment of local electric resistance heating includes heater, insulation, power source and other controlling devices.

Different kinds of heaters are detailed in AWS10.10, among them then flexible ceramic pad (FCP) is most commonly used. The heater is a multi-stranded Ni-Cr electric resistance heating wire woven with interlocking sintered Alumina ceramic

beads. The multi-stranded Ni-Cr wires produces the durability and dielectric Alumina which acts as insulation during heating is also abrasion resistant. The attachment of heaters depends on the heater types. The heated band of FCP may be comprised of one or more heaters [121], thus direct contact is not allowed as there is a risk of wire slips induced shorting.

In-situ residual stress measurement using neutron diffraction were performed while electric heating the components [122],[123]. It was proved that with increased temperature, residual stress is relaxed as a result of decreased yield stress. However, at even high temperature, creep plays a dominant role.

2.5.3.4 Alternative heating approaches

Heating methods are not only limited to induction heating and electric resistance heating, other heating approaches include exothermic heating, gas-flame generated infrared heating and radiant heating by quartz lamp. Exothermic heating is low cost for initial setups and has good portability, but it is seldom used for PWHT. Gas infrared and quartz infrared heating provide high heating rates and good portability, but they are in high cost for initial setups and fragile quartz lamp may increase the operation costs. They offer limited capability to create control zones around girth weld or sometimes additional equipment is required to accommodate the change in diameter. The selection of the heating methods greatly depends on the understanding of their advantages and limitations [121].

2.6 Discussion

This chapter has reviewed related literatures to understand the formation and the relieve of the residual stresses in welded structures, especially in girth welds. In terms of determining the distributions and magnitudes of the residual stresses in a component of interest, various measurement techniques can be used to make the material either destructive or non-destructive. The principles, applications, advantages and disadvantages of several popular measurement techniques have been summarized and compared. When selecting one or more technique for stress measurement, the condition of the material, the configuration of the component, the stresses in the desired area and the feasibility of the measurement technique are all worthy to be taken into consideration.

With respect to residual stress relieve by heating, the process can be performed in an enclosed furnace or using local heating methods. Although furnace heating has ideal effect on stress relieve, local PWHT has been investigated and standardized for industrial applications and practical purpose. A number of studies have been focused on investigating appropriated local heating to a certain volume of material which could achieve almost the same level of stress relieve as that carried out in a furnace. Among the heating methods, electric resistance heating has been widely used due to its flexibility, reliability and low cost for setting up. In addition, it is not restricted to material character such as induction heating can only be used for heating up ferromagnetic materials.

Residual stresses were also simulated using FEA approach for prediction or measurement validation. Either 2D or 3D model can be employed. For a girth weld, 2D model assumes the pipe in a rotational axisymmetric condition. Required computational power and time are much less that of a 3D model when the secretion has a large thickness.

2.7 Concluding remarks

Research carried out previously have provided a large number of information for residual stress measurement, stress relieve using furnace and local PWHT, and stress simulations using numerical modelling. The following conclusions are drawn for this study:

1. Residual stresses in girth welded pipe spools will be measured using non-destructive neutron diffraction technique because it has the ability to obtain through-thickness stresses in a thick-walled component. In addition, as the stress states will be evaluated in both as-welded condition and after PWHT process, damage due to destructive measurement process is not desired.

2. Residual stresses in girth welded pipe spools will be relieved using both furnace and electrical resistance local PWHT method. The effect of the heating band width will be investigated with a small number of pipe spools.

3.Resiudal stresses will be simulated using a 2D model which can greatly reduce the computational calculation. Results will be compared with the experiment outcomes.

Reference

[1] P. Withers and H. Bhadeshia, "Residual stress. Part 1–measurement techniques," *Mater. Sci. Technol.*, vol. 17, no. April, pp. 355–365, 2001.

[2] E. J. Hearn, "Contact stress, residual stress and stress concentrations," in *Mechanics of Materials-2An Introduction to the Mechanics of Elastic and Plasyic Deformation of Solids and Structural Materials*, Third Edit., 1997, pp. 381–442.

[3] N. Bailey, *Weldability of Ferritic Steels*. Cambridge, England: Woodhead Publishing Ltd., 1994.

[4] R. H. Leggatt, "Residual stresses in welded structures," *Int. J. Press. Vessel. Pip.*, vol. 85, no. 3, pp. 144–151, Mar. 2008.

[5] R. D. Stout, "Postweld Heat Treatment of Pressure Vessels," *WRC Bull. 302*, 1985.

[6] F. M. Burdekin, "Local Stress Relief of Circumferential Butt Welds in Cylinders," *Br. Weld. J.*, pp. 483–490, 1963.

[7] R. F. D. Scaramangas, A. and Porter Goff, "Residual stress and deformation in welded pipe joints.," in *Joints in Structural Steelwork, Proc. Int. Conf.*, 1981.

[8] R. F. D. Scaramangas, A.and Porter Goff, "Residual Stresses in cylinder girth butt weld," in *17th Offshore Technology Conference,OTC-5024-MS,* 1985, pp. 25–30.

[9] R. H. Leggatt, "Residual stressesat girth welds in pipes," *Weld. Energy-Related Proj.*, pp. 429–440, 1984.

[10] R. H. Leggatt, "Residual stresses at circumferential welds in pipes.," *Weld. Inst. Res. Bull. 23*, pp. 181–188, 1982.

[11] T. M. HOLDEN, B. M. POWELL, S. R. MACEWEN, and R. B. LAZOR, "Axial Strains at a Girth Weld in a 914 mm Linepipe," in *2nd Int Symposium on Non Destructive Characterisation of Materials*, 1986, p. 625–633.

[12] B. L. Josefson, "Stress redistribution during Annealing of a Multipass Butt-Welded Pipe," *ASME J Press. Vessel Technol.*, vol. 105, pp. 165–170, May 1983.

[13] B. L. Josefson, "Stress redistribution during Local Annealing of a Multipass Butt-Welded Pipe," *ASME J Press. Vessel Technol.*, vol. 108, pp. 125–130, May 1986.

[14] M. Jonsson and B. L. Josefson, "EXPERIMENTALLY DETERMINED TRANSIENT AND RESIDUAL STRESSES IN S BUTT-WELDED PIPE," *J. Strain Anal.*, vol. 23, pp. 25–31, 1988.

[15] M. Josson, B. L. Josefson, and M. Nasstrom, "Experimentally Determined Deformations and Stresses in Narrow-Gap and Single-U Multi-Pass Butt-Welded Pipes," *J. Offshore Mech. Arct. Eng.*, vol. 115, pp. 116–122, 1993.

[16] S. Sarkani, V. Tritchkov, and G. Michaelov, "An efficient approach for computing residual stresses in welded joints," *Finite Elem. Anal. ...*, vol. 35, pp. 247–268, 2000.

[17] E. F. Rybicki, W. D. Schmueser, and R. Stonesifer, "A Finite-Element model for residual stresses and deflections in Girth-Butt welded pipes," *J. Press. Vessel Technol.*, vol. 100, no. 3, pp. 256–262, 1978.

[18] E. F. Rybicki and R. Stonesifer, "Computation of residual stresses due to multipass welds in piping system," *J. Offshore Mech. Arct. Eng.*, vol. 101, no. 2, pp. 149–154, 1979.

[19] B. Brickstad and B. Josefson, “A parametric study of residual stresses in multi-pass butt-welded stainless steel pipes,” *... J. Press. Vessel. Pip.*, vol. 75, 1998.
[20] E. F. Rybicki, E. Merrick, J. Wert, and P. A. McGuire, “The Effect of Pipe Thickness on Residual Stresses due to Girth Welds,” *J. Press. Vessel Technol.*, vol. 104, no. 3, pp. 204–209, 1982.
[21] A. Yaghi, T. H. Hyde, A. A. Becker, W. Sun, and J. A. Williams, “Residual stress simulation in thin and thick-walled stainless steel pipe welds including pipe diameter effects,” *Int. J. Press. Vessel. Pip.*, vol. 83, no. 11–12, pp. 864–874, Nov. 2006.
[22] C. Liu, J. X. Zhang, and C. B. Xue, “Numerical investigation on residual stress distribution and evolution during multipass narrow gap welding of thick-walled stainless steel pipes,” *Fusion Eng. Des.*, vol. 86, no. 4–5, pp. 288–295, Jun. 2011.
[23] B. L. Josefson and C. T. Karlsson, “FE-calculated stresses in a multi-pass butt-welded pipe—A simplified approach,” *Int. J. Press. Vessel. Pip.*, vol. 38, no. 3, pp. 227–243, Jan. 1989.
[24] D. Deng and H. Murakawa, “Prediction of welding residual stress in multi-pass butt-welded modified 9Cr–1Mo steel pipe considering phase transformation effects,” *Comput. Mater. Sci.*, vol. 37, no. 3, pp. 209–219, Sep. 2006.
[25] A. H. Yaghi, T. H. Hyde, A. A. Becker, and W. Sun, “Numerical simulation of P91 pipe welding including the effects of solid-state phase transformation on residual stresses,” *Proc. Inst. Mech. Eng. Part L J. Mater. Des. Appl.*, vol. 221, no. 4, pp. 213–224, Jan. 2007.
[26] A. H. Yaghi, T. H. Hyde, A. A. Becker, and W. Sun, “Finite element simulation of welding and residual stresses in a P91 steel pipe incorporating solid-state phase transformation and post-weld heat treatment,” *J. Strain Anal. Eng. Des.*, vol. 43, no. 5, pp. 275–293, May 2008.
[27] P. Dong, “Residual Stress Analyses of a Multi-Pass Girth Weld: 3-D Special Shell Versus Axisymmetric Models,” *J. Press. Vessel Technol*, vol. 2, no. 123, pp. 207–213, 2000.
[28] P. Dong and F. W. Brust, “Welding residual stresses and effects on fracture in pressure vessel and piping components: a millennium review and beyond,” *J. Press. Vessel Technol.*, vol. 122, no. 3, pp. 329–338, 2000.
[29] D. Stamenković and M. Perić, “Determination of Residual Stresses in Welded Pipes Using a Simplified Heat Source,” *Sci. Tech. Rev.*, vol. 61, no. 1, pp. 12–16, 2011.
[30] J. Mazumder, “Finite Element Analysis of Three-Dimensional Transient Heat Transfer in GMA Welding,” *Weld. J.*, no. July, pp. 150–156, 1988.
[31] C.-H. Lee and K.-H. Chang, “Three-dimensional finite element simulation of residual stresses in circumferential welds of steel pipe including pipe diameter effects,” *Mater. Sci. Eng. A*, vol. 487, no. 1–2, pp. 210–218, Jul. 2008.
[32] C.-H. Lee and K.-H. Chang, “Prediction of residual stresses in high strength carbon steel pipe weld considering solid-state phase transformation effects,” *Comput. Struct.*, vol. 89, no. 1–2, pp. 256–265, Jan. 2011.
[33] N. U. Dar, E. M. Qureshi, and M. M. I. Hammouda, “Analysis of weld-induced residual stresses and distortions in thin-walled cylinders,” *J. Mech. Sci. Technol.*, vol. 23, no. 4, pp. 1118–1131, May 2009.
[34] D. Z. L. Hodgson, C. M. Gill, B. M. E. Pellereau, P. R. Hurrell, and J. Francis,

"Finite Element Modelling of 5- and 8-Pass Ferritic Steel Welds Using Phase Transformation Material Models," *ASME 2011 Press. Vessel. Pip. Conf. Vol. 6, Parts A B*, pp. 1589–1597, 2011.
[35] C. J. Hamelin, V. Luzin, and P. Bendeich, "PVP2011-57426 ACCOUNTING FOR PHASE TRANSFORMATIONS DURING WELDING OF FERRITIC," pp. 1–9, 2011.
[36] N. S. Rossini, M. Dassisti, K. Y. Benyounis, and A. G. Olabi, "Methods of measuring residual stresses in components," *Mater. Des.*, vol. 35, pp. 572–588, Mar. 2012.
[37] N. Kalakoutsky, "The Study of Internal Stresses in Cast Iron and Steel," 1888.
[38] N. Tebedge, G. Alpsten, and L. Tall, "Residual-stress Measurement by the Sectioning Method," *Exp. Mech.*, no. February, pp. 88–96, 1973.
[39] G. Alpsten and L. Tall, "Residual Stresses in Heavy Welded Shapes," *Weld. Res. Suppl.*, no. March, pp. 93–105, Mar. 1970.
[40] M. B. Prime and A. T. Dewald, "The Contour Method," in *Practical Reisudal Stress Measurement Methods*, G. S. Schajer, Ed. John Wiley & Sons, 2013, pp. 109–138.
[41] H. Bueckner, "The propagation of cracks and the energy of elastic deformation," *Trans. Am. Soc. Mech. Eng.*, vol. 50, pp. 1225–1230, 1958.
[42] M. B. Prime, "CROSS-SECTIONAL MAPPING OF RESIDUAL STRESSES BY MEASURING THE SURFACE CONTOUR AFTER A CUT," *J. Eng. Mater. Technol.*, vol. 123, p. pp.162-168, 2001.
[43] M. B. Prime and A. R. Gonzales, "THE CONTOUR METHOD: SIMPLE 2-D MAPPING OF RESIDUAL STRESSES," in *Sixth International Conference on Residual StressesSixth International Conference on Residual Stresses, July 10-12,* 2000, vol. 836, pp. 617–624.
[44] Y. Zhang, S. Ganguly, L. Edwards, and M. E. Fitzpatrick, "Cross-sectional mapping of residual stresses in a VPPA weld using the contour method," *Acta Mater.*, vol. 52, no. 17, pp. 5225–5232, Oct. 2004.
[45] P. Pagliaro, M. B. Prime, H. Swenson, and B. Zuccarello, "Measuring Multiple Residual-Stress Components using the Contour Method and Multiple Cuts," *Exp. Mech.*, vol. 50, no. 2, pp. 187–194, Aug. 2009.
[46] D. W. Brown *et al.*, "Critical comparison of two independent measurements of residual stress in an electron-beam welded uranium cylinder: Neutron diffraction and the contour method," *Acta Mater.*, vol. 59, no. 3, pp. 864–873, Feb. 2011.
[47] M. B. Prime, "Contour Method Advanced applications: Hoop Stresses in Cylinders and Discontinuities," in *Conference Proceeding of Society for Experimental Mechanics Series 999*, 2011, vol. 8, pp. 13–29.
[48] G. S. Schajer, "Relaxation Methods for Measuring Residual Stresses: Techniques and Opportunities," *Exp. Mech.*, vol. 50, no. 8, pp. 1117–1127, Jul. 2010.
[49] H. W. Walton, "Deflection methods to estimate residual stress," in *Handbook of Residual Stress and Deformation of Steel. ASM International*, G. Totten, M. Howes, and T. Inoue, Eds. 2002, pp. 89–98.
[50] W. M. Baldwin, "Residual stresses in metals," in *American Society for Testing and Materials*, 1949, p. 49.
[51] G. G. Stoney, "The Tension of Metallic lFilnms depostted by Electrolysis .," *Proceeding R. Soc. London. Ser. A, Contacting Pap. a Math. Phys. Character*, vol. 82, no. 553, pp. 172–175, 1909.

[52] R. G. Treuting and W. T. Read, “A Mechanical Determination of Biaxial Residual Stress in Sheet Materials,” *J. Appl. Phys.*, vol. 22, no. 2, p. 130, 1951.
[53] K. Mashbuchi, “Measurement of Residual Stresses in Weldments,” in *Analysis of Welded Structures: Residual Stresses, Distortion, and their Consequences*, 1st ed., D. W. Hopkins, Ed. Robert Maxwell, M.C., 1980, pp. 112–147.
[54] M. B. Prime, “Plasticity effects in incremental slitting measurement of residual stresses,” *Eng. Fract. Mech.*, vol. 77, no. 10, pp. 1552–1566, Jul. 2010.
[55] G. S. Schajer, “Hole-Drilling Residual Stress Measurements at 75 : Origins , Advances , Opportunities,” *Exp. Mech.*, vol. 50, pp. 245–253, 2010.
[56] J. Mathar, “Determ ination of Initial Stresses by M easur - ing the D eform ations A round D rilled Holes,” *Trans. ASME*, vol. 56, no. 4, p. pp.249-254, 1934.
[57] W. Soete and R. Vancrombrugge, “An industrial method for the determination of initial stresses,” *Proc SESA*, vol. 8, no. 1, pp. 17–28, 1950.
[58] G. S. Schajer, M. T. Flaman, G. Roy, and J. Lu, “Hole-Drilling and Ring Core Methods,” in *Handbook of measurement of reisdual stresses*, 1996, pp. 5–34.
[59] Vishay Precision Group, “Measurement of residual stresses by the hole drilling strain-gage method-Revision,” *Tech Note Tn-503*, 2010. .
[60] A. G. Olabi and M. S. J. Hashmi, “The effect of post-weld heat-treatment on mechanical-properties and residual-stresses mapping in welded structural steel,” *J. Mater. Process. Technol.*, vol. 55, no. 2, pp. 117–122, Nov. 1995.
[61] A. . Olabi and M. S. Hashmi, “Effects of the stress-relief conditions on a martensite stainless-steel welded component,” *J. Mater. Process. Technol.*, vol. 77, no. 1–3, pp. 216–225, May 1998.
[62] A. Paradowska and J. Price, “Measurement of residual stress distribution in tubular joints considering post weld heat treatment,” *Mater. Forum*, vol. 30, 2006.
[63] G. S. Schajer, “Advances in Hole-Drilling Residual Stress Measurements,” *Exp. Mech.*, vol. 50, no. 2, pp. 159–168, Feb. 2009.
[64] E. Procter and E. M. Beaneys, “THE TREPAN OR RING CORE METHOD , CENTRE-HOLE METHOD , SACH ’ S METHOD , BLIND HOLE METHODS , DEEP HOLE TECHNIQUE,” in *Advances in Surface Treatment: Technology - Application and Effects*, 4th ed., New York: Pergamon Press, 1987, pp. 165–198.
[65] P. Šarga and F. Menda, “Comparison of Ring-Core Method and Hole-drilling Method Used for Determining Residual Stresses,” vol. 1, no. 7, pp. 335–338, 2013.
[66] Gunnert, “Residual Welding Stresses, Method for Measuring Residual Stress and its Application to a Study of Residual Welding Stresses,” 1955.
[67] R. H. Leggatt, D. J. Smith, S. D. Smith, and F. Faure, “Development and experimental validation of the deep hole method for residual stress measurement,” *J. Strain Anal. Eng. Des.*, vol. 31, no. 3, pp. 177–186, May 1996.
[68] H. Kitano, S. Okano, and M. Mochizuki, “A study for high accuracy measurement of residual stress by deep hole drilling technique,” *J. Phys. Conf. Ser.*, vol. 379, p. 012049, Aug. 2012.
[69] A. Mirzaee-Sisan, A. J. Fookes, C. E. Truman, D. J. Smith, T. B. Brown, and

T. A. Dauda, “Residual stress measurement in a repair welded header in the as-welded condition and after advanced post weld treatment,” *Int. J. Press. Vessel. Pip.*, vol. 84, no. 5, pp. 265–273, May 2007.

[70] A. H. Mahmoudi, S. Hossain, C. E. Truman, D. J. Smith, and M. J. Pavier, “A New Procedure to Measure Near Yield Residual Stresses Using the Deep Hole Drilling Technique,” *Exp. Mech.*, vol. 49, no. 4, pp. 595–604, Aug. 2008.

[71] S. Hossain, C. E. Truman, and D. J. Smith, “Finite element validation of the deep hole drilling method for measuring residual stresses,” *Int. J. Press. Vessel. Pip.*, vol. 93–94, pp. 29–41, May 2012.

[72] C. O. Ruud, “A review of selected non-destructive methods for residual stress measurement,” *NDT Int.*, no. February, pp. 15–23, 1982.

[73] N. JH and R. D, “Application of the x-ray method of stress measrement to problems involving residual stress in metals,” in *Proceedings of the Society for Experimental Stress Analysis*, 1944, pp. 81–90.

[74] N. JH and R. D, “Stress measurement by x-ray diffraction,” in *Proceedings of the Society for Experimental Stress Analysis*, 1944, pp. 73–76.

[75] P. S. Prevey, “X-RAY DIFFRACTION RESIDUAL STRESS TECHNIQUES,” in *Metal Handbook*, 1986, pp. 380–392.

[76] P. S. Prevey, “Current applications of X-ray diffraction residual stress measurement,” *Dev. Mater. Charact. Technol. Symp. held Dur. 28th Annu. Tech. Meet. Int. Metallogr. Soc.*, no. 513, pp. 103–110110, 1996.

[77] V. I. Monin, T. Gurova, X. Castello, and S. F. Estefen, “STEEL PLATES BY X-RAY DIFFRACTION METHOD,” *Rev.Adv.Mater.Sci*, vol. 19, pp. 172–175, 2009.

[78] W. U. X. Diffraction, “Residual Stress Characterization of Thick-Plate Weldments Using X-Ray Diffraction,” *Weld. Res. Counc. Bull. 452*, no. March, pp. 87–91, 1993.

[79] A. Sugahara, S. Okano, T. Hashimoto, and M. Mochizuki, “Comparison of weld residual stress measurement results in low alloy welds between X-ray diffraction and stress relief methods,” *J. Phys.*, vol. 379, p. 7, Aug. 2012.

[80] F. A Kandil, J. D. Lord, A T. Fry, and P. V Grant, “A review of residual stress measurement methods - A guide to technical selection,” 2001.

[81] W. Reimers *et al.*, “Evaluation of residual stresses in the bulk of materials by high energy synchrotron diffraction,” *J. Nondestruct. Eval.*, vol. 17, no. 3, pp. 129–140, Sep. 1998.

[82] P. J. Withers and P. J. Webster, “Neutron and Synchrotron X-ray Strain Scanning,” *Strain*, vol. 37, no. 1, pp. 19–33, Feb. 2001.

[83] R. V. Preston, H. R. Shercliff, P. J. Withers, D. J. Hughes, S. D. Smith, and P. J. Webster, “Synchrotron X-ray Measurement and Finite Element Analysis of Residual Strain in TIG Welded Aluminium Alloy 2024,” *Metall. Mater. Trans. A*, 2006.

[84] A. Allen, C. Andreani, M. T. Hutchings, and C. G. Windsor, “Measurement of internal stress within bulk materials using neutron diffraction,” no. October, 1981.

[85] A Stacey, H. J. MacGILLIVARY, G. A Webster, P. J. Webster, and K. R. A Ziebeck, “Measurement of residual stresses by neutron diffraction,” *J. Strain Anal. Eng. Des.*, vol. 20, no. 2, pp. 93–100, Apr. 1985.

[86] G. A. Webster and R. C. Wimpory, “Non-destructive measurement of residual stress by neutron diffraction,” *J. Mater. Process. Technol.*, vol. 117, no. 3, pp. 395–399, Nov. 2001.

[87] T. Lorentzen, “Nondestructive evaluation of residual stresses by neutron diffraction,” *NDT Int.*, vol. 21, no. 6, pp. 385–388, Dec. 1988.
[88] P. J. Withers, “Mapping residual and internal stress in materials by neutron diffraction,” *Comptes Rendus Phys.*, vol. 8, no. 7–8, pp. 806–820, Sep. 2007.
[89] R. D. Haigh *et al.*, “Neutron diffraction residual stress measurements on girth-welded 304 stainless steel pipes with weld metal deposited up to half and full pipe wall thickness,” *Int. J. Press. Vessel. Pip.*, vol. 101, pp. 1–11, Jan. 2013.
[90] T. Neeraj, T. Gnäupel-Herold, H. J. Prask, and R. Ayer, “Residual stresses in girth welds of carbon steel pipes: neutron diffraction analysis,” *Sci. Technol. Weld. Join.*, vol. 16, no. 3, pp. 249–253, Apr. 2011.
[91] M. J. Park, H. N. Yang, D. Y. Jang, J. S. Kim, and T. E. Jin, “Residual stress measurement on welded specimen by neutron diffraction,” *J. Mater. Process. Technol.*, vol. 155–156, pp. 1171–1177, Nov. 2004.
[92] S. V. Pearce and V. M. Linton, “Neutron diffraction measurement of residual stress in high strength, highly restrained, thick section steel welds,” *Phys. B Condens. Matter*, vol. 385–386, pp. 590–593, Nov. 2006.
[93] D. Dini, X. Song, S. Y. Zhang, and A. M. Korsunsky, “Residual strain analysis in polycrystalline aggregates using diffraction measurement and finite element modelling,” *J. Strain Anal. Eng. Des.*, vol. 44, no. 1, pp. 55–70, 2008.
[94] W. Callister and D. Rethwisch, “Materials science and engineering: an introduction,” in *Materials Science and Engineering*, 2007, p. 64.
[95] R. E. Dinnebier and S. J. L. Billinge, *Powder Diffraction - Theory and Practice*. Cambridge: Royal Society of Chemistry, 2008.
[96] P. M. B. Piccoli, T. F. Koetzle, and A. J. Schultz, “SINGLE CRYSTAL NEUTRON DIFFRACTION FOR THE INORGANIC CHEMIST – A PRACTICAL GUIDE,” *Comments Inorg. Chem.*, vol. 28, no. 1–2, pp. 3–38, 2007.
[97] S. W. Peterson and H. A. Levy, “The Use of Single-Crystal Neutron Diffraction Data for Crystal Structure Determination,” *J. Chem. Phys.*, vol. 19, no. 11, pp. 1416–1418, 1951.
[98] C. L. Bull, M. Guthrie, R. J. Nelmes, and J. S. Loveday, “Time-of-flight single-crystal neutron diffraction to 10 GPa and above,” *High Press. Res.*, vol. 29, no. 4, pp. 780–791, 2009.
[99] AWS, “Preheating and Postweld Heating treating,” in *Welding Inspection Handbook*, Third., 2000.
[100] J. E. JONES and Y. LUO, “Welding - Theory and Practice,” in *Materials Processing: Theory and Practices*, vol. 8, L. OLSON, R. DIXON, and A. L. LIBY, Eds. 8: Elsevier, 1990, pp. 293–323.
[101] D. J. Smith and S. J. Garwood, “Influence of postweld heat treatment on the variation of residual stresses in 50 mm thick welded ferritic steel plates,” *Int. J. Press. Vessel. Pip.*, vol. 51, no. 2, pp. 241–256, Jan. 1992.
[102] D N Crofft, *Heat Treatment Of Welded Steel Structures*. 1996.
[103] R. T. Rose, “Stress in Cylindrical Vessels due to Local Heating Stress Relief of Circumferential Welds,” *Br. Weld. J.*, pp. 19–21, 1960.
[104] E. G. Shifrin and M. I. Rich, “Effect of Heat Source Width in Local Heat Treatment of Piping,” *Weld. J.*, vol. 53, no. 12, pp. 792–799, Dec. 1973.
[105] C. Bloch, J. Hill, and D. Connell, “Proper PWHT Can Stop Stress-Induced Corrosion,” *Weld. J.*, vol. 76, no. 5, pp. 31–41, 1997.
[106] S. L. Semiatin and D. E. Stutz, “HEAT TREATMENT METHODS,” in *Induction Heat Treatment of Steel*, 1986, pp. 4–5.

[107] L. V Khomlyak, V. N. Maksimovich, and A. Z. Kuz, “Reduction of Residual Stress in Welded Plates by Local Heat Teatment Using Moving Heat Sources.,” no. i, pp. 89–93, 1990.
[108] C.-J. Rosen, A. Gumenyuk, H. Zhao, and U. Dilthey, “Influence of local heat treatment on residual stresses in electron beam welding,” *Sci. Technol. Weld. Join.*, vol. 12, no. 7, pp. 614–619, Oct. 2007.
[109] D. Tawfik, P. J. Mutton, and W. K. Chiu, “Experimental and numerical investigations: Alleviating tensile residual stresses in flash-butt welds by localised rapid post-weld heat treatment,” *J. Mater. Process. Technol.*, vol. 196, no. 1–3, pp. 279–291, Jan. 2008.
[110] ANSI/AWS D10.10/10.10M, *Recommended Practices for Local Heating of Welds in Piping and Tubing,An American National Standard*. 1999.
[111] P. M. Korol’kov, “Equipment and technology for local heat treatment of welded joint in pipelines,” *Weld. Int.*, vol. 12, no. 10, pp. 818–821, Jan. 1998.
[112] V. V Tsarevskii, “SELECTION OF THE PARAMETERS OF LOCAL HEAT TREATMENT OF CIRCULAR WELDED JOINTS V.,” no. 8, pp. 29–30, 1985.
[113] A. A. Shulyak, A. V. Startsev, E. M. Korovin, and P. M. Korol’kov, “Local heat treatment of large welded pressure vessels by induction heating,” *Weld. Int.*, vol. 25, no. 8, pp. 652–655, Aug. 2011.
[114] R. E. Haimbaugh, *Practical Induction Heat Treating*. 2001.
[115] S. L. Semiatin and D. E. Stutz, “Application of Induction Heat Treatment,” in *Induction Heat Treatment of Steel*, 1986, pp. 189–210.
[116] P. G. Simpson, *Induction Heating-Coil and System Design*. 1960.
[117] S. L. Semiatin and D. E. Stutz, “Other Heat Treatment Processes Using Induction,” in *Induction Heat Treatment of Steel*, 1986, pp. 211–225.
[118] T. Shimizu, K. Enomoto, and S. Sakata, “Residual Stresses in Girth Butt Welded Pipes and Treatments to Modify These Test specimens,” vol. 16, 1984.
[119] R. E. Haimbaugh, “Theory of Heating by Induction,” in *Practical Induction Heat Treating*, 2001, pp. 5–18.
[120] British Electrical Development Association, “ELECTRIC RESISTANCE HEATING,” in *Electric Resistance Heating-Electricity and productivity series; no.5.*, British Electrical Development Association, 1953, pp. 31–50.
[121] J. W. McEnerney and P. Dong, “Recommended Practices For Local Heating Of Welds In Pressure Vessels,” in *Welding Research Council Bulletin 452*, 2000, p. 64.
[122] B. Chen *et al.*, “In situ neutron diffraction measurement of residual stress relaxation in a welded steel pipe during heat treatment,” *Mater. Sci. Eng. A*, vol. 590, pp. 374–383, Jan. 2014.
[123] S. Paddea, J. A. Francis, A. M. Paradowska, P. J. Bouchard, and I. A. Shibli, “Residual stress distributions in a P91 steel-pipe girth weld before and after post weld heat treatment,” *Mater. Sci. Eng. A*, vol. 534, pp. 663–672, Feb. 2012.

3 Experimental – sample preparation and testing

3.1 Introduction

This chapter introduces the experimental procedures of sample preparations and the general mechanical testing for material characterization. In section 3.2 the welding process of the pipe girth welds is described. Details of the material data, welding parameters as well as the measurements of the transient temperate and strains by thermocouples and strain gauges are included in this section. All experimental data will be used to compare with the predicted welding thermal cycle and residual stresses using the Finite Element Analysis (FEA) which will be reported in Chapter 7 and points the importance of the obtained results for the follow-up study. Section 3.3 demonstrates the post weld heat treatment procedures which were carried out on the welded pipes and the reference samples as the state of the residual stress in a pipe spool will be evaluated using a strain-free reference sample which experienced same thermal treatment. Section 3.4 presents the conventional tensile tests and hardness tests conducted to gain more information regarding the material properties. Finally, a brief discussion is given in section 3.5, which concludes the experimental achievements Girth welds fabrication

3.1.1 Overview

A numbers of pipe girth weld spools were fabricated in UK by an industrial member of TWI, four of them were used for subsequent residual stress measurement and post weld heat treatment for stress relief. During the welding process, transient temperature and strains were recorded on two pipe spools by pre-attached thermocouples and strain gauges. Data collection was fulfilled with the acquisition system produced by TWI.

3.1.2 Material selection

The parent material of the pipe spool is APL 5L X65 pipeline steel. Chemical compositions of the parent and filler metal are listed in Table 3-1. The specifications of the pipes used in this study are: 750mm long with an outer diameter D in 355.6mm (14 inch.) and a wall thickness t in 19.05mm (3/4 inch.). As the dimension ratio D/t of the pipe is 18, it is regarded as thick-wall pipe.

Table 3-1 Chemical composition of the parent and filler metals

material	Composition (wt%)							
	C	Mn	Si	Ni	Cr	Mo	V	Cu
Parent metal	0.1	1.13	0.25	0.11	0.14	0.1	0.06	0.16
Filler metal	0.07	1.55	0.68	0.92	0.03	0.004	0.008	0.08

3.1.3 Welding process

1.1.1.1 Narrow-gap grove geometry

Welding of the pipe spools was carried out in accordance with a conventional industrial manufacturing specification. The fabricated final pipe spool was 1500mm long with a multi-pass narrow-gap girth weld in the middle. Figure 3.1 exhibits the geometry of the weld groove and is the schematic representation of the welding procedure. The small angled J-bevel groove geometry and a slight bevel offset created a narrow-gap weld profile. Six passes of the filler metal were deposited.

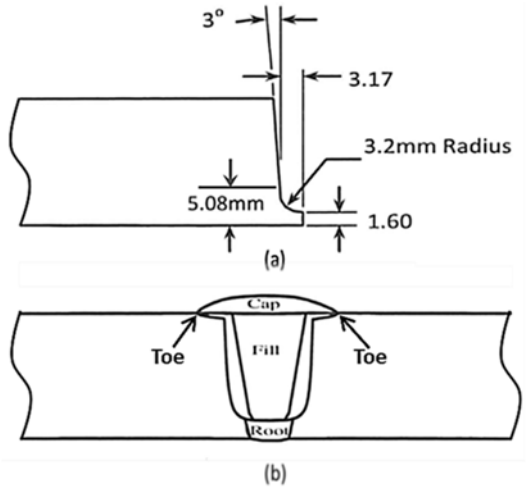

Figure 3.1 (a) Geometrical details of the weld groove and (b) Schematic representation of the welding procedure

Before welding, a pipe piece was initially bullet tacked to an anchor pipe to fix pipe end. The second pipe piece was skin tacked with the first one at four locations based on the welding specification (2, 4, 7 and 11 o'clock circumferential locations). Each tack was approximately 25mm long.

1.1.1.2 Preheating

The weld groove and adjacent parent metal (150mm on each side) were preheated by induction heating (figure 3.2). Pipe spools 1 and 2 (to be denoted as "P1" and "P2" respectively) were preheated on only one side of the weld groove and the adjacent

parent metal, because a numbers of strain gauges and thermocouples for monitoring were attached on the other side. Pipe spools 3 and 4 (denoted as “P3” and “P4”) were preheated on both sides. A probe was inserting underneath the induction heating cable for the measurement of the pipe surface temperature. Preheat temperature was in the range 80-90°C. Preheating is intended to avoid hydrogen cracking. The effect (if any) of preheating [1], [2] on welding residual stress was also part of the investigation in the study.

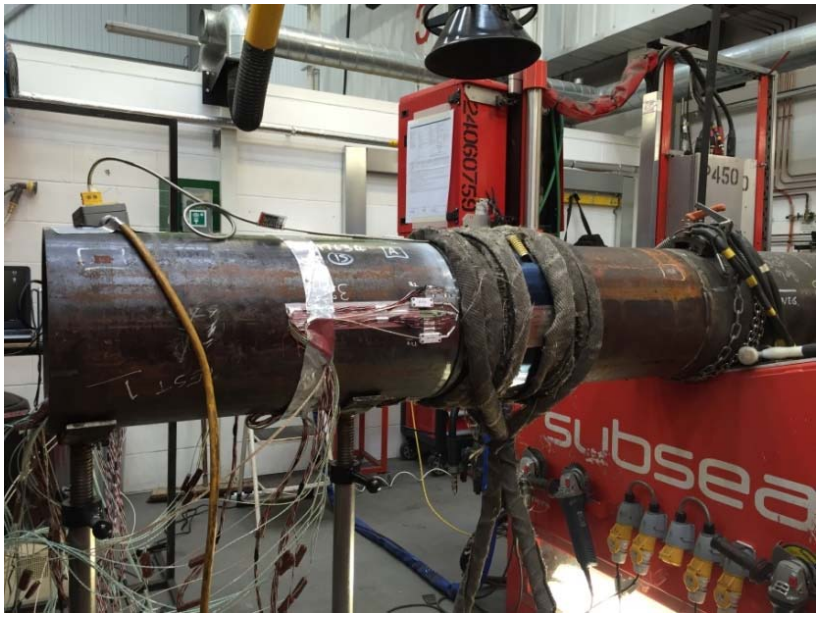

Figure 3.2 Induction preheating conducts on one side of the groove on the pipe that attached with thermocouples and strain gauges

1.1.1.3 Welding procedure

During welding, the pipe sections were fixed horizontally, and no clamping was employed. Two mechanically and electrically controlled welding torches were used, and welds were laid simultaneously on both sides. Each of them was deposited a weld along the pipe circumference 180 degree from the 12 o’clock (weld start) to the 6 o’clock (weld stop) position. The weld contains a root pass, a hot pass, three fills and the cap. The root pass was completed by using cold metal transfer (CMT) technique and the rest of the passes were fabricated by pulsed gas metal arc welding (PGMAW) process.

CMT is a modified GMAW process that uses a new method of droplet detachment based on short circuit welding [3]. It is generally performed on sheet material. Due to the root face being only 1.6mm thick, CTM was used for the benefits of low thermal

input and stable arc. PGMAW is subsequently conducted for the other passes. With precise control of arc dynamics, it was able to be run as a high deposition rate, fast-fill process. Due to the pulsing behaviour, during which the current is periodically modulated between a relatively low base current and high peak current, globular transfer will happen when the mean current level falls within a certain range while axial spray transfer of smaller droplets will happen the peak current level far exceeds the transition value. Advantages of this welding process include: better arc characteristics, greatly reduced spatter and fume generation, less incomplete fusion and lower heat input. In industrial production, low heat input applied in the multi-pass narrow-gap weld is able to create smaller heat affected zone and introduce lower levels of residual stresses [4].

Between each pass, a short period of time was allowed for air cooling. Inter-pass temperature was recorded, and it was observed that the inter-pass temperature was in the range of 80-160°C. Table 3-2 lists the welding parameters for the pipe spools fabricated.

Table 3-2 Welding parameters for X65 pipes

Parameters	Root	Hot pass/fill	Cap
Shielding gas composition	50%Ar / 50%CO2		
Flow rate (l/min)	28	28	28
Filler wire diameter(mm)	1.0	1.0	1.0
Voltage (V)	14-15	21-22	21-22
Current (A)	210-230	150-220	120-130
polarity	DC+	DC+	DC+
Travel speed (mm/s)	5.8-6.2	4.8-7	3.1-4.5
Heat input (kJ/mm)	0.5-0.55	0.6-0.9	0.6-0.9

3.1.4 Temperature and strain recording

3.1.4.1 Apparent thermal strain calibration

Because of the difference in the thermal-expansion coefficient of the test material, gauge backing and foil alloy, and changes in the electrical propertied of the gauge alloy which occur with a change in temperature, apparent thermal strains are produced during welding process [5]. However, it is difficult to develop a gauge alloy with the same expansion coefficient as of the test material to eliminate apparent thermal strains. Therefore, “self-temperature-compensated” strain gauges, whose

expansion coefficient and electrical properties have been developed to match the test material over a specified temperature range, were used in this study.

In order to identify the mechanical strains from the overall measured strains, apparent thermal strains were characterised beforehand. A strain gauge (SG) and a thermocouple (TC) were attached on an instrumented dummy pipe metal to record the strain output at corresponding temperatures [6], [7]. The measurement was made while the dummy metal was placed in an enclosed furnace and heated up to 260°C and cooled back to room temperature.

Welding thermal cycle was recorded by NI-SCXI-1102 32-channel input modules. All the modules were installed on a chassis. A USB Data Acquisition and Control Module were connected as well to achieve data logging at 600 times per second. The applied software was a production of TWI which recorded the binary data in ASCII file. All data were converted to decimal for further analyses.

3.1.4.2 Thermocouple and strain gauge installation on the pipe

In order to measure the transient change of temperature and strains during the welding process, high temperature thermocouples and strain gauges were installed onto the inner and outer surfaces of the pipes at 3 o'clock location in terms of the 5G welding position (horizontal fixed).

Figure 3.3 is an example showing the layout of the thermocouples and strain gauges on the outer surface of one pipe at 3 o'clock location. Thermocouples were attached along the line and the uniaxial strain gauges were attached correspondingly for the measurement of the transient surface strains in axial and hoop directions.

There were in total 7 thermocouples installed from the edge of the weld groove. They are respectively 3mm, 5mm, 10mm, 15mm, 25mm, 35mm, and 55mm away from the groove edge. Two types of the high temperature thermocouples were applied in the experiment.

As shown in Figure 3.3, TC1 and TC2 are the R-type thermocouples. They are composed by platinum wire (99.99% purity) and Platinum/Rhodium wires (Pt87/Rh13) and is able to work at temperature up to 1500°C. Joined by Nickel-

Chromium/Nickel-Aluminium wires, the rest of the thermocouples are K-type and can survive up to 1260°C.

Eight weldable AW-6-350-11-01LT strain gauges (SG) were attached close to the K-type thermocouples for the measurement of the transient strains at corresponding temperature-measurement locations. Because this type of strain gauge was specified to be able to work under 300°C, they were attached not too close to the weld, starting from the point 15mm away from the groove edge. For instance, starts at CT4 location, SG1 was used to measure the transit axial strain and SG5 was for the transient hoop strain.

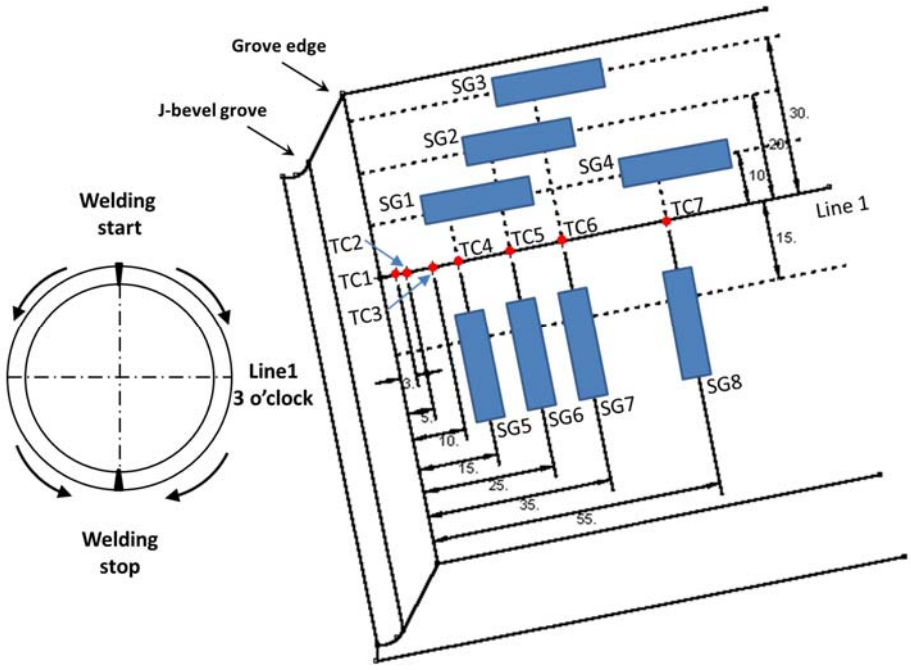

Figure 3.3 The layout of the thermocouples and strain gauges on pipe outer surface

Two pipe pieces were prepared with thermocouples and strain gauges for two different girth welds. They were joined respectively to create pipe spools P1 and P2 as mentioned before.

3.1.5 Data process and discussion

3.1.5.1 Apparent thermal strain

Two K-type thermocouples K1 and K2 were welded on a dummy metal for calibration of the apparent thermal strain. Thermal history was recorded by the thermocouples when the meatal was heated in an enclosed furnace from room

temperature up to 260 °C and in cooling back. K1 and K2 display almost identical temperature results in Figure 3.4, proving the measurement stability of the thermocouples.

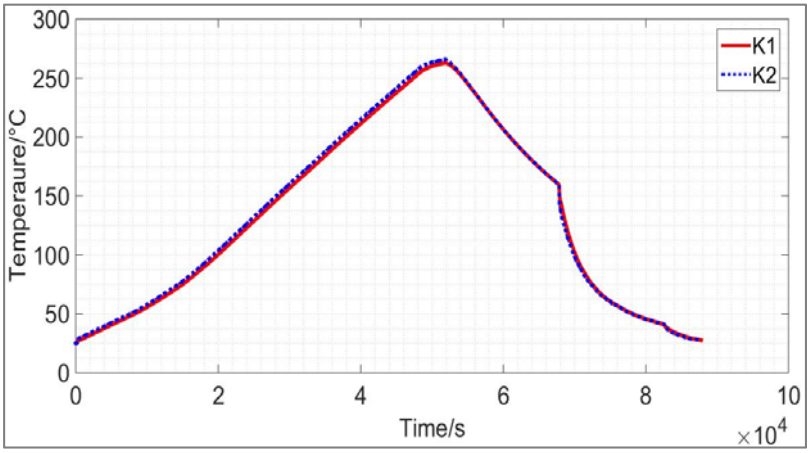

Figure 3.4 Recorded temperature from K-type thermocouples when heating up and cooling down in the furnace for calibration

Strain gauge generated temperature-strain output (apparent thermal strain) is shown in Figure 3.5. It is noticed that although values of apparent thermal strains were higher during cooling than that of heating process, the levels were maintained in the small range of ±100μm. This is the advantage of the self-compensate strain gauge.

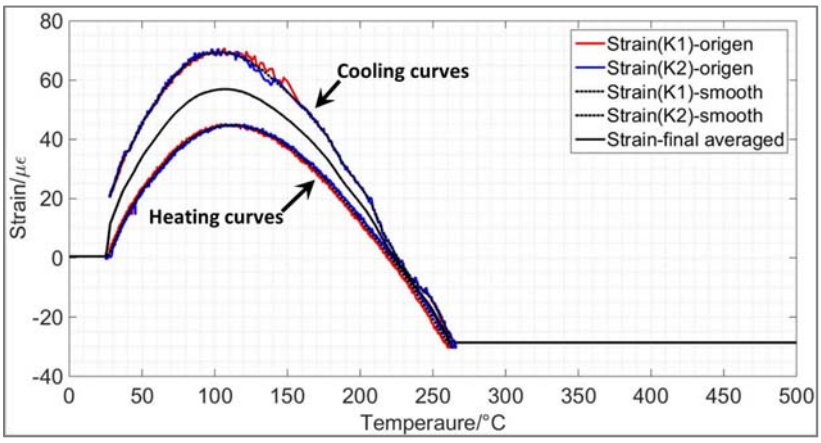

Figure 3.5 Calibrated apparent thermal strains from K-type thermocouple and strain gauge

Because the differences of the strain values between the heating and cooling process were not significant, averaged values (Figure 3.5) of the two stages were used as the effective apparent thermal strains. They were thereafter deducted from measured welding transient strains to obtain transient mechanical strains.

3.1.5.2 Transient temperature

Transient temperatures at measurement points were obtained on both outer and inner surfaces of the pipes. On the outer surface of P1 and P2 (Figure 3.6), thermal cycles and temperature magnitudes at the measurement locations were quite similar for both pipes. Only the temperature information was missing for the last pass. This is because the deposition of the weld caps destroyed the R-type thermocouples which were located too close to the weld grove edge.

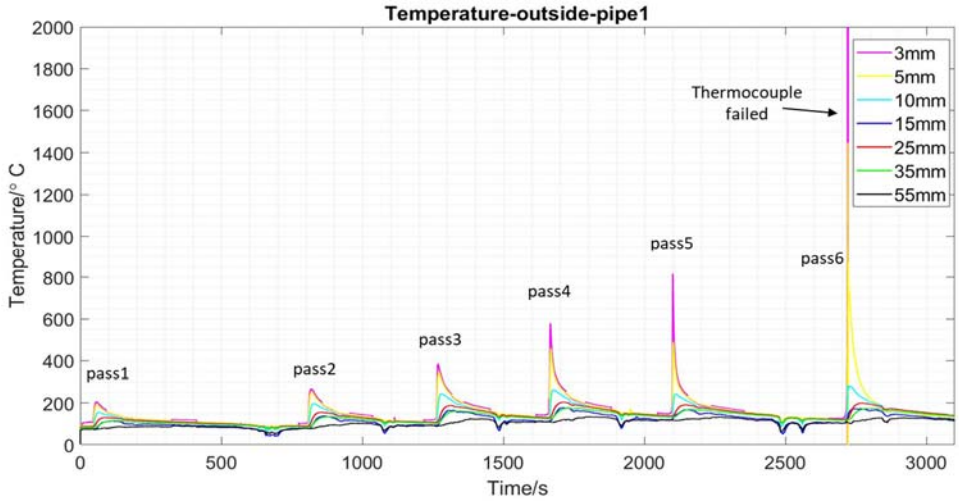

(a)

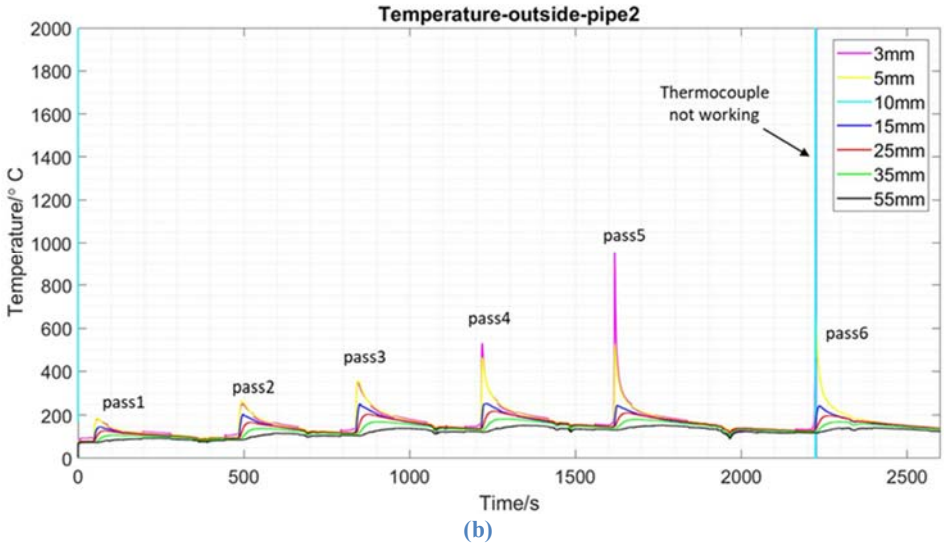

(b)

Figure 3.6 Measurement of the temperature history at 3 o'clock location on the outer surface of (a) P1 and (b) P2

For the pipe inner surface (Figure 3.7), temperature recordings from R-type thermocouples on P2 (3mm and 5mm away from grove edge) were much lower than that of P1. There was a high chance that the thermocouples were either not well

bonded by spot welding initially or unattached when plugged them to the data logger.

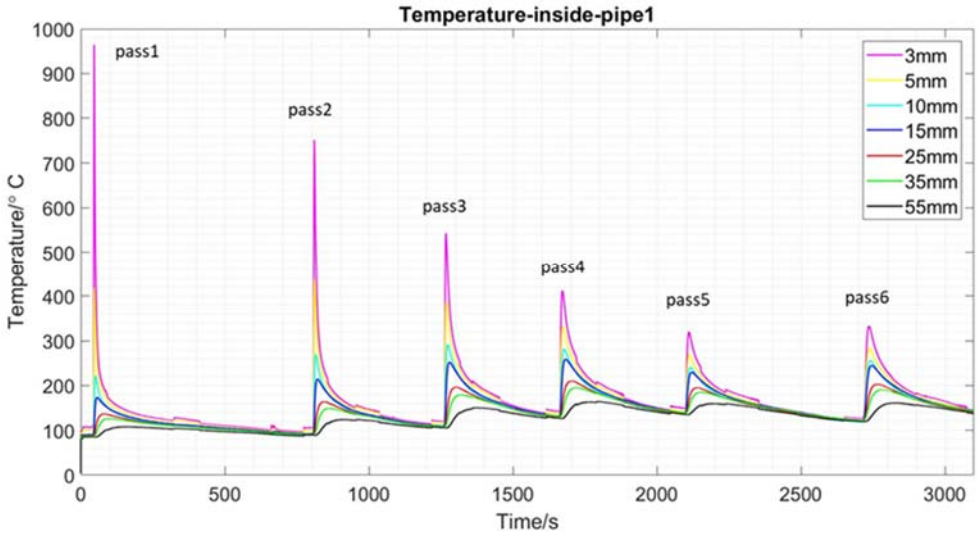

(a)

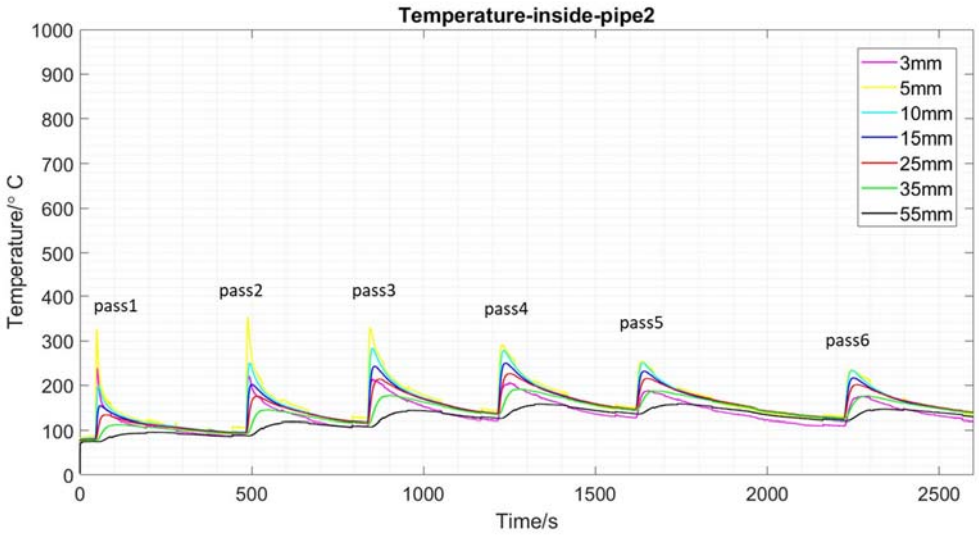

(b)

Figure 3.7 Measurement of the temperature history at 3 o'clock location on the inner surface of (a) P1 and (b) P2

3.1.5.3 Transient strains

Original experimental transient strains were measured near K-type thermocouples in both axial and hoop directions. At these locations the peak temperature was all below 260°C - in the specified temperature measurement range of the strain gauges. The finalized mechanical strain profiles, shown in Figure 3.8, Figure 3.9, Figure 3.10 and Figure 3.11, were obtained by subtracting the apparent thermal strains from the time-compensated experimental strains.

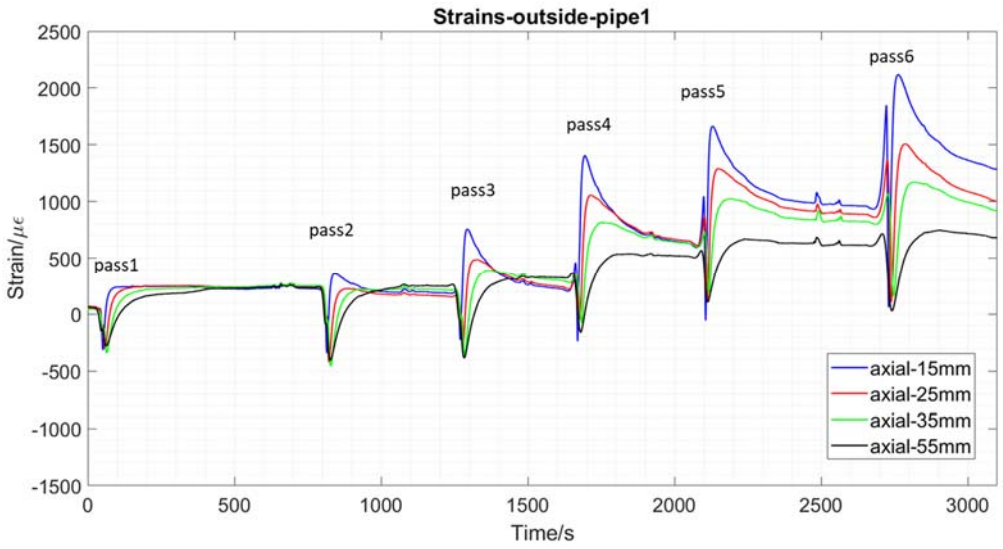

(a)

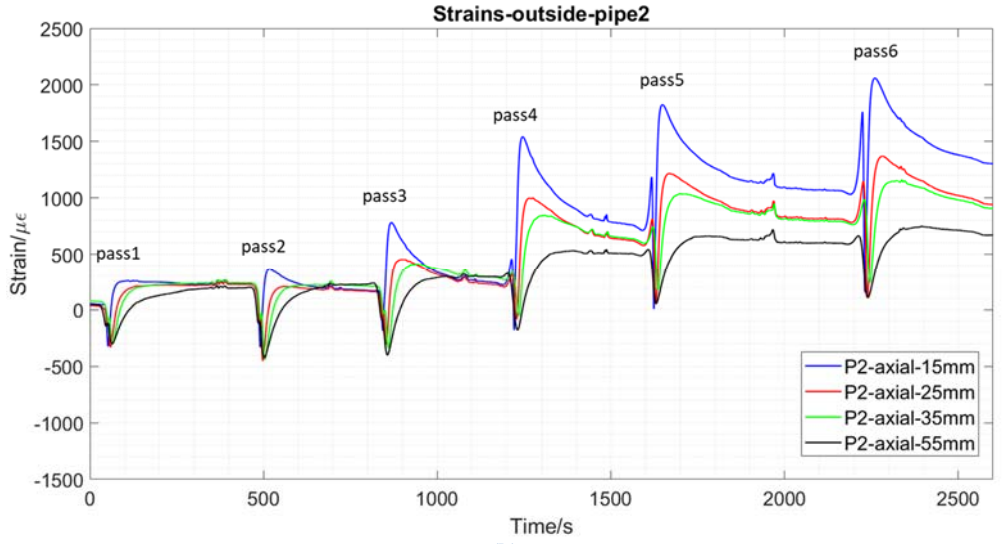

(b)

Figure 3.8 Transient axial strains at 3 o'clock positions of the outer surface of (a) P1 and (b) P2

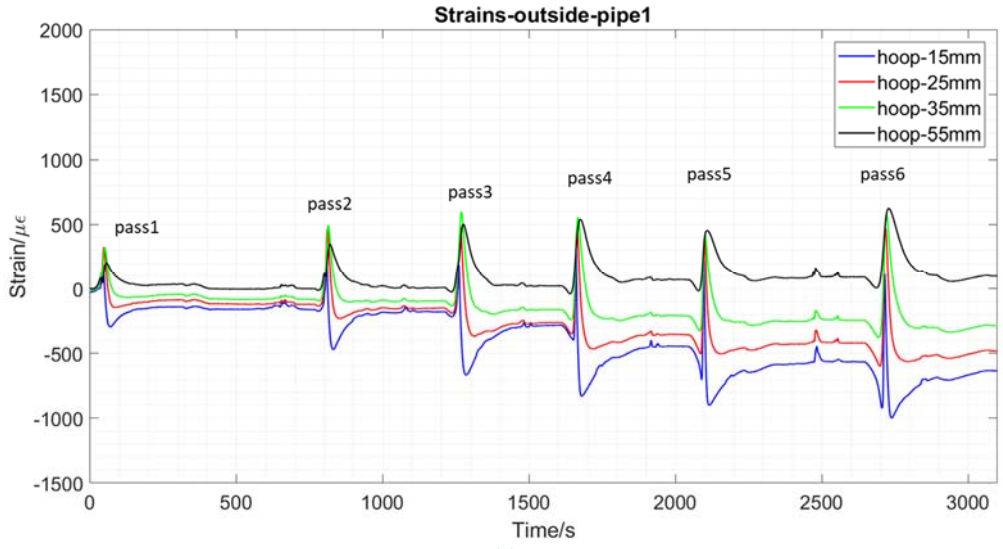

(a)

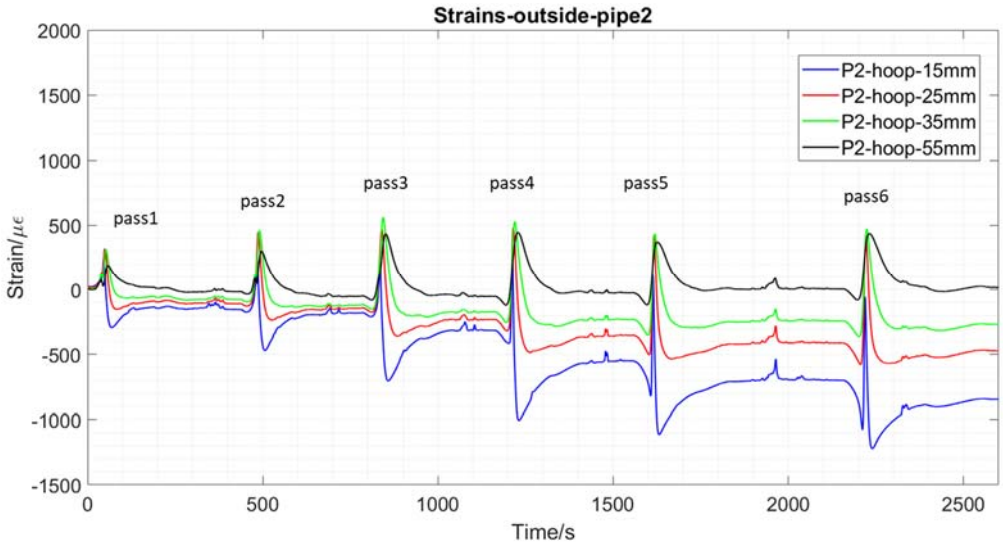

(b)

Figure 3.9 Transient hoop strains at 3 o'clock positions of the outer surface of (a) P1 and (b) P2

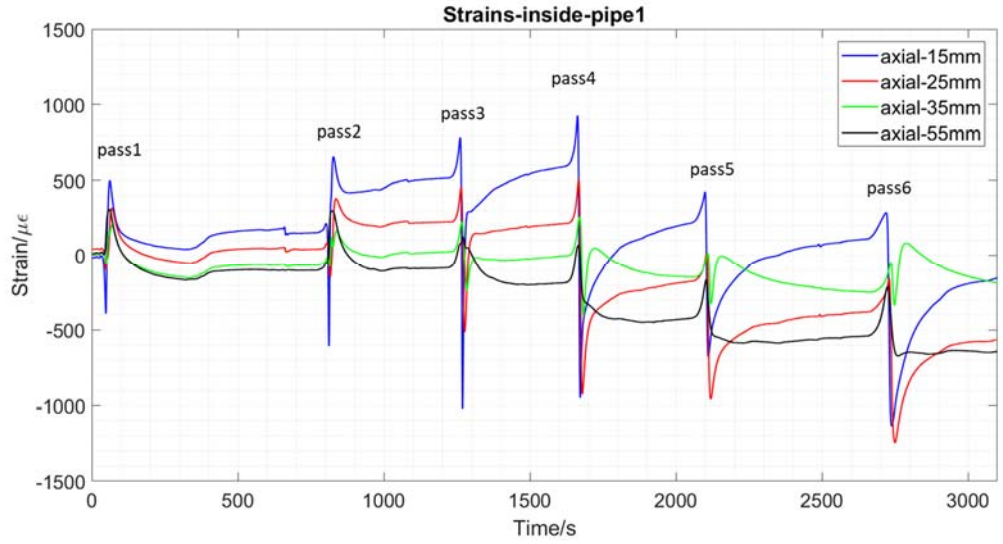

(a)

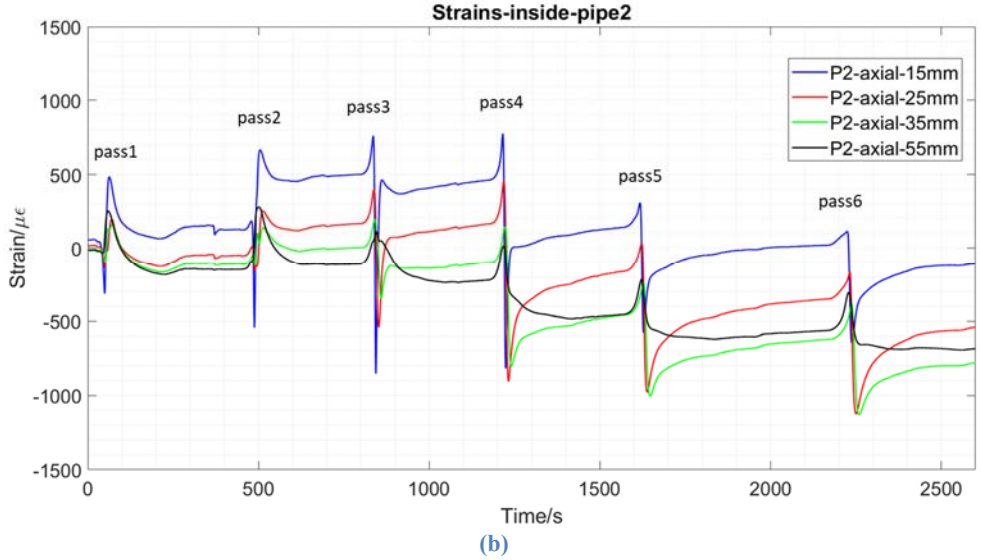

(b)

Figure 3.10 Transient axial strains at 3 o'clock positions of the inner surface of (a) P1 and (b) P2

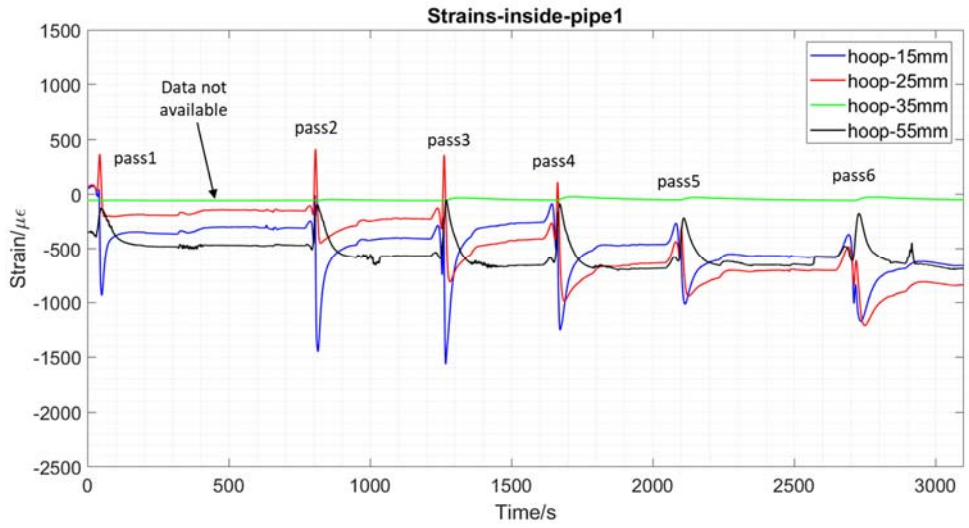

(a)

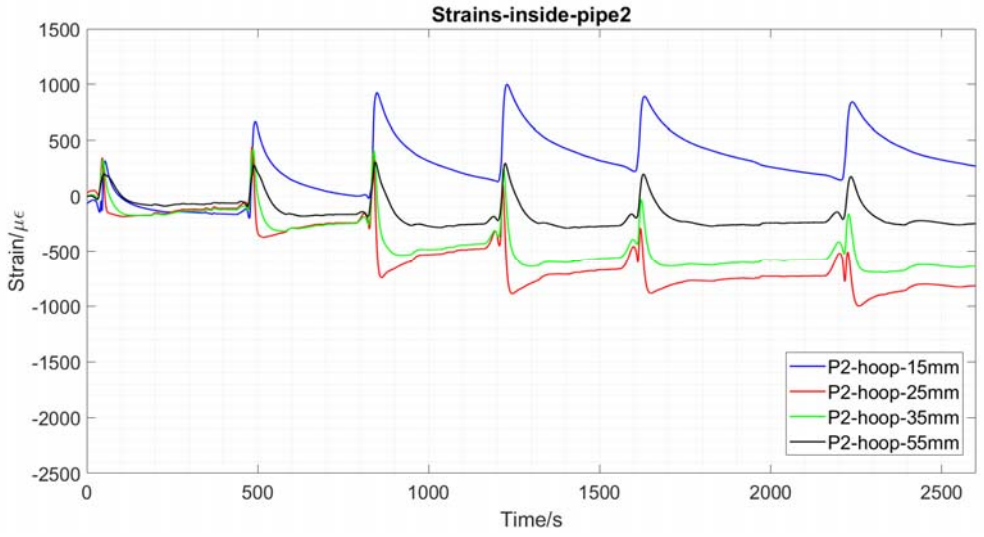

(b)

Figure 3.11 Transient hoop strains at 3 o'clock positions of the inner surface of (a) P1 and (b) P2

Shown in Figure 3.8 and Figure 3.9 are the axial and hoop strain profiles on the outer surface of P1 and P2, respectively. Two pipes display similar strain magnitudes at corresponding location for six passes. Figure 3.10 and Figure 3.11 show the final strain profiles on pipe inside surface. Similar to the temperature plots, strain gauges at the 3 o'clock position recorded 6 peaks representing the transient strains during the process of the welding procedure.

On the pipe outside surface, tensile axial residual strains and compressive hoop residual strains were accumulated pass by pass. The magnitude of both strains decreased with the increase of the distance from the weld groove edge along the pipe

length. Measurement points at 55mm from the grove edge were nearly strain-free in hoop direction.

In comparison, the change of strains after each pass was less regular on the pipe inside surface. It is noticed that at individual locations, especially at 25mm points from the grove edge, the axial strain changed after third pass from tensile to compressive. However, hoop strains were constantly compressive at all the measurement locations. It is clear that the nearer the location measured to the weld the higher the compressive hoop strain values. Oppositely, axial strains were lower magnitudes but preliminary compressive.

It is worthy to note that at the 15mm position of P2 (Figure 3.11b), hoop strains plots was not correct because transient tensile strains were displayed during the entire welding process. Due to the moving heat source, large thermal expansion occurred on the parent metals nearby. Hence the parent metals in front of and outside the heated area was subjected to compression. Because of this effect, strain gauges recorded compressive hoop strains before the heating source passed the circumferential measurement locations at which large tensile strains were captured. Once the cooling started, hoop strains dropped and altered to become compressive due to the weld metal shrinkage [8].

3.2 Post weld heat treatment

3.2.1 Heating methods

In order to investigate the stress states inside the narrow-gap girth welds and evaluate the effectiveness of the PWHT on stress relief, non-destructive neutron diffraction technique was carried out on the pipes in as-welded condition and after PWHT. After the welded pipes were measured for residual stress, they were sent to an external laboratory for PWHT for stress relief, then measured again for remaining residual stresses. Details regarding the application of the neutron diffraction technique in this study will be introduced in Chapters 4 to 6.

For post weld heat treatment, P1 was heated globally in an enclosed furnace while the other three pipes were heated treated locally. Local PWHT conducted on pipes P2, P3 and P4 was achieved by the electric resistance heating method, for which Flexible Ceramic Pad (FCP) heaters were applied. FCP heater consists of high grade

nickel-chromium flexible core wires and alumina ceramic beads. Ceramic fibre blankets, were applied on pipe outer surfaces and inserted into the pipe two ends as insulation to reduce the heat loss during heating.

The dimension of the FCP and the insulation blanket determine the widths of the heated band and the gradient control band (GCB) respectively, which should provide minimum values that required in the recommended practice for local PWHT. A general sketch of the local circumferential PWHT parameters as well as their terminologies is shown in Figure 3.12.

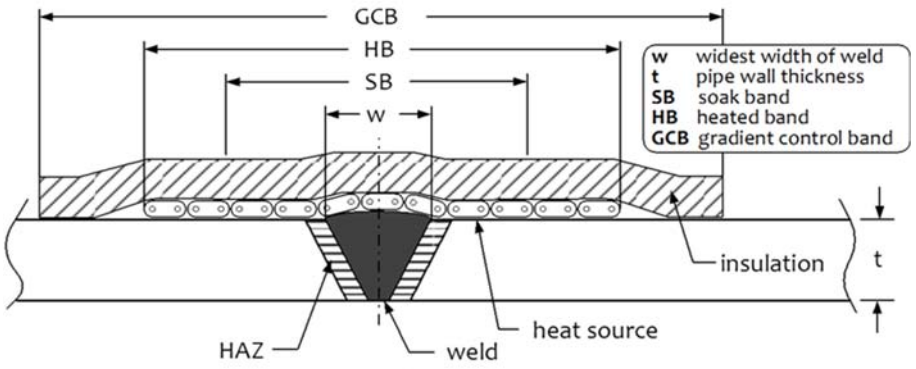

Figure 3.12 Sketch of the local circumferential PWHT with standard terminologies [9]

3.2.2 Heating parameters

For fabricated girth welds, standard widths of the SB, the HB and the GCB were calculated, following recommendations in AWS 10.10 [9] and applied on P2, listing in Table 3-3. The values of HB and GCB are listed in Table 3-4. In practical operations, the standard width of HB was 280mm for P2 and 500mm for GCB (Table 3-4). With regard to P3 and P4, varied widths of the HB with GCB remaining the same were applied respectively.

It is known that a too fast rate of a heating and cooling may affect the structure integrity by introducing additional residual stresses [10]. For instance, fast heating increases the temperature difference between outer and inner surfaces. Owing to the external heating source, hoop stresses variations are generated with the existence of the through-thickness temperature gradient. The heated outer layer is restrained by the cooler core inside, leading to a change through the pipe thickness from compressive stresses on the outer layer to tensile stresses on the inner layer.

Table 3-3 Calculated widths of SB, HB and GCB based on various practices

Standards	Soak band (SB)	Heated band (HB)	Gradient control band (GCB)
BS EN 13445	W + 2HAZs <20mm	$5\sqrt{Rt}$ =275mm	$10\sqrt{Rt}$ =550mm
PD 5500	W + 2HAZs <20mm	$5\sqrt{Rt}$ =275mm	$10\sqrt{Rt}$ = 550mm
BS 2633	-	$W + 5\sqrt{Rt}$ = 294mm	-
ASME III	W + min[100mm,2t] =55mm	Temperature is gradually diminished to avoid harmful thermal gradient	-
ASME VIII	W + min[100mm,2t] =55mm	Temperature is gradually diminished to avoid harmful thermal gradient	-
ASME B31.1	$3t_{max}$ = 57mm	-	-
ASME B31.3	$3t_{max}$ =57mm	-	-
AWS D10.10	W + min[100mm,2t] =55mm	Maximum [HB1, HB2, SB+50mm] HB1 =SB + $4\sqrt{Rt}$ =275mm HB2 = Hi[$\frac{OD^2-ID^2}{2}$ + (ID)(SB)]/OD =256mm (H_i=3) 105mm	HB + $4\sqrt{Rt}$= 495mm or 476mm or 325mm

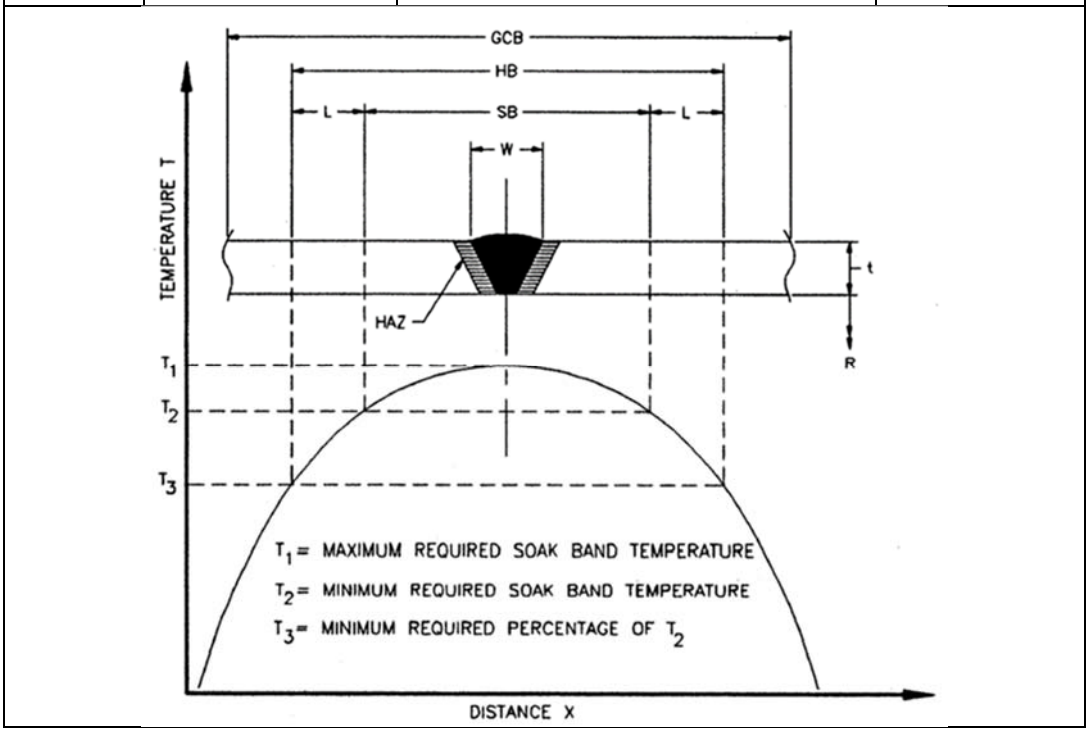

Table 3-4 Furnace and local post weld heat treatment parameters applied for all the pipes

PWHT parameters	P1	P2	P3	P4
Method	Furnace	Local	Local	Local
HB	1000mm	280mm	170mm	430mm
GCB	no	500mm	500mm	500mm
Heating rate	Maximum 200°C/h over 200 °C			
Soaking temperature	620°C			
Soaking time	1hour			
Cooling rate	Maximum 220°C/h			

Fast cooling is over more problematic. If stresses induced from heating are likely to relax during holding, those induced from cooling tend to remain. Values of the heating and cooling rates, soaking temperatures and durations were selected based on a comparison of the recommendations given in various fabrication codes which were made in the literature review and are shown in Table 3-4.

3.2.3 Measurement of the temperature

For measuring temperature during PWHT, K-type thermocouples were installed at various locations on the outer surface of the pipe, as shown in Figure 3.13, at the edge of SB and HB bands. The control thermocouples were placed on the centreline of the weld, aimed at assuring appropriate heat supplied to the weld, and achieving but not exceeding the temperatures required.

The use of the monitoring thermocouples assists to achieve the specified parameters for local heating. For instance, monitoring thermocouples at the edge of the SB band verifies whether the minimum temperature haven been reached throughout the SB band. Similarly, at the edge of the HB band, the maximum allowed temperature drop was check not to exceed.

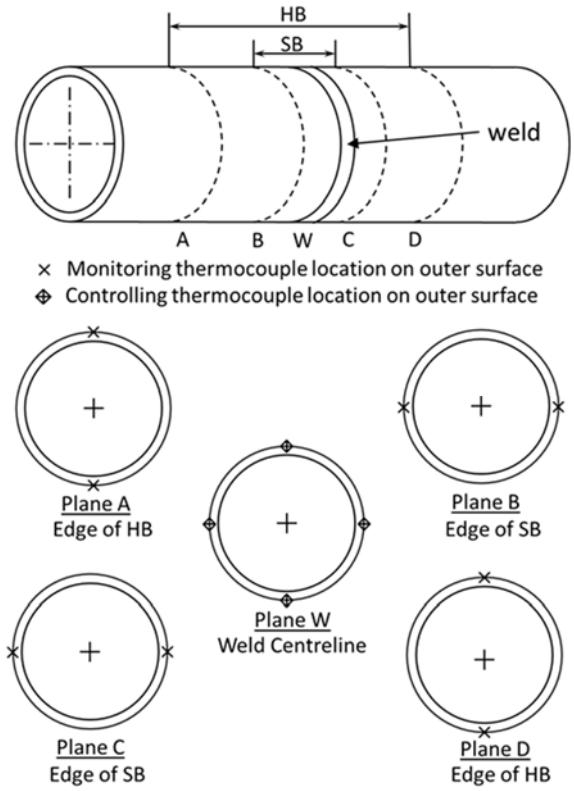

Figure 3.13 The locations of the control and monitoring thermocouples on the pipe with four control zones

3.2.4 PWHT on d_0 samples

It is essential to obtain the correct value of the strain-free lattice spacing d_0 in the reference sample [11] for calculating the residual stresses in the pipes. Details are explained in Chapter5. Six reference samples were prepared in this study (Figure 3.14). They were extracted at the 3 o'clock location from another pipe spool which was fabricated using the same welding parameters. Electro discharge machining (EDM) was employed to obtain the grid-like samples d_{01} and d_{02}. The lattice spacing at specific locations in the samples was measured by neutron diffraction in both as-welded and after PWHT conditions.

For the PWHT carried out on d_0 samples (Table 3-5), d_{01} was cut into small cuboid samples and heat treated individually in a furnace. The parameters of the thermal cycle were the same as those applied to the P2. Rest of the samples were heated together with the pipes to minimize potential errors. The determination of residual stresses was further discussed in chapter 6.

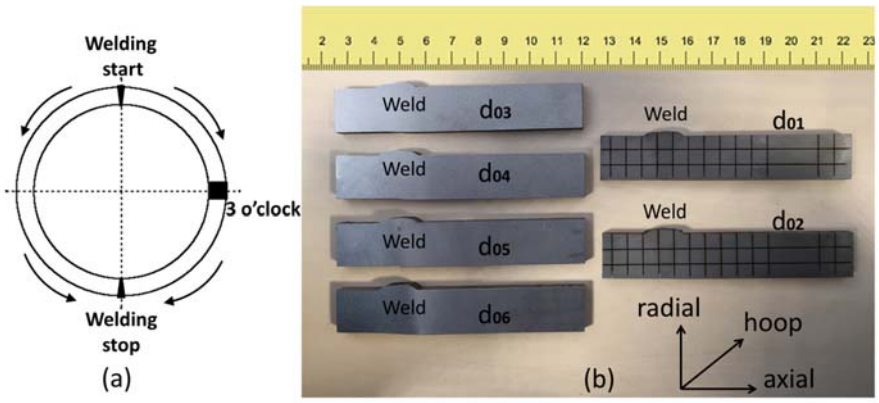

Figure 3.14 The preparation of the different types of the d0 samples (a) Extraction location on the pipe weld spool, (b) d_0 samples dimensions

Table 3-5 List of the PWHT carried out on d_0 samples

Reference sample	Type	PWHT methods		Accompanying pipe
d_{01}	"Grid"cut by EDM	Furnace		Not with pipe (individual cubes)
d_{02}		Local PWHT	(HB 280mm)	P2
d_{03}	Flat piece from weld cross-section	Furnace	(HB 1000mm)	P1
d_{04}		Local PWHT	(HB 280mm)	P2
d_{05}			(HB 170mm)	P3
d_{06}			(HB 430mm)	P4

3.2.5 Thermal history of the pipes

PWHT thermal cycles measured at weld zone of all the pipes are shown in Figure 3.15. The heating and the cooling rates for each pipe were controlled properly not to exceed the proposed temperature values. With sufficient widths of the heated band, pipe P1, P2 and P4 were heated successfully at the targeting soaking temperature for 1 hour.

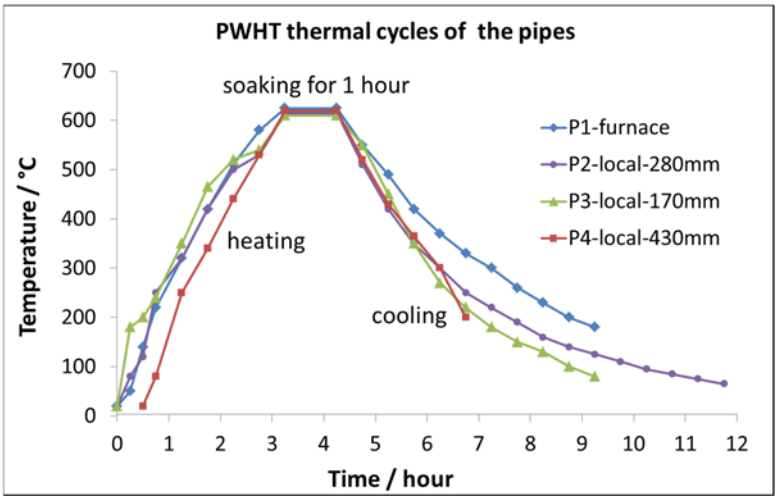

Figure 3.15 PWHT thermal cycles of the pipes

By contrast, the soaking temperature for P3 was slightly below 620 °C from the thermal profile recorded. Moreover, the heaters burned out three times when the temperature reached 450 °, 520 ° and 570 °C during the heating of P3 and they were replaced immediately after the first two times. The burn out is thought to be caused by the generation of the localized overheat, which can be avoid by using an ammeter for the monitoring of the electric current.

3.3 Material characterization

3.3.1 Tensile test

Tensile properties of both parent and weld material were obtained from tests carried out on the specimens extracted from one of the girth welded pipe spools. All weld metal specimens were extracted along the girth weld in the hoop direction. Parent metal samples were extracted parallel to the pipe axis. All tests were conducted according to British Standard BS EN ISO 6892 at ambient temperature, and the results are presented in Figure 3.16 and Table 3-6.

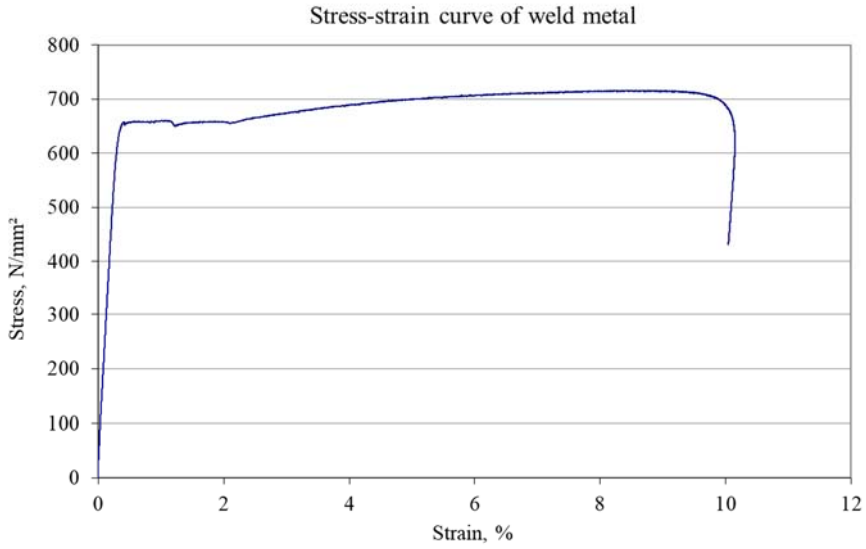

(a)

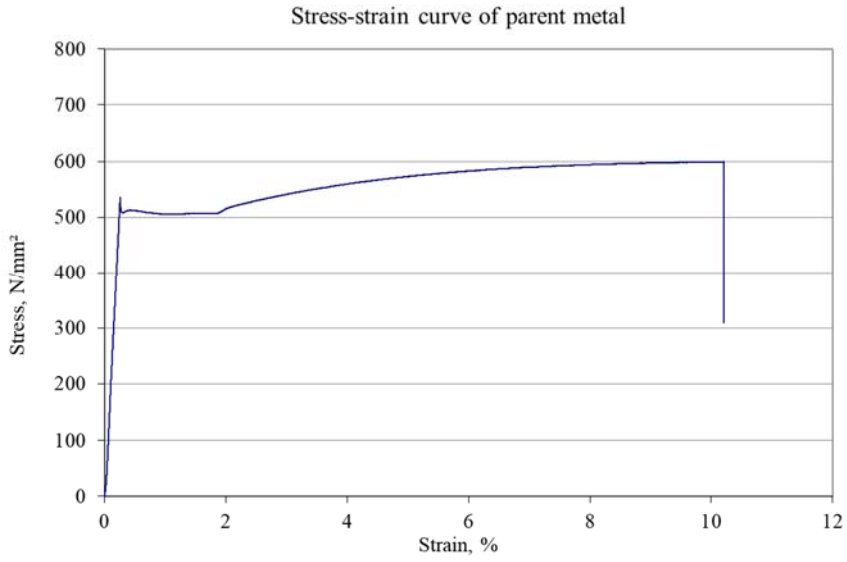

(b)

Figure 3.16 Material tensile properties of (a) weld metal and (b) parent metal

Table 3-6 Typical tensile properties of the parent and weld metals

Mechanical properties	Yield strength (MPa) 0.2% proof stress	UTS (MPa)	Elongation (%)	Reduction area (%)
Parent metal	510	600	27	79
Weld metal	657	719	19	71

3.3.2 Vickers hardness test

Vickers hardness testing, in as-welded condition, was conducted on a sample which has the identical geometry as the flat d_0 samples. Measurements were carried out in the axial direction, preliminarily 2mm from the top (represented pipe outer surface) and bottom (represented pipe inner surface) edges of the parent metal as well as at

the mid-thickness of the sample (Figure 3.17). It was suggested that in previous research that the hardness variation in the welded component may indicate the distribution of the residual stresses [12]. Besides, it was believed that the hardness of the weld and parent metal may represent that of all the fabricated pipes, hence the prediction of residual stress distribution.

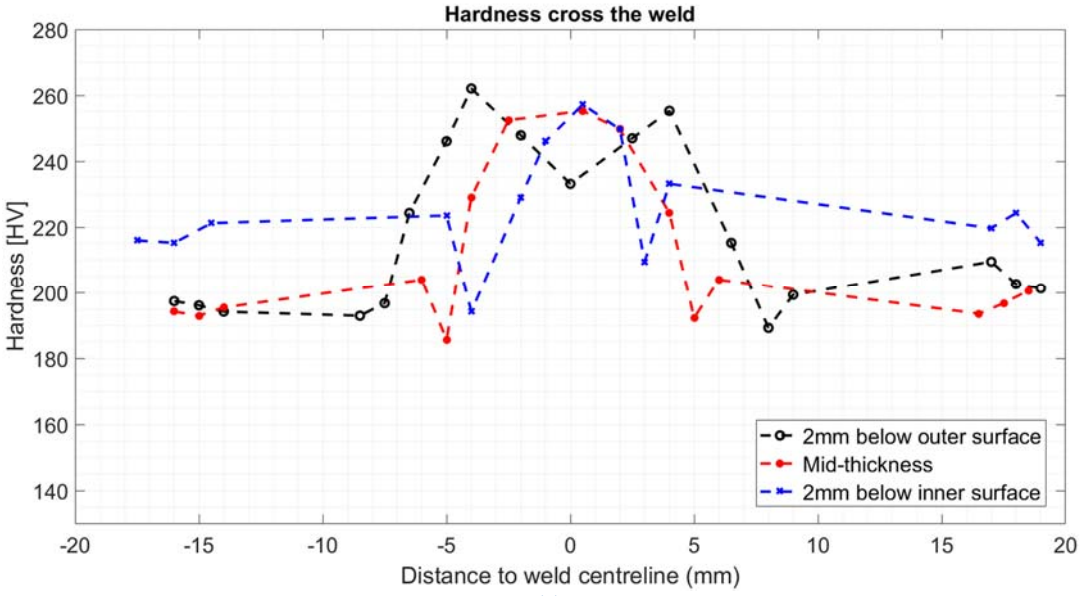

(a)

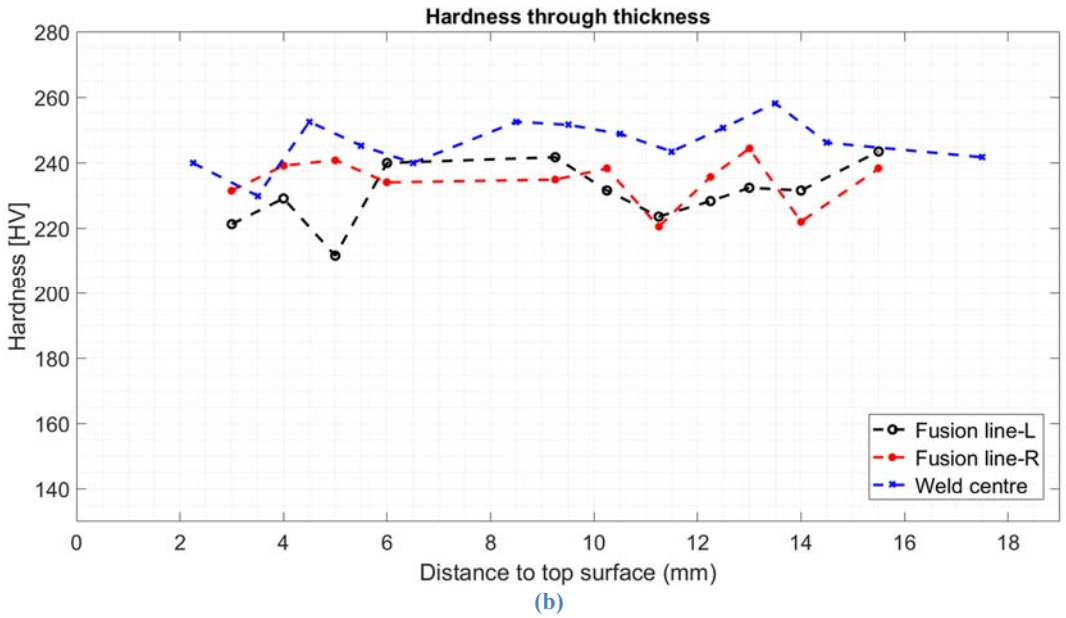

(b)

Figure 3.17 Vickers hardness measured (a) cross the weld at near pipe outer and inner surfaces and mid-thickness and (b) through thickness at weld zone

3.4 Discussion

This chapter has introduced the procedures for girth weld fabrication, PWHT and material mechanical testing carried out in the research work. The design of the experiment details should be highlighted.

First of all, for pipe welding process, a large number of thermocouples and strain gauges have been installed in the outer and inner surface of the pipes. A pro-test was performed on a pipe dummy metal to calibrate the used thermocouple and strain gauges to ensure during welding process they would be picking up correct temperature and transient strain readings. By recording the behaviour of strain gauges and the temperature change, the mechanical strain values will be determined by removing the apparent thermal strain from the measured total strains.

Global and local post weld heat treatment were carried out on narrow-gap pipes fabricated using similar welding procedures, aiming to investigate the effect of various heating condition for the stress relieve in welds which were assumed had similar residual stress state after welding. Parameters selected for PWHT were determined by comparing a number of guidelines recommended in current engineering codes and practices. Nevertheless, not all the PWHT variables parameters could be taken into account. In this work, only the effect of width of heating band on stress relieve was investigated.

Room temperature tensile test was conduct on weld and parent metals. It was difficult to perform such test on a specimen extract from HAZ because for a narrow-gap weld, HAZ was only approximately 1.5mm wide.

3.5 Concluding remarks

From the experimental work performed above, the following outcome could be achieved:

1. Fabricated pipes as well as manufactured reference samples were used for the evaluation of the residual stresses by neutron diffraction technique. The stress states in the pipes will be compared and evaluated in as-welded and after PWHT conditions.

2. Readings from thermocouples and strain gauges will be used to provide essential information for evaluating the accuracy of the thermal and the stress models developed from subsequent FEA approach.

3. Mechanical testing provided room temperature material properties for weld and parent metal, which will be assigned to corresponding sections in the FE model.

Reference

[1] Y. C. Lin and K. H. Lee, "Effect of preheating on the residual stress in type 304 stainless steel weldment," *J. Mater. Process. Technol.*, vol. 63, pp. 797–801, 1997.

[2] S. M. Adedayo and M. B. Adeyemi, "Effect of preheat on residual stress distributions in arc-welded mild steel plates," *J. Mater. Eng. Perform.*, vol. 9, no. 1, pp. 7–11, 2000.

[3] R. Fokens, "Cold Metal Transfer - CMT - A Revolution in Mechanized Root Pass Pipeline Welding," in *4th Pipeline Technology Conference*, 2009, p. 2.

[4] A. M. Paradowska, J. W. H. Price, R. Ibrahim, and T. R. Finlayson, "The effect of heat input on residual stress distribution of steel welds measured by neutron diffraction," *J. Achiev. Mater. Manuf. Eng.*, vol. 17, no. 1–2, pp. 385–388, 2006.

[5] R. Slaminko, "Strain Gages on Composite - Gage-Selection Criteria," in *Manual on Experimental Methods for Mechanical Testing of Composites*, R. L. Pendleton and M. E. Tuttle, Eds. London: Elsevier Applied Science Publishers, 1989, pp. 27–30.

[6] A. Lundbäck, H. Alberg, and P. Henrikson, "Simulation and validation of TIG-welding and post weld heat treatment of an Inconel 718 plate," *Math. Model. weld Phenom. 7 [papers Present. Seventh Int. Semin. "Numerical Anal. Weldability" held from 29th Sept. to 1st Oct. 2003 Schloss Seggau near Graz, Austria]*., pp. 683–696, 2005.

[7] M. Jonsson and B. L. Josefson, "Experimentally determined transient and residual stresses in a butt-welded pipe," *J. Strain Anal. Eng. Des.*, vol. 23, no. 1, pp. 25–31, 2007.

[8] M. Jonsson and B. L. Josefson, "EXPERIMENTALLY DETERMINED TRANSIENT AND RESIDUAL STRESSES IN S BUTT-WELDED PIPE," *J. Strain Anal.*, vol. 23, pp. 25–31, 1988.

[9] ANSI/AWS D10.10/10.10M, *Recommended Practices for Local Heating of Welds in Piping and Tubing,An American National Standard*. 1999.

[10] D N Crofft, *Heat Treatment Of Welded Steel Structures*. 1996.

[11] P. J. Withers, M. Preuss, A. Steuwer, and J. W. L. Pang, "Methods for obtaining the strain-free lattice parameter when using diffraction to determine residual stress research papers," *J. Appl. Crystallogr.*, vol. 40, pp. 891–904, 2007.

[12] A. M. Paradowska, N. Larkin, H. Li, Z. Pan, C. Shen, and M. Law, "Neutron diffraction residual stress measurements of welds made with pulsed tandem gas metal arc welding (PT-GMAW)," *Powder Diffr.*, vol. 29, no. December, pp. S24–S27, 2014.

4 Residual stress evaluation by neutron diffraction

4.1 Introduction

This chapter firstly describes the principles of the neutron diffraction technique and its capability in the determination of the residual stress non-destructively in bulk engineering materials. The following section introduces the equipment utilised and the methodology adopted in this study for the residual strain scanning of the weld components. Finally discusses and compares the residual stress profiles recommended in the current British engineering critical assessment procedure such as BS 7910 [1] and R6 [2].

4.2 Principles of neutron diffraction

4.2.1 Fundamentals

The Principle of applying neutron diffraction for the evaluation of the residual stresses in the components is based on Bragg's law. In a polycrystalline material, only the grain lattice planes which allow Bragg reflection will contribute to the scattering. The principle of the Bragg's law is illustrated in Figure 4.1 [3], [4].

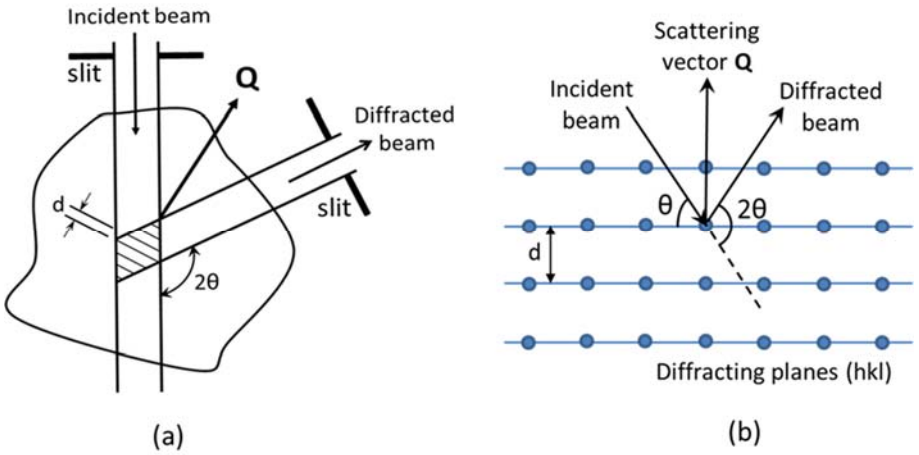

Figure 4.1 Principle of neutron diffraction showing the Bragg's reflection from the crystal plane d.

Once a beam of neutrons of a wavelength λ is incident upon a crystalline material that contains crystallographic planes hkl, a diffraction pattern is produced with peaks. Let d_{hkl} represent the lattice spacing in the direction of scattering vector Q with scattering angle $2\theta_{hkl}$, then Bragg's law gives the position of the peaks value:

$$2d_{hkl}\,sin\,\theta_{hkl} = \lambda \qquad (4.1)$$

With the ability of penetration into the steel up to a few centimetres, neutron beams are able to probe the change of the atomic lattice spacing due to stress. The relative changes in spacing are calibrated using a stress-free material sample (i.e. d_0 sample) to calculate absolute strain and hence stress values.

Monochromatic 2θ strain scanning, commonly found at a reactor source and is based on a single wavelength neutron beam, was applied in this study. It measures the changes in the peak diffraction angle of a single diffraction peak, 2θ, relating to a particular lattice spacing, d, due to residual stresses. When a beam of neutron is diffracted on a stressed crystal plane, any change in lattice spacing Δd would result in a corresponding shift in the angular position Δθ of Bragg reflection (Figure 4.2). If the stress-free lattice spacing d_0 is known and $2\theta_0$ is the corresponding angular position of diffraction peak for the stress-free sample, then the lattice elastic strain can be calculated as:

$$\varepsilon = \frac{d-d_0}{d_0} = \frac{\Delta d}{d_0} = -\Delta\theta \cot\theta_0 \qquad (4.2)$$

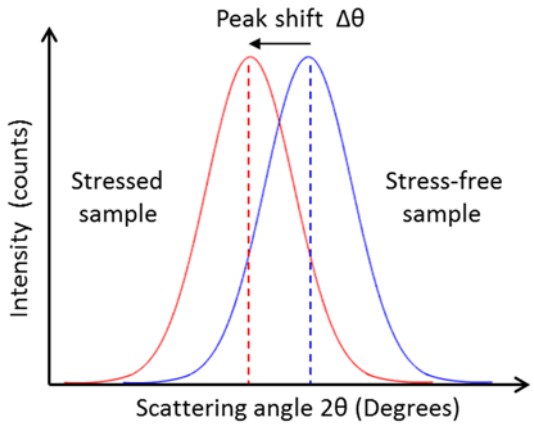

Figure 4.2 Illustration of the peak shift with Bragg reflection in stressed sample, fitted with Gaussian distribution

It is important to note that for the determination of the stress state at a measurement point, six independent components are required to define the accurate stress tensor. However, it will be sufficient to measure the strain components on the orthogonal directions of the principle stresses. Here principal stresses are defined as whose normal components of stress that act on the planes have shear stress components with zero magnitude. Therefore, the stress tensor reduces to a diagonal matrix and is fully characterised by the three measured stresses.

In pipe girth weld, three main directions are defined as: axial (x) is perpendicular to the weld along pipe length; hoop (y) is parallel to the welding direction and radial (z) is perpendicular to the pipe wall thickness. Hence strain measurements are made in the (x), (y) and (z) directions of the weld to define the stress tensor. When principal strain components ε_{xx} , ε_{yy} and ε_{zz} are known, the corresponding stresses can be obtained based on continuum mechanics using the general Hooke's law:

$$\sigma_{xx}=\frac{E}{(1+\nu)(1-2\nu)}[(1-\nu)\varepsilon_{xx}+\nu(\varepsilon_{yy}+\varepsilon_{zz})] \quad (4.3)$$

$$\sigma_{yy}=\frac{E}{(1+\nu)(1-2\nu)}[(1-\nu)\varepsilon_{yy}+\nu(\varepsilon_{zz}+\varepsilon_{xx})] \quad (4.4)$$

$$\sigma_{zz}=\frac{E}{(1+\nu)(1-2\nu)}[(1-\nu)\varepsilon_{zz}+\nu(\varepsilon_{xx}+\varepsilon_{yy})] \quad (4.5)$$

Where E is the Young's modulus and ν is the Poisson's ratio of the material. Based on the Kröner model, the scattering plane for ferritic steel is Fe (211) and therefore the values of E=223.8 GPa and ν=0.27 are used for X65 steel in this work. Calculation are carried out using software DECcal [5].

4.2.2 Uncertainties of the calculated results

The errors, or uncertainties in both the measured stressed and unstressed lattice spacing (Δd and Δd_0) were calculated by using an general multiplication error propagation method [6]. There are a few possibilities contributing to Δd and Δd_0, among which the error in the peak position (data fitting) can be easily quantified. This source of uncertainty is dependent on the counting time of the measurement and is present in all lattice spacing measurements. Other sources of experimental uncertainty may be present, including thermal, grain size and texture effects [7]. The source of errors such as positioning, gauge volume size or misalignment during the experiment procedure could be minimised but not easily quantified. Derived from the error propagation method, considering only the peak fitting, the errors of elastic strains ε_{xx}, ε_{yy} and ε_{zz} are written as:

$$\Delta\varepsilon_{xx} = \frac{d_{xx}}{d_0}\sqrt{\left(\frac{\Delta d_{xx}}{d_{xx}}\right)^2+\left(\frac{\Delta d_0}{d_0}\right)^2} \quad (4.6)$$

$$\Delta\varepsilon_{yy} = \frac{d_{yy}}{d_0}\sqrt{\left(\frac{\Delta d_{yy}}{d_{yy}}\right)^2 + \left(\frac{\Delta d_0}{d_0}\right)^2} \quad (4.7)$$

$$\Delta\varepsilon_{zz} = \frac{d_{zz}}{d_0}\sqrt{\left(\frac{\Delta d_{zz}}{d_{zz}}\right)^2 + \left(\frac{\Delta d_0}{d_0}\right)^2} \quad (4.8)$$

Errors of the stress components can then be derived as:

$$\Delta\sigma_{xx} = \frac{E}{(1+\nu)(1-2\nu)}\sqrt{(1-\nu)^2\Delta^2\varepsilon_{xx} + \nu^2\Delta^2\varepsilon_{yy} + \nu^2\Delta^2\varepsilon_{zz}} \quad (4.9)$$

$$\Delta\sigma_{yy} = \frac{E}{(1+\nu)(1-2\nu)}\sqrt{(1-\nu)^2\Delta^2\varepsilon_{yy} + \nu^2\Delta^2\varepsilon_{zz} + \nu^2\Delta^2\varepsilon_{xx}} \quad (4.10)$$

$$\Delta\sigma_{zz} = \frac{E}{(1+\nu)(1-2\nu)}\sqrt{(1-\nu)^2\Delta^2\varepsilon_{zz} + \nu^2\Delta^2\varepsilon_{xx} + \nu^2\Delta^2\varepsilon_{yy}} \quad (4.11)$$

The reported errors are ± 15 MPa on average. Note that these are the peak fitting errors and do not take into account other possible sources of errors such as partial illumination. The chance of partial illumination is considered low as there are no unexpected high stress results close to edges, and the error in sample positioning is estimated to be less than 0.1mm.

4.3 Instrumentations and measurement methodology

4.3.1 The KOWARI Strain Scanner at ANSTO

Residual stress measurements were carried out by the KOWARI strain scanning diffractometer at the Australia Nuclear Science and Technology Organization (ANSTO). Figure 4.3 shows the layout of the major hardware elements of the KOWARI instrument, including the adjustable jaws that define the neutron beam cross-section, the collimators for the detector, and the x, y, z, ω positioning table on which the sample is mounted. This heavy-duty table with unique telescopic design is capable to bear a sample with maximum weight up to 1 metric ton, while the dimension of the sample in horizontal direction should not exceed 1000mm.

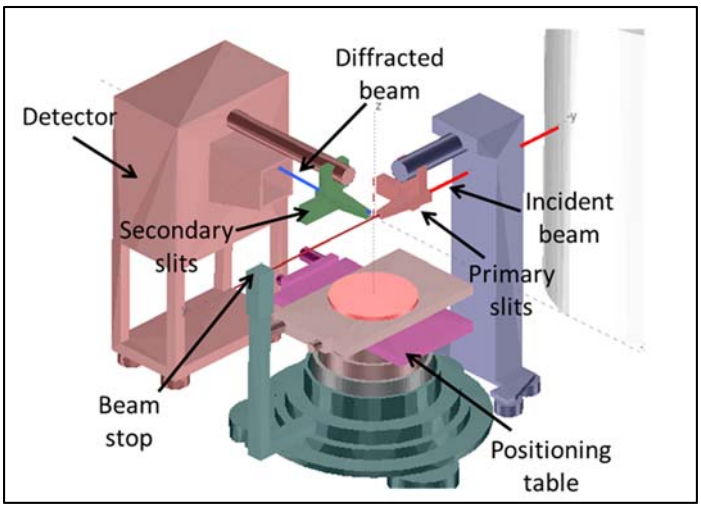

(a)

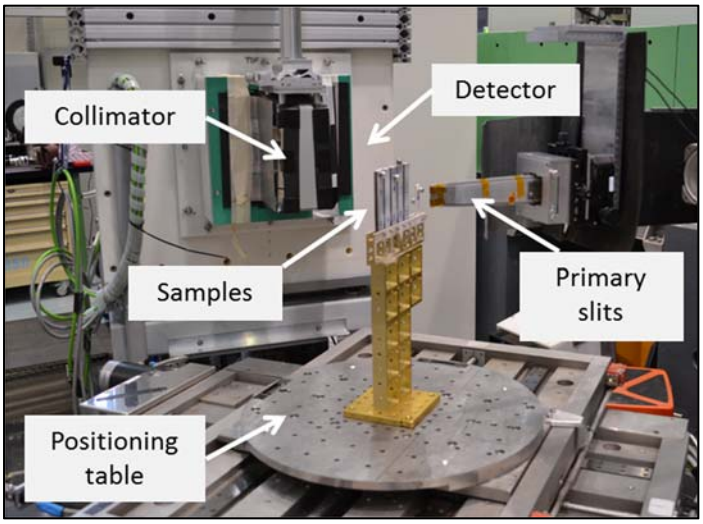

(b)

Figure 4.3 View of the main components and layout of the KOWARI strain scanning diffractometer from (a) alignment in the model and (b) d_0 sample measurement

Equipped with reactor source, neutrons of 1.67 Å wavelength are extracted from a double focusing Si (4 0 0) monochromator at a take-off angle of 76° to look at α-Fe (211) reflection for radial, hoop and axial components. Obtained beam of the neutrons with monochromatic wavelength enables single diffraction peaks to be sampled.

The gauge volume, over which the diffraction data are collected, is defined by adjustable jaws and the choice of collimator. The dimensions of the gauge volume are controlled in the x direction (parallel to the beam) by the choice of the collimator and in the y and z directions by the adjustable horizontal and vertical jaws which determine the cross-section of the neutron beam. In this experiment a gauge volume

of 3x3x4 mm^3 was used: the horizontal dimension perpendicular to the beam was 3 mm and the height of the gauge volume was 4 mm. The position of the detector was 90°, creating cubic gage volume for the measurement of the axial, hoop and radial components.

4.3.2 Use of Strain Scanning Simulation Software (SScanSS)

Due to the large scale and complexity of the components to be measured as well as the fact of time-consuming for sample positioning and alignment, and instrument control during strain measurement, a careful planning of the experiment is of great importance. To overcome these difficulties, Strain Scanning Simulation Software (SScanSS) [8], [9] which was developed by The Open University in collaboration with staffs at the ISIS neutron source was used together with the KOWARI virtual instrument to position measurement points and automatically calculate instrument movements required to execute measurements

Prior to neutron diffraction scanning 3D model geometry of the sample were captured by laser scanning. Measurement points were positioned on the sample model and the scanning sequence was displayed as the point number. Each scan was simulated to predict the measurement time and to check the orientation of the sample from which the actual experiment can be controlled. Figure 4.4 is an example which demonstrates the procedures of using SScanSS for the planning of the measurement locations and pre-scan simulation of on a pipe sample model.

4.3.3 Importance of sample positioning

The SScanSS based approach to instrument control relies on the accurate measurement of the position of the sample on the instrument. This is routinely achieved on KOWARI by attaching a number of fiducial marks, in the form of stainless steel spheres to the outside of the sample in the region of the measurement points. These spheres can be identified on the virtual sample and their position measured using touch probes when the real sample is on the instrument. By matching the real and virtual fiducial points, the position of the sample is accurately reproduced in the virtual laboratory. Once this step has been completed, the accuracy of the alignment is checked by bringing the sample to the test measurements position and checking the position of the fiducial points with the

touch probe. Usually the accuracy of the procedure is in the order of ~0.05 mm, however for this relatively large component the positioning precision was relaxed, typically between 0.05-0.1 mm depending how off centre was the component.

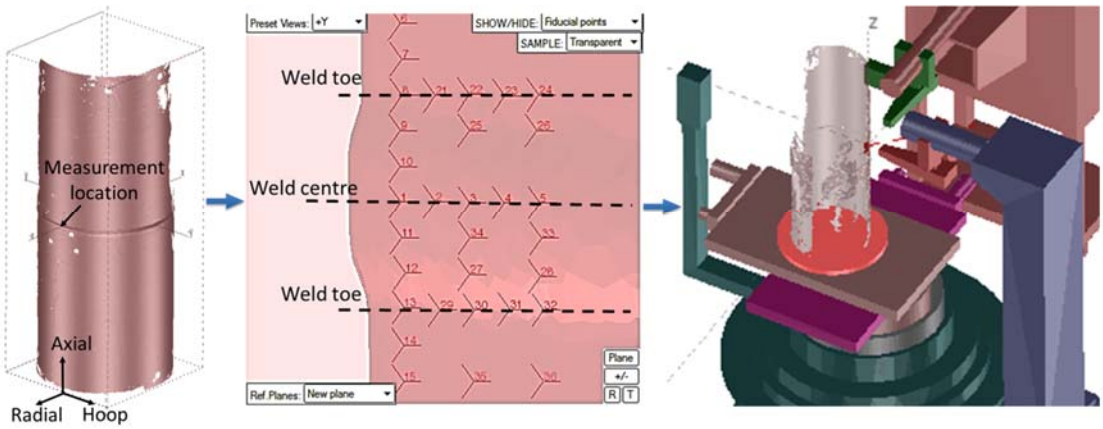

Figure 4.4 The application of SScanSS software to pre-design the measurement points on the laser scanned 3D pipe model

4.3.4 Lattice spacing measurements

Un-stressed lattice parameter measurements were performed on the reference samples in the three orthogonal directions. The selections of the measurement points were positioned depended on the configuration of the d_0 samples. For instance, on a grid sample, there were only 24 points measured in the sample due to the additional slits cut in both axial and hoop directions. With the given gauge volume 3x3x4mm^3, the measurements at each point were carried out focusing the beam at the centre of each grid. By contrast, a flat d_0 sample had almost 40 measurement points; the proposed locations were quite similar as those in the pipes. However, in the recomposed cuboid samples, measurements were made at the points with every 1mm interval. Details will be introduced in next chapter.

For each pipe residual stresses were measured at up to 40 locations. At each location, lattice spacing was determined in three principal directions: axial, hoop and radial. Three line-scans were carried out at a).3mm below the outer surface, b).mid-thickness and c).3mm above the inner surface. This allows full residual stress maps to be generated for compare of the stress states of the pipe spools in as-welded condition and after PWHT. Besides, the through-thickness strains were measured mainly at weld centreline and the toe area. There were still several additional points were measured in the vicinity of the weld to generate the full stress maps.

In as-welded condition, residual stresses were evaluated on four reference samples and two pipes. After PWHT, the measurements were repeated on all the six reference samples and four pipes. The scanning time was greatly reduced by the introduction of the slits on the pipes after PWHT, enabling the neutron beam avoid penetrating the double thickness of the pipe wall. The measurements of the pipe and the reference samples were made with separate experimental sessions.

4.4 Residual Stress Profiles in Current Engineering Critical Assessment Procedures

4.4.1 Residual stress in as-welded condition

Engineering Critical Assessment (ECA) procedures such as BS7910 and R6 recommend through wall residual stress profiles to be used in the assessment of structures containing flaws in the absence of residual stress measurements and/or simulations.

R6 provides three levels of measurement for determining the magnitude and spatial distribution of residual stresses. In Level 1, the structure with a defect is assessed assuming that the residual stresses are uniform and tensile with a magnitude equal to the appropriate yield stress of the parent metal or weld material. This level is equivalent to the assessment procedure described in section 7.1.8 of BS 7910. Non-uniform residual stress distributions for a range of structures are presented in Level 2 of R6, as well as in Annex Q of BS 7910. Level 2 profiles are based on published compendia of conservative residual stress profiles for a range of as-welded structures. They are upper bounds, and less conservative compared to the uniform tensile stress distribution advised in Level 1. In both BS7910 and R6 procedures, it is advised that for residual stress profile, longitudinal stresses are normalized with respect to the greater yield strength (at room temperature) of the weld or parent material (represented by σ_y^+) for the level 2. The transverse stresses, in contrast, are advised to be normalized with respect to the lower yield strength of the two (represented by σ_y^*). The Level 3 approach (measurement and/or analysis of a specific joint) is expected to lead to less conservative results but is more complex, requiring both experimental measurements and numerical analysis.

In terms of the stress components in pipeline girth welds, the longitudinal stress designates the stresses acting in the hoop direction (i.e. along the weld) and the transverse stress designates the stresses acting in the axial direction (i.e. transverse to the weld). The residual stress in the radial direction is negligible provided that the pipe can be considered as a thin-walled structure.

In the case of pipe butt weld geometry, Level 2 recommends a longitudinal through-thickness residual stress distribution as a linear profile. At the outer surface, the longitudinal residual stress $\sigma_R^{L,O}$ equals to σ_y^+. In contrast, the residual stress at the bore (inner surface) $\sigma_R^{L,B}$ can be calculated by equation (4.12). In this study, the pipe wall thickness is in the range between 15 and 85mm, A_b is calculated using equation (4.13) [1]. The specific Level 1 and 2 profiles are displayed in Figure 4.5(a).

$$\sigma_R^{L,B}=A_b\,\sigma_y^+ \tag{4.12}$$

$$A_b=1-0.0143(t-15) \tag{4.13}$$

The through-wall transverse residual stress profiles are defined in terms of the fractional distance from the inner surface, z/t, and depend on the weld electrical energy per unit run length per unit thickness [(q/v)/t], where q is equal to current × voltage (J/sec), v is the welding torch advance rate (mm/sec), z is the radial distance from the pipe inner surface (mm) and t is the pipe wall thickness (mm). For the welding technique used in this work, the heat input [(q/v)/t] was less than 50 J/mm^2 and is 'low heat input' as defined in BS 7910. The transverse residual stress profiles following BS 7910 and R6 procedures are shown in Figure 4.5(b).

$$\sigma_R^T=\sigma_y^*\,[1-6.80(z/t)+24.30(z/t)^2-28.68(z/t)^3+11.18(z/t)^4] \tag{4.14}$$

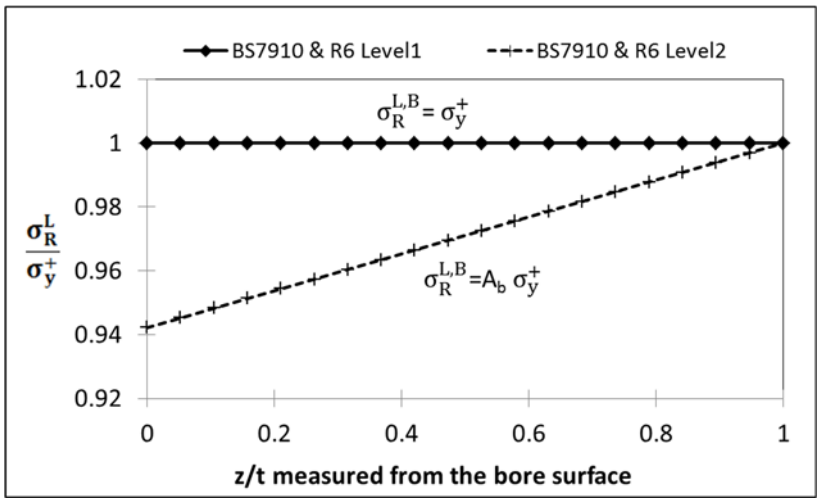

(a)

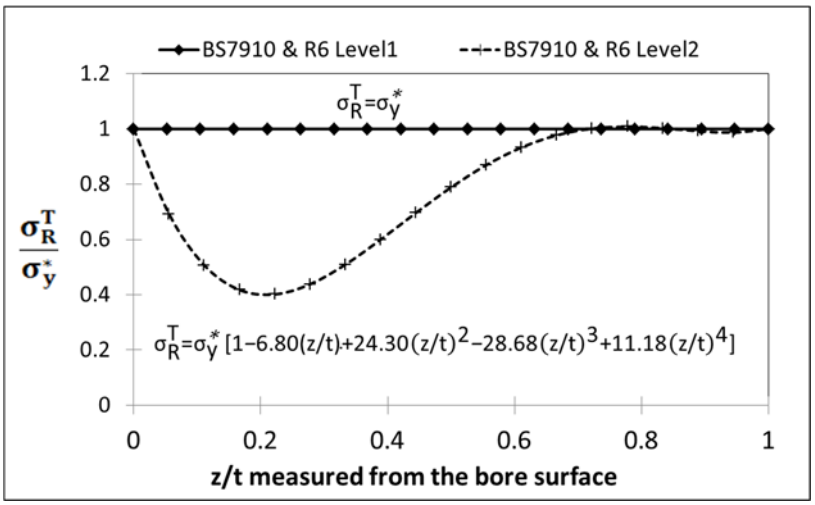

(b)

Figure 4.5 Calculated levels 1 and 2 through-thickness residual stress distribution based on BS 7910 and R6 (a) Longitudinal (hoop direction in pipe) stress distribution and (b) transverse (axial direction in pipe) stress distribution

In BS 7910, there is currently no guidance on the residual stress distributions along the pipe length showing how residual stresses fade away from the weld centre-line outwards. With regard to the surface residual stress profiles, parameter r_0, given in R6, is used to define the yield zone dimension of the weld in thick materials. Ideally, residual stresses in the yield zone would be entirely tensile with infinite material restraints. In practice, finite restraints enable redistribution of residual stresses between the yield zone and the adjacent material. As a result, the hoop residual stress in the butt weld next to the yield zone is usually compressive. To determine the radius of the yield zone r_0 (mm), Equation 4.15 was applied, based on the R6 procedure when $r_0 \leq t$,

$$r_0 = \sqrt{\frac{K}{\sigma_{YP}} \cdot \frac{\eta q}{v}} \tag{4.15}$$

Where t is the pipe wall thickness (mm), K is the material constant (Nmm/J), σ_{YP} is the yield or 0.2% proof strength of the parent metal (N/mm^2), q is the arc power, v is the welding speed and η is the process efficiency.

Taking a typical value of efficiency of 80% i.e. η = 0.8, K · η= 122Nmm/J can be assumed for ferritic steels [23]. Using the heat input experienced by the cap and measured from the fusion boundary, the yielded zone radius r_0 in this experiment was conservatively selected as the lowest value during welding. The residual stress magnitude was then assumed to be constant and equal to σ_{YP} in the weld and reduced to zero at the boundary of the yield zone.

The calculated yield zone for outer surface is shown in the Figure 4.6. Welding width was determined using the distance between two toes. Yielded zone radius r_0 was calculated using the welding parameters for cap listed in Table 3-2. A combination of lowest power voltage and current and highest welding speed were applied. For pipe inner surface, the weld width should be the dimension the root.

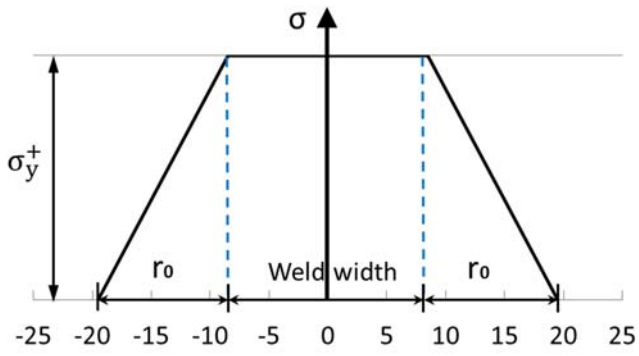

Figure 4.6 Surface hoop residual stress distribution and calculated radius of the yield zone at butt weld in the pipe

Currently there are no recommended profiles for axial residual stress in restrained material in ECA procedures. This is because the tensile stress on the un-yielded material would spread outwards. The decay of the transverse stresses with distance varies for different cases. Conservatively, they are assumed to be constant and equal in the magnitude to the 0.2% proof strength of either parent material or the weld metal, whichever is lower.

4.4.2 Residual stress after PWHT

The level of residual stress relief after furnace PWHT is given in BS 7910:2013 for the carbon manganese and 2¼Cr1Mo steels. It is assumed that the residual stress remaining in the welds after an enclosed furnace PWHT with the range of 580°C to 620°C would be 20% of the lesser of the room temperature yield strengths of the weld or the parent metal for the stress component transverse to the weld; 30% of the room temperature yield strength of the material (the weld or the parent metal) where the flaw is located for the stress component parallel to the weld. It should be noted that this is treated as a membrane stress. It needs to be highlighted that there is currently no guidance in the procedures to estimate the level of residual stresses after local PWHT.

4.5 Discussion

There were a few challenges in the use non-destructive neutron diffraction technique to measure residual stresses in this research. For examples, to accurately locate the measurement positions on such large component was not as easy as on a sample with a small dimension and simple geometry. The ability of relocating the reference (start) point ensured the subsequent stress component measurement were made at the region of interest. Particularly, strain measurement after PWHT should be repeated at same region as that in as-welded condition.

The use of the virtual model created by SScanSS depends on the scales and configurations of the component being measured. For large scale and complicated sample, such as in this work the sample was one metre long with large thickness and a girth weld in the middle length, a virtual model had great convenience and accuracy to positioning samples.

For the examination of residual stress states in the pipe, current EAC procedures were introduced in which distribution and magnitude of the stress were recommended for certain thicknesses. Although the guidance was developed for generally case with wide grove welds, the degree of conservatism could be evaluated.

4.6 Concluding remarks

This chapter introduced the principles of using neutron diffraction technique for the determination of residual stresses in pipe girth weld, the following conclusion can be made:

1. Residual stress state in the pipe girth weld can be determined by measuring the three principle stress components in axial, hoop and radial directions.

2. Prior to neutron beam scanning, measurement points were selected and measurement procedure was simulated using SScanSS software, which not only guarantee the accuracy of the measurement locations, but also provided information such as the time required to complete a set (stress component at each direction) of measurement on large scale and complex geometry components

3. Current ECA procedures are widely used for the evaluation of residual stresses in conventional wide-gap weld. Stress profile recommended in these standards did not consider the profiles measured from non-destructive neutron diffraction in the narrow-gap weld in as-welded and after PWHT conditions.

4. When using BS7910 or R6 procedures for the evaluation of the residual stresses, recommended stress profiles should be obtained by applying correct value of the component thickness and understanding the level of heat input.

Reference

[1] "BSI, 'BS7910:2013 Guide to methods for assessing the acceptability of flaws in metallic structures,' 2013," 2013.

[2] "British Energy. Assessment of the Integrity of Structures Containing Defects. Procedure R6 Revision 4. British Energy Generation Ltd; 2014." .

[3] G. A. Webster and R. C. Wimpory, "Non-destructive measurement of residual stress by neutron diffraction," *J. Mater. Process. Technol.*, vol. 117, no. 3, pp. 395–399, Nov. 2001.

[4] A. Stacey, H. J. MacGILLIVARY, G. A Webster, P. J. Webster, and K. R. a Ziebeck, "Measurement of residual stresses by neutron diffraction," *J. Strain Anal. Eng. Des.*, vol. 20, no. 2, pp. 93–100, Apr. 1985.

[5] T. Manns; B. Scholtes, "DECcalc - A Program for the Calculation of Diffraction Elastic Constants from Single Crystal Coefficients," *Mater. Sci. Forum*, vol. 681, pp. 417–419, 2011.

[6] J. R. Taylor, *An Introduction to Error Analysis*. Oxford University Press, 1982.

[7] A. J. Allen, "Errors in Analysis, in Measurement of Residual and Applied Stress Using Neutron Diffraction," 1992.

[8] J. A. James, J. R. Santisteban, L. Edwards, and M. R. Daymond, "A virtual laboratory for neutron and synchrotron strain scanning," *Phys. B Condens. Matter*, vol. 350, no. 1–3 SUPPL. 1, pp. 743–746, 2004.

[9] J. A. James and L. Edwards, "Application of robot kinematics methods to the simulation and control of neutron beam line positioning systems," *Nucl. Instruments Methods Phys. Res. Sect. A Accel. Spectrometers, Detect. Assoc. Equip.*, vol. 571, no. 3, pp. 709–718, 2007.

[10] I. Milne, R. Ainsworth, A. Dowling, and A. Stewart, "Assessment of the integrity of structures containing defects," *Int. J. Press. Vessel. Pip.*, vol. 32, no. 1–4, pp. 3–104, Jan. 1988.

5 Determination of strain-free lattice spacing using neutron diffraction technique

5.1 Introduction

The estimation of residual strains hence the residual stresses are based on the difference in the measured lattice spacing between a stressed component and a stress-free or unstrained sample from the same material. The fundamentals of elastic strain can be interpreted using Bragg's and Hook's laws which have been introduced in the previous chapter.

This chapter discussed the design, preparation and experimental neutron diffraction measurement procedures for the determination of the strain-free lattice parameter (d_0) in different types of reference samples and in the required directions. Various configurations of the reference samples can be used to determine the effect of specimen manufacture methods on the variability of lattice spacing. The work began with thin slice samples manufactured to create plane-stress condition. Two of them were designed with vertical and horizontal slits, turning them into comb configuration which allowed for further residual stress relieve. One of the comb samples was reduced to smaller cuboid samples with the intent to achieve the optional strain-relieve condition.

All the measurements were carried out using neutron diffraction technique which allowed the measurement of the lattice spacing in the direction normal to the free surface. Reference samples were manufactured using electro-discharge machining to generate desired strain-relief condition at macroscopic level. Cooling fluid was used during machining to avoid overheating.

The idea of the "relative changes in the strain", a pseudo micro-strain of the reference samples after stress relief could be established. Following the analysis and comparison of the measured lattice spacing, recommendations were made on the selection of appropriate d_0 values to calculate residual stresses in both as-welded and PWHT conditions.

5.2 Reference sample preparations and measurement design

5.2.1 Background

A stress-free condition is strictly defined when tri-axial components are strain-free therefor the principle values of macroscopic stress and strain tensors are zero [1]. However, there are cases when stress tensor is zero, i.e. in plane stress condition, the corresponding strains are not necessarily zero. Factors affecting the lattice spacing include compositional gradient, phase transformation, changes in temperature, geometrical effect as well as intergranular strains [2].

For the measurement of stress-free (d_0) lattice spacing, various methods have been adopted in previous investigation [3]–[7]. A common approach is to use a far field d_0 value in the sample as reference which is expected to be strain-free or with small level of stress exists [6], [8]. This idea of using a reference sample assumes the material is stress-free and remains unaffected by surrounded macrograph stress field. However, this method has not been recommended for the cases involving local heating since the process may introduce possible change in local composition [9].

As the principle of manufacturing small reference samples is to obtain a d_0 which long-range macro residual stresses cannot be sustained in certain directions after the excision of the materials of concern. For this reason, the lattice spacing measured from powders, cubes as well as comb samples have been widely used as strain-free values [10]–[12]. Using any one of these samples for the measurement of the strain-free lattice spacing allows users to determine the strain states either locally or globally, near surface or in-depth, 3-D full map may be achievable, but it is often time consuming and required good coordination. Nevertheless, it is still important to determine the d_0 in the required directions, because using accurate value/values of the reference lattice spacing will generate reliable residual stress estimation.

As introduced in previous chapter, the d_0 samples in this study were manufactured from an additional pipe girth weld. The welding procedure conducted on fabricating this pipe was identical to that for the other four pipes. Three types of d_0 samples were prepared: 1) thin slice samples (flat sample without slits), 2) comb samples (flat sample with slits), and 3) cuboid samples. Inter-planar lattice spacing in axial, hoop and radial directions at the positioning locations of the samples were measured using

neutron diffraction technique. Measurements were carried out on the samples in both as-welded and after PWHT conditions. Measurement locations were designed to cover the regions containing the weld and parent materials.

5.2.2 Manufacturing of the d_0 samples

5.2.2.1 Flat samples

Six flat reference (d_0) samples were initially manufactured from the additional girth weld. They were taken at the 3o'clock location of the girth weld where the compositional and thermal variations were unlikely to be affected compared to the weld start and stop regions. An example of the sample manufacturing procedure is shown in Figure 5.1.

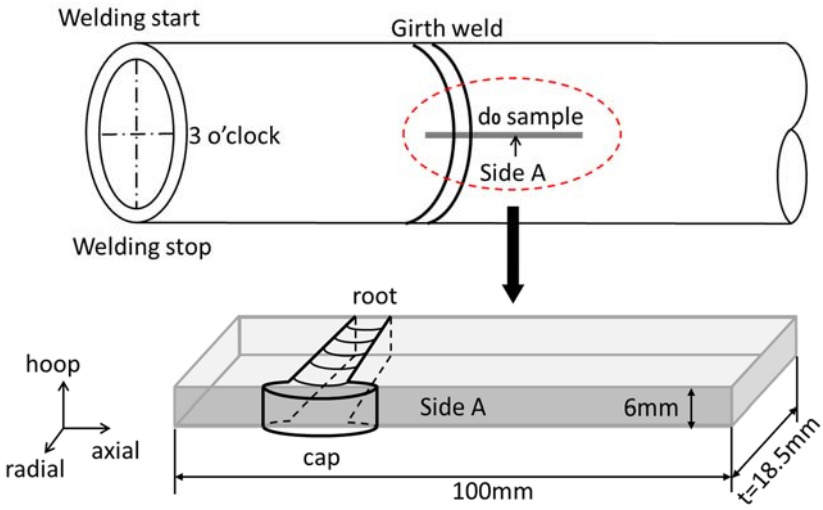

Figure 5.1 Demonstration of the manufacturing location and the dimensions a d_0 sample

All the flat samples were manufactured by EDM technique. The diameter of the cutting wire was 0.25mm. The flat samples were measured 100 mm long (axial direction) and 6mm thick (hoop direction). The width of the samples was 18.5mm which was the maximum achievable from pipe wall thickness during machining. Following the specific welding procedure, the stress states were assumed symmetric with regard to the weld centre. Therefore, prepared flat sample contains full profile of the weld and enough volume of the parent material on one side of the weld.

Two comb samples denoted as d_{01} and d_{02} were manufactured from the flat samples by introducing additional slits using EDM to create a "grid-like" configuration. Each slit was 0.25mm wide which equals the diameter of the cutting wire. The "teeth-cut"

was made at every 6mm wide from the surface of the cap side down to the locations 1mm away to the root side. Two line-cuts in the horizontal direction divided each "tooth" into three grids with a height of in 6mm. These two slits were cut 5mm deep in the hoop direction. Figure 5.2 illustrates the manufacture of the comb samples from flat metal pieces.

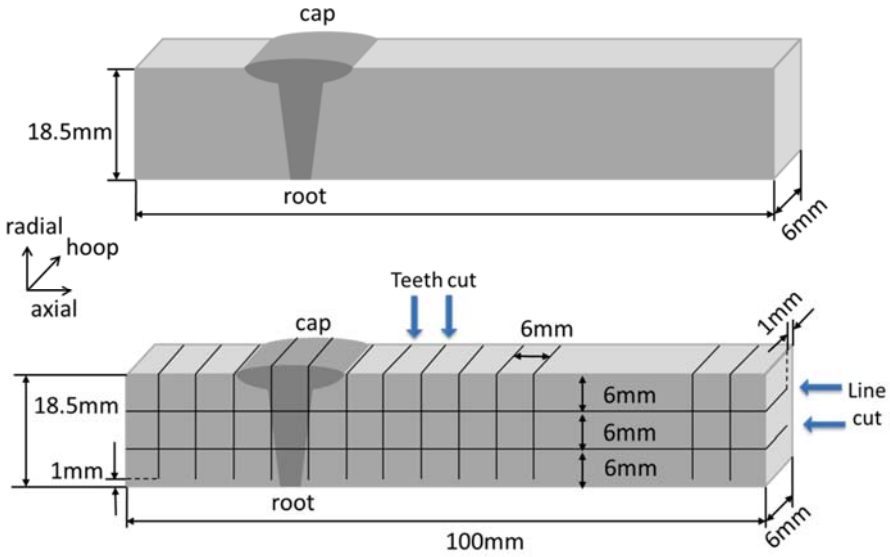

Figure 5.2 Manufacture of the comb sample with "teeth-cuts" and "line-cuts"

Four pipes were prepared for the purpose of investigating the effect of PWHT and they were couple individuals with four flat thin-slice samples (denote as d_{03}, d_{04}, d_{05} and d_{06}), which were used for the determination of the corresponding reference lattice spacing under different heat treatment.

5.2.2.2 Cuboid samples

After the completion of the d-spacing measurement in as-welded condition, cuboid samples were subsequently manufactured from d_{01} of the weld and parent metal (Figure 5.3a). This procedure was believed to further relieve any remaining residual stresses inside the comb sample. Every grid, except for the weld cap region, was divided into four small cubes with a gauge volume of 3x3x3mm^3 (Figure 5.3b). In comparison, the cuboid samples made of weld cap metal were slightly larger in volume, i.e. 3x3x4.5 mm^3 (Figure 5.3c). All machined cubes were re-assembled using super glue to construct two columns to retain the original positions and configurations of the weld metal (Figure 5.3d) and parent metal (Figure 5.3e), respectively. Table 5.1 summarises the type of the d_0 sample manufactured in this study.

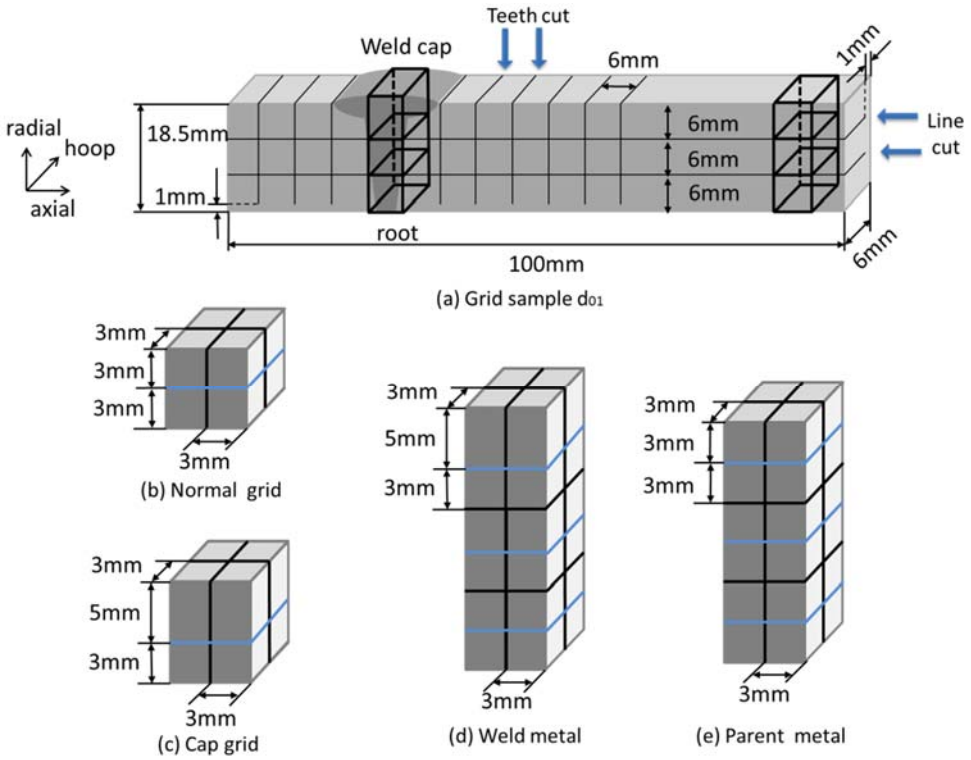

Figure 5.3 Preparation of the cuboid samples - manufactured from d_{01} and re-assembled to columns for neutron diffraction measurements

Table 5-1 Summary of the d_0 samples manufactured in this study

Type	EDM flat samples from pipe section						cuboid
	comb		Thin-sliced				
Sample	d_{01}	d_{02}	d_{03}	d_{04}	d_{05}	d_{06}	d_{01}
Preparation	EDM slits on the flat sample		As in EDM flat samples from pipe section				EDM from as-welded d_{01}

5.2.3 Measurement locations on d_0 samples

5.2.3.1 Comb samples

For comb samples d_{01} and d_{02}, measurements of lattice parameter were performed on 24 designated locations (Figure 5.4). The numbers marked on the grids represent the neutron beam scanning sequence. The neutron beam was adjusted and positioned such that it was focused at the centre of each grid (i.e. designated location) of a $3x3x3mm^3$ or $3x3x4mm^3$ gauge volume.

At the weld centre, three measurements (points 1 to 3) were first made through the section of the weld. Subsequent measurements were carried out as illustrate in Figure 5.4, in the region of the material containing HAZ and thermally affected parent metal (points 4-9 and 19-24). The far-field lattice spacing was also measured in the parent metal (point 16, 17 and 18). Along the axial direction, three line-scans results were

obtained at 3mm below the pipe outer surface (weld cap), middle section and 3mm above the pipe inner surface (weld root).

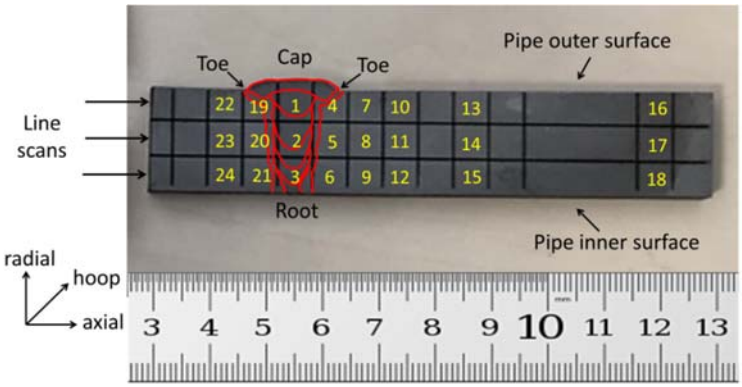

Figure 5.4 Measurement locations and sequence on comb samples d_{01} and d_{02}

5.2.3.2 Thin-sliced samples

For each thin-sliced sample, measurements were carried out at 37 designated points. As shown by the number in Figure 5.5, line scans were carried out at 3mm below the outer surface, along mid-thickness and 3mm above the inner surface. Additional measurement locations were, along the dash lines at 6mm below the outer surface and 6mm above the inner surface.

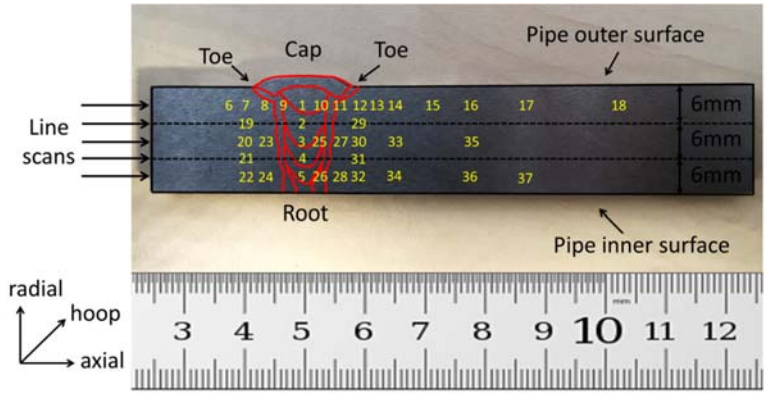

Figure 5.5 Measurement locations and sequences on thin-piece samples

5.2.3.3 Cuboid samples

Lattice parameters of the weld and parent metals were measured respectively in the re-assembled cuboid samples (Figure 5.6a). The neutron beam was aligned to focus at the centre of the gauge volume of the cuboid-sample column. For each column sample, neutron diffraction measurements were performed at 13 locations. The scanning of the lattice spacing initiated at the location at 3mm below the outer surface and terminated at 3mm above the inner surface. The movement of the gauge

volume centre was made every 1mm along radial direction over a distance of 12mm (Figure 5.6b).

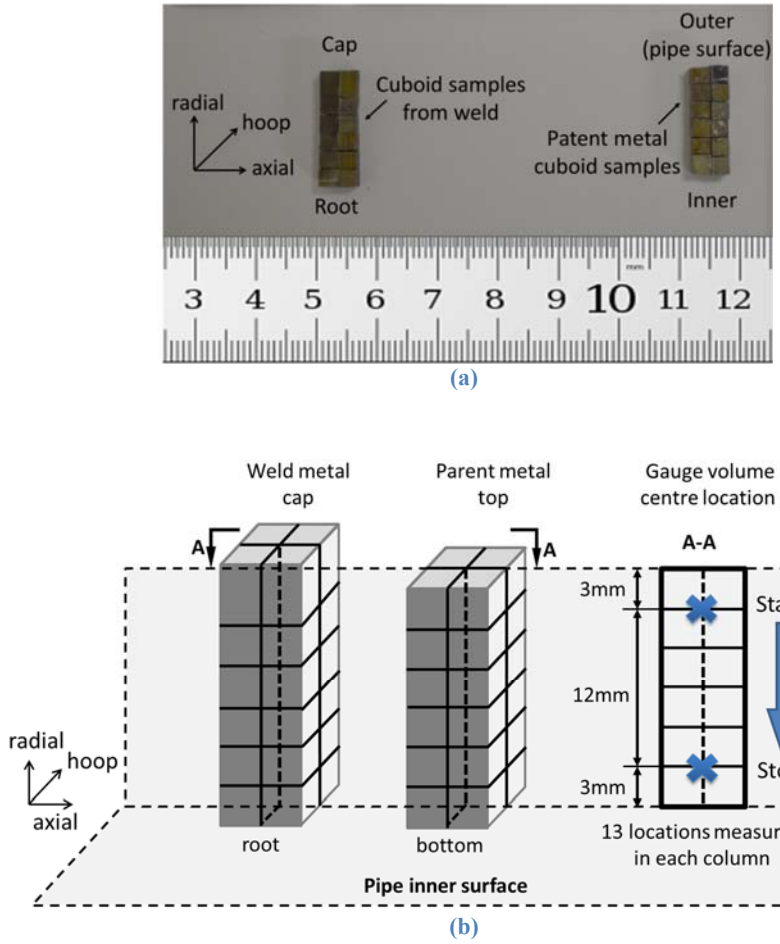

Figure 5.6 Illustration of the measurement locations and sequence in cuboid samples from weld and parent materials

5.2.4 Neutron diffraction measurement procedures

5.2.4.1 As-welded condition

In order to examine the effectiveness of the various specimen manufacturing techniques on the stress relief in reference samples, the measurements of the lattice spacing were conducted on four as-welded reference samples - two comb samples (d_{01} and d_{02}) and two thin-sliced samples (d_{03} and d_{04}). The measurement was carried out at the 24 locations in comb samples and 37 locations in each thin-slice sample. Since it was assumed the stress states of all the thin-slice samples were similar, measurements were not repeated on d_{05} and d_{06}.

Prepared samples were mounted for the measurements as shown in Figure 5.7. Samples were secured by screws on a holder to ensure all of them were vertically

fixed, and the axis of the weld centreline was all aligned. In this way, all the samples were positioned at the same height and separated by a known interval distance, which in turn, facilitated the measurement sequence in an efficient manner.

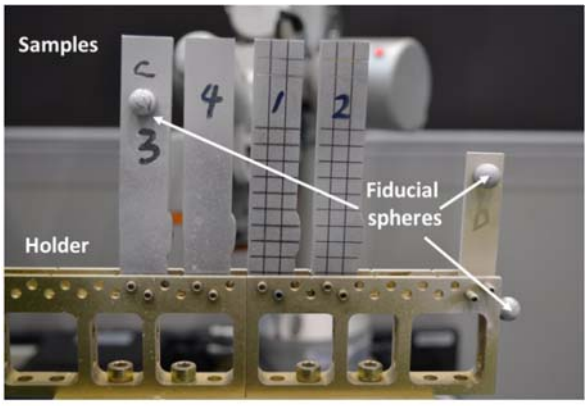

Figure 5.7 Prepared reference samples place on a holder with fiducial spheres for the measurement of the lattice parameter in as-welded condition

Several preparation steps were essential before conducting the measurement. The roughness of sample surface was increased using white particle spray to assist creating a high-quality 3D virtual model of the sample geometry by laser scanning. Additional stainless-steel spheres in diameter of 10mm were attached to the samples and the holder as fiducial marks. The function of these marks is to complete the sample alignment on the instrument, thus corresponding locations in the virtual model would match the fiducial points of the physical sample in the test measurement positions.

5.2.4.2 Post weld heat treated condition

Comb sample d_{02} and thin-slice samples d_{03}, d_{04}, d_{05} and d_{06} were post heat treated with their corresponding pipes to ensure the same thermal process either globally or locally. Before the neutron diffraction measurement on these heat-treated samples, they were polished manually using sandpaper to remove a thin layer of the oxides on the surface. Measurement locations on the samples were the same as those without heat treatment - 24 locations in comb samples and 37 locations in each thin-slice sample. Figure 5.8 shows the samples positioning on the instrument during the measurement of the lattice pacing in the radial direction.

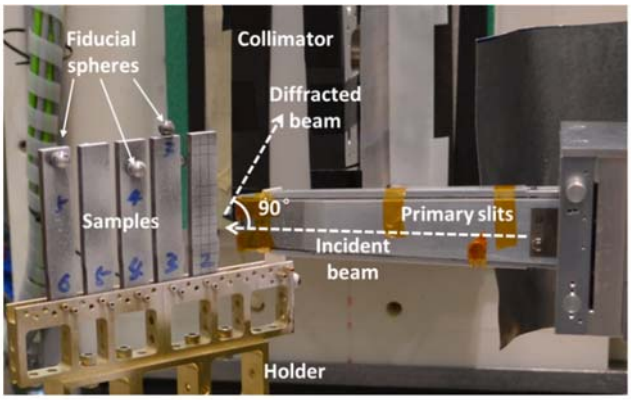

Figure 5.8 Measurement of the lattice parameters in radial direction on reference samples after post weld heat treatment process

5.2.4.3 Measurements on cuboid samples

The measurements of the lattice parameters were carried out on the cuboid samples with and without PWHT. Cuboid samples were manufactured from sample d_{01} after completing the first round of the neutron diffraction measurement on four d_0 samples in as-welded condition. The inter-planar lattice spacing in three principles directed were re-evaluated in the two re-assembled cube columns to examine the potential strain variations in the weld and parent metals due to additional machining.

Samples were then placed in an enclosed furnace for post weld heat treatment aiming to relieve residual stresses. The variations of the lattice spacing were compared with those in the heat-treated comb and thin-sliced samples. This allowed a comprehensive and direct comparison of the measured values and an evaluation of the effectiveness of sample preparation. Table 5-1 summarises the neutron diffraction measurements that carried out on all the reference samples.

Table 5-2 Measurements of the lattice parameters on all the d_0 samples

Sample	type	PWHT		Number of Neutron diffraction measurement locations	
		methods	accompanying pipe	as-welded condition	PWHT condition
d_{01}	comb	-	-	24	-
	cuboid	furnace	-	weld - 13 parent metal - 13	
d_{02}	comb	Local	P2-standard band	24	
d_{03}	thin slice	Furnace	P1	37	
d_{04}		Local	P2-standard band	37	
d_{05}		Local	P3-narrow band	-	37
d_{06}		Local	P4-wider band	-	37

5.3 Evaluation of the relative strains in reference samples

5.3.1 Methods for selecting d_0 values

The selection of an appropriate value of strain-free lattice spacing d_0 from a given reference sample can affect the calculated residual stresses. Ideally, the d_0 measured at a location and orientation in a reference sample, in either parent or weld metal or HAZ, should be used to calculate the residual strains of the exact corresponding areas in the investigated material. This allows better and more accurate estimation of the residual stresses magnitude since the intergranular strains and compositional variations in both stressed and stress-free samples will cancel out [6].

The compositional and microstructural variations resulted from welding thermal cycle gives rise to uneven lattice spacing in three principle directions. Therefore applying a single value of d_0 is likely to introduce significant error in strain calculation [7], [13]. For this reason, position-dependent values of d_0 have been used for the calculation of the residual stresses [3], [13].

However under certain conditions where the compositional variations are within an allowance range, the reference value d_0 can be taken from either the far-field region of the sample [11] or an averaged of measured values throughout the specimen [5], [8], [14].

In this study, relative strains which are defined as the relative changes in lattice spacing in various reference samples were characterised and compared in the axial, hoop and radial directions. From this analytical procedure, values of d_0 could be found whether independent to the measurement directions and/or locations or identical in prepared reference samples. Also, suitable forms of the d_0 samples for measurement were explored.

5.3.2 De-convoluted lattice spacing in flat samples

The flat samples, either in a form of comb or thin slice, were manufactured in a sufficient small thickness such that the out-of-plane stress in the hoop direction could be assumed negligible. Instead of selecting a d_0 value from far-filed of the sample or using an averaged value, de-convoluted lattice spacing (denote as d_c) was used to evaluate the variations of the relative strains within the reference samples. At

each measurement point, a value of d_c was determined using inversed Hook's Law. This is applied to the values of the three principle lattice spacing d_{xx}, d_{yy} and d_{zz} measured from neutron diffraction technique. Macro-stresses in the hoop direction in the flat samples were assumed to be thoroughly relieved:

$$\sigma_{yy} = \frac{E}{(1+\nu)(1-2\nu)}[(1-\nu)\varepsilon_{yy} + \nu(\varepsilon_{xx} + \varepsilon_{zz})] = 0 \quad (5.1)$$

therefore, the hoop strain and the associated d_c can be calculated using the following equations:

$$\varepsilon_{yy} = \frac{d_{yy}-d_c}{d_c} = \frac{\nu\,(\varepsilon_{xx}+\varepsilon_{zz})}{\nu-1} \quad (5.2)$$

$$d_c = \frac{(1-\nu)d_{yy}+\nu(d_{xx}d\varepsilon_{zz})}{(1+\nu)} \quad (5.3)$$

In this assumed plane stress condition in which the hoop macro-stress is zero, the variation of the measured d_c values at the selected locations may reveal an inherent difference in lattice spacing of the weld, HAZ and parent metal. In the flat sample, the variation of the d_c is illustrated as strain relative to a reference value d_c^0, which is obtained by averaging the values of dc at several measurement points in the parent metal:

$$\varepsilon_c = \frac{d_c - d_c^0}{d_c^0} \quad (5.4)$$

Figure 5.9 shows the selected locations from in the comb and flat samples where the values of d_c^0 were calculated using inversed Hook's Law. In the as-welded condition, d_c^0 was calculated from the selected locations on comb sample. The variations of d_c, hence the relative strains in both comb and thin slice samples were compared.

For heat-treated samples, d_c^0 was obtained from the measurement points in the thin slice d_{03} which was heat treated entirely in the furnace with its accompanied pipe. This full body PWHT is believed to be the most effective procedure for the relief of the residual stresses. Relative strains in the other heat-treated thin slice samples were compared to this d_c^0 in order to understand the relative change of the lattice spacing in the d_0 samples that underwent various local PWHT procedures.

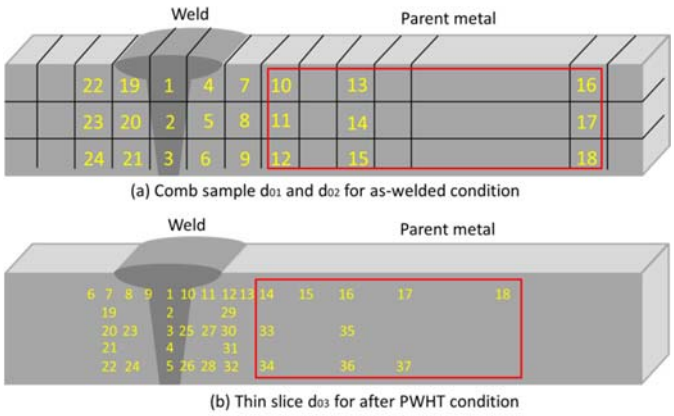

Figure 5.9 Selected locations in parent metal of the sample to obtain d_c^0

5.3.3 Averaged lattice spacing in cuboid samples

Relative strains in three principle directions were evaluated in the weld and parent metals of the cuboid samples. A reference value d_{ave}^0 was obtained by averaging all measured d_0 values in the hoop direction from the parent metal. The method of obtaining $d\,{}_{ave}^{0}$ from the parent metal of the cuboid samples was applicable for both as-welded and after the stress relief process.

After determining the value of d_{ave}^0 for cuboid samples, the relative strains could be compared to firstly, demonstrate the difference in lattice spacing in weld and parent metal. Secondly, compositional variations in either the weld or parent metal would be examined through the thickness of the pipe wall. In addition, the sensitivity of the relative strains with respect to the direction of the measurements may be also brought to light.

5.3.4 Relative strain calculation and comparison

Selecting an accurate d_0 value from the reference sample can reduce the risk of underestimating the residual stresses in the structures. Therefore, it is essential to determine the correct type of the reference samples for specific stress analysis. Since it was uncertain that any selected values of the d_0 could be exactly strain-free, the primary interest is to understand the relative changes in strain distributions, rather than the absolute values in the reference samples.

In this study, the values of either d_c^0 from flat samples and d_{ave}^0 from cuboid samples was used as an assumed “strain-free” lattice parameter to determine the

relative strain state in the corresponding samples. Relative strains in three principle directions were determined using the following equations:

$$\varepsilon_{rel} = \frac{d - d_c^0}{d_c^0} \tag{5.5}$$

$$\varepsilon_{rel} = \frac{d - d_{ave}^0}{d_{ave}^0} \tag{5.6}$$

where d is the lattice spacing of the material at any point measured using neutron diffraction, in either axial, hoop or radial direction.

Comparisons of the relative strains in comb, thin slice and cuboid samples were made under the same thermal condition [6]. Using these different types of samples is expected to indicate the effectiveness of different manufacturing methods on the macro-stress relief. And the other assumption is that the extent of the strain variations across the weld, HAZ and parent metal, if measurable, can be affected by the inherent lattice spacing due to various metallurgical composition in conjunction with the retained stresses.

As introduced in Chapter 4, the error propagation method [15] was used to determine the error of the lattice spacing measured in reference samples. The (fitting) uncertainties are estimated not to exceed 100 micro-strains.

5.4 Result analysis

5.4.1 Variation of the de-convoluted lattice spacing

The comparison of the calculated values of the de-convoluted lattice spacing in comb samples d_{01} and d_{02}, in as-welded condition, are shown in Figure 5.10. The de-convoluted relative strains in the parent metal vary within a range of ±50με; Showing a small deviation of the de-convoluted values of the lattice spacing d_c to their averaged value d_c^0. Since a plane stress condition was assumed in hoop direction, lattice spacing of the parent metal are suggested close to strain-free condition. Therefore, value of d_c^0 was used for the calculation of the relative strains in all the welded reference samples (Equation 5.5). Moreover, a good agreement of relative strains in d_{01} and d_{02} at corresponding measurement locations proved the extent of stresses relief in the samples were similar using EDM.

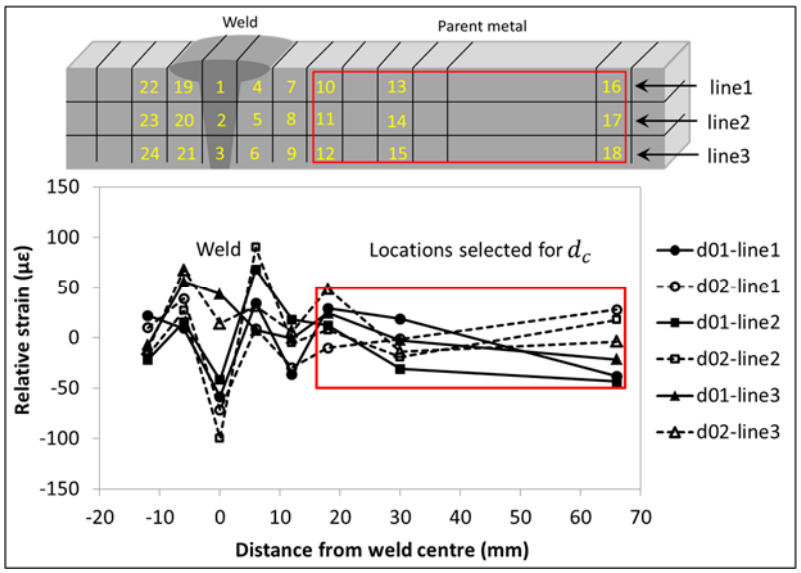

Figure 5.10 Variations of the de-convoluted lattice parameters in comb samples in as-welded condition

The value of d_c^0 was obtained from a heat-treated thin-slice reference sample d_{03}. The relative changes in the de-convoluted lattice spacing d_c were evaluated at the three lines and two additional points at weld centre (Figure 5.11).

The variations of the d_c at the selected points are less than ±25με, which was an even better strain-free condition achieved from PWHT procedure. Therefore, the value of d_c^0 , obtained from d_{03}, was used as a datum for the subsequent calculation of the relative strains in all reference samples which were locally heat treated for stress relief.

However, bigger variations of d_c were revealed in comb samples d_{01} and d_{02} in as-welded condition. The relative strains of the d_c vary from +50με to -150με in the weld metal. While after furnace PWHT, the magnitudes of the relative strains in the weld region of the thin-slice d_{03} exhibit only negative values, which could be as low as -150με.

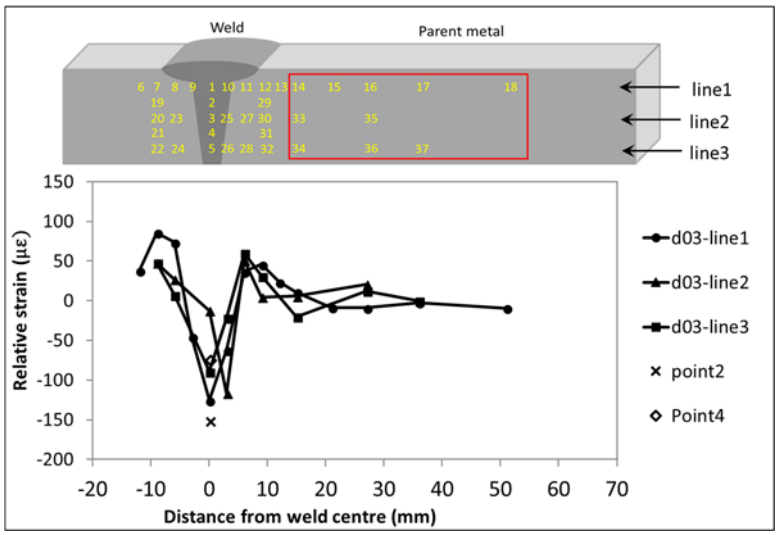

Figure 5.11 Variations of the de-convoluted lattice spacing in d_{03} after furnace PWHT

It can be concluded from these initial comparisons that first of all, the weld and parent metals used in this study have different values of the inherent lattice spacings. Then, from the results of Line3 in both Figure 5.10 and Figure 5.11, the relative strain variations in comb samples might be caused by a certain level of residual stresses unrelieved near the weld root (due to the requirement of the EDM cutting to maintain the sample configuration or there exists the chemical compositional variation through the thickness of the weld).

It has been suggested elsewhere [7] that material near the weld cap of the comb samples has least constrains from the surrounding material in weld region. Therefore, the value of the lattice spacing from the end of the tooth of comb samples were used as the strain-free reference due to fewer errors.

5.4.2 Evaluation of the relative strains in flat samples

Relative strains in the comb and thin-slice samples were evaluated in in both as-welded condition and after PWHT procedures. As shown in Figure 5.12, the profiles of the relative strain, with respect to the three principle directions, would be compared along weld centreline (red marks) as well as the line-scan directions. Three main line-scans were carried out at 3mm below the (pipe) outer surface, at mid-thickness and at 3mm above the (pipe) inner surface.

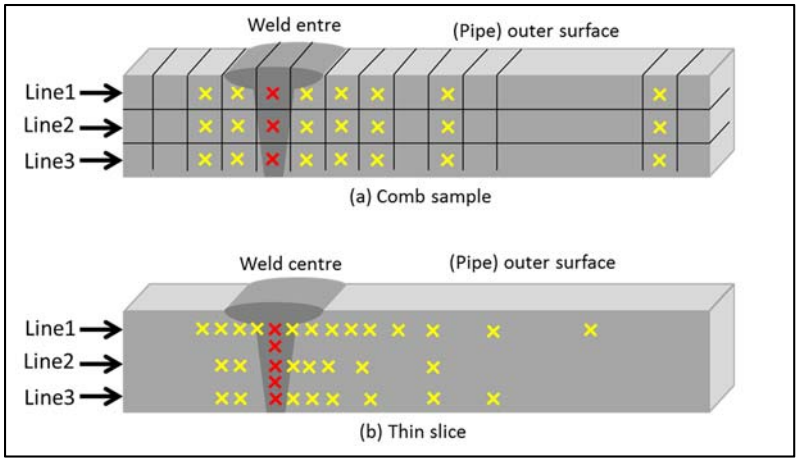

Figure 5.12 Measurement locations in comb and thin-sliced samples

The results of the relative strain profiles are demonstrated in subsequent sections 5.4.2.1 (as-welded condition) and 5.4.2.1 (PWHT condition). More measurements results from cuboid samples, either extracting from the weld region or far-field parent material will, be shown subsequently. This investigation was aimed at examining if the values of the lattice spacing, in the similar material, were direction-dependent and/or might vary from point to point in measurement each direction.

5.4.2.1 In as-welded condition

5.4.2.1.1 Weld centreline

The changes in the relative strain distribution and the magnitude in the comb samples d_{01} and d_{02} and thin-sliced samples d_{03} and d_{04} were compared in as-welded condition. The relative strain plots at the weld centreline are shown in Figure 5.13.

At weld centreline, comb samples d_{01} and d_{02} exhibit similar trends and values of the relative strains. Axial (Figure 5.13a) relative strains are in negative values, varying from the magnitude of -100με to -200με approximately. Similar behaviour has been observed in hoop direction (Figure 5.13b) but the calculated relative strain values were close to zero with max +100με to minimum -100με. Relative strains in radial direction (Figure 5.13c) display an acceding trend with a value from less that -200με near the cap to almost zero close to the root.

In contrast, the patterns as well as the magnitudes of the calculated relative strains in the thin-slice samples d_{03} and d_{04} are in good agreement. However, variations were

observed along the weld centreline. For instance, high axial relative strains (Figure 5.13a) which were over 400με existed at the regions near the weld cap while dropped sharply to less than -200με and maintained to the region close to the root.

With regard to the hoop relative strains (Figure 5.13b), a value of 200με occurred at the locations at upper half of the weld in compression and at the lower half in tension. Radial relative strains (Figure 5.13b) near the cap and root were in the similar level as that in the comb samples while at the rest of the corresponding locations, strains were in tension.

By comparing the relative strain profiles of the flat reference samples, it is known that first of all at weld centreline, thin-slice samples contained higher strains magnitude than those in comb samples, especially for axial strain components. It was proved that introducing the additional slits on the flat sample in this direction allowing the stresses further relieved.

Besides, as relative strains in comb samples did not vary in the same range while they were prepared with strain relieved at three directions, lattice spacing at these principle directions might not be the similar values when subjected to zero strains.

In addition, comb samples only exhibited strain variation in radial direction; therefore, it was of an interest to compare the strain condition in the comb and cuboid samples subsequently to understand if the strain-free lattice spacing at weld region was sensitive to the specific locations where material was deposited.

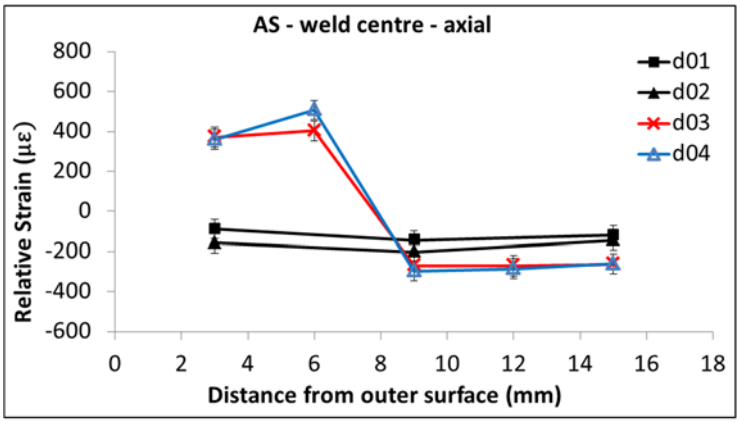

(a) Axial relative strains at weld centre

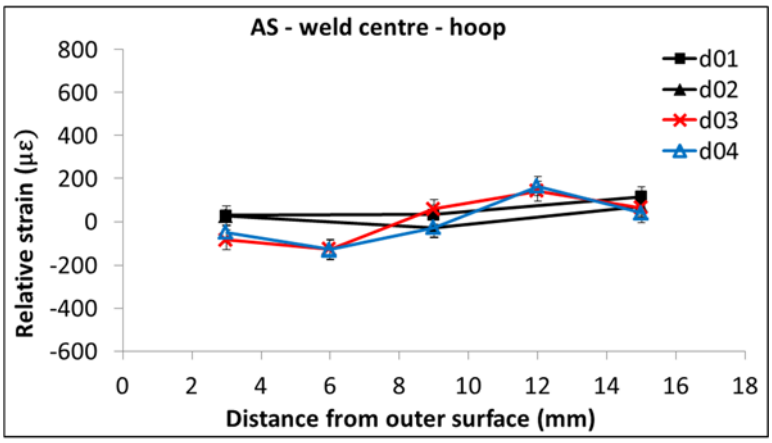

(b) Hoop relative strains at weld centre

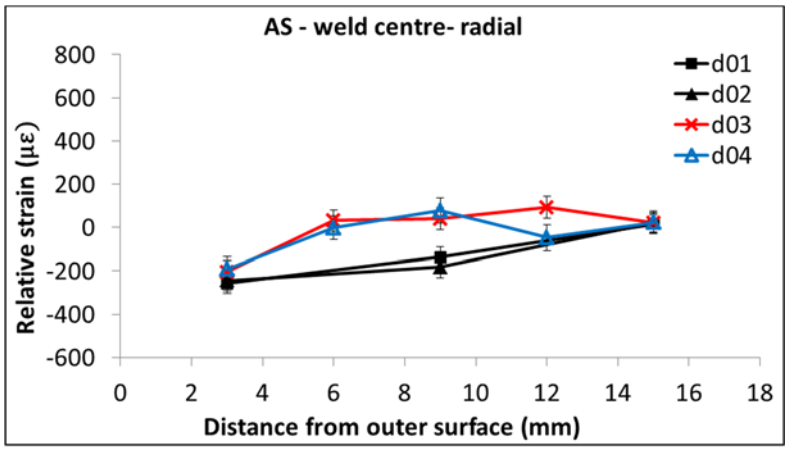

(c) Radial relative strains at weld centre

Figure 5.13 Relative strains at the weld centre of the comb and thin slice samples in as-welded (AS) condition

5.4.2.1.2 Axial line-sans

The profiles of the relative strains in the comb (d_{01} and d_{02}) and thin–slice samples (d_{03} and d_{04}), in three principle directions, from line-scans are shown in Figure 5.14, Figure 5.15 and Figure 5.16, respectively. Beyond the location 20mm from the weld centreline, the magnitudes of the relative strains, for all the reference samples, were around zero value in parent metal. While at the weld metal and the region adjacent to it significant variations of the relative strains were observed.

For comb samples d_{01} and d_{02}, relative strain variations are only observed at weld centre in axial and radial directions while for hoop they were in negligible values. The trend of the strain variations along the weld are as those discussed in previous section. In comparison with the slice sample d_{03} and d_{04}, significant strain variations were revealed at weld metal region closed to the cap.

In line1, axial relative strains of d_{03} and d_{04} soared into 600με where 3mm from the weld centreline and greatly reduced to near zero value at toes (Figure 5.14a). Hoop and radial relative strains displayed variations ranging 200με and 400με, respectively, in compression (Figure 5.14b and Figure 5.14c) but decreased to near zero value where approximately ±10mm from the weld centreline.

In the weld and HAZ of the line2 and line3, axial relative strains varied less significantly and the distributions were similar as those in comb samples; i.e. the magnitudes were averagely 100με higher in compression (Figure 5.15a and Figure 5.16a). Hoop and radial relative strains at line 2 were slightly in tension but less than 200με (Figure 5.15b and 5.15c); while near the root, they shown least variations in thin slice samples (Figure 5.16b and 5.16c).

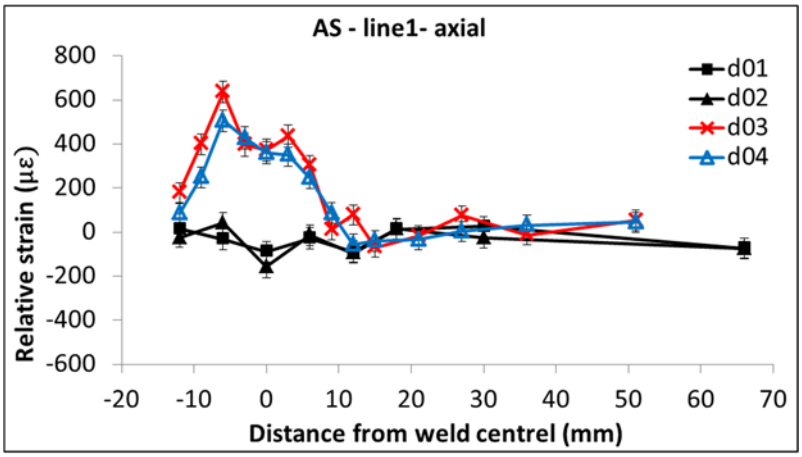

(a) Axial relative strains of line 1

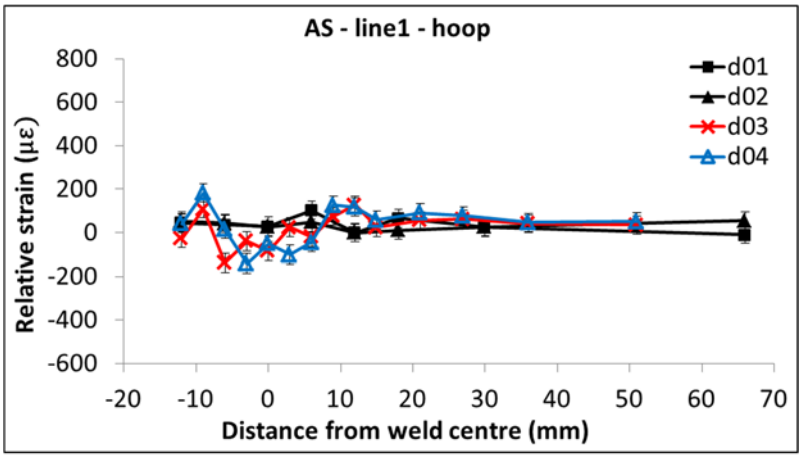

(b) Hoop relative strains of line 1

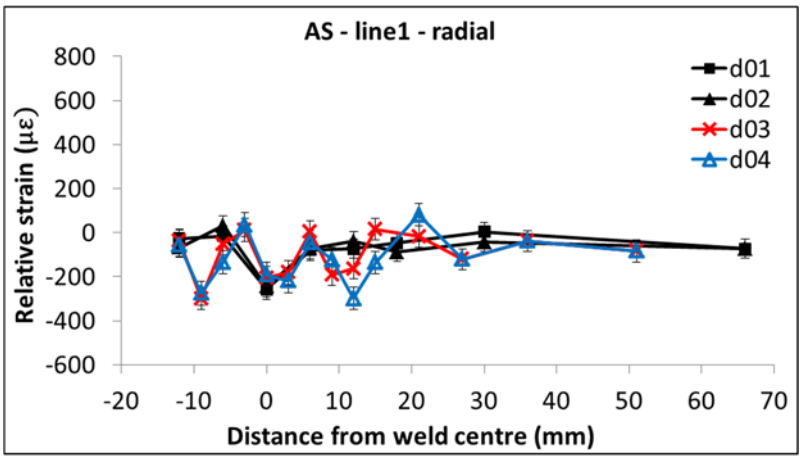

(c) Radial relative strains of line 1

Figure 5.14 Relative strains of line1--3mm below the (pipe) outer surface in as-welded condition

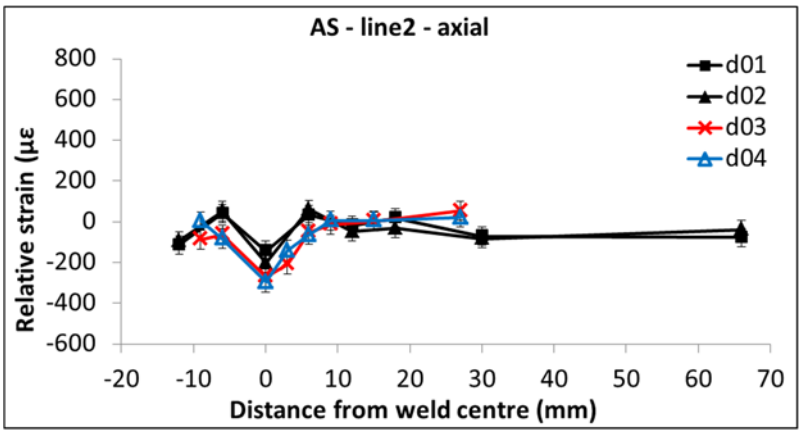

(a) Axial relative strains of line 2

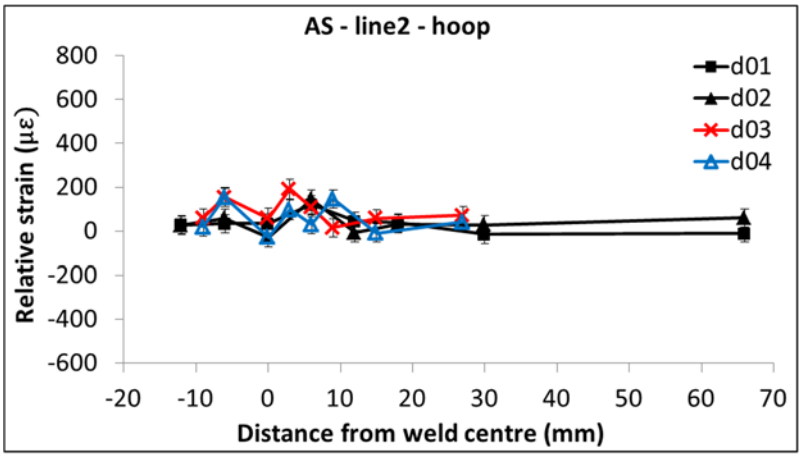

(b) Hoop relative strains of line 2

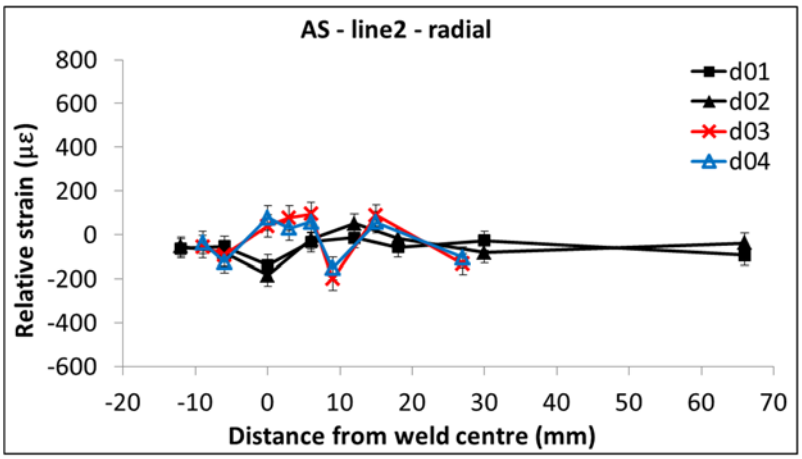

(c) Radial relative strains of line 2

Figure 5.15 Relative strains of line2--mid-thickness of (pipe) wall in as-welded condition

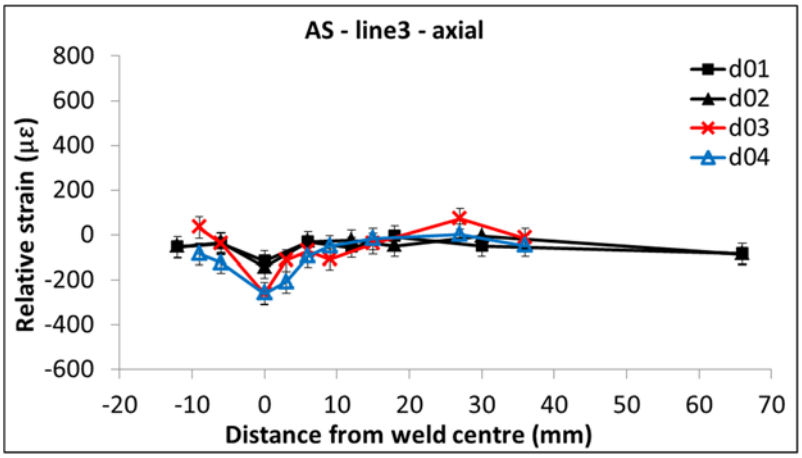

(a) Axial relative strains of line 3

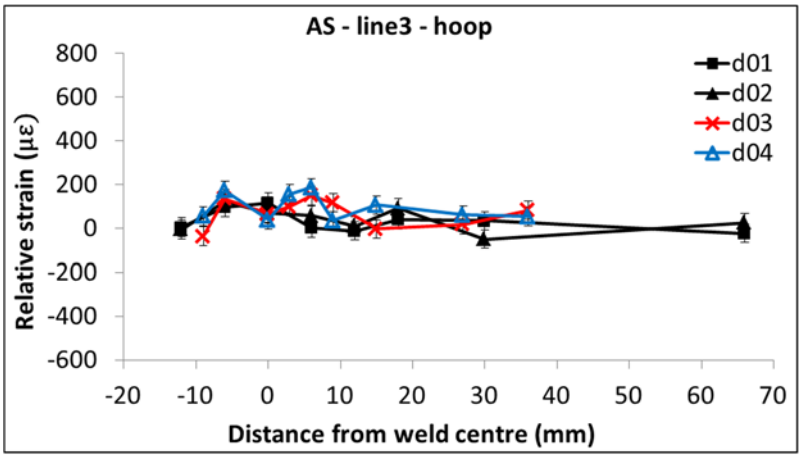

(b) Hoop relative strains of line 3

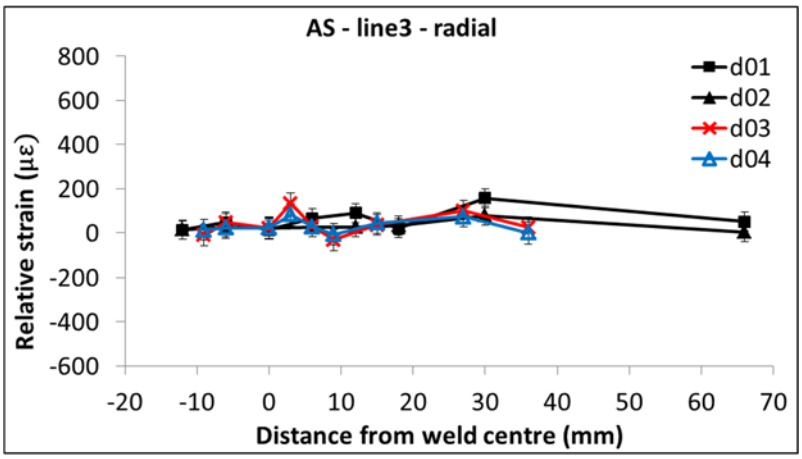

(c) Radial relative strains of line 3

Figure 5.16 Relative strains of line3--3mm above the (pipe) inner surface in as-welded condition

It is concluded that, first of all, constant relative strains in the parent metals of all the reference samples indicated similar lattice spacing values of the materials after stress relief. Besides, the relief of the residual stress in axial direction in the thin slice samples is least effective. Accordingly, it is recommended not to apply thin slice sample directly as a reference for residual stress calculation unless its own stress states are known.

5.4.2.2 After stress relief

5.4.2.2.1 Weld centreline

After post weld heat treatment, the relative strains, in the five d_0 (samples d_{02}, d_{03}, d_{04}, d_{05} and d_{06}), along weld centreline were remeasured. As shown in Figure 5.17, no significant variations in the relative strains were observed from cap to root in all three directions and the relative strains were consistently in the negative magnitude ranging from 0 to -200με.

The axial relative strains measured from thin slices d_{03} and d_{04} (Figure 5.17a) which were over 400με near the cap region before heat relief (Figure 5.13a), greatly reduced to the strain level equivalent to those in comb sample d_{02}. Because d_{05} and d_{06} were assumed to exhibit the same level of strain in as-welded condition as that of d_{03} and d_{04}, the residual stress induced from welding were believed to have been relieved through local post weld heat treatment.

In hoop and radial directions (Figure 5.17b and Figure 5.17c), the relative strains near the root were less negative than those close to the cap. Nevertheless, the strains were still in the range of 200με considering the error margins. It can be deduced that either local or global post heat treatment could both achieve the same level of strain/stress relief as long as the thermal cycles were identical.

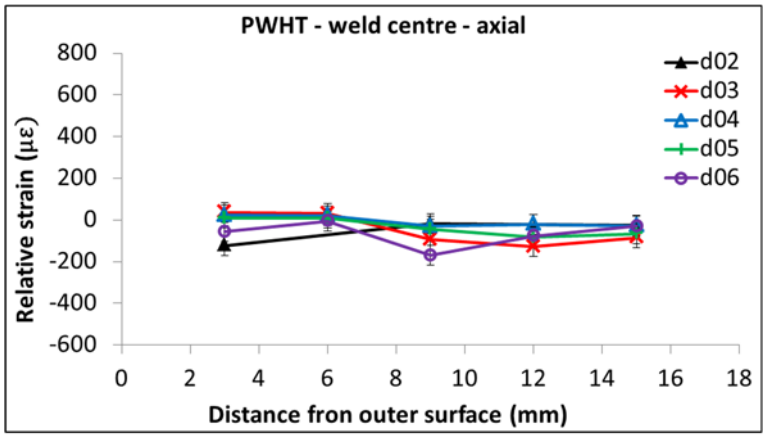

(a) Axial relative strains at weld centre

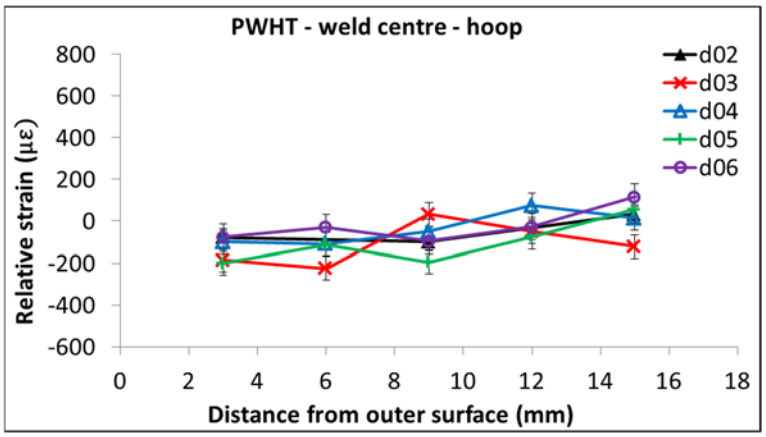

(b) Hoop relative strains at weld centre

1

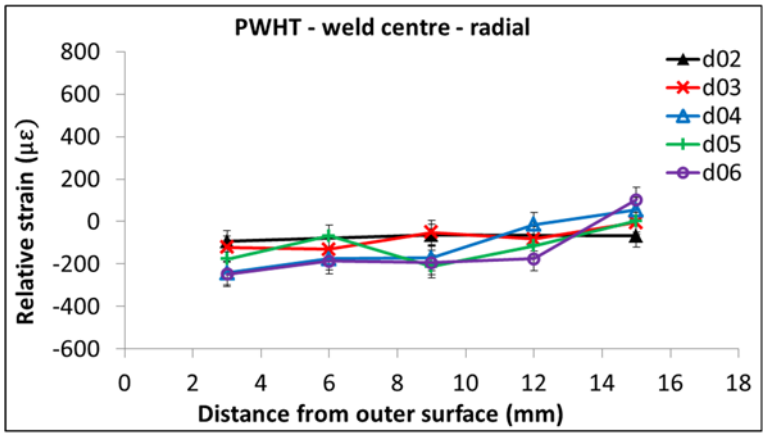

(c) Radial relative strains at weld centre

Figure 5.17 Relative strains at the weld centre of the comb and thin slice samples after PWHT

5.4.2.2.2 Axial line-scans

The results of the three-axial line-scans are presented in Figure 5.18, Figure 5.19 and Figure 5.20. The relative strains in the weld were maximum 200με in compression while in the parent metals they were varied around 0με. In the parent metal of all samples, the comb sample d_{02} and thin slice d_{03} exhibited the least variations around zero value in all three directions. Thin slice d_{03} with its accompanied pipe were heat treated in the furnace which was believed to be most efficient method for stress relief. In comparison, although comb sample d_{02} was locally heat treated its grid-like configuration allowed it to achieve greater degree of stress relief.

Along Line1, tensile relative strains have been observed in the parent metal of thin slice samples in the axial direction (Figure 5.18a). The highest value of the relative strain was 200με in d_{04} at a location 36mm from weld centreline. In the hoop direction, sample d_{05} varied with a larger range from weld to parent metal. The magnitudes of the relative strains were -200με at the weld centre and at approximately 20mm away it peaked at 200με (Figure 5.18b). Thin slice d_{06} which had been heat treated with the narrowest band showed the highest compressive relative strain in the weld in radial direction (Figure 5.18c). At 51mm away from weld metal, the relative strains, in all the directions, in all the reference samples were nearly 0. At far field of the parent metal, the zero value of the relative strain illustrated that the material was in the strain-free condition.

Along line2 and line3, the relative strains in parent metal were only measured at a few points at approximately 30mm from the weld centreline (Figure 5.19 and Figure 5.20). Strain magnitude in the parent metal varied within in a range of ±100με in axial, hoop and radial directions. While in comb sample d_{02} the relative strain variations was least pronounced, i.e.±50με.

The variations in relative strains from the weld to the parent metals suggested that lattice spacings of the materials were significantly different. In light of this, the calculation of their residual stresses in the pipe girth welds in either as-welded or after PWHT conditions, it was crucial to differentiate the strain-free d_0 values by the measurement direction, macro region (parent metal or weld), and if possible by the micro material regions (i.e. coarse-grained or fine-grained or HAZ). Material lattice

spacing of the cuboid samples was subsequently examined to understand if they were showing similar variation.

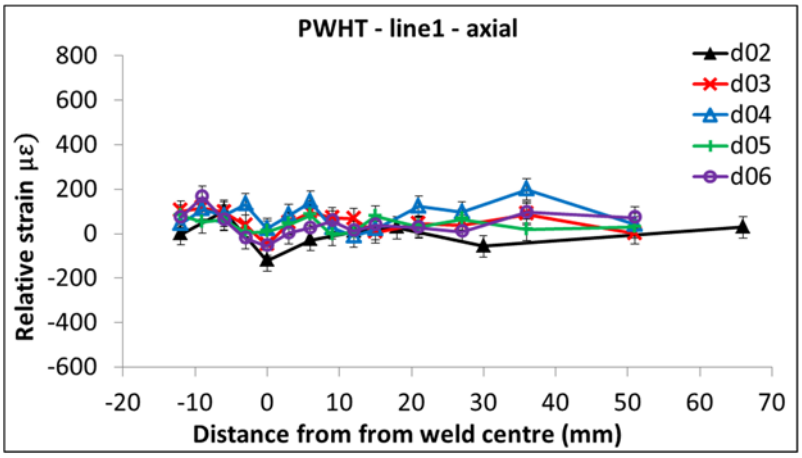

(a) Axial relative strains of line 1

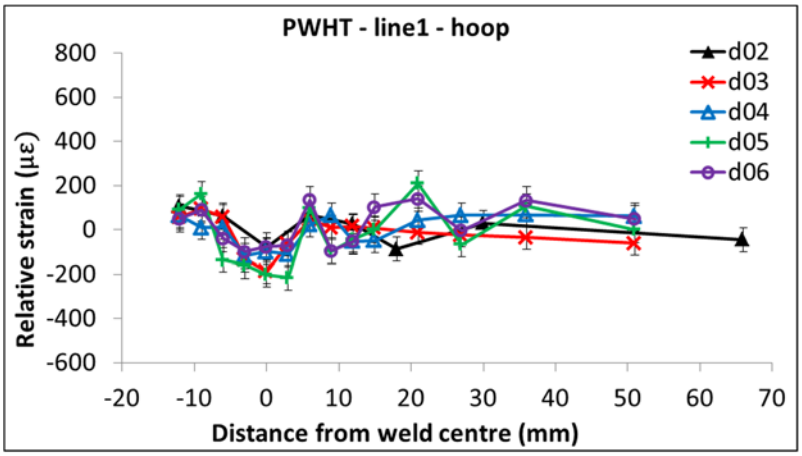

(b) Hoop relative strains of line 1

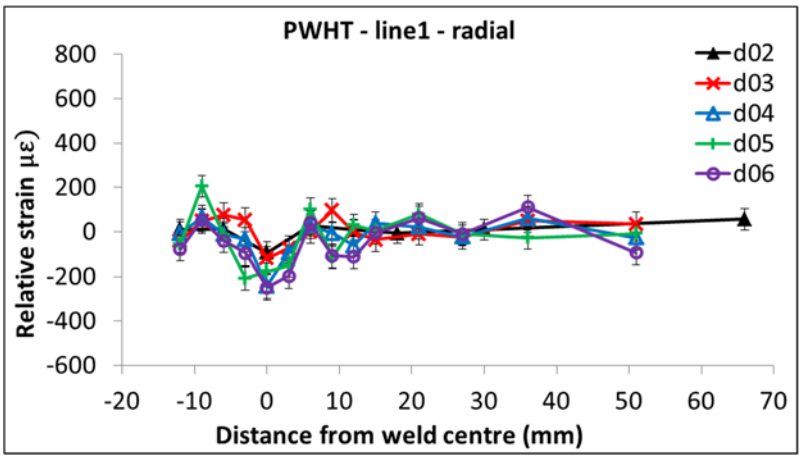

(c) Radial relative strains of line 1

Figure 5.18 Relative strains of line1--3mm below the (pipe) outer surface after PWHT

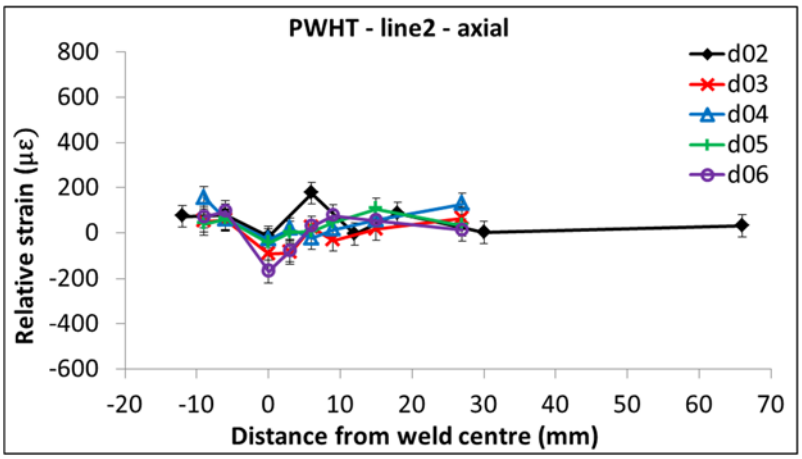

(a) Axial relative strains of line 2

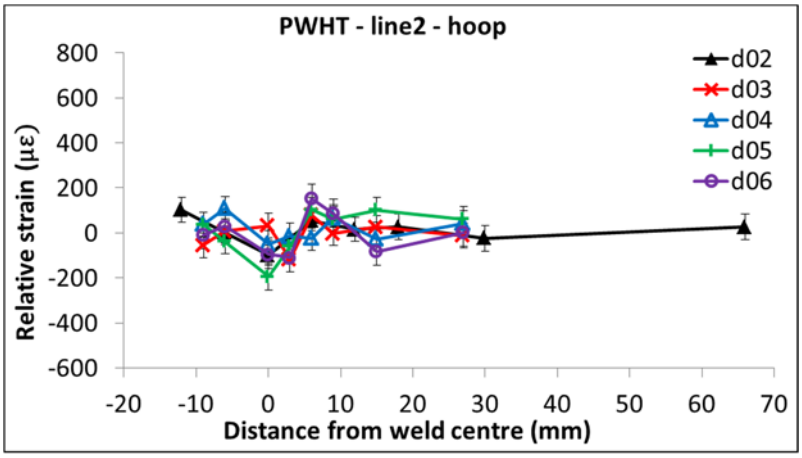

(b) Hoop relative strains of line 2

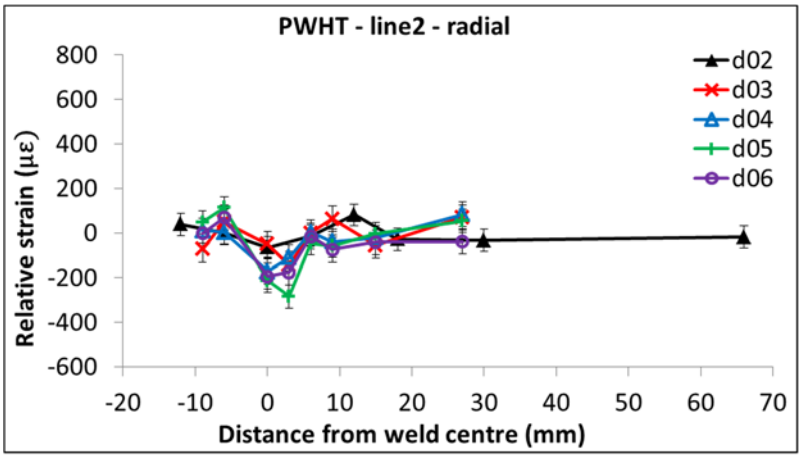

(c) Radial relative strains of line 2

Figure 5.19 Relative strains of line2--mid-thickness of (pipe) wall after PWHT

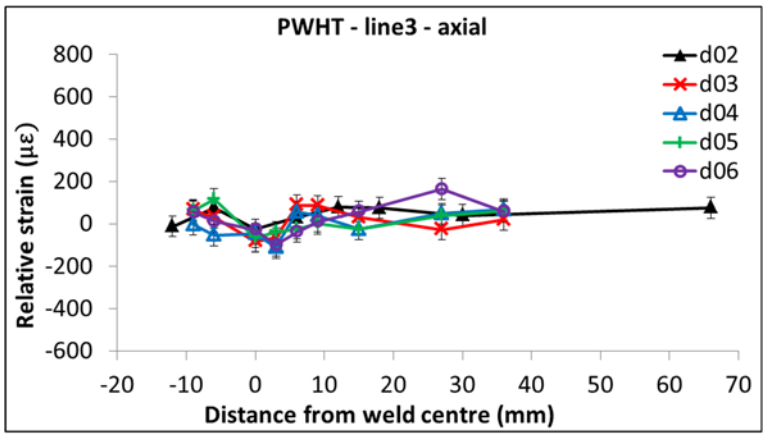

(a) Axial relative strains of line 3

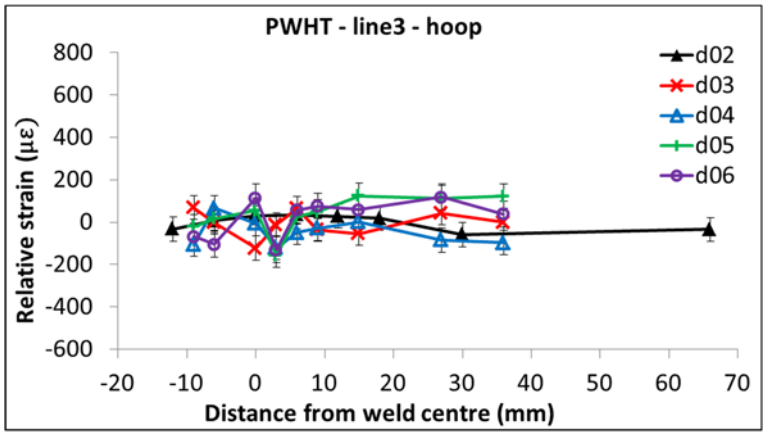

(b) Hoop relative strains of line 3

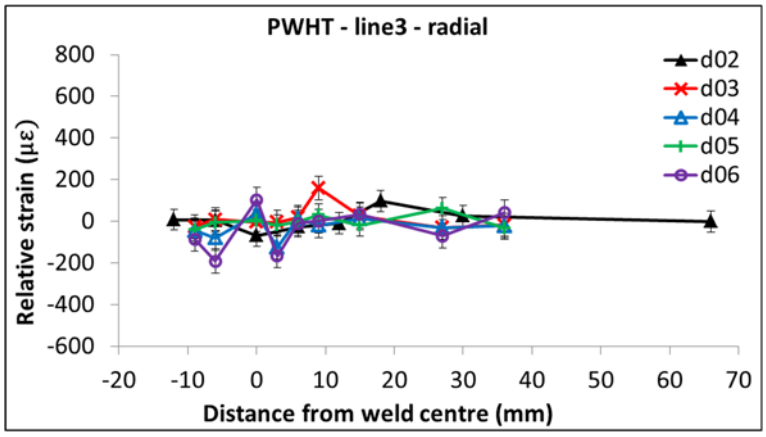

(c) Radial relative strains of line 3

Figure 5.20 Relative strains of line3--3mm above the (pipe) inner surface after PWHT

5.4.3 Evaluation of relative strains in cuboid samples

5.4.3.1 In as-welded condition

Excision of the comb sample into small cuboid samples allowed further relaxation of residuals stresses. The results of the relative strain of these specimens are shown in

Figure5.21. Similar to earlier observation, the parent metal showed negligible variations in the lattice spacing in all three principle directions (Figure5.21a). The strains in the weld were less consistent. Variations up to approximately -380με has been observed in weld metal in the radial direction (Figure5.21b).

Most measurements (for each direction) showed the strains vary within the range of ±100με between the smallest and largest measurement values, suggesting that compositional gradient at microscopic level did not significantly affect the lattice spacing. The lattice spacing of the weld metal were more direction-dependent and less dependent on position.

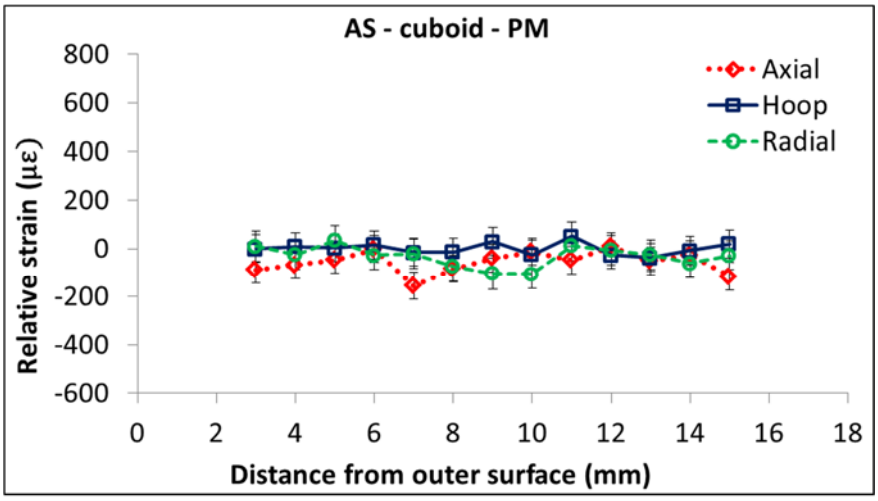

(a)

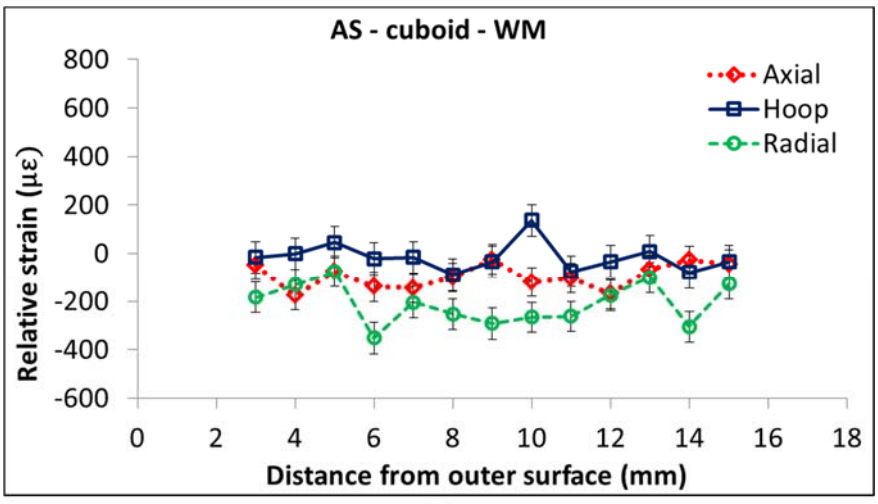

(b)

Figure 5.21 Relative strains in the (a) parent metal (PM) and (b) weld metal (WM) of the cuboid samples in as-welded condition

5.4.3.2 After stress-relief

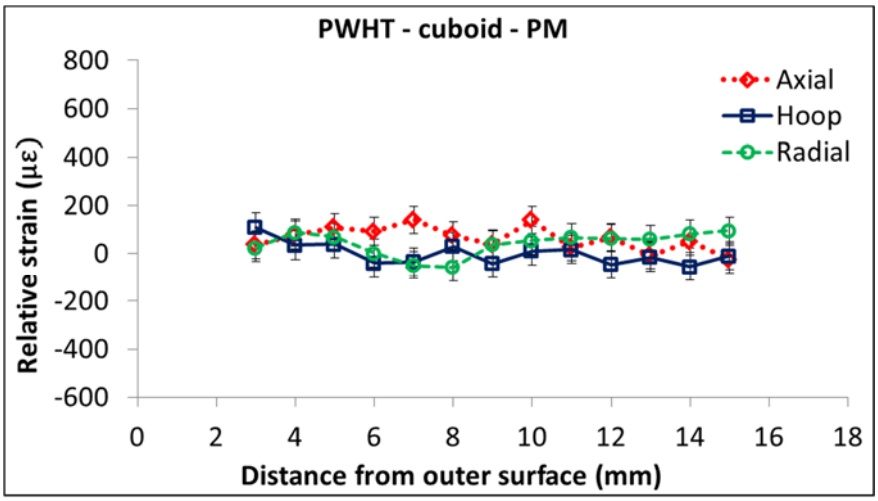

(a)

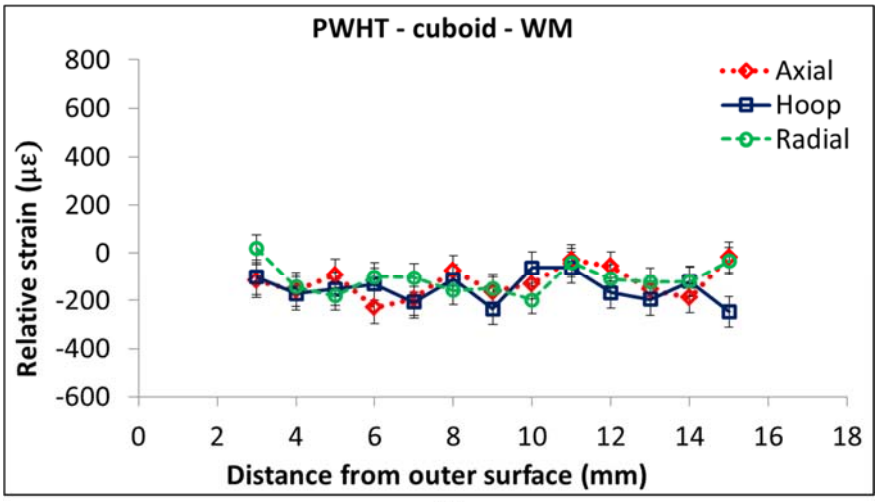

(b)

Figure 5.22 Relative strains in the (a) parent metal (PM) and (b) weld metal (WM) of the cuboid samples after PWHT

The overall shifts in the relative strains between weld (Figure 5.22b) and parent metals (Figure 5.22a) could be interpreted as the difference in the absolute lattice parameters. In addition, the relative strains of the cuboid samples, in terms of the measurement directions, showed less significant variation in the same material. Stress relief was more efficient and uniform in all three directions especially when a smaller sample in cuboid shape as used. When determining residual stresses in a post heat treated weldment, the averaged values of strain-free lattice parameters, from either the weld or base material of cuboid samples, can be used accordingly.

5.5 Discussion

5.5.1 Stress relief in various samples

The presentation of results obtained from various reference samples allowed the users to examine the effectiveness in measured lattice spacing using various samples. This could be used to establishe effect of reference sample configuration and manufacturing methods on stress relief in both as-welded and after PWHT conditions.

When determining level of residual stresses in a component in as-welded condition, selected reference (strain-free) samples was manufactured using mechanical cutting for stress relief. For instance, in this study samples were prepared in configurations as flat, comb, and cuboid for stress relief. In contrast, residuals stresses after PWHT would be determined using values of lattice spacing in these reference samples which also experienced heat treatment.

The results of the lattice spacing obtained from the parent metal of the reference samples showed parent metal was practically strain-free within the error range, so the discussion in following sections would only concentrated to discuss the effect of the using various reference samples to obtain lattice-spacing in weld metal.

5.5.2 Comparison of relative strains in samples in as-welded condition

The results relative strains in comb (d_{01} and d_{02}) and cuboid samples shown in Figure 5.23 suggested that the measured d-spacing from both samples could be used for the calculation of weld metal residual stresses.

It was observed relative strains varied in range of 0 to -200με in axial direction (Figure 5.23a), 100με to -100με in hoop direction (Figure 5.23b) and -100με to -300με in radial direction (Figure 5.23c) in the weld metal of cuboid samples. Since there was no significant variation of the relative strains in weld metal in each direction, averaged value of lattice spacing (for each direction) could be used for the calculation of weld metal residual stresses.

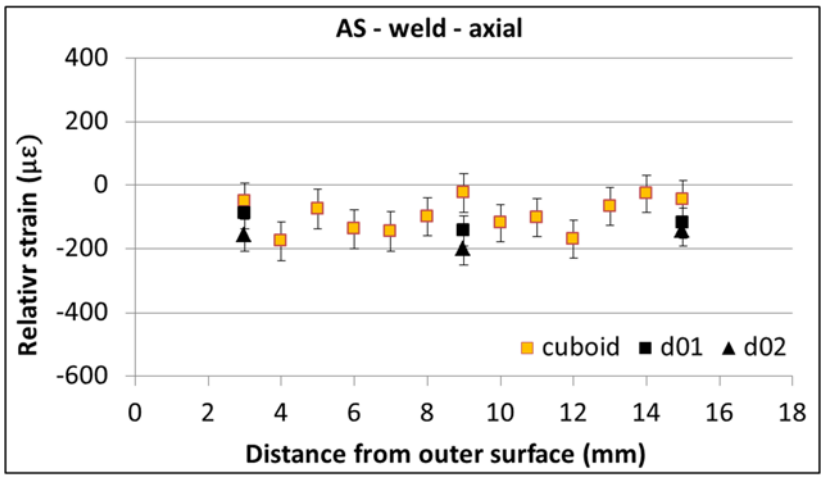

(a)

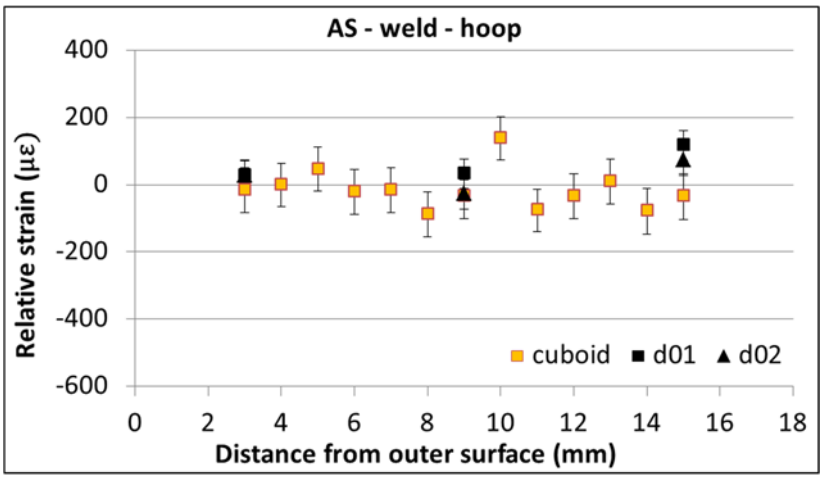

(b)

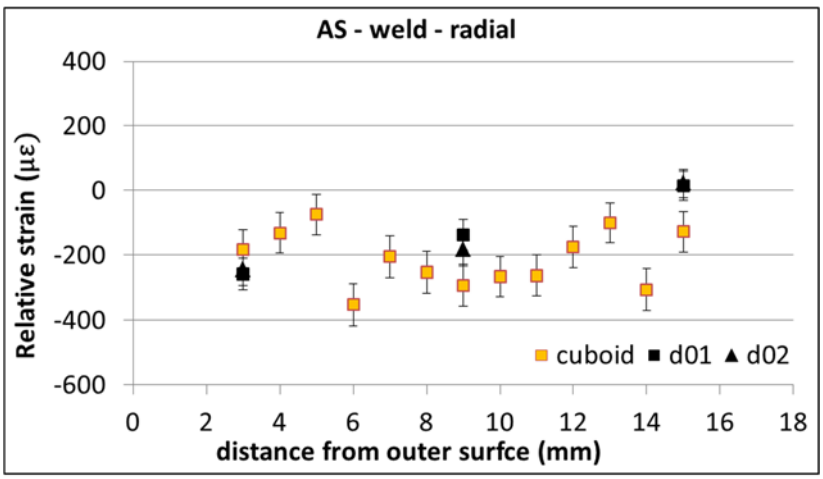

(c)

Figure 5.23 Comparisons of the relative strains in the weld of the cuboid and comb samples in (a) axial (b) hoop and (c) radial directions in as-weld condition

Similar results were observed in comb samples except for that in radial direction (Figure 5.23c), obtained relative strain values near weld root (at 15mm distance from

outer surface) was not in the error range. It could be believed in comb samples, material closer to the root had higher restraint in radial direction when manufacturing therefore in this direction relative strains in comb samples exhibited large value. Averaged value of measured lattice spacings still could be used if it is in the error range.

5.5.3 Comparison of relative strains in samples after PWHT condition

The results of relative strains obtained in section 5.4.2 have showed that the level of axial relative strains in weld metal of thin slice samples (d_{03}, d_{04}, d_{05}, d_{06}) have been dropped to the strain level similar to that of comb sample (d_{02}) after PWHT, which could be only observed in hoop and radial directions in as-welded condition.

Relative strains of the weld metals in three principle directions in various reference samples, after PWHT, were compared in Figure 5.24. It was observed the relative strains were within similar error range for using either furnace (for d_{03} and cuboid samples) or local PWHT (for d_{02}, d_{04}, d_{05} and d_{06}) process.

Relatives strains in all directions of all the weld metals were varied in the range from 0 to -200με. Therefore, using an averaged value of the d-spacing from post weld heat treated samples, either flat (comb or thin slice) or cuboid samples, as a strain-free lattice spacing was unlikely to introduce significant errors when determining residual stresses after PWHT process.

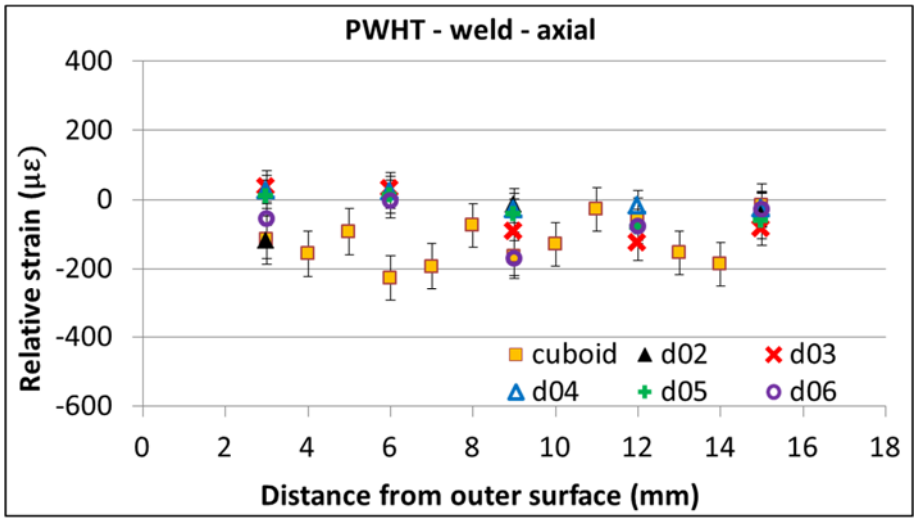

(a)

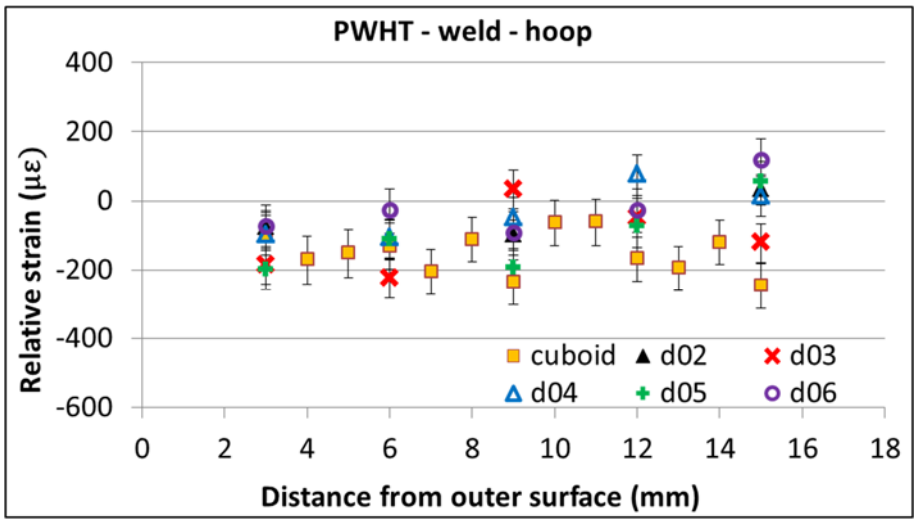

(b)

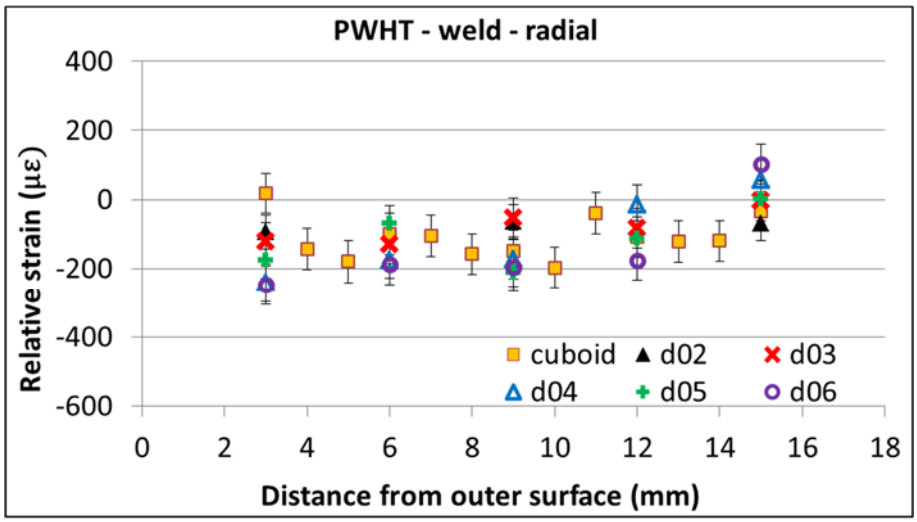

(c)

Figure 5.24 Comparisons of the relative strains in the weld of the cuboid and flat in (a) axial (b) hoop and (c) radial directions after PWHT

5.5.4 Reference sample design

To obtain strain-free lattice spacing values from reference samples, both mechanical cutting and heat treatment could be conducted for stress relief. In as-welded condition, only mechanical cutting was used. Since residual stresses in thin slice were not completed relieved, introducing grid/teeth in the reference samples allowed stresses in axial and radial directions further relieved.

Comb samples with a grid-like configuration is highly recommended. First of all, it improves the efficiency of the neutron diffraction measurement process. Preparation of the samples takes less time than manufacturing small cuboid sample or some

comb samples with narrower teeth and gap which also requires smaller neutron gauge volume, which are even more time and resource consuming. In addition, this sample contains almost the entire configuration of the weldment and can be used for the stress states evaluation in both as-welded condition and after PWHT procedure.

Obtaining lattice spacing from smaller cuboid sample could achieve best results in this study. Residual stresses in the material of interest could be relieved in all three directions. Especially in multi-pass weld or thick section, the effect of chemical composition on lattice spacing at various locations can be revealed from the variation of the relative strains.

5.6 Concluding remarks

This chapter discussed the designing, preparation and neutron diffraction measurements procedures for the determination of the strain-free lattice parameter, in the different types of the reference samples, in in both as welded condition and after PWHT procedure. Conclusions are drawn as follows:

1. Regardless of the configuration of the samples and their thermal conditions, materials lattice spacing of the parent metal should not be used as reference value for the evaluation of the residual stresses of the weld region.
2. The lattice spacing of parent metal did not exhibit significant variation in terms of the measurement direction and through the thickness (of the pipe). An averaged value of d-spacing was obtained from all the measurement results.
3. The value of the lattice spacing of the comb and cuboid samples produced from a welded joint is readily used as strain-free reference for the calculation of the residual stresses in as-welded condition. The values of d_0 vary with respect to the measurement directions, however it is not necessarily use then as position-dependent variables. For each direction, an averaged value can be used with provided errors range.
4. After either global or local PWHT, the values of the lattice parameters in the weld material were found insensitive to the measurement direction. This means an identical averaged value will be used to derive residual stresses after PWHT.

5. The axial and radial residual strain/stresses were high in thin-slice sample in as-welded condition. Therefore thin-slice sample is not recommended to apply d-

spacing values directly to establish stress state unless it can be demonstrated that the d values obtained are similar to those obtained from thinner slice or comb or cuboid samples.

6. Stress relief in reference samples was achieved using both local and global PWHT processes and the level was stresses were similar. It is recommended local PWHT can be substitute for stress relief as long as it is applied properly and in accordance with a recognised practice.

Reference

[1] P. J. Withers, M. Preuss, A. Steuwer, and J. W. L. Pang, "Methods for obtaining the strain-free lattice parameter when using diffraction to determine residual stress research papers," *J. Appl. Crystallogr.*, vol. 40, pp. 891–904, 2007.

[2] M. T. Hutchings, P. J. Withers, T. M. HOLDEN, and LORENTZEN.T., *Introduction to the characterization of residual stresses by neutron diffraction*. 2005.

[3] S. Paddea, J. a. Francis, a. M. Paradowska, P. J. Bouchard, and I. a. Shibli, "Residual stress distributions in a P91 steel-pipe girth weld before and after post weld heat treatment," *Mater. Sci. Eng. A*, vol. 534, pp. 663–672, Feb. 2012.

[4] B. Chen *et al.*, "In situ neutron diffraction measurement of residual stress relaxation in a welded steel pipe during heat treatment," *Mater. Sci. Eng. A*, vol. 590, pp. 374–383, Jan. 2014.

[5] A. Paradowska, T. R. Finlayson, J. W. H. Price, R. Ibrahim, A. Steuwer, and M. Ripley, "Investigation of reference samples for residual strain measurements in a welded specimen by neutron and synchrotron X-ray diffraction," *Phys. B Condens. Matter*, vol. 385–386, pp. 904–907, 2006.

[6] P. J. Withers, M. Preuss, A. Steuwer, and J. W. L. Pang, "Methods for obtaining the strain-free lattice parameter when using diffraction to determine residual stress," *J. Appl. Crystallogr.*, vol. 40, no. 5, pp. 891–904, 2007.

[7] S. Ganguly, L. Edwards, and M. E. Fitzpatrick, "Problems in using a comb sample as a stress-free reference for the determination of welding residual stress by diffraction," *Mater. Sci. Eng. A*, vol. 528, no. 3, pp. 1226–1232, 2011.

[8] A. M. Paradowska, J. W. H. Price, R. Ibrahim, and T. R. Finlayson, "The effect of heat input on residual stress distribution of steel welds measured by neutron diffraction," *J. Achiev. Mater. Manuf. Eng.*, vol. 17, no. 1–2, pp. 385–388, 2006.

[9] M. T. Hutchings, P. J. Withers, T. M. Holden, and T. Lorentzen, *Introduction to the Characterization of Residual Stress by Neutron Diffraction*, 1 edition. CRC Press, 2005.

[10] A. Krawitz and R. Winholtz, "Use of position-dependent stress-free standards for diffraction stress measurements," *Mater. Sci. Eng. A*, vol. 185, no. (1-2), pp. 123–130, 1994.

[11] P. J. Hutchings, M. T., Bouchard, P. J. & Withers, "Characterization of the Residual Stress State in a Double 'V' Stainless Steel Cylindrical Weldment Using Neutron Diffraction and Finite Element Simulation," in *6th International Conference on Residual Stress*, 2000.

[12] W. Woo, V. T. Em, B. S. Seong, P. Mikula, and G. B. An, "Residual stress determination in a thick ferritic steel weld plate using neutron diffraction," *J. Mater. Sci.*, vol. 47, no. 14, pp. 5617–5623, Apr. 2012.

[13] M. Rogante, "Stress-free reference sample: The problem of the determination of the interplanar distance d0," *Phys. B Condens. Matter*, vol. 276–278, pp. 202–203, 2000.

[14] A. M. Paradowska, J. W. H. Price, T. R. Finlayson, U. Lienert, P. Walls, and R. Ibrahim, "Residual stress distribution in steel butt welds measured using neutron and synchrotron diffraction," *J. Phys.*, vol. 124213, p. 8, 2009.

[15] J. R. Taylor, *An Introduction to Error Analysis*. Oxford University Press, 1982.

6 Residual stress in narrow-gap girth welds

6.1 Introduction

Narrow-gap multi-pass welding is widely used in the pipeline production for its heat input which reduces the magnitude of residual stresses [1]. The relief of the welding residual stresses is generally achieved by applying PWHT which is conventionally to be conducted in an enclosed furnace. For some full scale pipeline structures, PWHT is normally restricted to using local means limited by the equipment availability and working environment condition [2].

In this study the effectiveness of the global (furnace-based) and local PWHT on residual stress relaxation in narrow-gap multi-pass girth welds was investigated. The atomic lattice spacing, *d*, was measured on the pipe spools using neutron diffraction technique in both as-welded and PWHT-ed conditions. Measurement details are described in the following sections.

Neutron diffraction measurement was conducted in this research due to its through-thickness ability and non-destructive nature. The residual strains hence the residual stresses in the pipe spools were determined after measuring the un-strained lattice spacing from a set of reference samples. The residual stress profiles before and after various PWHT were compared. The through-thickness and near-surface stress profiles were also compared with the recommended practice given in British Standard BS 7910 “Guide to methods for assessing the acceptability of flaws in metallic structures” [3] and the UK nuclear R6 procedure [4].

6.2 Neutron diffraction (ND) measurement on pipes

6.2.1 Measurement plan

In this project, all the girth welds (in as-welded condition) were fabricated using identical procedures. Assuming little deviation in terms of heat input, welding speed etc., the residual stresses measurement was carried out only on a few pipe spools before and after PWHT. Pipe spools P2 and P3 which underwent different levels of preheat were selected for the evaluation of the residual stresses in as-welded condition. Partly aimed at verifying the stability of the welding processes, this study also served to investigate the effect of preheat on welding residual stresses.

Details of the PWHT procedures have been introduced in Chapter 3. Table 6-1 summarises the residual stress measurements carried out on each pipe ND technique.

Table 6-1 Summary of the neutron diffraction measurements carried out on the pipes.

Experiments on the pipes		P1	P2	P3	P4
As-welded condition	Preheat	Applied on one side of grove		Applied on both sides of grove	
	Residual stress measurement	Not measured	Measured using ND		Not measured
After PWHT	Heat band width	Furnace	280mm	170mm	430mm
	Residual stress measurement	All measured using ND			

Because the main intention was to investigate the effect of welding procedure under a steady state condition, ND measurements were conducted at 3 o'clock along circumferential position of the girth welds where the effect of start-stop was minimal. It was also assumed that the stress state was symmetric regarding the girth weld at the middle length of the pipe spool, allowing the measurement to be taken only on one side of the weld. This approach enabled an optimal use of the available beam time.

6.2.2 Sample preparation

The longest sample that can be measured by the KOWARI instrument is up to 1000mm. The length of the pipe spools was thus reduced symmetrically to 500 mm at both sides of the girth weld.

Before commencing the neutron scanning, seven stainless steel spheres were attached on to the pipe outer surface and used as fiducial marks. They were located close to the regions where measurements were taken. These fiducial points were used as initial identification points for creating a virtual model for to lay out the measurement points. Thereafter, their exact positions were measured using a touch probe and matched with the virtual positions. In this way it was possible to know accurately where the measurement positions were. This step ensured the sample was aligned correctly to meet the desired measurement requirements.

Due to the nature of the pipe geometry, the neutron beam was forced to penetrate the pipe wall thickness twice when measuring the axial and hoop strain components at

any given location. Therefore, a window cut was introduced which allowed the reflection beam to pass through and reduced the neutron travel path therefore minimized the measurement time.

6.2.3 Measurement design

A virtual model was constructed for the following purposes (Figure 6.1). The dimension of the virtual pipe should represent its actual size. It was not always necessary to acquire the whole geometry if a laser probe could be used to scan the pipe outer surface such that the full length and girth dimensions of the pipe could be obtained. It was also expected the locations and the sizes of the fiducial marks as well as the two window cuts would be captured.

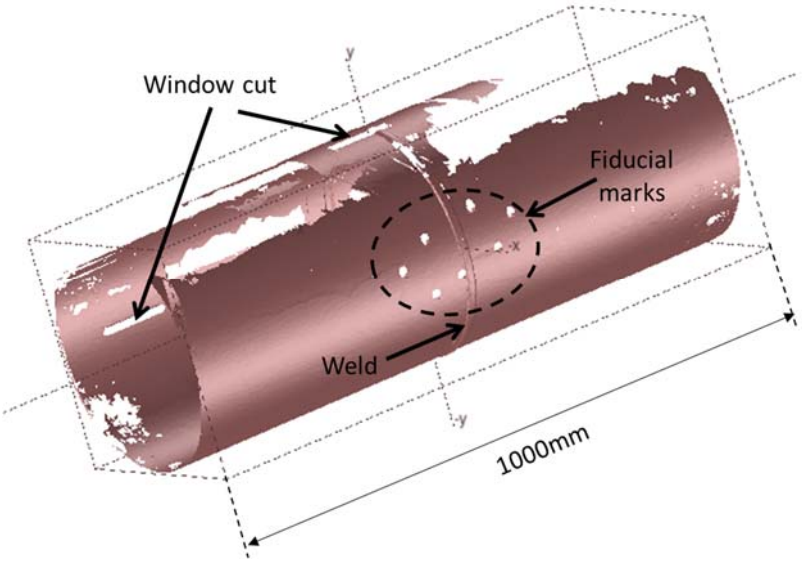

Figure 6.1 A virtual model of the pipe created after the attachment of the fiducial spheres and insertion of the window cuts.

As shown in Figure 6.2, a window cutting was introduced to allow for the measurement of the axial strain components (Figure 6.2a). The window, was needed to allow reflected beams to be detected directly, was located at the side of the 9 o'clock position and close to the pipe end and measured 150mm in length and 20mm in width. The excision was only made, on the parent metal near the end, on the pipes of which the residual stresses were measured in as-welded condition to avoid stress relieve close to the weld metal due to mechanical cutting.

An additional window was introduced for the hoop strain measurements (Figure 6.2b) after the pipes underwent PWHT. The window was cut across the weld and sat at the position 90 degree to the measurement points to reduce the measurement time. For the measurement of radial strain components, neutron beams only went through single pipe wall (Figure 6.2c). The measurement time of each point was dependent on its depth relative to the pipe wall thickness.

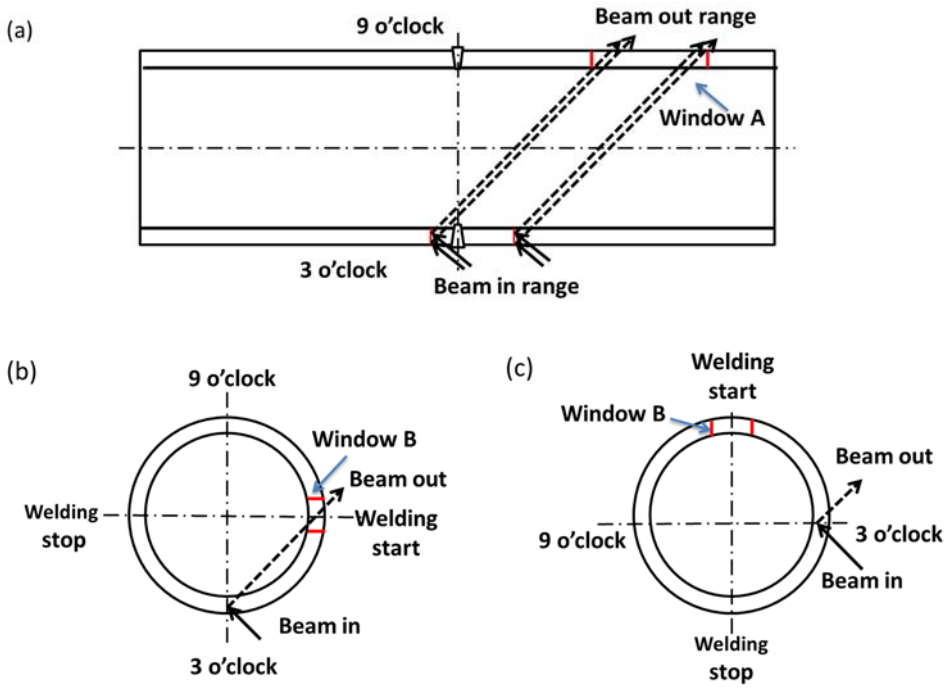

Figure 6.2 Insertion of small windows on the pipe spool to minimize neutron travel path

Before conducting neutron diffraction measurements, the pipe wall thickness was measured at several locations at both the pipe ends and the window cuts. It was found that the thickness was uneven and varied from 18mm to 19mm in parent metal. This error was acceptable since for an API 5L welded pipe with a thickness greater than 15mm and the allowable tolerance for wall thickness is $\pm$1.5mm. Therefore, It was assumed that pipe thickness to be an averaged value of 18.5mm.

6.2.4 Measurement details

On each pipe, three line-scans were carried out at a) 3mm below the outer surface; b) mid-thickness; and c) 3mm above the inner surface. Neutron scanning began at the points near the outer surface and moved every 3mm along the axial direction. Once a

line scan had been completed, the neutron beam was adjusted inwards to a greater depth through the section.

Through wall thickness measurements were carried out at the weld centres and weld toes. Two additional locations were also measured, and they sat 6mm below the outer and above the inner surfaces. The measurement points taken in the vicinity of the weld are illustrated in Figure 6.3.

For each pipe, the residual stresses were measured at up to 40 locations. At each location of measurement, the strain components, in all three principal directions: axial, hoop and radial, were determined. This allowed a full residual stress mapping to be generated for both as-welded and PWHT-ed conditions. As shown in Figure 6.4; the pipe was fixed horizontally at the positioning stage for the axial strain measurements. The hoop and radial components were measured with the pipe "standing" ie in a vertical position.

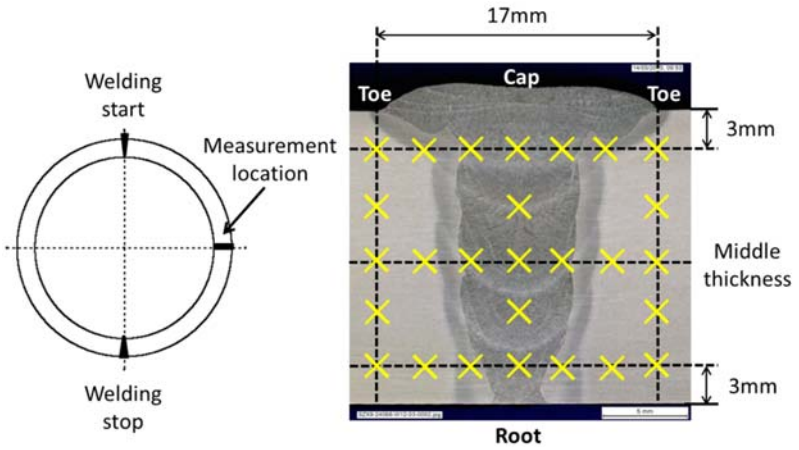

Figure 6.3 Schematic overview of the welding procedure (left), macrograph of the weld cross section and measurement points in the vicinity of the weld centre (right).

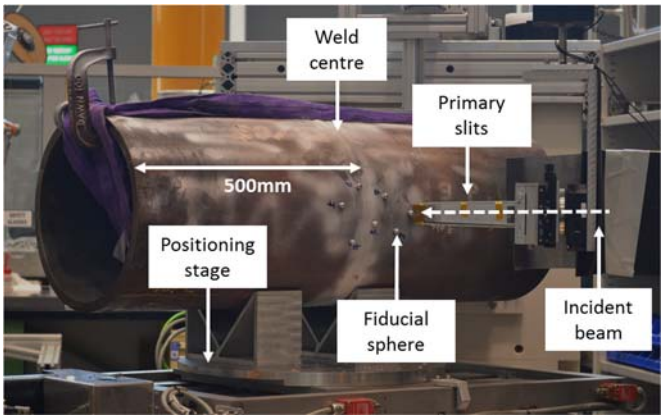

Figure 6.4 Measurement of the axial residual strains in the pipe spool using KOWARI instrument at ANSTO

6.2.5 Evaluation of residual stresses

The residual stresses, in both as-welded (AS) and PWHT (HT) conditions, were calculated using the measured d-spacing (ie lattice spacing) from the pipes and the d_0 values from the reference samples. The residual stresses in the weld metal (WM) and parent metal (PM) were determined using different values of d_0 due to the nature of the compositional variations which affects the lattice spacing. This part has been investigated and discussed in detail in Chapter 5.

For the calculation of the residual stresses in the parent metal, the d_0 values used was an averaged value from the radial, axial and hoop components. While those of the weld metal were evaluated using direction-dependant d_0 values measured in as-welded condition. The lattice spacing in the post-PWHT welds did show significant variation in all four flat samples (d_{03}, d_{04}, d_{05} and d_{06}), so the averaged value of strain free lattice spacing measured from d_{03} was applied based on engineering judgement. Table 6-2 lists the reference lattice spacing applied for stress evaluation.

Table 6-2 Application of the reference lattice spacing for the evaluation of the residual stress in pipes

Condition and region		Pipes			
		P1	P2	P3	P4
AW	WM	-	Averaged d_{xx}, d_{yy}, d_{zz} from weld of d_{01} and d_{02}		-
	PM	-	Averaged d-spacing from parent metal of d_{01} and d_{02}		-
HT	WM	Averaged d-spacing from weld of d_{03}			
	PM	Averaged d-spacing from parent metal of d_{03}			

6.3 Results

6.3.1 RS in welded pipes

In as-welded condition, the two measured pipes P2 and P3 exhibited similar stress distribution and magnitude. The profiles of the through-thickness and line-scan residual stresses are shown in Figure 6.5 and Figure 6.6, respectively.

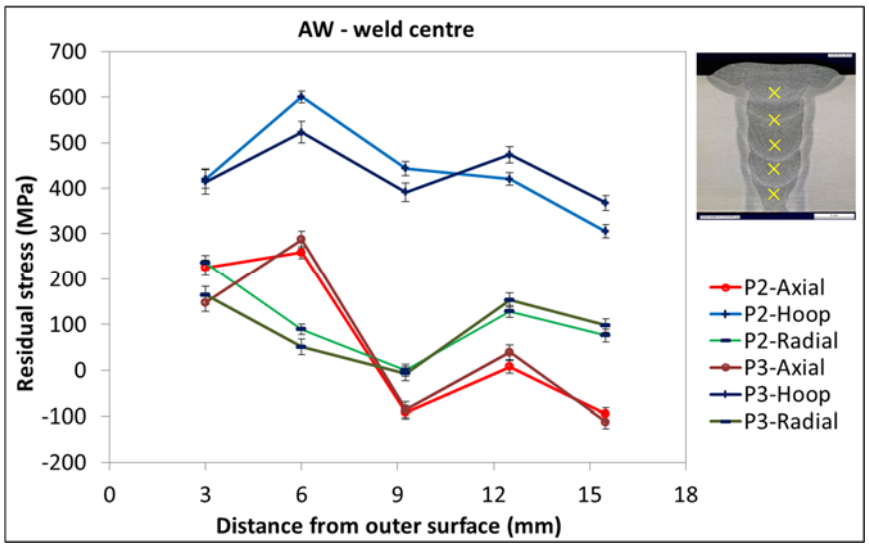

(a)

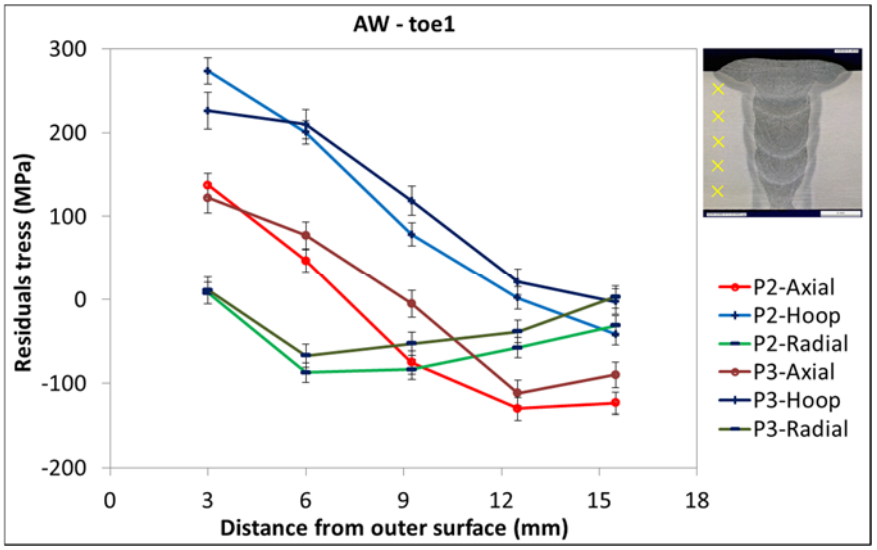

(b)

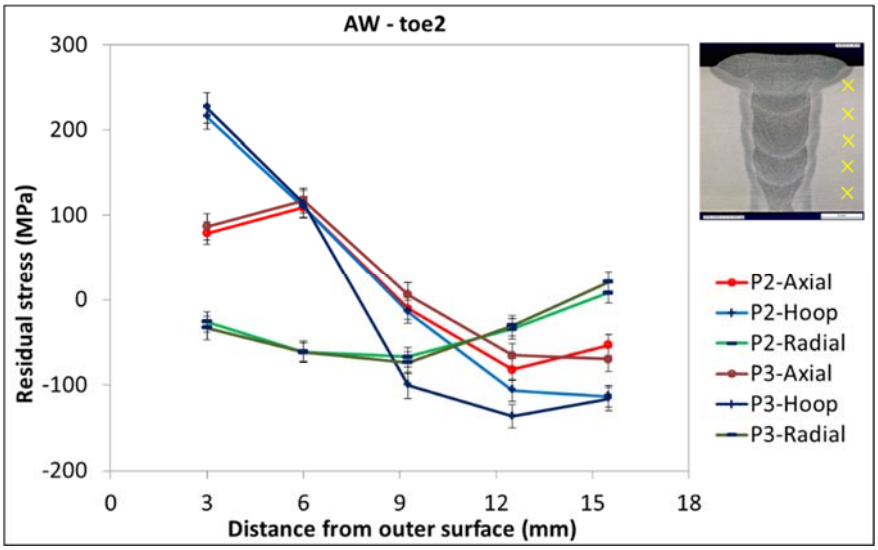

(c)

Figure 6.5 Through-thickness residual stress profiles at (a) weld centreline, (b) and (c) toe areas

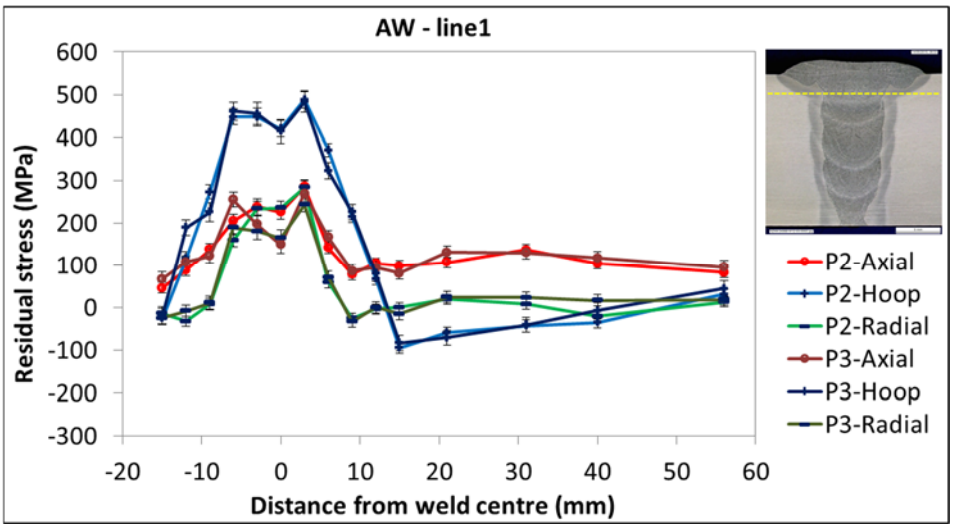

(a)

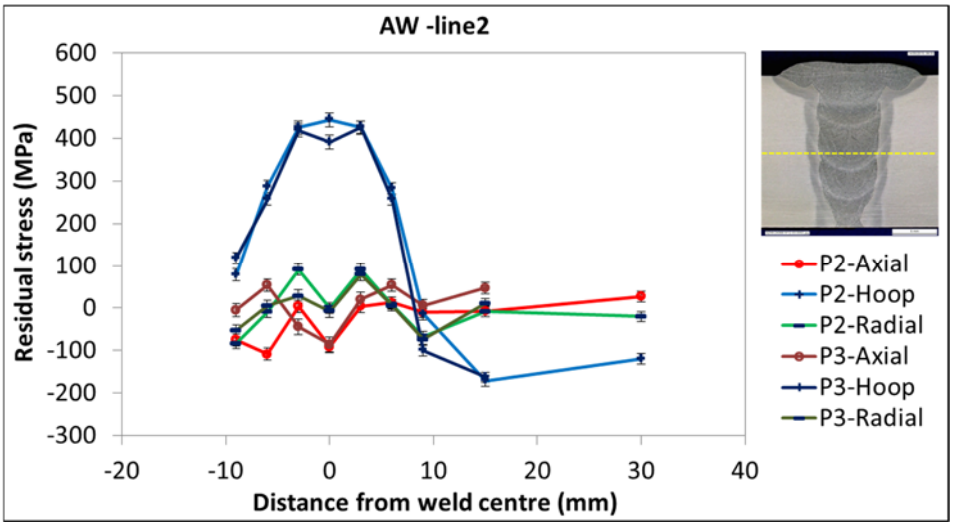

(b)

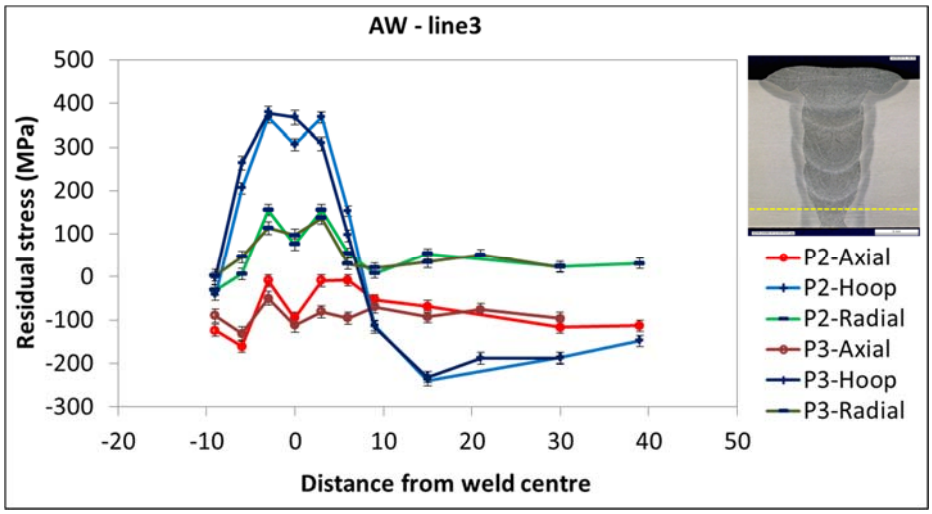

(c)

Figure 6.6 Line-scan residual stress profiles at (a) near outer surface, (b) pipe mid-wall thickness and (c) near inner surface in AW condition

At the weld centre (Figure 6.5a) the highest residual hoop stress occurred in the region at 6mm below the pipe outer surface. The stress magnitude was above 600MPa in P2 which was almost equivalent to the yield strength (657MPa). In terms of the axial component, the tensile residual stress through the pipe wall did not reach beyond 300MPa, which was less than 50% of the yield magnitude. The residual stresses were tensile near pipe outer surface and became compressive at the pipe inner wall.

In the region below the weld toes, the through-thickness residual stress profiles are shown in Figure 6.5b and 6.5c. The hoop and axial stresses at both sides of the weld varied from tensile to compressive inwards the pipe wall. An approximate 50MPa of differences in magnitude were found at the right toe/side. It might be caused by an offset in the centre of the gauge volume at the measurement locations, as the left toe was found to be 8mm from the weld centreline and the right toe 9mm. It was safe to say 1mm offset within the gauge volume of 3mm x 3mm x 4mmwas unlikely to introduce any significant errors.

The residual stress profiles of the line-scans are presented in Figure 6.6. In the weld metal close to the pipe outer surface (Figure 6.6a), the residual stresses in hoop, axial and radial directions were all in tension. The highest stress magnitude was seen in the hoop direction in the HAZ and were approximately 500MPa. The magnitudes of residual stresses decreased rapidly to zero and became compressive beyond the toe locations.

The highest measured axial and radial residual stress were up to 300MPa in the HAZs (approximately 3mm from the weld centre). They decreased to the lowest magnitudes close to the toes and then stayed at a level of less than $\pm$100MPa in the parent metals.

At the mid-thickness (Figure 6.6b) and near inner surface (Figure 6.6c) of the pipe wall, the residual stress variations occurred in the weld region and within an area 9mm from the weld centreline. In the weld region the hoop and radial stresses were tensile while the axial stresses were compressive. It has been observed the highest stresses were in the hoop direction and ranging from 400 to 500MPa. The level of axial and radial stresses was in the range of $\pm$150MPa in the weld metal. Beyond the

weld toes, the residual stresses in all measurement directions became stable with a low magnitude.

6.3.2 RS after PWHT

The post-PWHT residual stresses were measured and compared with each other in the four selected pipes. It is worth noting that P1 was post heat treated in a furnace to achieve a complete stress relief, while the other three pipes were heat treated locally using heating pads which were made of various widths of heating bands.

6.3.2.1 Through-thickness stresses at weld centreline

The residual stress profiles measured at the weld centreline of the four pipes are shown in Figure 6.7. It has been observed the highest measured magnitude of the axial residual stresses close to the pipe outer surface were less than 100MPa which then decreased gradually inwards the pipe wall thickness and became compressive at approximately 7mm from pipe outer surface (Figure 6.7a). Near the pipe inner surface, the axial stresses reached the lowest magnitude, which was approximately -125MPa in P3 and was approximately 50MPa lower than those in the other three pipes.

The stress profiles in both hoop and radial directions are shown in Figure 6.7b and Figure 6.7c, respectively. There were no significant stress variations observed through the weld thickness. Whilst one measurement in P3 showed residual stress of approximate 100MPa close to the pipe inner surface, all the other pipes exhibited residual stress levels close to zero. In the radial direction, the residual stresses remained at a level of less than ±50MPa.

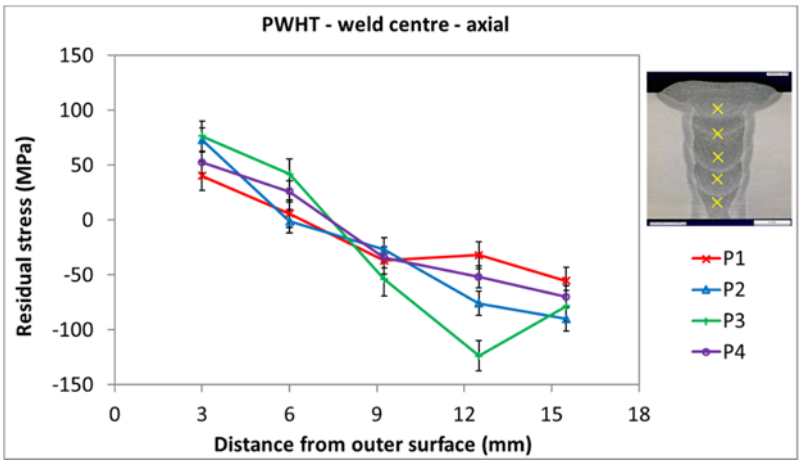

(a)

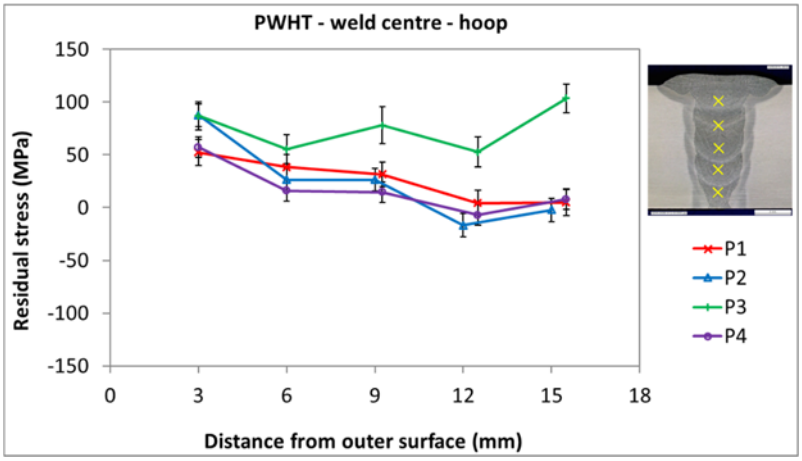

(b)

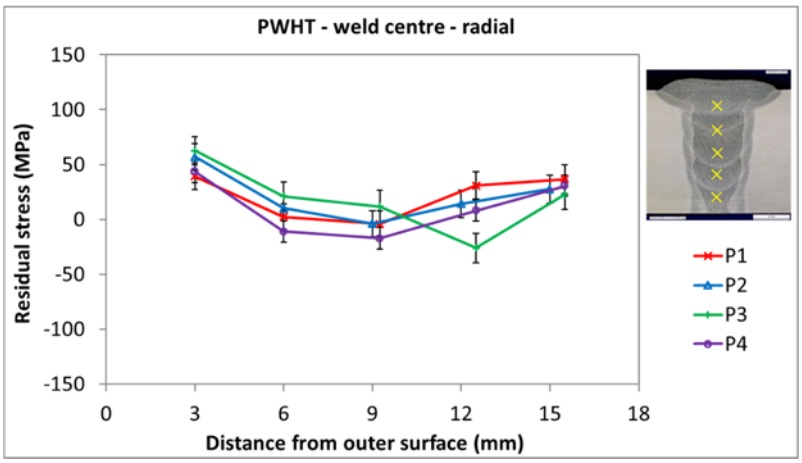

(c)

Figure 6.7 Through-thickness residual stress profiles at weld centreline in (a) axial, (b) hoop and (c) radial directions

6.3.2.2 Through-thickness residual stresses at weld toes

The through-thickness residual stresses below toe1 were evaluated, as shown in Figure 6.8. The axial residual stresses close to the pipe outer surfaces were tensile and measured up to 50MPa (Figure 6.8a). The residual stress magnitude fell to zero at the pipe wall mid-thickness and became compressive. The lowest measured value was found in P3 near the inner surface and was approximately -80MPa. The hoop stresses measured just below the weld toes were less than 50MPa for all the pipes after PWHT (Figure 6.8b). Deeper into the pipe wall, the hoop stresses reduced gradually to 0MPa.

Unlike the hoop component, the radial stresses were compressive (Figure 6.8c). Through the entire wall thickness, the residual stress level was slightly greater than -50MPa in P1, P2 and P4 while that of P3 went as low as -75MPa at approximately 6mm below the pipe outer surface.

Overall, weld toe2 exhibited similar trends in terms of the residual stresses as those in weld toe1 (Figure 6.9). For instance, the axial stresses showed a transition from tensile to compressive through the pipe wall thickness (Figure 6.9a). Their magnitudes were in the range of ±50MPa. The radial stresses, in comparison, were all compressive and the distributions were almost the same as those of toe1(Figure 6.9c), ranging from -75MPa to 0MPa.

The hoop stresses in toe2 of all the pipes were different from those in toe1. For example, in P1, P2 and P4 the measured hoop stresses varied from tensile to compressive and returned to neutral ie zero through the section thickness. The lowest stress magnitude recorded as in the region which sat 12mm from the outer surface. In P3 the hoop stresses became increasingly compressive as the measurement locations moved further from the pipe outer wall (Figure 6.9b). At mid-thickness and close to the inner surface, the measured stresses in P3 were as low as -75MPa.

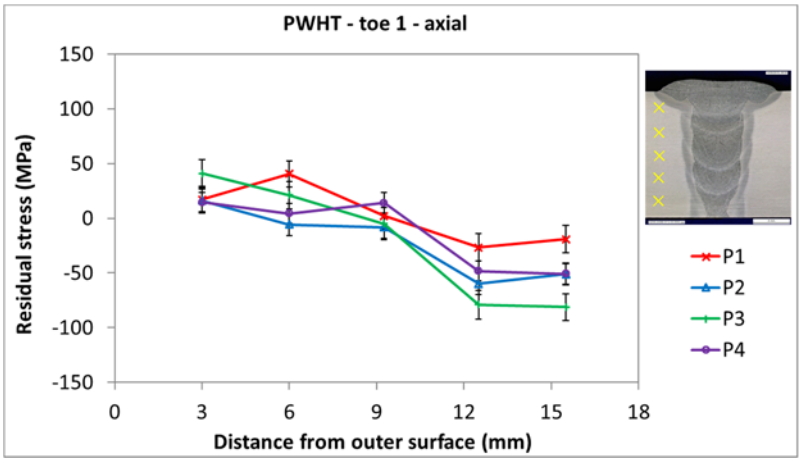

(a)

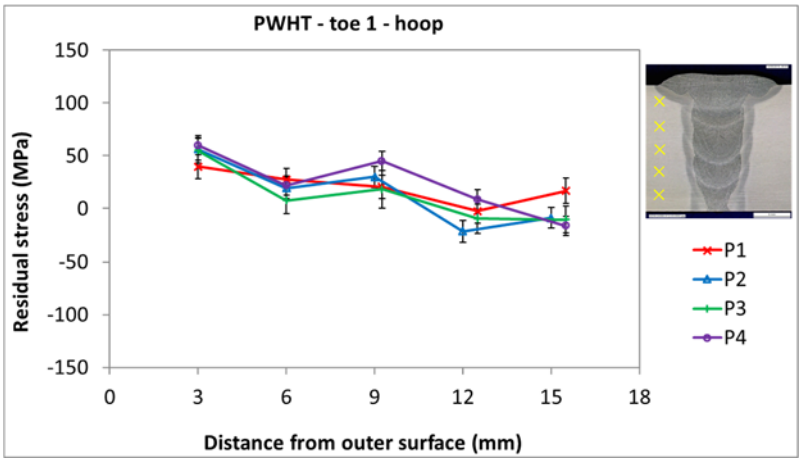

(b)

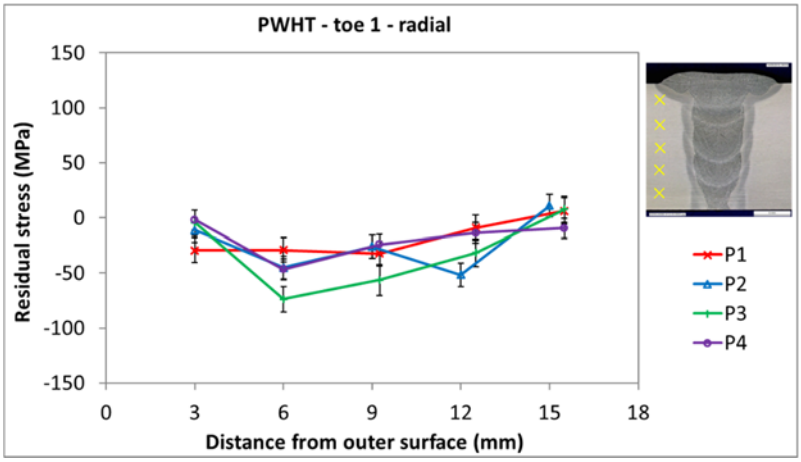

(c)

Figure 6.8 Through-thickness residual stress profiles below left toe in (a) axial, (b) hoop and (c) radial directions

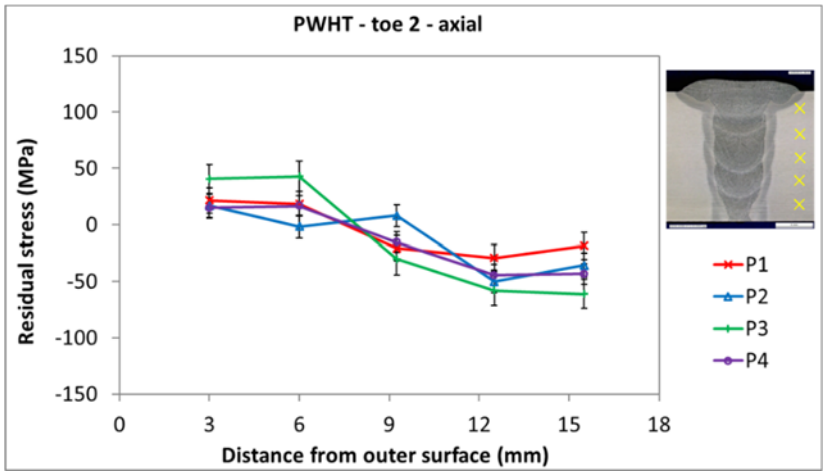

(a)

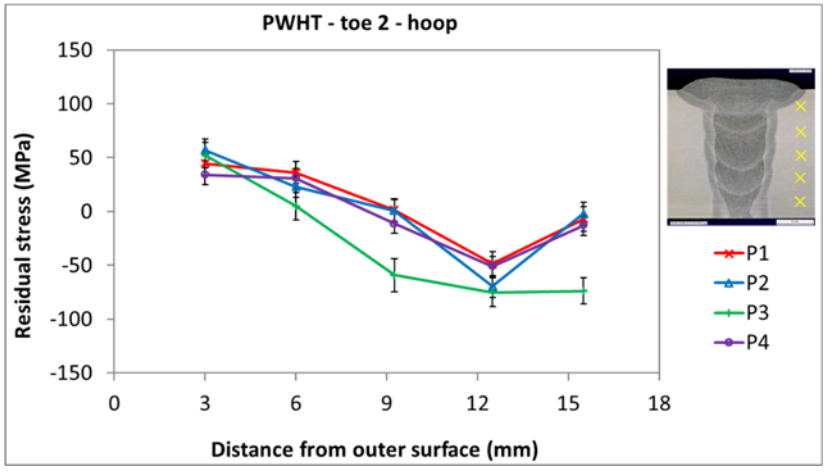

(b)

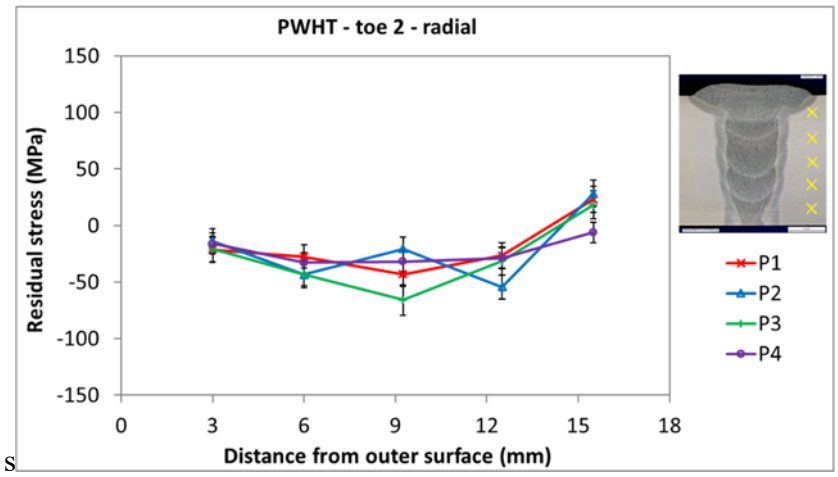

S

(c)

Figure 6.9 Through-thickness residual stress profiles below right toe in (a) axial, (b) hoop and (c) radial directions

6.3.2.3 Residual stresses along pipe length

The residual stresses close to the outer surface, at pipe wall mid-thickness and at near pipe inner surface were measured in all the pipes (P1, P2, P3 and P4). It is worth a reminder that P1 underwent heat treatment in a furnace while the other pipes were heat treated locally using heating pads of which the band widths were 280mm for P2, 170mm for P3 and 430mm for P4 respectively.

The results of the measured residual stresses profiles in all pipes at near pipe outer surface (line1) are shown in Figure 6.10. The magnitudes and the distributions of the stresses, for each measurement direction, in four pipes were similar. The residual stresses at weld zone were at a magnitude of approximately 150MPa or less.

The highest recorded magnitude was found at the region which was 3mm from weld centreline It was believed these measurements either fully or partially sampled the HAZ. The axial (Figure 6.10a) and radial (Figure 6.10c) peak stresses dropped to a level of near zero in the parent metal which was 9mm from weld centreline and showed minor fluctuation along the measurement line. The tensile hoop stresses were found to affect a wider region from weld to parent metal and a noticeable drop to the neutral state was only observed when it was sufficiently far from the weld metal i.e. approximately 18mm (Figure 6.10b).

The residual stresses profiles at the pipe wall mid-thickness (line2) are shown in Figure 6.11. For all the pipes, the measured residual stresses in the weld region

between 100MPa and -100MPa. The axial and radial stresses were in the range of ±100MPa before PWHT (as seen in Figure 6.6b) and decreased to a lower magnitude after PWHT (Figure 6.11a and Figure 6.11c).

Some stress variations have been observed in both the weld and parent metals in P3 in axial and hoop directions (Figure 6.11a and Figure 6.11b). At locations close to the pipe inner surface (line3), P3 exhibited greater variations in residual stresses than the other pipes did (Figure 6.12). In general, the residual stress levels had been reduced to less than either 30% of weld metal yield strength or 20% of parent metal yield strength, which were in good agreement with the recommendations for heat-treated components given in fitness-for-service procedures

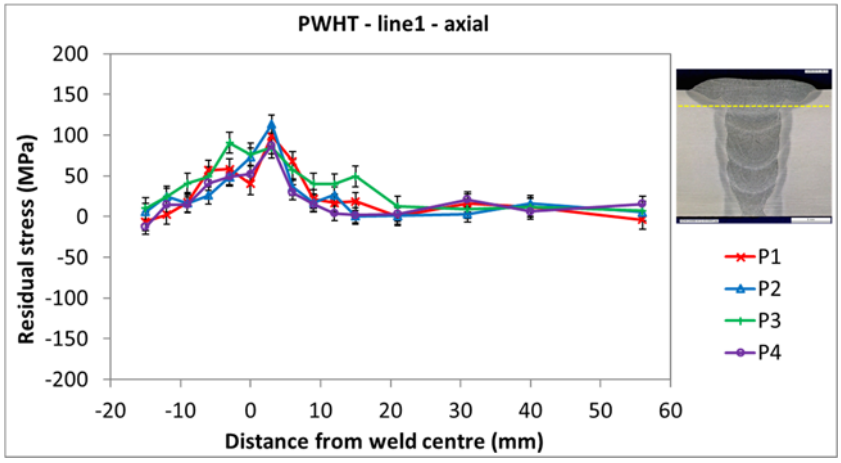

(a)

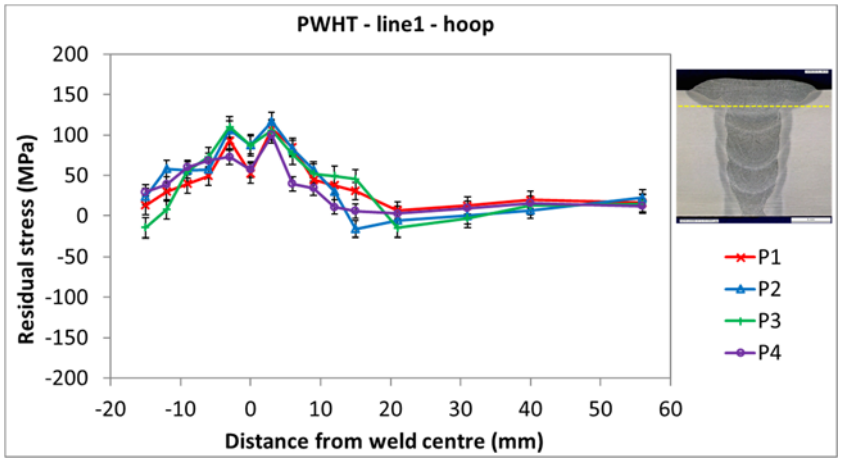

(b)

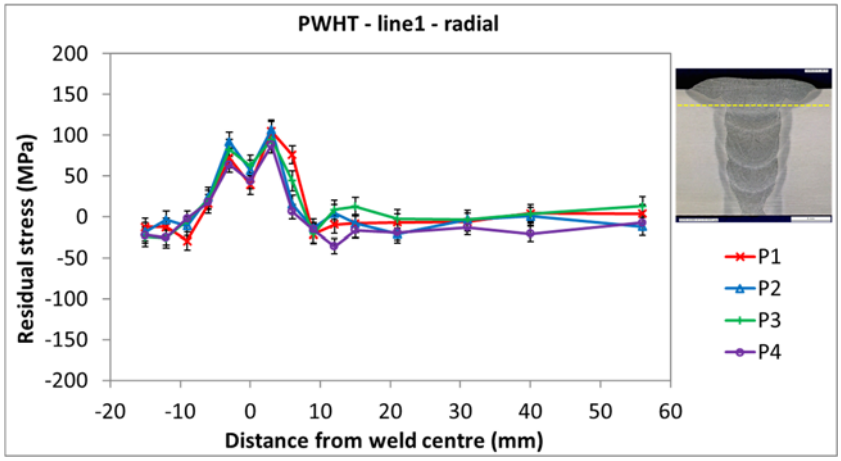

(c)

Figure 6.10 Line-scan residual stress profiles near pipe outer surface in (a) axial, (b) hoop and (c) radial directions after PWHT

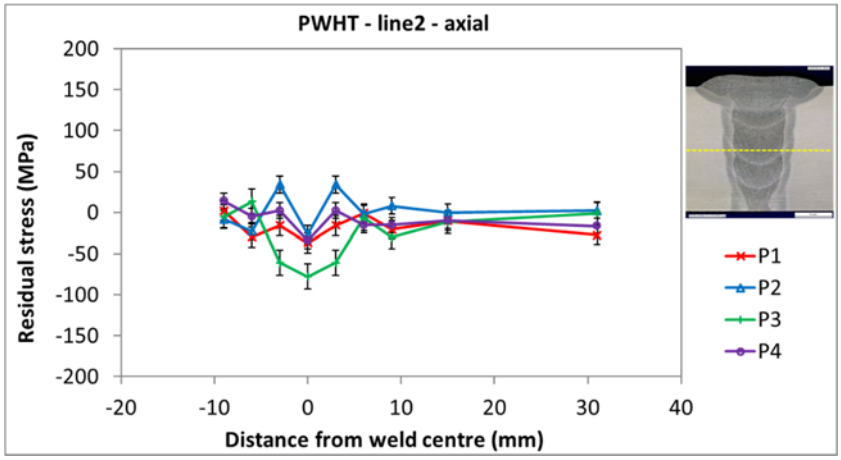

(a)

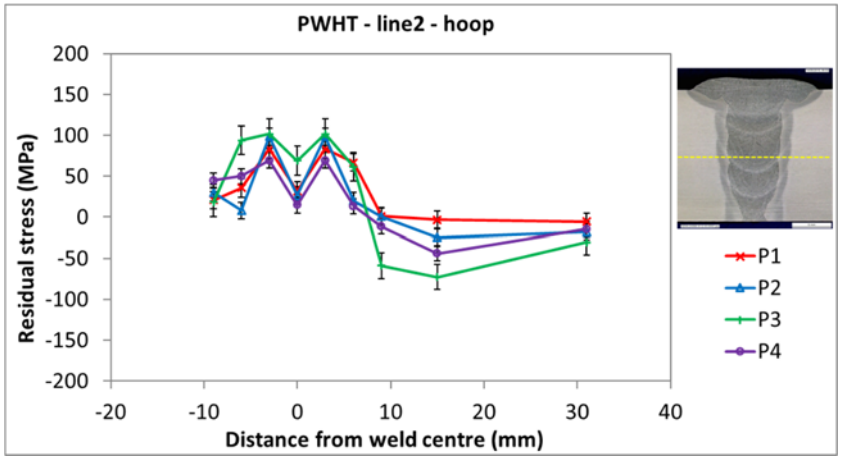

(b)

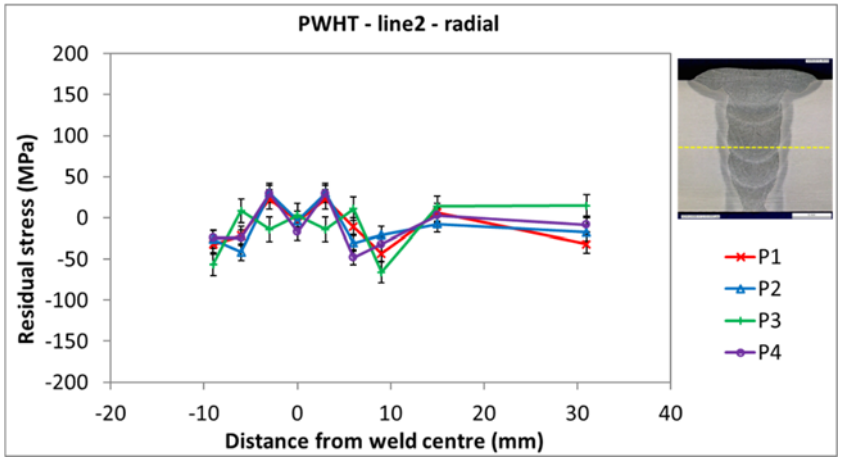

(c)

Figure 6.11 Line-scan residual stress profiles at pipe wall mid-thickness in (a) axial, (b) hoop and (c) radial directions after PWHT

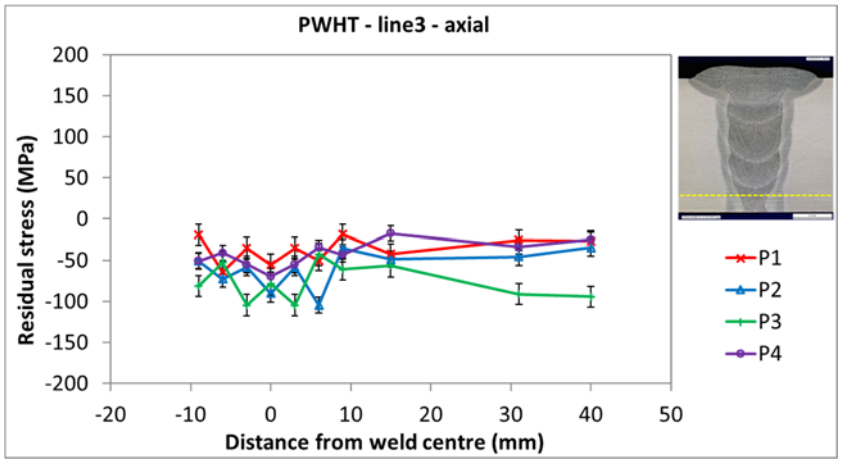

(a)

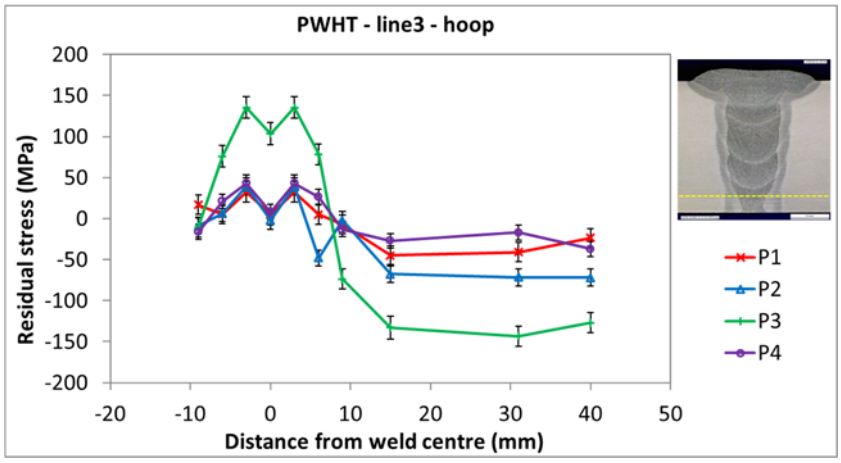

(b)

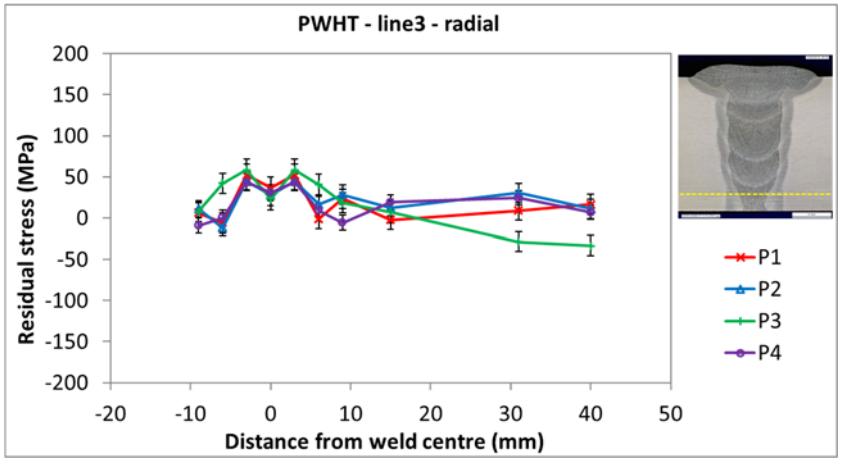

(c)

Figure 6.12 Line-scan residual stress profiles at near pipe inner surface in (a) axial, (b) hoop and (c) radial directions after PWHT

6.4 Discussion

6.4.1 The effect of heating methods on residual stress relief

From the stresses profiles measured after PWHT, it could be said that all four pipes experienced stress relief under various heating conditions in which they were seeing a reduction in the hoop residual stresses to a level of less than 30% of weld metal yield strength. P3 has been stress relieved using local the narrowest heating band still showed tensile hoop residual stress of almost 150MPa near the weld root (Figure 6.12b).

The cause of the stresses variations in P3 could be a combination of two factors. Firstly, the heating pad used was in contact with the outer surface of the pipe wall. With increased thickness of wall thickness, a steep thermal gradient could be induced. The applied heat band used on P3 was 170mm wide which approximately equalled to $3\sqrt{Rt}$ (R is the pipe inner radius and t is the pipe wall thickness). However, it was recommended in many PWHT practices the minimum heat band should be $5\sqrt{Rt}$ (see Table 3-3) or wider to avoid undesirable thermal gradient. During the experimental work, some thermocouples were installed on the pipe inner surface to record temperature changes during PWHT, it could not be said for certain if applied heat (via heating band) on P3 was sufficient to bring the temperature at the pipe inner surface up to a level sufficient to relieve the residual stresses in the weldment.

Another factor contributing to potential insufficient thermal energy in P3 could be that the PWHT had been interrupted during heating stage after the heating pad burnt out several times at 450°C, 520°C and 580°C. All efforts were made to ensure the heating pad was replaced immediately after the burnt-out, but the time taken to re-attach the replacement units would have reduced the heating period and caused inconsistency. It had an impact on the temperature at the final stage which was reported to be lower than the target soaking temperature. Under these circumstances the unusual variation in residual stress of P3 could be justified.

6.4.2 Full mapping of the residual stresses

Full mapping of residual stress in the measurement direction of interest could be generated using the values calculated at each measurement point. This extrapolation was able to provide an indication of the stress distribution as well as the magnitude within a certain volume of the material. The residual stresses measured in P2 and P3 in as-welded condition are shown in Figure 6.13. Those in P1 and P2 were compared after furnace and local PWHT, as seen in Figure 6.14. The original plan was to use P3 with the narrowest heating band to investigate the effect of band width on stress relief but due to the unforeseen interruption, it was not recommended to use the measured data for further analysis.

It was known $P_{AW}2$ (labelled as "$P_{AW}2$" for the residual stress measurement in as-welded condition for P2) was only preheated on one side of the weld and the other side was kept for attaching strain gauges and thermocouples. $P_{AW}3$ (labelled as "$P_{AW}3$" for the residual stress measurement in as-welded condition for P3) underwent preheating on both sides of the girth weld. Preheating was intended to avoid hydrogen cracking, the effect (if any) of preheating [5], [6] on welding residual stresses was also part of the investigation in the study.

It can be seen from Figure 6.13 that the two pipes were in a similar stress condition after welding. This implies that the differences in the preheat condition did not affect the stress profile significantly. The highest hoop residual stresses were observed in the vicinity of the weld, 6mm below the outer surface. The axial residual stresses were slightly tensile on the outer surface, close to zero at mid-thickness and compressive at the inner surface.

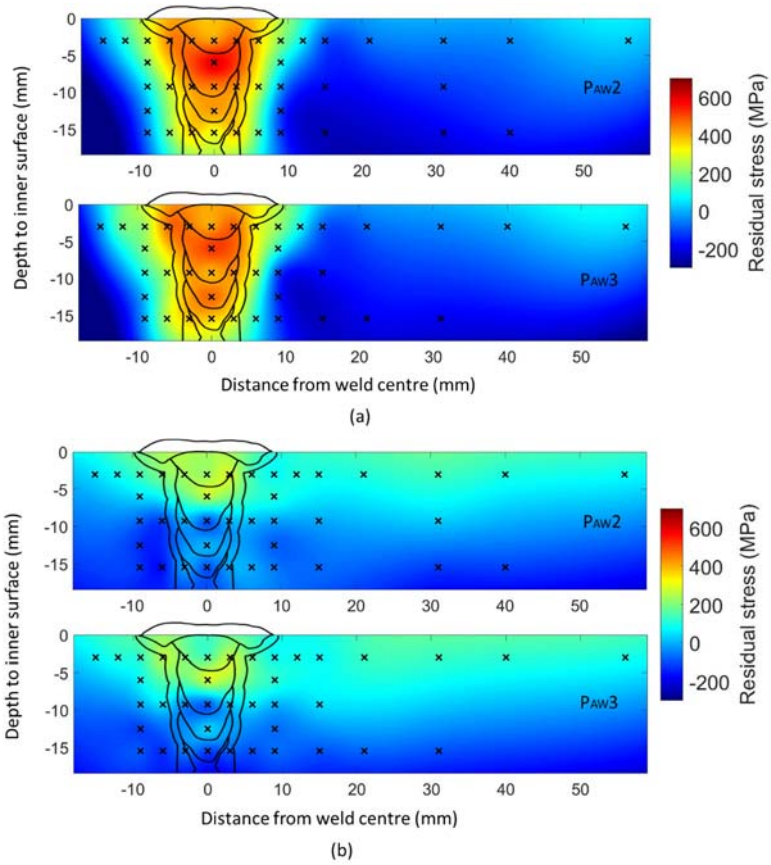

Figure 6.13 Residual stress maps in as-welded condition in hoop (a) and axial (b) direction for $P_{AW}2$ and $P_{AW}3$

In Figure 6.14, the residual stress maps of $P_{HT}1$ (in furnace) and $P_{HT}2$ (local PWHT) after PWHT were presented which both showed a significant reduction in residual stress. The measured residual stresses in $P_{HT}1$ were mostly relieved via conventional furnace PWHT. The remaining stresses were less than 100 MPa which were lower than 20% of the parent metal room temperature yield strength.

In $P_{HT}2$, a slight variation of stress near the pipe outer surface could be observed, as indicated by a small patch of greenish blue shade. At the inner surface, the residual stresses compressive.

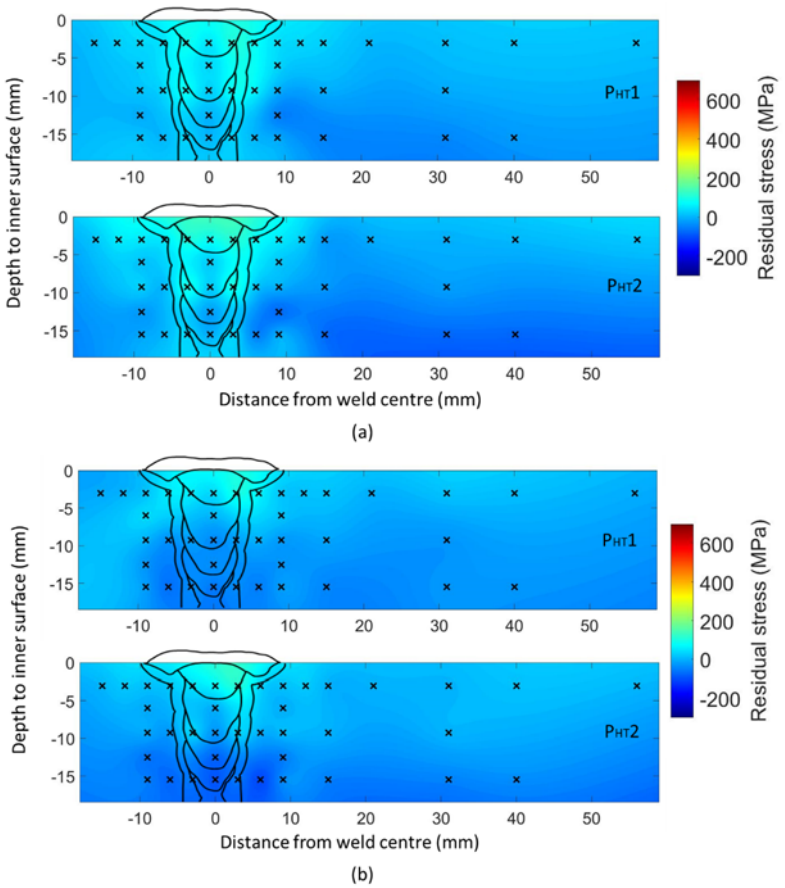

Figure 6.14 Residual stress maps in after PWHT in hoop (a) and axial (b) direction for PHT1 and PHT2

6.4.3 A comparison with recommendations given in BS 7910 and R6

Information on the effectiveness of PWHT had been incorporated into Engineering Critical Assessment (ECA) procedures such as BS 7910 and R6, which assume that in wide-groove welds, different levels of stress relief occurr in both transverse and longitudinal directions following a conventional furnace PWHT. BS 7910 also provides some information on the effect of PWHT temperature on stress relief. However, the guidance is not applicable to narrow-gap welds. The literature data on stress relief after local PWHT is rather limited although some experimental and analytical work had been carried out to investigate the effective heating band width for optimum stress relaxation [7]–[10] and through-thickness temperature gradient variation [11]–[13].

6.4.3.1 Through-thickness residual stress evaluation

A comparison of the through-thickness residual stresses at the weld centre before (P2 vs. P3) and after furnace and local PWHT (P1 vs. P2) are shown in Figure 6.15 for

the hoop and axial direction respectively. The residual stress profiles given in R6 and BS 7910 are also included. The residual stress profiles near the outer surface were also compared and are shown in Figure 6.15.

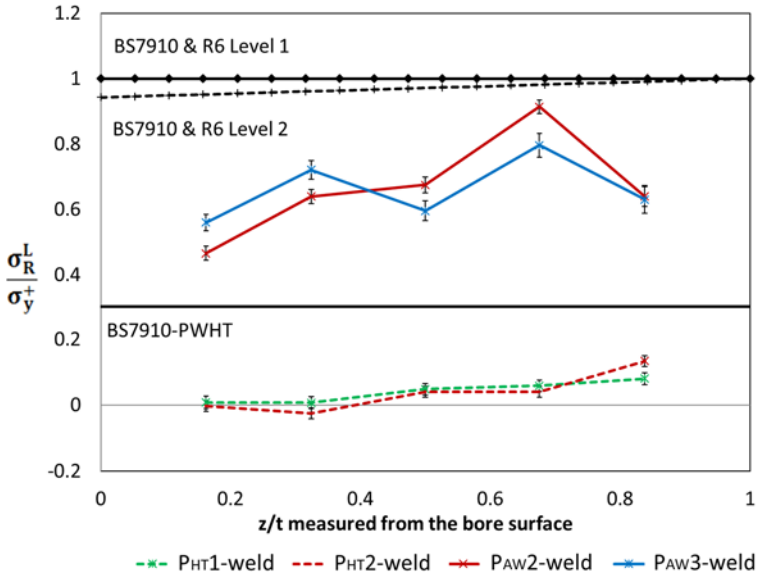

(a) Normalized hoop residual stresses

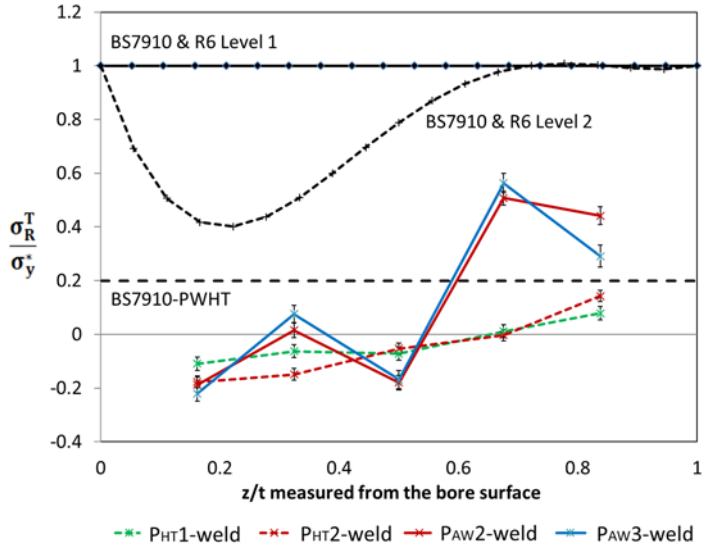

(b) Normalized axial residual stresses

Figure 6.15 Comparison of the through-thickness residual stresses at weld centre and weld toe before and after local and furnace PWHT with R6 and BS 7910

Figure 6.15a showed that the through-thickness hoop residual stresses at the weld centre of two pipes were at a much lower magnitude than those assumed in BS 7910 and R6 Level 2. With the neutron diffraction technique employed and a gauge

volume of 3x3x4mm^3, it was not possible to measure the residual stresses at the surface. The closest measurements (both inner/bore and outer) were therefore 3mm below the surfaces. As shown in Figure 6.15a, the greatest magnitude of the hoop component in the as-welded condition occurred at 6mm (z/t=0.69) below the outer surface and was close to the upper bound value.

The axial residual stresses near the pipe outer surface were tensile and balanced by the compressive ones near the inner surface; as shown in Figure 6.15b. The highest measured axial residual stress was 50% of the room temperature yield magnitude of the parent metal. The measured values were less than the upper bounds as advised in handbook solutions.

6.4.3.2 Line-scan stress evaluation

The next set of comparisons with the codes looked at the line scan which sat 3mm below the outer surface/ This set of measurement indicated the highest as-welded hoop residual stresses occurred within the weldment. From the measurement results, it can be seen that the two as-welded pipes exhibited identical stress profiles along the line 3mm below the outer surface in both hoop and axial directions (Figure 6.16). The hoop stress could be as high as 75% of the weld metal yield strength, then dropped to less than 30% at the toe and reduced to zero at 15mm away from the weld centre line (Figure 6.16a).

The calculated radius of the yield zone r_0 near the outer surface (see in Figure 4.6) was approximately 11.6mm. To simplify the calculation and keep the results conservative, r_0 was taken as 11mm and was demonstrated in Figure 6.16a. It could be seen R6 recommendations for the yield zone were conservative. This could be a significant advantage in using narrow-gap weld procedure for its low heat input and smaller HAZ and the resultant lower residual stresses.

The as-welded axial residual stresses (Figure 6.16b) were predominantly tensile close to the outer surface and measured up to 55% of the material yield strength in the HAZ. After PWHT, they were found to be less than 20% of the material yield strength.

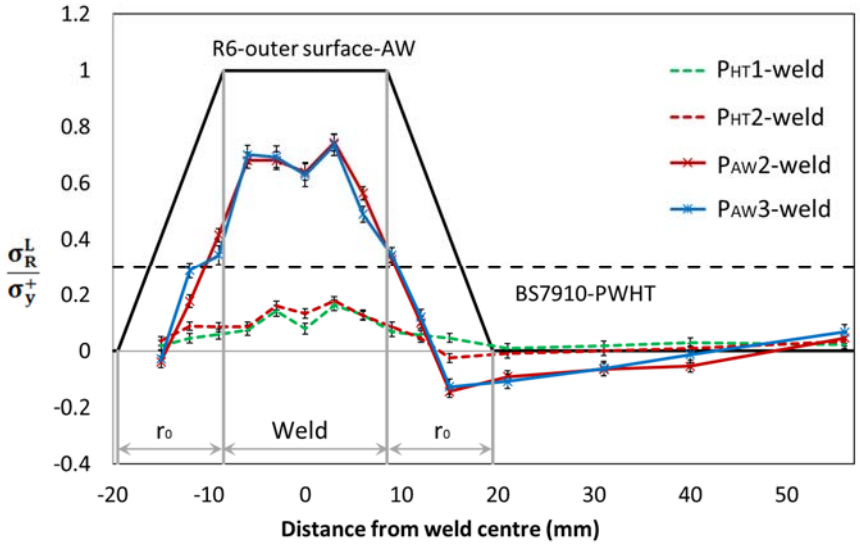

(a) Normalized hoop residual stresses

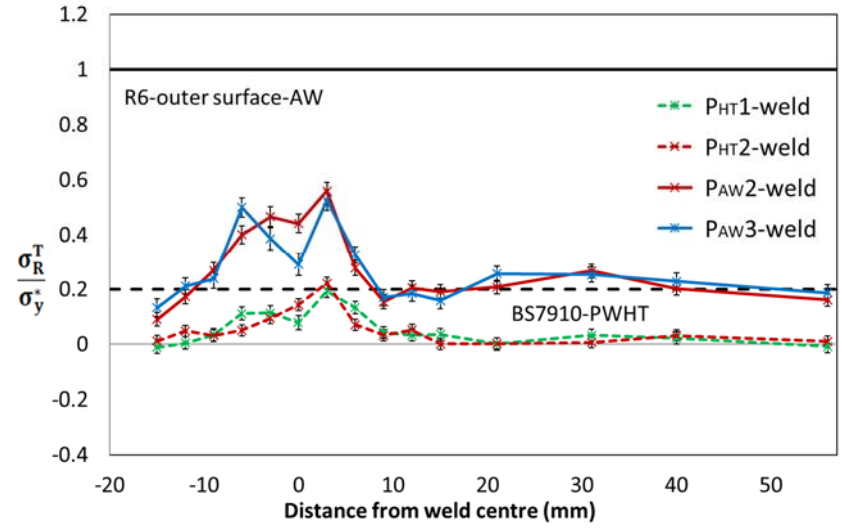

(b) Normalized axial residual stresses

Figure 6.16 Comparison of the near outer-surface residual stress before and after local and furnace PWHT with R6 and BS 7910-PWHT

R6 procedure also provides some recommendations in terms of the hoop stresses at pipe inner surface. The stress values measured at 3mm from inner surface were evaluated and compared with those given in R6 and BS 7910 as shown in Figure 6.17. The value of yield zone radius r_0 was calculated using the welding parameters (for weld root) from Table 3-2 and the Equation 4.15. As a conservative estimate, r_0 was applied as 10mm. The hoop stress reached to a level less than 60% of the yield strength in the weld, then dropped to zero at approximately 8.5mm away from the weld centre line (Figure 6.17). After PWHT, the residual stresses in the weld were less than 10% of the yield strength in the weld.

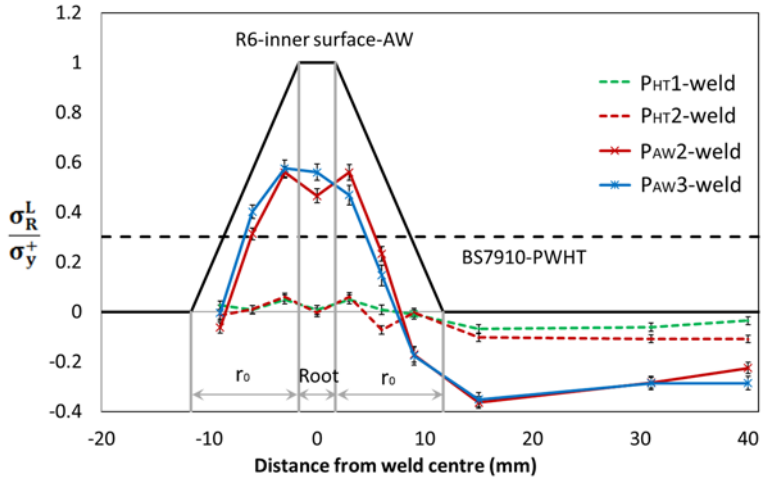

Figure 6.17 Comparison of the near inner-surface hoop residual stress before and after local and furnace PWHT with R6 and BS 7910-PWHT

For those pipes subject to local PWHT, the axial residual stress at the weld centre line in PHT1 was greatly reduced to approximately zero. PHT2, which was heated locally, saw a reduction in residual stresses at the outer surface to 20% of the material yield strength. From the line sans, the hoop stresses near pipe outer and inner surfaces were much lower than the upper bounds recommended for engineering critical assessment. Comparing the stress reduction in general, it could be said that local PWHT in this study exhibited identical effect on stress relief effect as those achieved by furnaces (Figures 6.15-6.17).

6.5 Concluding remarks

In this chapter, the residual stresses in narrow-gap girth welds were determined for both as-welded and PWHT (global and local) conditions. The stress profiles at the locations close to the pipe outer and inner surfaces and through section thickness were compared with the recommended upper bound profiles given in BS 7910 and R6. The key findings from this investigation were:

1. Small temperature differences during preheating had little or no effect on the overall residual stress of pipe spools.

2. Current recommendations in the codes are conservative for the narrow-gap welds, based on the results of this work, in both as-welded and PWHT conditions.

3. Local PWHT can achieve the same magnitude of stress relief as that of global PWHT, if it is applied correctly, following prescribed procedure.

4. With regard to the studied narrow-gap multi-pass welds, residual stresses can be relieved effectively by local PWHT using a band width smaller than the recommended standard size in general practice.

Reference

[1] A. M. Paradowska, J. W. H. Price, R. Ibrahim, and T. R. Finlayson, "The effect of heat input on residual stress distribution of steel welds measured by neutron diffraction," *J. Achiev. Mater. Manuf. Eng.*, vol. 17, no. 1–2, pp. 385–388, 2006.

[2] D. N. Crofft, *Heat Treatment Of Welded Steel Structures*. 1996.

[3] "BSI, 'BS7910:2013 Guide to methods for assessing the acceptability of flaws in metallic structures,' 2013," 2013.

[4] I. Milne, R. Ainsworth, A. Dowling, and A. Stewart, "Assessment of the integrity of structures containing defects," *Int. J. Press. Vessel. Pip.*, vol. 32, no. 1–4, pp. 3–104, Jan. 1988.

[5] Y. C. Lin and K. H. Lee, "Effect of preheating on the residual stress in type 304 stainless steel weldment," *J. Mater. Process. Technol.*, vol. 63, pp. 797–801, 1997.

[6] S. M. Adedayo and M. B. Adeyemi, "Effect of preheat on residual stress distributions in arc-welded mild steel plates," *J. Mater. Eng. Perform.*, vol. 9, no. 1, pp. 7–11, 2000.

[7] W. Soete and R. Vancrombrugge, "An industrial method for the determination of initial stresses," *Proc SESA*, vol. 8, no. 1, pp. 17–28, 1950.

[8] R. T. Rose, "Stress in Cylindrical Vessels due to Local Heating Stress Relief of Circumferential Welds," *Br. Weld. J.*, pp. 19–21, 1960.

[9] J. I. Bluhm, "Fracture Mechanics, SAE Technical Paper 630101," Jan. 1963.

[10] H. MURAKAWA, H. LU, and J. WANG, "Mechanical Behavior in Local Postweld Heat Treatment (Report II) : Determination of Critical Heated Band during Local PWHT(Mechanics, Strength & Structure Design)," *Trans. JW RI*, vol. 27, pp. 89–95, 1998.

[11] E. G. Shifrin and M. I. Rich, "Effect of Heat Source Width in Local Heat Treatment of Piping," *Weld. J.*, vol. 53, no. 12, pp. 792–799, Dec. 1973.

[12] C. Bloch, J. Hill, and D. Connell, "Proper PWHT Can Stop Stress-Induced Corrosion," *Weld. J.*, vol. 76, no. 5, pp. 31–41, 1997.

[13] H. LU, J. WANG, and H. MURAKAWA, "Mechanical Behavior in Local Postweld Heat Treatment (Report III) : Criteria for heated band width based on through-thickness temperature distribution(Mechanics, Strength & Structure Design)," *Trans. JW RI*, vol. 27, pp. 89–95, 1998.

7 Finite Element Modelling of Welding Residual Stress

7.1 Introduction

The macroscopic transient temperature, displacement, stress and strains during a welding process can be predicted from a welding simulation. It is also possible to simulate microscopic details of metal phase transformation such as grain growth, dissolution and precipitation.

In this work, finite element analysis (FEA) was employed to simulate an arc welding process for the prediction of welding residual stresses using ABAQUS software. The FE models were validated against measured stresses from the neutron diffraction technique.

A two-dimensional axisymmetric model of a six-pass 19mm thick girth-welded pipe was developed and validated against a series of measurements including temperature, transient strains and residual stresses.

7.2 Principles of modelling of welding residual stresses

7.2.1 Overview

7.2.1.1 The physics of welding process

Arc welding is a complex physical process which involves a series of material physical interactions during the process such as heat transfer from the arc source to the component to be joined, melting, fluid flow with mass transport, interaction between liquid and solid phases, metallurgical phase transformation and solidification.

In arc welding process, the welding arc acts as a heat source which is quantified by arc power. The power is determined by the applied arc voltage V and the effective welding current I. The electromagnetic force, produced in the weld pool, encourages the superheated liquid flow downwards to the bottom of the weld pool and hence produces deeper weld penetration.

Most of the energy generated from the arc can be transferred to a weld pool effectively via thermal conduction and radiation. However, some heat is still lost to

the surrounding environment. The proportion of the arc power transferred to the work piece is defined as welding efficiency η.

The solidification of a weld pool can be affected by several factors such as the cooling rate and the compositional gradient. As different alloying elements solidify over a range of temperatures, the material may or may not experience solid-state phase transformation upon cooling. Depending on the cooling rates, the composition of a given transformed phase can vary.

Residual stresses in a weldment can be evaluated from numerical thermal analysis of the welding process. However, it is difficult to employ an analytical or numerical tool to include all the physical aspects of welding [1]. Some simplification can be made when simulating a welding process. The extent of complexity of simulations depends on the requirement of the outcome, it is not always necessary to consider all the physical aspects as long as the welding residual stresses can be realistically predicted [1].

7.2.1.2 Development of finite element analysis for welding process

FEA, one of numerical techniques, which employs thermal and mechanical analysis for the prediction of welding residual stresses, has been in use since late 1970s. It has been favoured in comparison to experimental method because of the advancement in computing technologies, particularly in improved processing speed, storage capacity and numerical algorithms for thermal and mechanical analysis [1]. The availability and development of commercial software such as ABAQUS, SYSWELD and ANSYS have encouraged the use of FEA to simulate welding processes.

There has been extensive research carried out to evaluate welding residual stresses in different types of welded joints using either experimental measurement techniques or FEA, or a combination of them. Data of welding residual stresses has been documented, including open publication, and shows scatters in both distributions and magnitudes. This implies that experimental techniques and numerical procedures still require further enhancement if residual stresses are to be determined more consistently, accurately and realistically.

Guidelines for simulating welding residual stresses are detailed in Section III.15 of R6 Rev.4 [2] which defines the main steps for modelling of welding residual stresses

and identifies the input data for each step, such as temperature–dependent conductivity, general convection and radiation boundary conditions for heat transfer analysis and hardening mechanism for stresses analysis.

7.2.2 Heat transfer modelling

7.2.2.1 Physical heat input

A transient thermal analysis is required for the simulation of heat transfer in welding process. This can be achieved by modelling the heat flow applied to either a two-dimensional (2D) or three-dimensional (3D) configuration accordingly to generate a temperature field for a subsequent thermal stress analysis. Physically, the total effective arc energy, in the unit of J/s, for an arc welding process can be evaluated using Equation 7.1:

$$Q = \eta V I \tag{7.1}$$

where, η is the process efficiency, V is the welding voltage and I is the welding current. The thermal efficiency of gas metal arc welding processes can be taken as 0.8, as recommended in R6 procedure.

Modelling of the heat input of a welding process can be achieved using three approaches: a static heat source with prescribed temperature, a static heat source with volumetric flux, and a moving heat source with volumetric flux, in the order of increasing complexity and accuracy.

Among the three approaches, a static heat source with prescribed temperature is the simplest method which models the heat input by defining the weld in the model being held at a fixed temperature above T_m (material melting temperature) for a period of time Δt, in units of seconds. The challenge of applying this method is to select a reasonable Δt. Too long a hold time introduces excessive amount of heat to the weld region with increased size of the plastic deformed zone surrounding the welding zone. Too short a hold time is not able to achieve a reasonable molten zone size. As a result, the accuracy of the residual stress field is difficult to predict.

A static heat source with volumetric flux, in comparison, defines the welding arc energy input (heat flux) instead of temperature and welding efficiency. With the calculated weld pool length, the flux duration τ can be estimated. With this

approach, the heat flux is applied simultaneously to the whole weldment, either the cross section of the weld in a 2D model or the whole weld in a 3D model.

A moving heat source with volumetric flux is only employed in 3D welding simulation. The heat source is allowed to travel along a predefined path which represents the most realistic form of welding process. In Abaqus, a user-subroutine is required to generate a moving heat source for welding simulation, in which the welding voltage, current, efficiency, speed, heat flux as well as the dimension of the heat source should be defined.

7.2.2.2 Three-dimensional heat source

The development of heat source models has been made since 1940s. The earliest generation of heat source model was pioneered by Rosenthal [3] who proposed a point or line moving heat source model to predict temperature in or near the fusion zone (FZ) and the heat affected zone (HAZ).

Experimental evidence has shown that the surface power density distribution of arc welding heat source is approximately Gaussian. In 1970s, Pavelic [4] and Rykalin [5] developed a moving heat source using a Gaussian distribution of flux deposited on the surface of the workpiece, which obtained significantly better temperature distribution in the HAZ than the classical moving point heat source solution of Rosenthal's. Complex interactions between the heat source and the weld pool mean that the heat input is effectively distributed throughout a volume in the work piece. As this 'disc' model only considered surface heat distribution, deep welding process could not be accurately simulated.

Thereafter, non-axisymmetric 3D heat source model was developed. It is able to predict the temperature field in a weldment, accommodating either deep or shallow welds. Among all the heat source models, the moving double ellipsoidal heat source model proposed by Goldak et al [6] has been widely used to simulate the heat input of welding processes as well as weld to predict welding residual stresses.

Goldak also achieved success in predicting the shape and size of the fusion zone using the moving double ellipsoidal power density distribution. The shape and the size of the ellipsoid is set equal to that of the molten weld pool. This more complex heat source model allows the power to be distributed asymmetrically forward. A

double-ellipsoid heat source configuration generated in an arc welding process is shown in Figure 7.1. The power density distribution of the front and rear quadrants of the moving heat source model are described with the following equations:

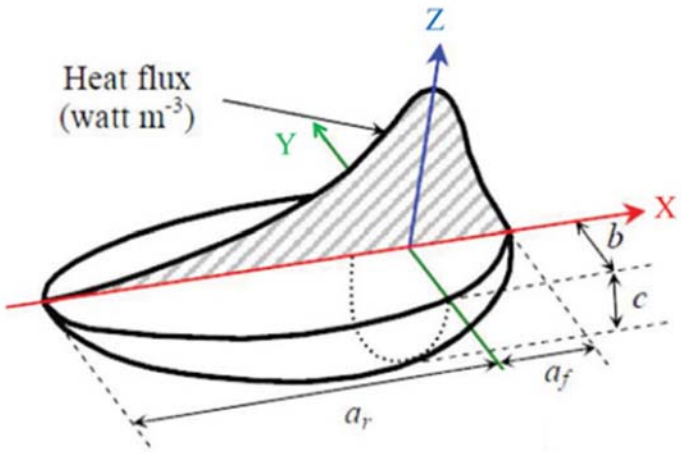

Figure 7.1 Double ellipsoid heat source configuration with the power distribution [7]

$$q_f\,(x,y,z,t) = \frac{6\sqrt{3}\eta Q f_f}{a_f bc\pi\sqrt{\pi}} exp\left(-\frac{3x^2}{a_f^2} - \frac{3y^2}{b^2} - \frac{3z^2}{c^2}\right) \tag{7.2}$$

$$q_r\,(x,y,z,t) = \frac{6\sqrt{3}\eta Q f_r}{a_r bc\pi\sqrt{\pi}} exp\left(-\frac{3x^2}{a_r^2} - \frac{3y^2}{b^2} - \frac{3z^2}{c^2}\right) \tag{7.3}$$

where x, y and z are the local coordinates of the double ellipsoid model, η is the arc efficiency, Q is the effective heat input as given in Equation 7.1. Parameters a, b and c are related to the definition of the ellipsoidal shape and can carry different values in the front and rear quadrants since they are independent. a_f and a_r are the front and rear semi-axes of the heat source, respectively. The fraction of deposited heat f_f and f_r represent the heat distributions in the front and rear quadrants of the double ellipsoid, where $f_f + f_r = 2$.

The double ellipsoidal model has the advantage of imposing the heat input in the FE model with a user subroutine which perform the weld deposition in a continuous and sequential manner. However, it is extremely difficult if the welded structure has complex configuration, i.e. multi-pass welds in a thick section, and/or the computer resource is restricted.

An alternative 3D model can apply moving welding simply dividing a weld pass into smaller weld blocks and consider sequentially heating of each block in the welding

direction with a constant heat input. The heat flux (h), in the unit of W/mm^3, applied to a weld block can be calculated using the following equation:

$$h = \frac{Q}{V_{wb}} \tag{7.4}$$

where, Q is given by Equation 7.1. V_{wb} is the volume of the weld block corresponding to the heating time Δt.

The heating time for each weld block can be calculated with Equation7.5:

$$\Delta t = \frac{L_{wb}}{v} \tag{7.5}$$

where, L_{wb} is the length of the weld block in welding direction, and v is weld electrode travel speed.

This method, compared to the double ellipsoidal model, comes with an easier implementation for the process of sequentially depositing weld fillers but not in a continuous manner. This drawback can be overcome by having smaller blocks of weld passes in the welding direction.

7.2.2.3 Two-dimensional heat source

Compared to 2D model, 3D analysis for heat transfer modelling is more time- and resource-consuming, especially, for thick section components fabricated from multi-pass welding. In such case, the use of 2D cross section model with an equivalent static heat source is a widely accepted practice.

The use of 2D has clear advantages. When predicting residual stresses in a thick-sectioned multi-pass circumferential weld, a 2D axisymmetric model which assumes rotational symmetry can be employed to reduce calculation and allow a high degree of mesh refinement to evaluate critical stresses within or adjacent to the weld.

However, there are limitations on what a simplified model can offer. In a 2D model the effect of heat flow in the (hoop) direction of motion of welding heat source is not taken into account. Hence, it is not easy to impose an equivalent welding heat input in a 2D model while excluding the heat conduction in this direction. The model is assumed to be in plane strain as displacements (strain) in the welding direction is

treated as zero, leading to a high constraint in this direction and hence an overestimate of the hoop stress levels.

In order to apply a proper imposition of equivalent welding heat input in a 2D residual stress model, the following considerations should be taken into account. The heat input is modelled by assigning distributed heat flux on individual elements, in the unit power/unit volume, for instance, W/mm^3. An equivalent heat flux (h) during a finite period of heating time (Δt) is estimated using Equation 7.6:

$$h = \frac{Q}{V_p} \tag{7.6}$$

where Q (the effective heat input) is given by Equation 7.1, V_p is the weld pass volume corresponding to the heating time in a 2D model.

Estimation of the weld pass volume V_p in a 2D model is not easy the fraction of the circumference that makes up the volume $V_p$is unknown. This issue comes from the approximation of a real 3D heat flow by using an axisymmetric 2D solution. Instead of modelling a heat source (electrode) travelling around the pipe circumference at specific welding speed in 3D, a 2D model assumes the heat flux is applied instantaneously around the circumference. Hence the fraction of the circumference is estimated in such a way that some empirical observations are satisfied [8].

If weld cross-section macrographs are available, then V_p can be conveniently estimated by the following relation [9]:

$$V_p = A_p v \Delta t \tag{7.7}$$

where A_p represents the area of the cross-sectional area of a weld pass. By combining Equations 7.6 and 7.7, the equivalent heat flux in a 2D model can be expressed as

$$h = \frac{Q}{A_p v \Delta t} \tag{7.8}$$

Equation 7.8 gives the equivalent heat flux applied to a 2D model of welding heat transfer which would be constant during the heating time Δt. Then the heating time Δt (Equation 7.9) can be approximately estimated when the heat source passing a weld pool length L_p:

$$\Delta t = \frac{L_p}{v} \tag{7.9}$$

The value of L_p can be estimated as two times of a typical weld bead width [9].

7.2.3 Mechanical modelling

Mechanical analysis, namely the welding residual stress simulation, which follows the thermal analysis, should be conducted using the results from the heat transfer analysis. Either a coupled or an un-coupled analysis can be employed.

A coupled analysis assumes that the stress/deformation field in a structure depends on the temperature field in the structure, involving each step of the thermal analysis being run and immediately followed by the corresponding time step of the mechanical analysis.

However, the temperature field can be found without knowledge of the stress/deformation response. As a result, the heat generated by deformation can be ignored in a welding analysis and it is not necessary to conduct coupled analyses. Therefore, most welding simulations are conducted as un-coupled analysis. In such a mechanical model, stress analysis reads the temperatures from the heat transfer analysis during which the temperature varies with position and is usually time dependent. The temperature is predefined because it is not changed by the stress analysis.

Apart from inputting the temperature field from a heat transfer model, the stress analysis employs a material model which aims to realistically represent the material's mechanical behaviour during a welding process, such as the elastic and plastic behaviours including plastic strain hardening in the thermal cycles of rapid heating and cooling.

In terms of hardening behaviour, a material can be assumed to exhibit either isotropic, linear kinematic or non-linear kinematic plastic strain hardening. Isotropic hardening model is developed based on the assumption that the yield surface remains the same shape but expands in size uniformly in all directions with the increasing stress, which implies that, the yield strengths in tension and compression are initially the same.

The kinematic hardening models are used to model Bauschinger effect, where a hardening in tension will lead to a softening (reduced yield strength) in reversed loading (compression). With this type of hardening behaviour, the yield surface remains the same shape and size and merely translates in the stress space. In theory, the kinematic hardening models are preferable in simulations of a welding process since the Bauschinger effect due to cyclic straining of the weld and adjacent parent metals which subjected to several thermal cycles in the multi-pass weld is taken into account.

7.3 Simulation of residual stresses in narrow-gap girth welds

7.3.1 Generation of FEA model

7.3.1.1 Weld geometry creation

A weld cross section was extracted from the 3'clock location of a girth weld in the cross-sectional view of the pipe, and a macrograph has been prepared to show the weld profile (Figure 7.2a). A 2D axisymmetric model of the pipe was created. The weld geometry has been made in an effort to recreate the actual weld profile as closely as possible but with simplified geometry to reduce potential complexity in sketching. Figure 7.2b shows the modelled weld zone with created partitions which took into account the HAZ region as well as the material overlap effect between every two sequential passes. Two sets of the materials, the parent metal and the weld metal, were defined (Figure 7.3).

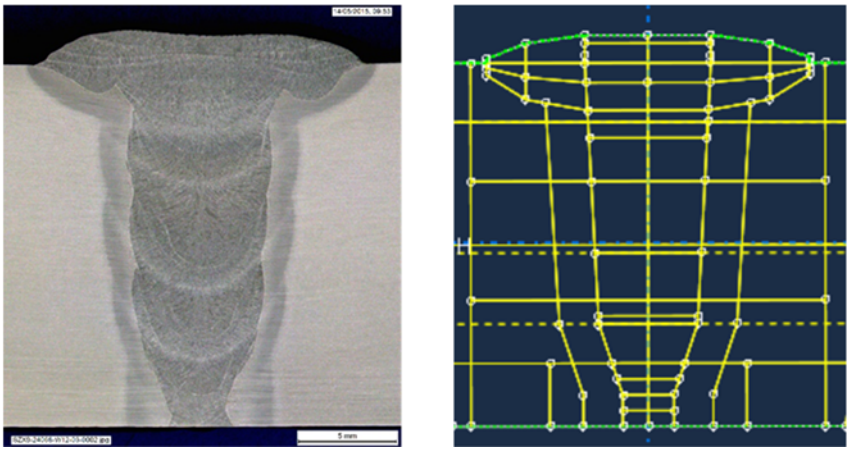

(a) (b)

Figure 7.2 Geometry of the weld cross section in (a) an experimental extracted weld macrograph and (b) a modelled weld profile

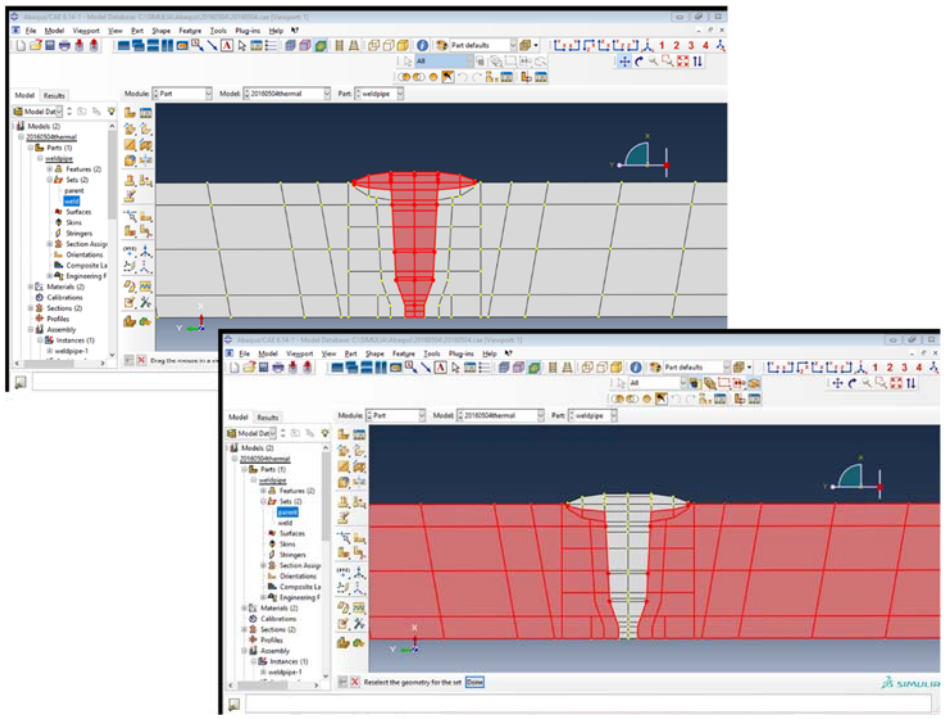

Figure 7.3 Display of the material sets, weld metal and parent metal as highlighted, in model.

7.3.1.2 Material properties

Material property data used for this study was collected from experimental measurement and literature surveys [10]. The thermal and mechanical properties, including conductivity, thermal expansion coefficient and specific heat, density, elasticity, plasticity, were defined with either fixed or temperature-dependent values.

For both parent and weld metals, same values of material properties were applied except for the yield strengths which are different determined from mechanical testing. The material property data used are listed in Table 7-1, Table 7-2, Table 7-3, Table 7-4 and Table 7-5. The mass density of the materials is $7.97E-6\ g/mm^3$.

Table 7-1 Temperature-dependent material conductivity

Temperature, °C	Conductivity, W/mm/K
0	0.06
62.6	0.0597
208.4	0.0547
323.7	0.0494
508.3	0.0406
746.4	0.0314
861.4	0.0281
1417.8	0.0333
1493.8	0.0358
1500.9	0.0392
1523.7	0.0397
1730	1

Table 7-2 Specific heat used for thermal analysis

Temperature, °C	Specific heat, J/ [kg. K]
0	361
198	410
443	492
619	575
657	617
718	675
802	818
840	1002
855	1136
895	456
1384	496
1560	570

Table 7-3 Material thermal expansion coefficient

Temperature, °C	Thermal expansion coefficient (α)
20	1.26E-05
688	1.44E-05
703	1.42E-05
811	1.33E-05
849	1.21E-05
864	1.12E-05
872	1.05E-05
1068	1.27E-05
1240	1.42E-05
1412	1.52E-05
1460	1.66E-05
1476	1.73E-05
1492	1.78E-05

Table 7-4 Material elastic modulus and Poisson ratio

Temperature, °C	E, MPa	Poisson ration, μ
0.0	207197	0.3
210.9	201269	0.3
390.6	184363	0.3
468.8	170407	0.3
523.4	156495	0.3
593.8	131503	0.3
632.8	106569	0.3
664.1	81650	0.3
695.3	56730.5	0.3
773.4	37249.7	0.3
914.1	23178.5	0.3
1070.3	17365.9	0.3
1210.9	6057.21	0.3

Table 7-5 Material plastic properties for stress analysis

Temperature, °C	Plastic strain	Yield stress, MPa	
		Parent metal	Weld metal
20	0	510	657
20	0.1	600	600
200	0	388	388
200	0.1	573	573
400	0	355	355
400	0.1	557	557
600	0	206	206
600	0.1	244	244
900	0	31	31
900	0.1	70	70
1200	0	4	4
1200	0.1	4	4

7.3.1.3 Element type and mesh design

Meshing of the weld model was applied in the assembly module not on the parts as the parts were out together to form an assembly. The geometry mesh was created on the assembly with a total of 8592 elements.

There are several selections of element types such as linear, quadratic, hybrid and reduced integration. In this study, the first order 4-node linear axisymmetric heat transfer quadrilateral elements (DCAX4) [11], [12] provided by the software was employed for thermal analysis. And the second-order 8-node biquadratic axisymmetric quadrilateral with reduced integration elements (CAX8R) [13] for nodes located at the corner and mid-side of each element, was employed in mechanical analysis.

Reduced integration elements were used for the stress analysis. As a welding process may introduce high level of plastic strain, element-locking, which may occur in fully integrated elements when material behaviour is almost incompressible, can be avoided.

There was a high degree of mesh refinement at the weld zone and adjacent HAZ (Figure 7.4) to capture the steep thermal and stress gradient during welding. The thermal effect on parent materials further away from the weld is less of a concern.

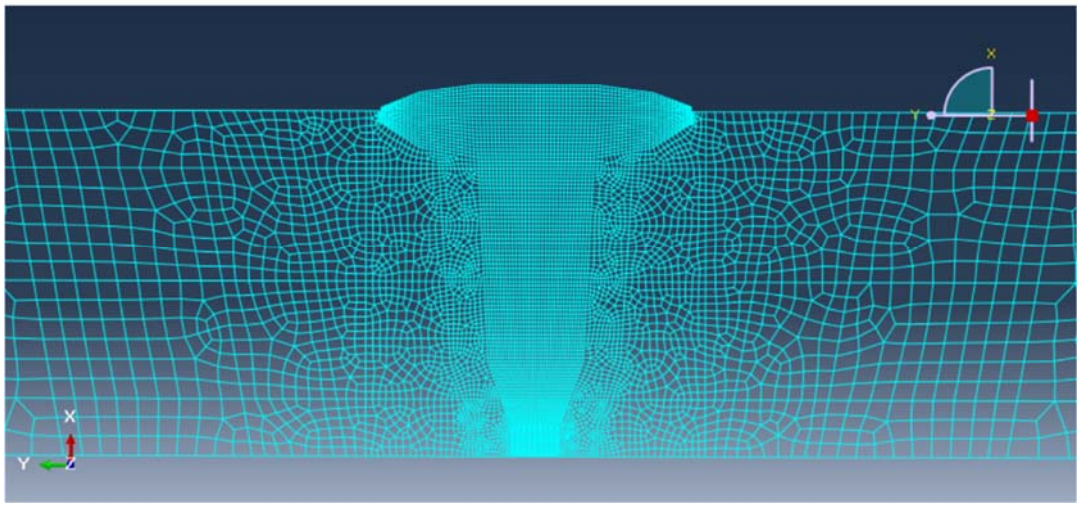

Figure 7.4 Mesh refinement at the weld zone and adjacent HAZ

7.3.2 Heat transfer modelling

7.3.2.1 Modelling of thermal cycles

Weld zone materials in a multi-pass welding process experienced a sequence of heating and cooling in certain time of period, which was modelled in STEP module (Figure 7.5). In each weld pass, a heating and a cooling steps were created with assigned heating time calculated using Equations 7.6, 7.7, 7.8 and 7.9 and cooling time recorded during welding process.

Step Manager

	Name	Procedure	Nlgeom	Time
✔	Initial	(Initial)	N/A	N/A
✔	Step-1weldremove	Heat transfer (Transient)	N/A	0.001
✔	Step-2heatpass1	Heat transfer (Transient)	N/A	1.6482
✔	Step-3coolpass1	Heat transfer (Transient)	N/A	437
✔	Step-4heatpass2	Heat transfer (Transient)	N/A	1.7725
✔	Step-5coolpass2	Heat transfer (Transient)	N/A	350
✔	Step-6heatpass3	Heat transfer (Transient)	N/A	1.976
✔	Step-7coolpass3	Heat transfer (Transient)	N/A	378
✔	Step-8heatpass4	Heat transfer (Transient)	N/A	2.22
✔	Step-9coolpass4	Heat transfer (Transient)	N/A	402
✔	Step-10heatpass5	Heat transfer (Transient)	N/A	2.52466
✔	Step-11coolpass5	Heat transfer (Transient)	N/A	608
✔	Step-12heatpass6	Heat transfer (Transient)	N/A	3.0622
✔	Step-13coolpass6	Heat transfer (Transient)	N/A	54000

Create... Edit... Replace... Rename... Delete... Nlgeom... Dismiss

Figure 7.5 Heating and cooling steps created for thermal model

The addition of filler material was modelled by de-activating and re-activating the elements that represented each pass. All passes were defined with the corresponding weld metals which were present in the model at outset, and all the elements in the weld region was deactivated before initiating the first heating step. The deposition of the weld metal was achieved by activating the elements defined for each pass, which were isolated from the previous passes.

7.3.2.2 Modelling of thermal loads

Thermal loads were modelled with a distributed body heat flux which assumed theat the heat was instantaneously applied to the weld cross section. As discussed in Section 7.2.2.3, an effective heat input (Equation 7.8) was calculated based on an estimation of the weld pool length and the area of the cross section of the heated weld bead.

Figure 7.6 is an example assuming that the weld material being added for of Pass 2 was only a part of the material being heated because of the re-heat in material in a multi-pass weld. The material volume for each pass was estimated from the weld macrograph (Figure 7.2). The heat input was only modelled in each heating step and the addition of heat flux was deactivated in the subsequent cooling step.

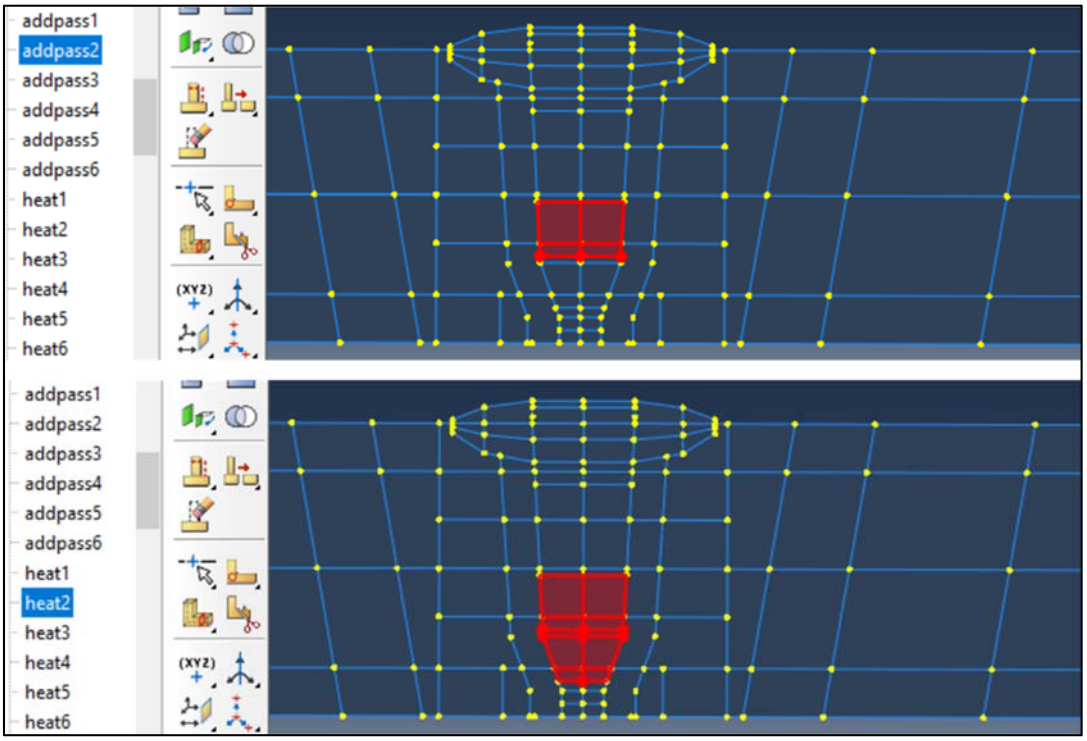

Figure 7.6 An example of showing the volumes of the material being added and heated for Pass 2 with the consideration of re-heat effect in multi-pass weld

7.3.2.3 Modelling of thermal boundary conditions

The heat transfer boundary conditions can incorporate both convection and radiation. Convective heat transfer was dominate for the near surface rate during cool-down, and radiative heat transfer was significant at high temperatures near the weld. The effect of radiative heat losses was excluded during weld metal deposition because an equivalent heat source was used which has taken into account the heat losses with applied weld efficiency. Thermal boundary conditions were applied to all boundaries of the pipe as well as the new boundaries created for each new pass. Figure 7.7 is an example of the surface created for Pass 2. Another important boundary condition is pre-heat. It was modelled by raising the initial temperature to 80 °C before any welds deposition were simulated.

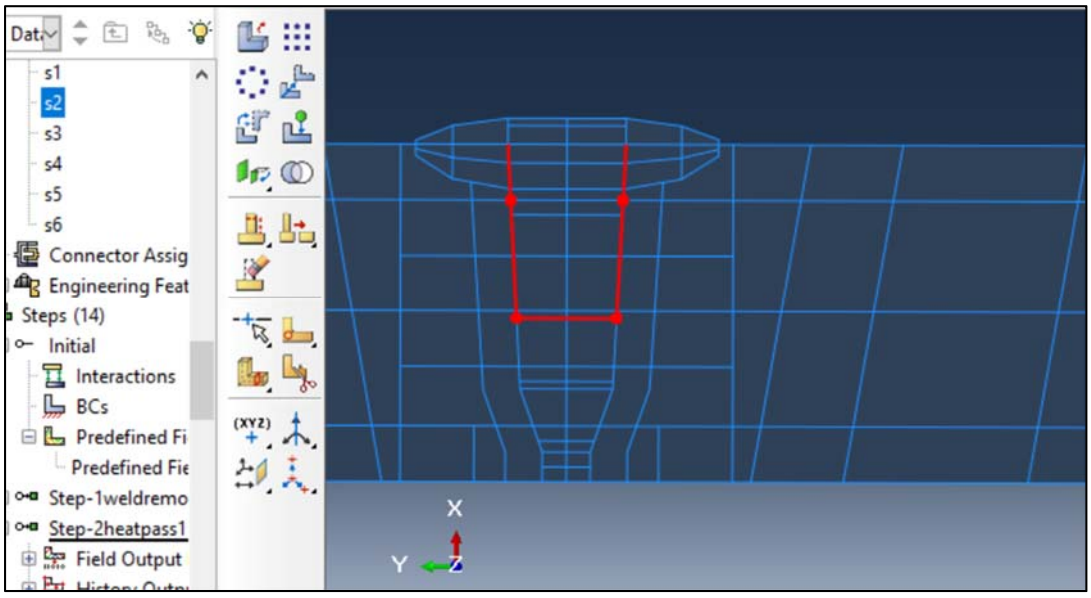

Figure 7.7 An example of the surface created for Pass 2

7.3.3 Mechanical modelling

A mechanical model was created based on the previously established thermal model. In a mechanical model, the weld geometry, material property and the sections (weld and parent metal regions) must be identical to that of the thermal model while some changes have been made in terms of step type, load and boundary conditions. Also, in this work, the element type was changed to CAX8R which was introduced in section 7.3.2.3.

In a stress analysis, there were also 13 steps created and each step time was in line with that of the thermal model (Figure 7.8). The approach of deactivation/activation of the weld beads was also employed to simulate metal depositions. However, the step type was changed from heat transfer (in the thermal model) to a general static which called for a history of stresses and strains.

For a mechanical model there was no external load applied to the pipe, the stresses/strains were generated from thermal history. There were also no axial restraints considered to approximate the realistic conditions at the fabrication of a pipe girth weld. Instead a mechanical boundary condition restraint was created at the outer surface at the centre of the weld root to prevent the component from rotating in the circumferential direction and moving along pipe length.

The temperature output from the thermal analysis was used in the mechanical analysis for the prediction of welding residual stresses, which was achieved by reading the temperature history of the step as predefined fields for the stress output for the same step. Such predefined fields were read into ABAQUS at nodes where interpolation was made at mid-side nodes for the determination of resultant stress within the given elements.

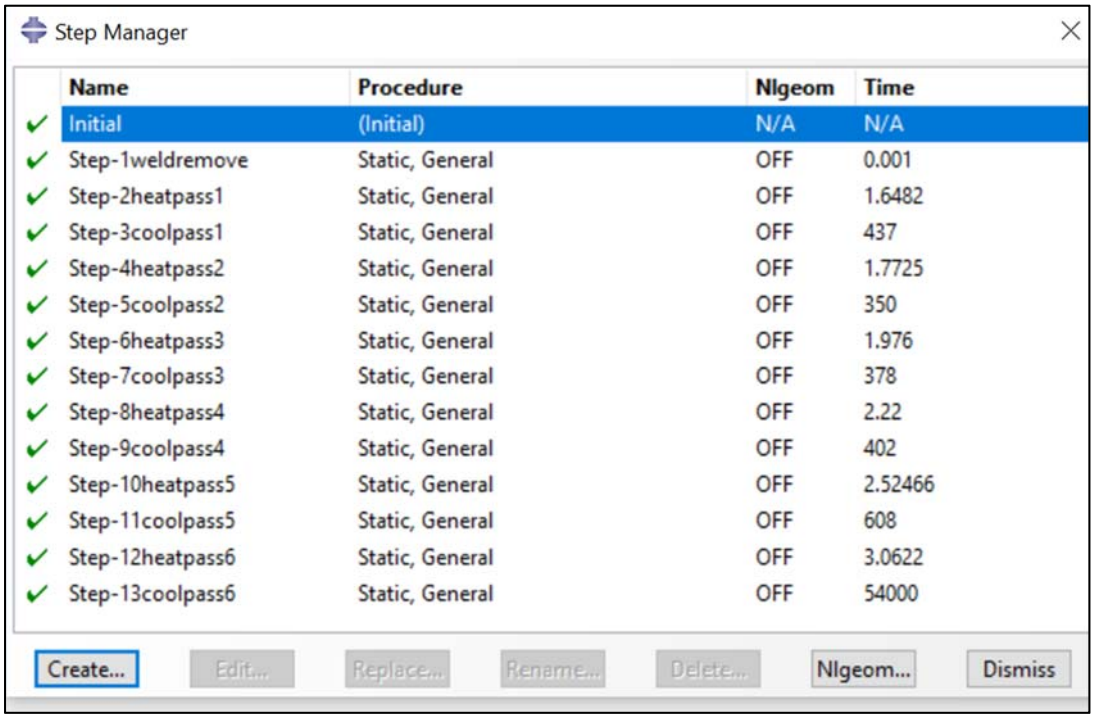

Figure 7.8 Heating and cooling steps created for stress analysis

7.4 Results

7.4.1 Simulated thermal field

The simulated cross-sectional thermal fields for each weld pass are given in Figure 7.9 and 7.10. A reasonable molten zone size was achieved when at least the melting temperature (assumed 1500°C) was reached in each weld pass (Figure 7.9). And the distance to the HAZ from the fusion boundary where the maximum temperature has reached 900°C (Figure 7.10) [8]. A comparison of the weld profile between the 2D simulated weld cross section (Figure 7.9) and the actual weld macrograph (Figure 7.2) showed both were in reasonable agreement with each other.

A further comparison was made between the measured and simulated thermal cycles, i.e. the transient temperatures of heating and cooling cycles at specific locations where thermocouples were installed (Figure 7.11 and Figure 7.12).

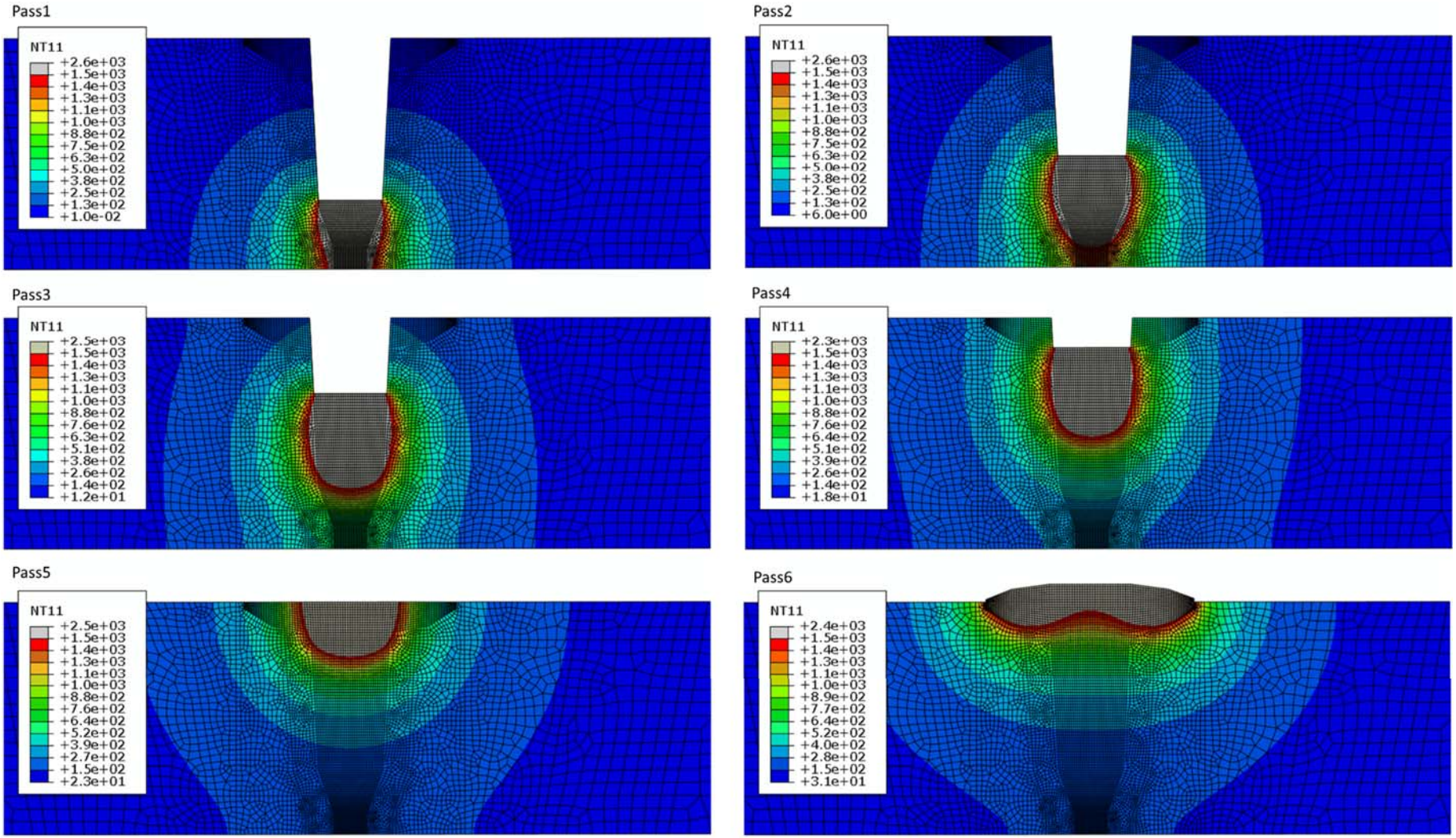

Figure 7.9 Simulated molten zone and fusion boundary for multi-pass weld

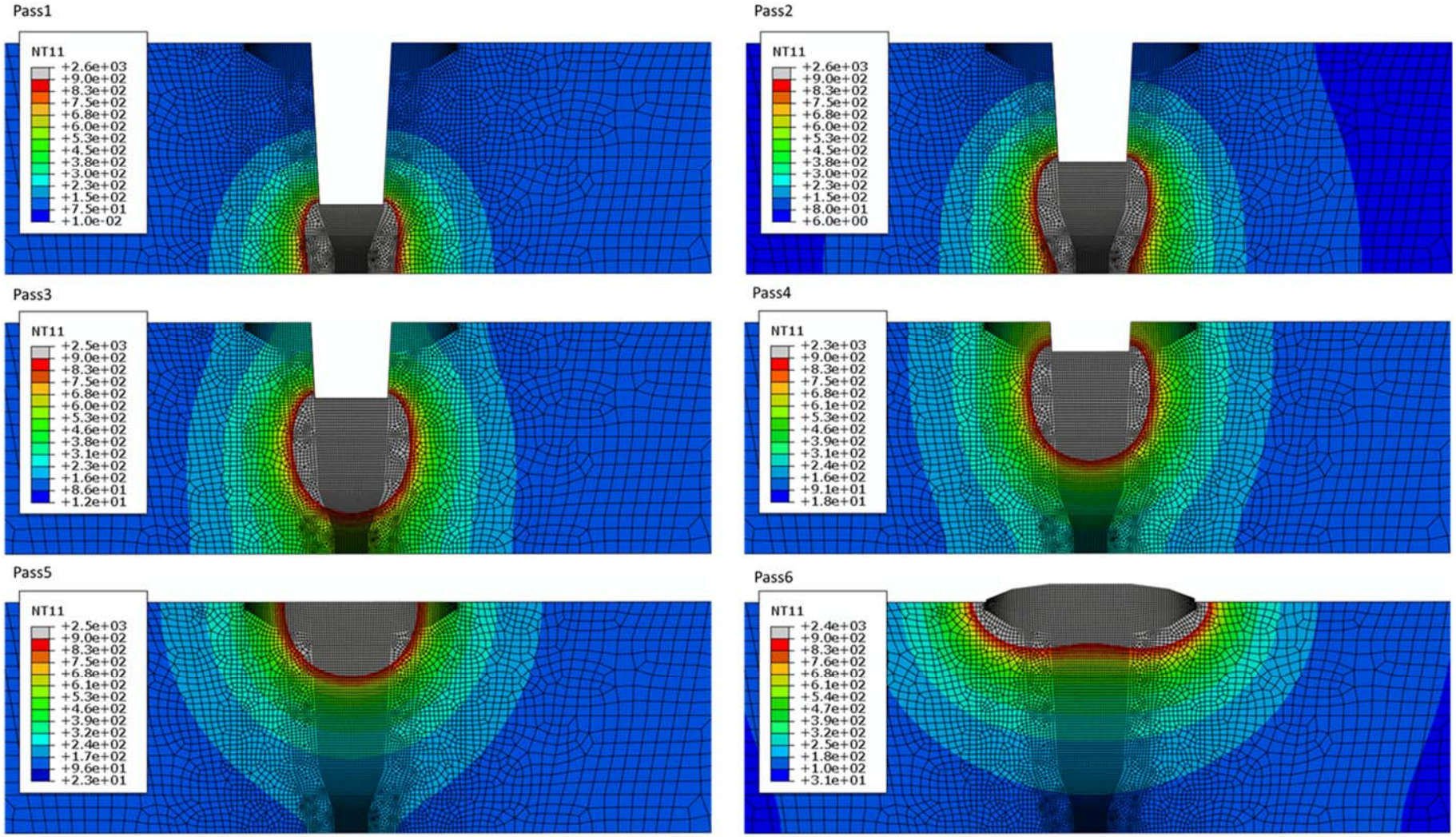

Figure 7.10 Simulated distance to HAZ from fusion boundary

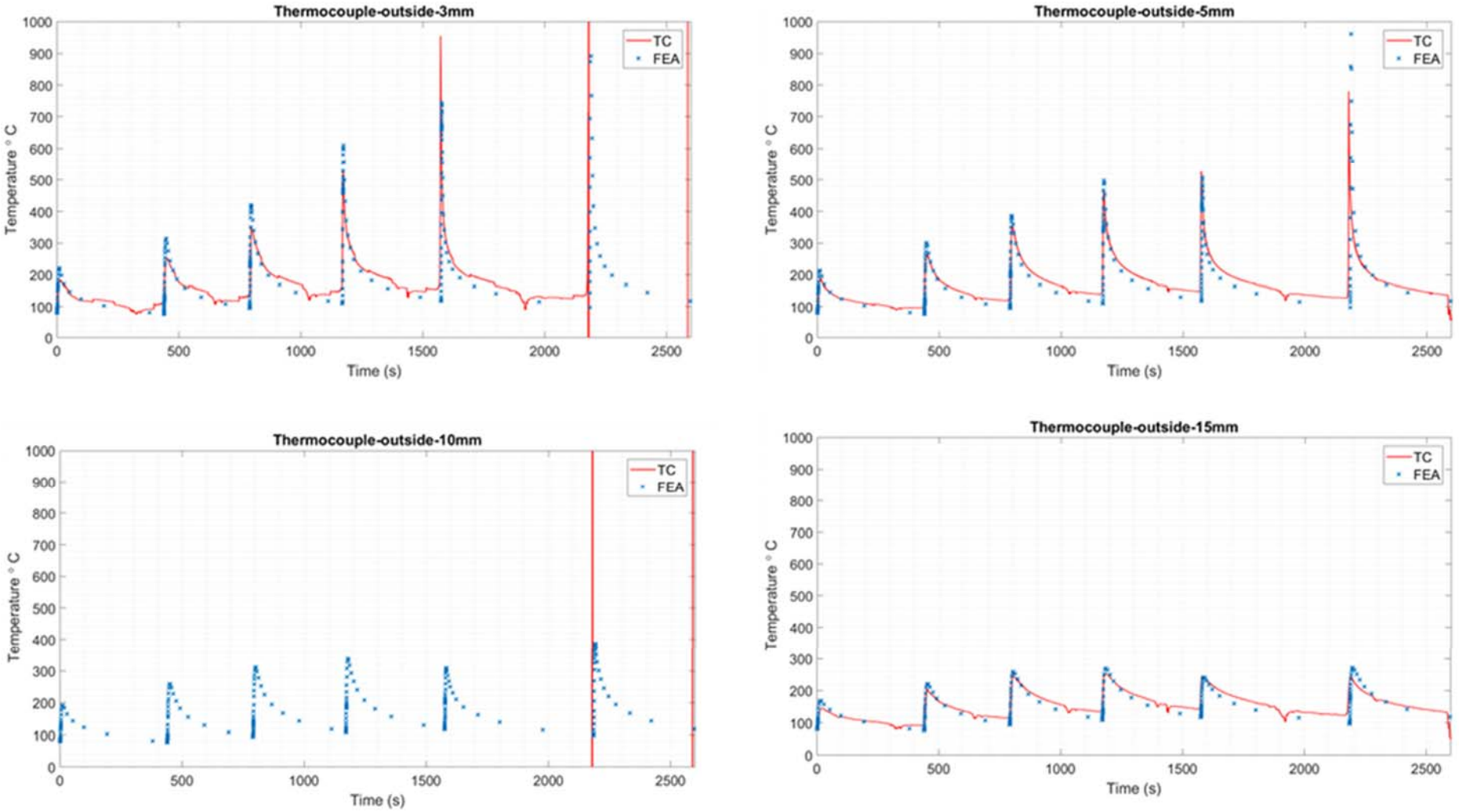

Figure 7.11 Comparisons of simulated and measured transient temperatures at the pipe outer surface

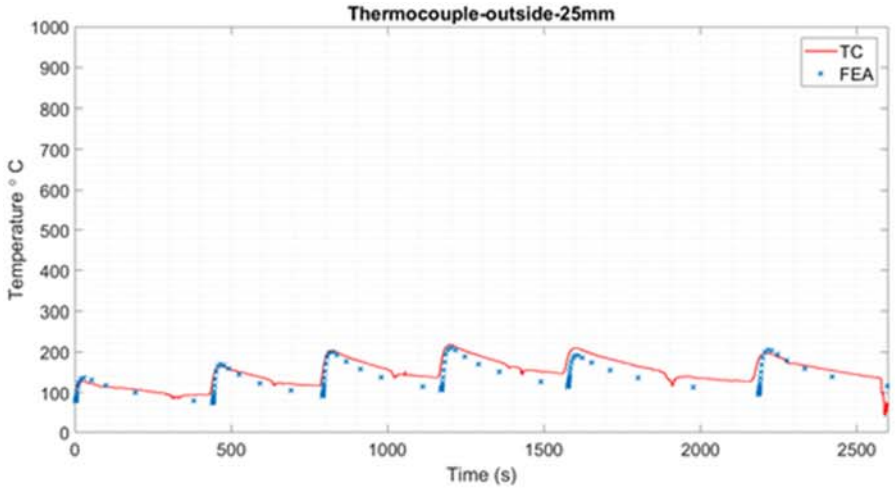

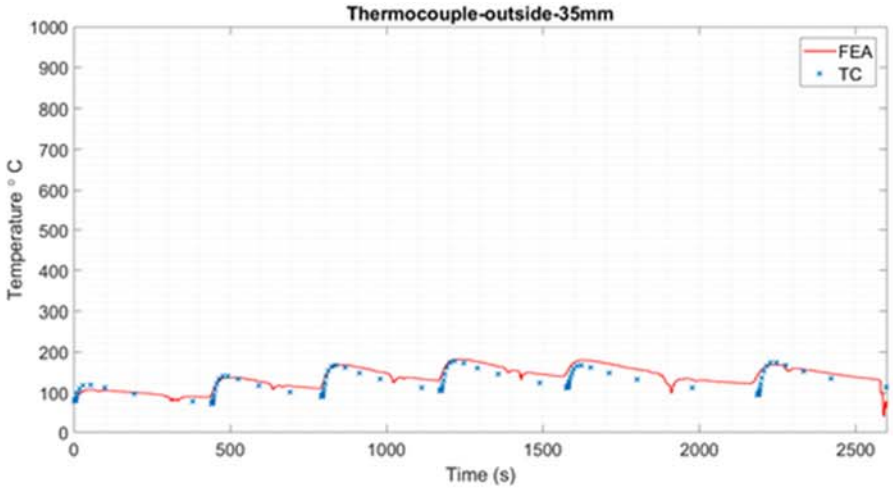

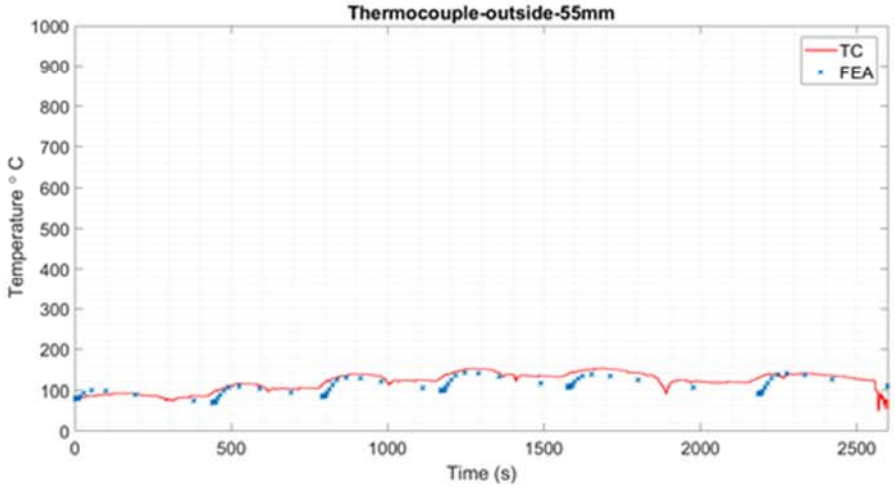

Figure 7.11 Comparisons of simulated and measured transient temperatures at the pipe outer surface (continued)

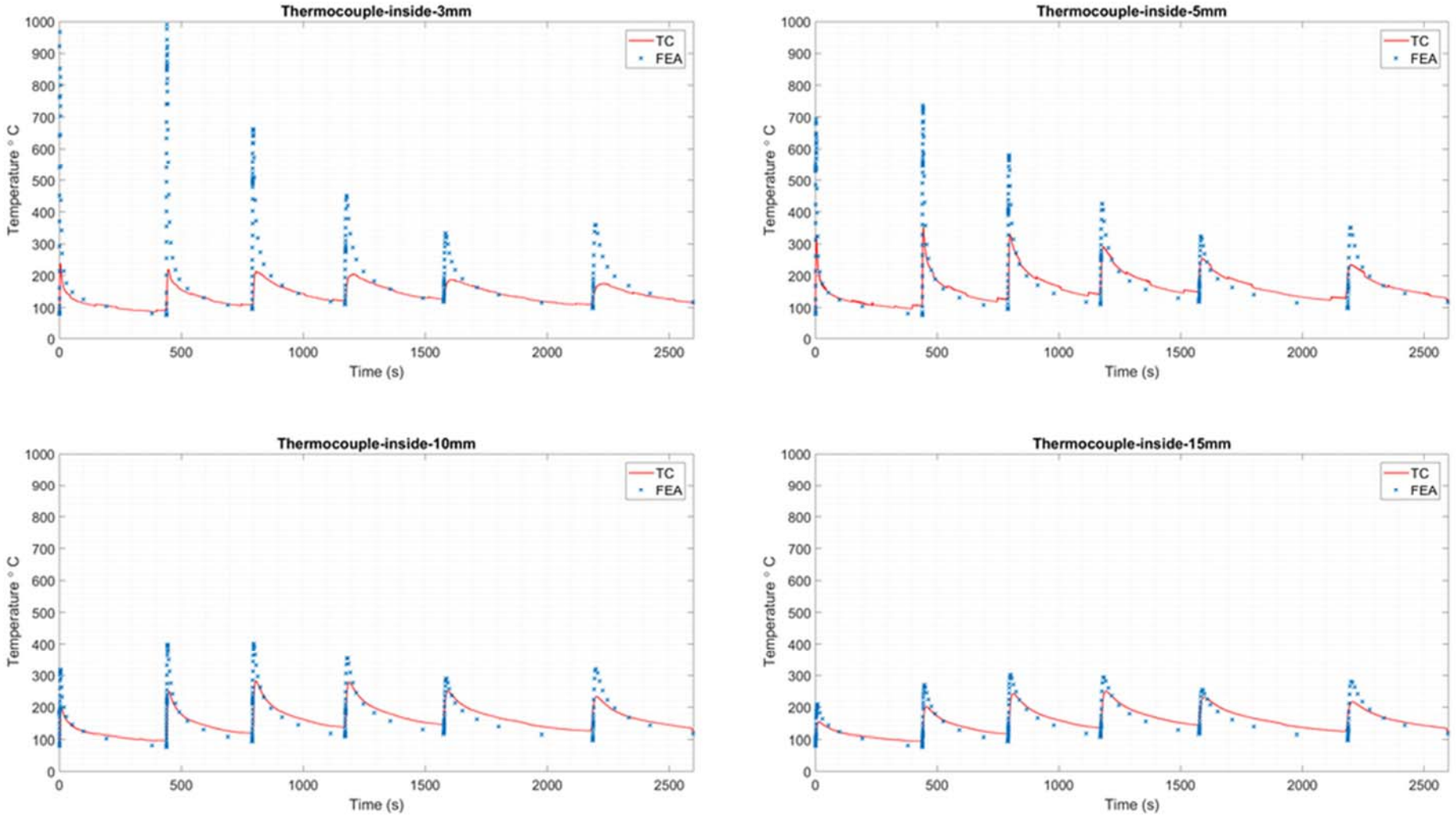

Figure 7.12 Comparisons of simulated and measured transient temperatures at the pipe inner surface

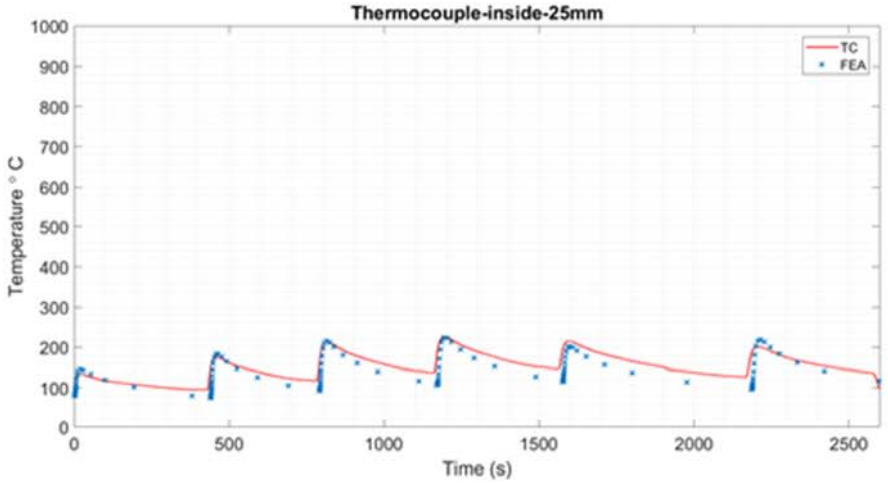

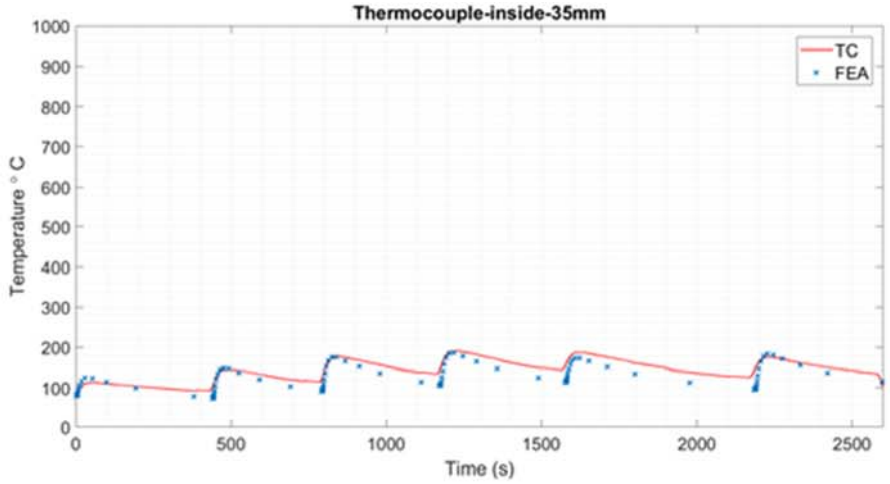

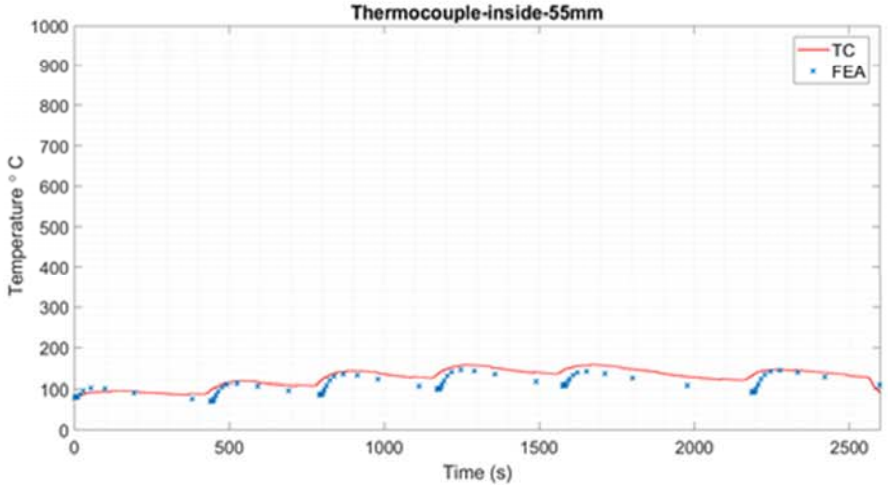

Figure 7.12 Comparisons of simulated and measured transient temperatures at the pipe inner surface (continued)

On the pipe outer surface (Figure 7.11), temperatures measured from thermocouples close to the weld grove edge (3mm, 5mm,10mm) were on average 50 °C lower than those predicted by the FEA model. Although the thermal history at the 10mm location was unknown due to thermocouple frailer, a prediction was made from another measured pipe (Figure 3.6a). Further away from the weld centre, recorded thermal cycles including inter-pass temperature were in good agreement with those simulated. Temperature deviations were less than ±5°C.

Figure 7.12 shows the measurement and FEA results for the pipe inner surface. At near-weld regions (3mm, 5mm), the peak temperatures predicted were much higher than the experimental data, which might have some inaccuracies due to the experimental setup and environment influence. At the 3mm location, the temperature measured from another pipe (Figure 3.7a) shown a peak value of up to 1000°C at the root pass, which is in good agreement with FEA results. Similar agreements have been found at the pipe outer and inner surfaces of on which the simulated peak temperatures match the experimental data.

7.4.2 Comparison of transient strains

Transient axial and hoop strains from FEA and recorded data, at locations 15mm, 25mm, 35mm and 55mm from the weld grove edge on the pipe's inner and outer surfaces, were compared and exhibited in Figures 7.13 and 7.14. Both simulated and measured peak temperatures at these locations never reached over 300°C within the working temperature range for the strain gauges used. Therefore, recorded strain values were valid.

For the welding process, generated total strains include thermal, elastic and plastic strains. In this FEA model, a mechanical strain of elastic and plastic components was calculated and then compared with recorded mechanical strain values from welding process. The trends in the whole field show a good agreement between the prediction and measurements. On pipe inner surface, hoop strains at 15mm from grove edge were not captured as the strain gauge was found to have failed (Figure 7.14b) and strains from FEA model was matched with the strain data from another measured pipe (P1 in Figure 3.11).

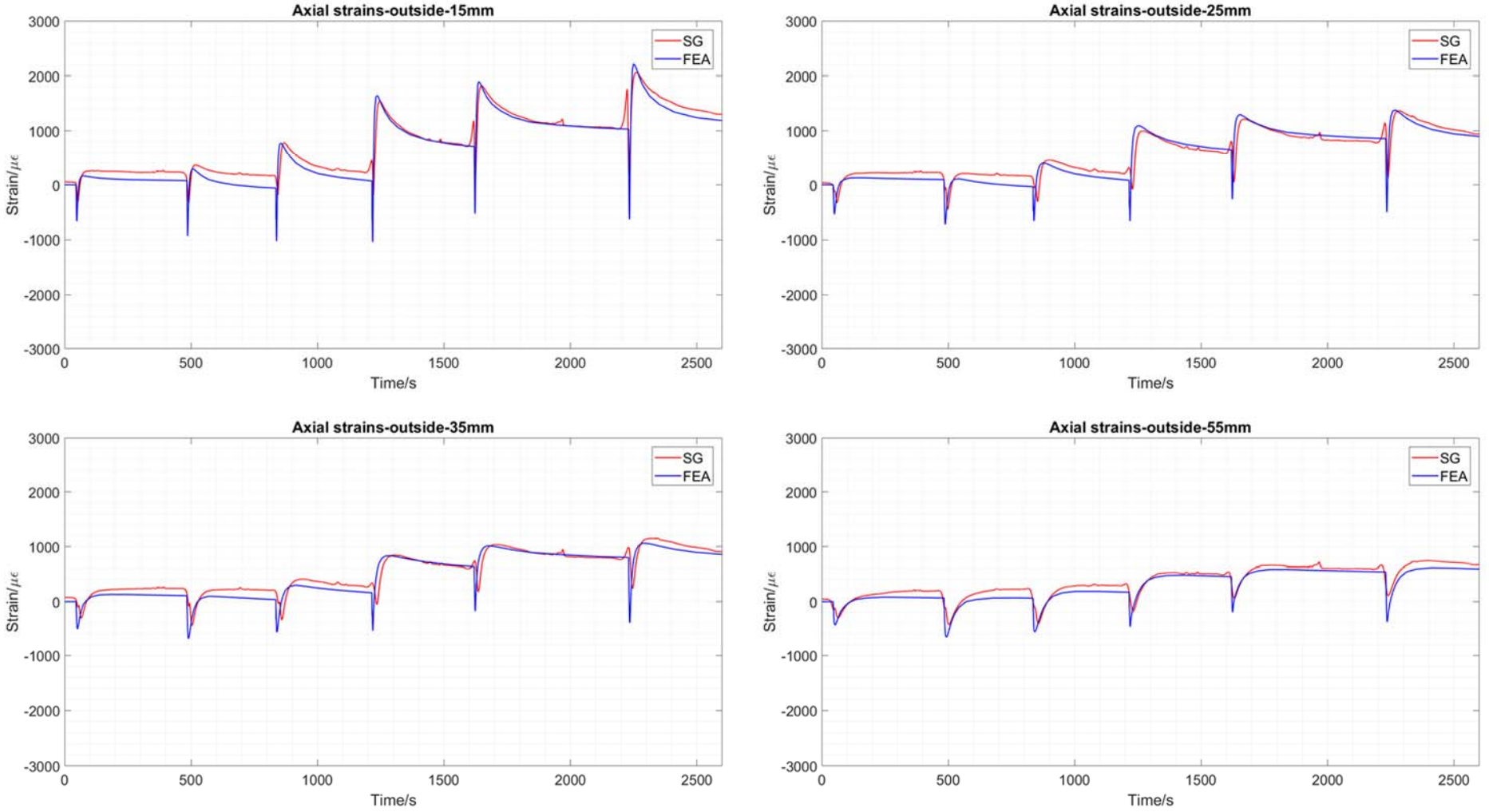
Axial strains-outside-15mm
Axial strains-outside-25mm
Axial strains-outside-35mm
Axial strains-outside-55mm
SG
FEA
Strain/με
Time/s
3000
2000
1000
0
-1000
-2000
-3000
0
500
1000
1500
2000
2500

(a)

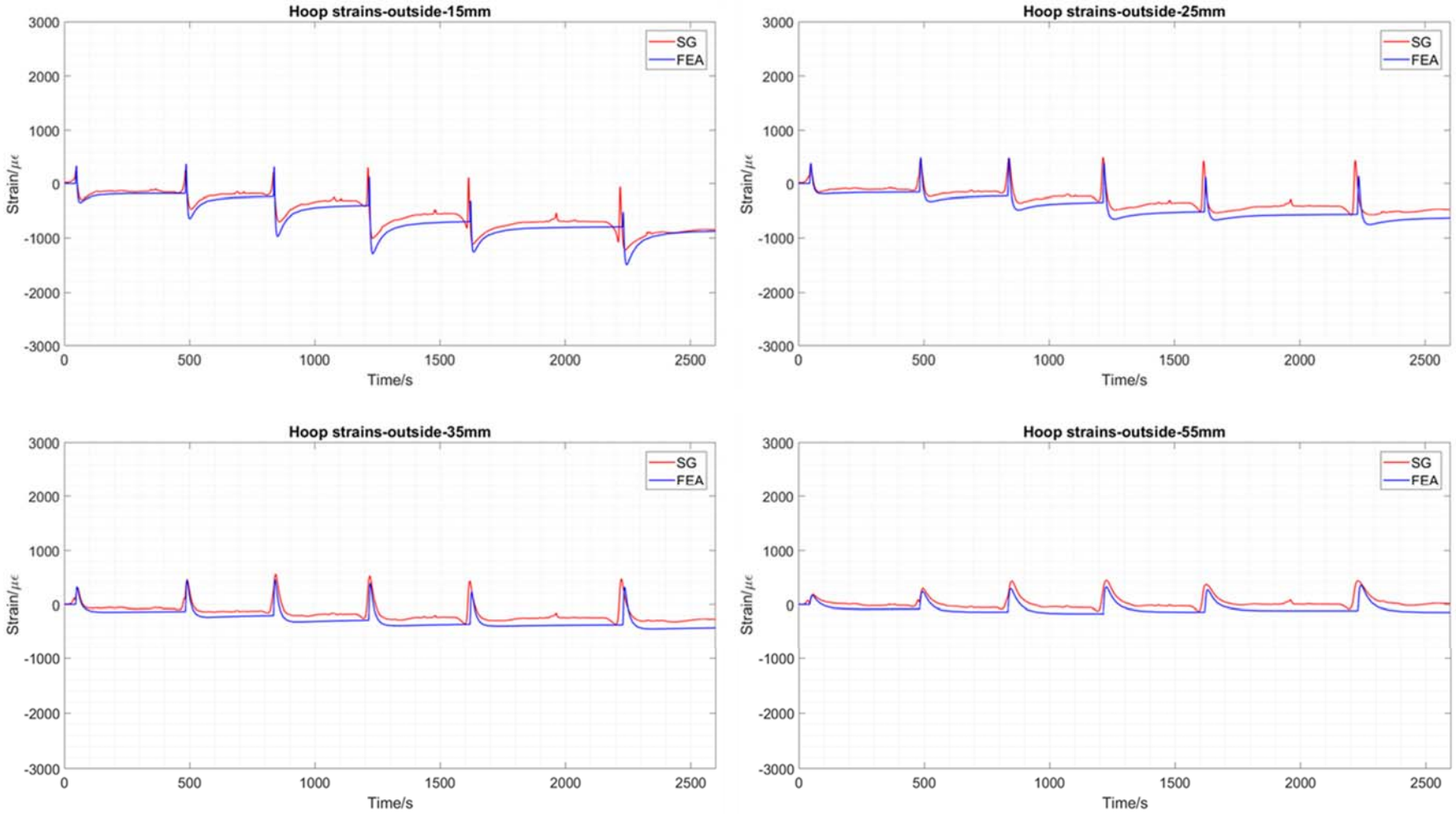

(b)

Figure 7.13 Transient (a) axial and (b) hoop strains measured at pipe outer surface

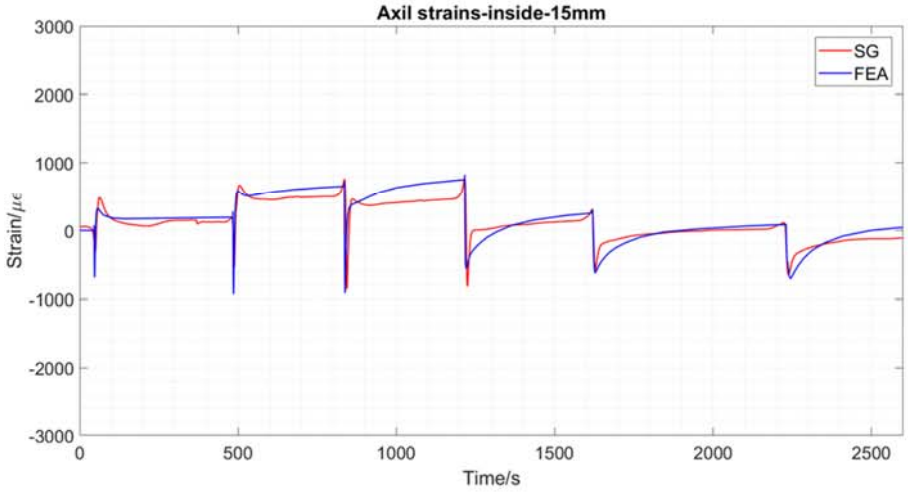
Axil strains-inside-15mm
SG
FEA
Strain/με
Time/s
3000
2000
1000
0
-1000
-2000
-3000
0
500
1000
1500
2000
2500

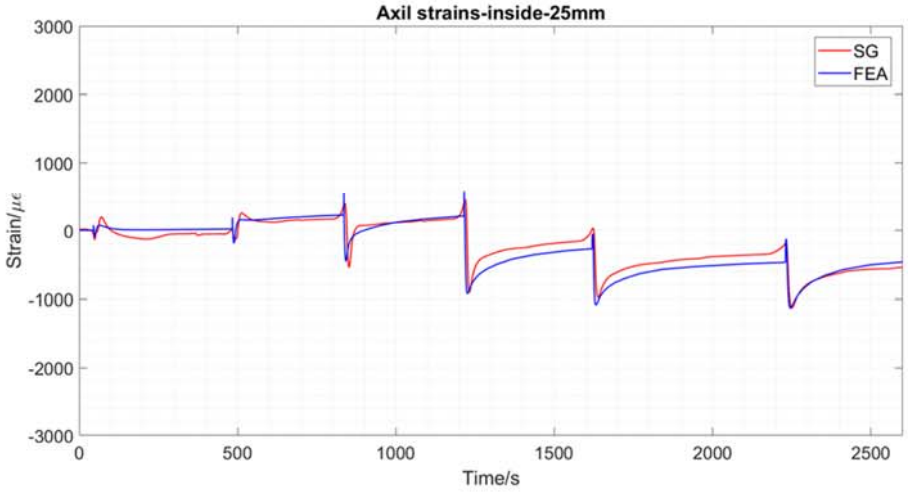
Axil strains-inside-25mm
SG
FEA
Strain/με
Time/s
3000
2000
1000
0
-1000
-2000
-3000
0
500
1000
1500
2000
2500

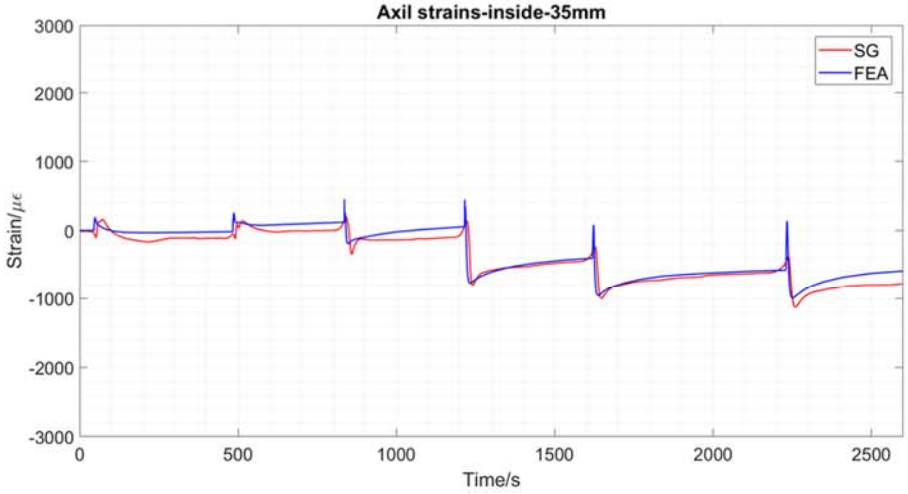
Axil strains-inside-35mm
SG
FEA
Strain/με
Time/s
3000
2000
1000
0
-1000
-2000
-3000
0
500
1000
1500
2000
2500

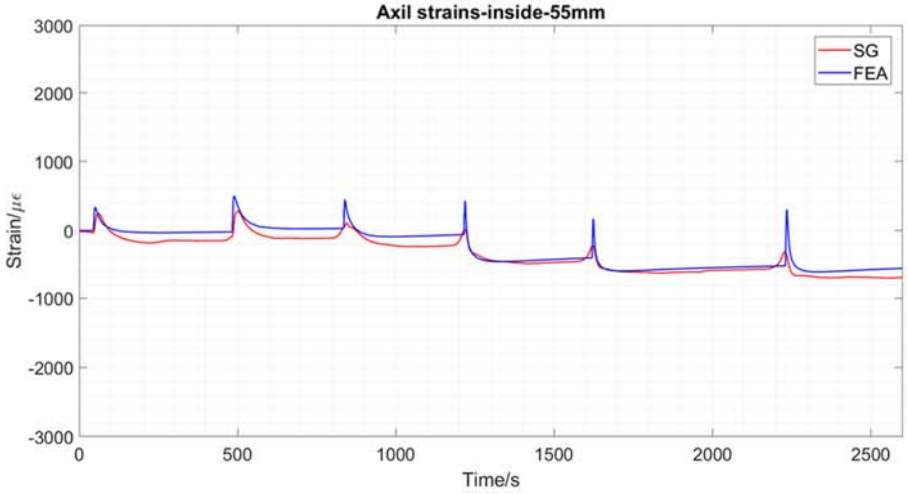
Axil strains-inside-55mm
SG
FEA
Strain/με
Time/s
3000
2000
1000
0
-1000
-2000
-3000
0
500
1000
1500
2000
2500

(a)

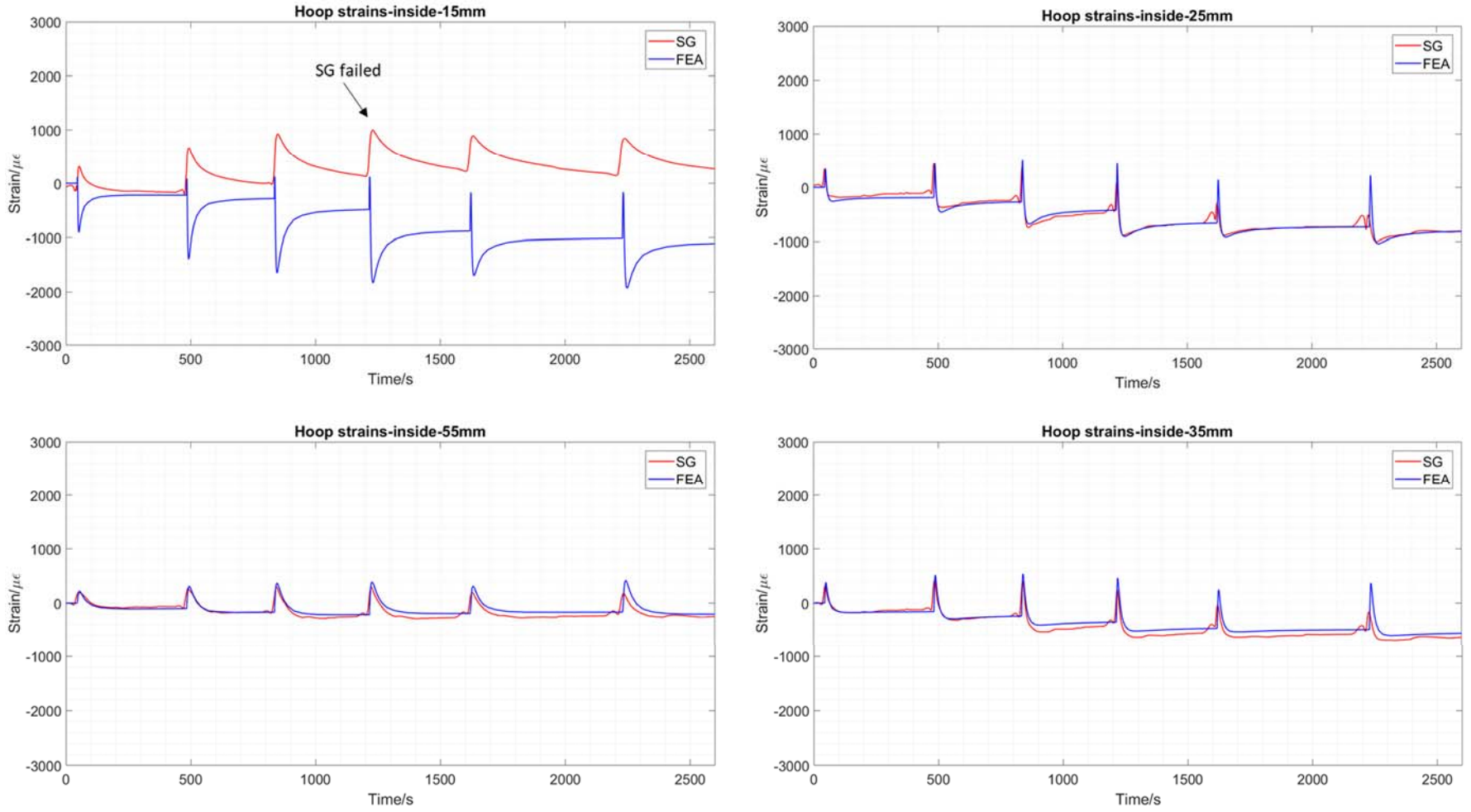

(b)

Figure 7.14 Transient (a) axial and (b) hoop strains measured at pipe outer surface

7.4.3 Predicted welding residual stresses

Predicted welding residual axial and hoop stresses at near pipe outer surface, at pipe wall mid-thickness, at near pipe inner surface, at weld centreline as well as at the weld toe were compared with the stress profiles obtained from the neutron diffraction measurement, as shown in Figure 7.15, 7.16, 7.17, 7.18 and 7.19 respectively.

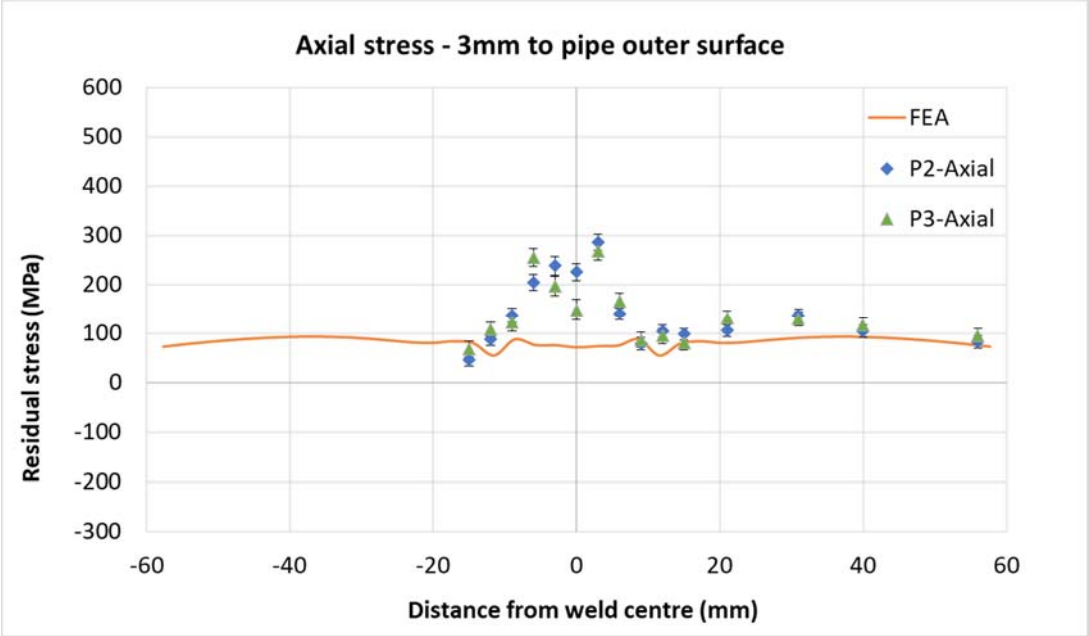

(a)

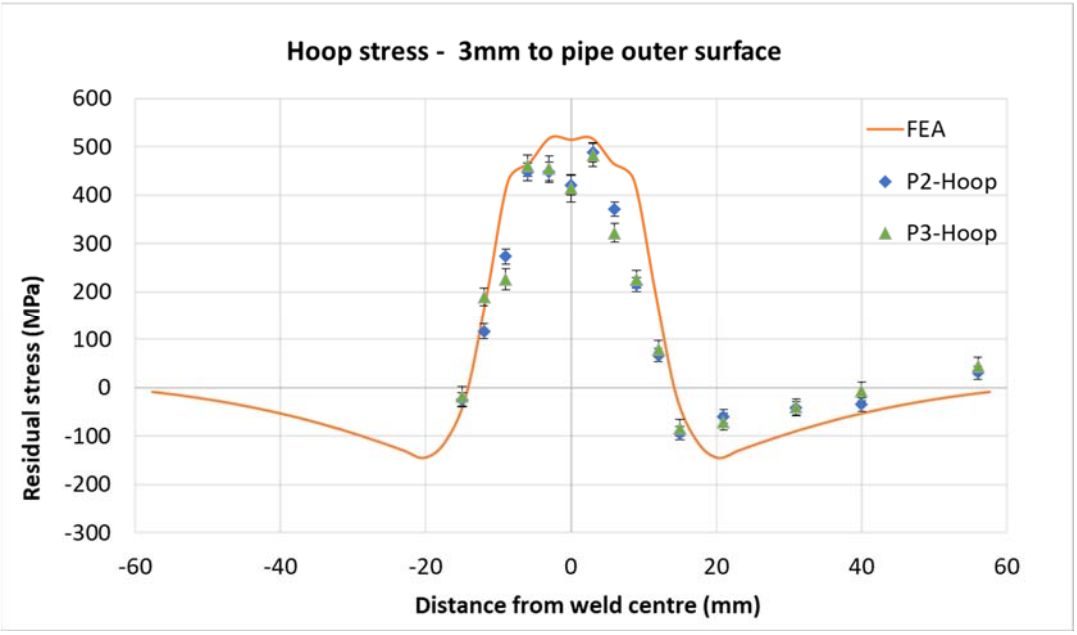

(b)

Figure 7.15 Comparison of residual (a) axial and (b) hoop stresses between FEA and mesurement profiles at loation near 3mm to pipe outer surfce

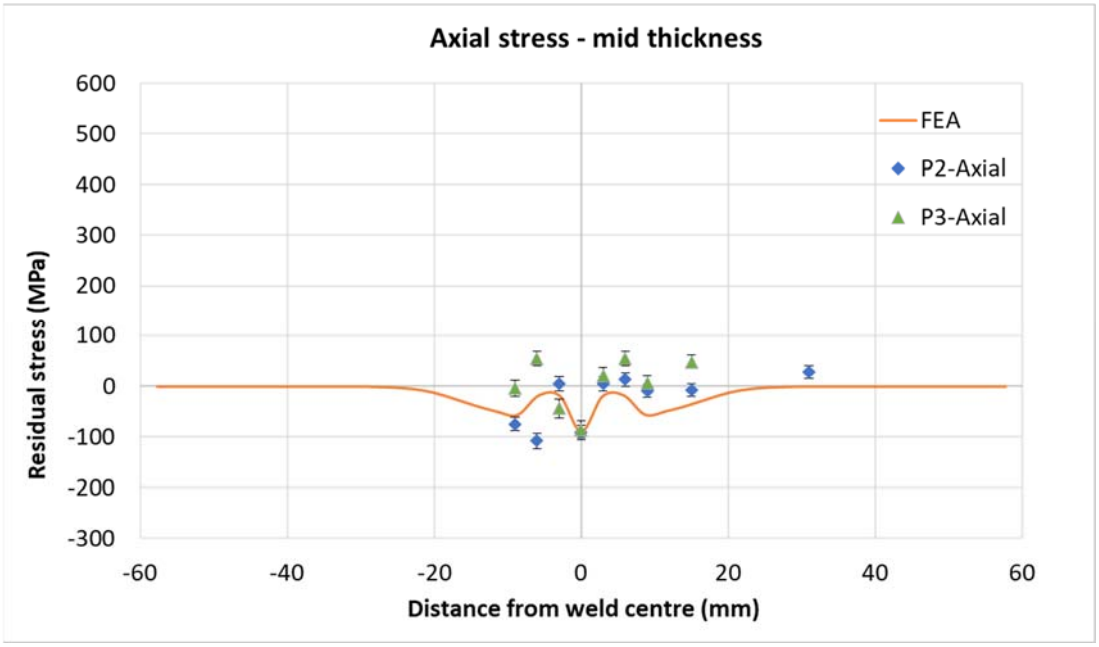

(a)

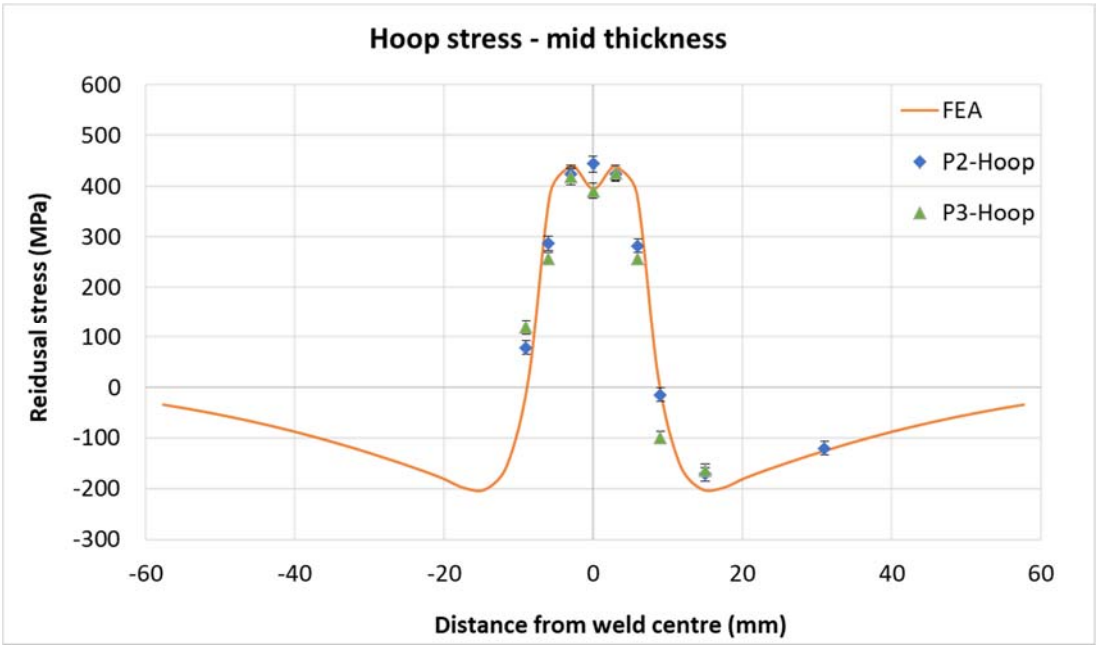

(b)

Figure 7.16 Comparison of residual (a) axial and (b) hoop stresses between FEA and mesurement profiles at pipe wall mid-thickness

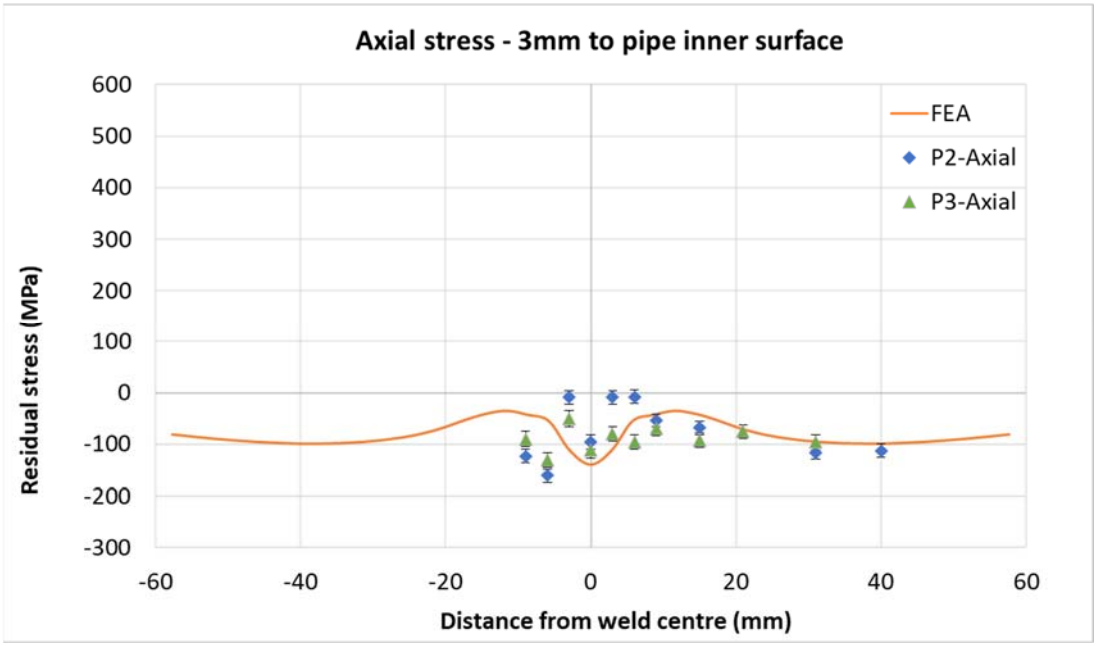

(a)

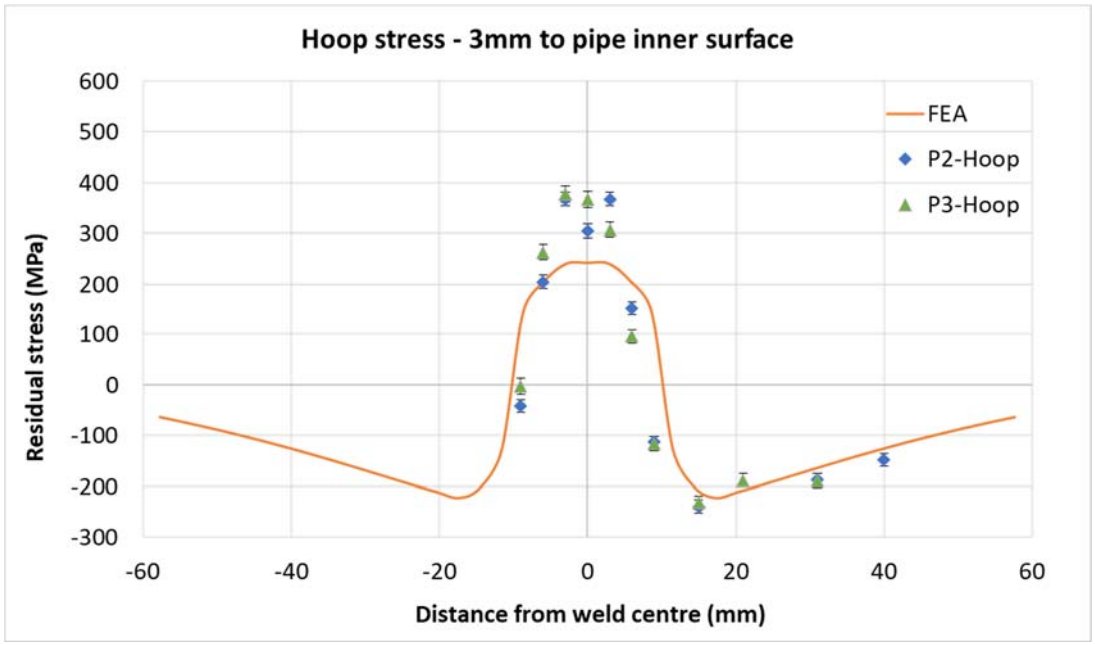

(b)

Figure 7.17 Comparison of residual (a) axial and (b) hoop stresses between FEA and mesurement profiles at loation near 3mm to pipe inner surfce

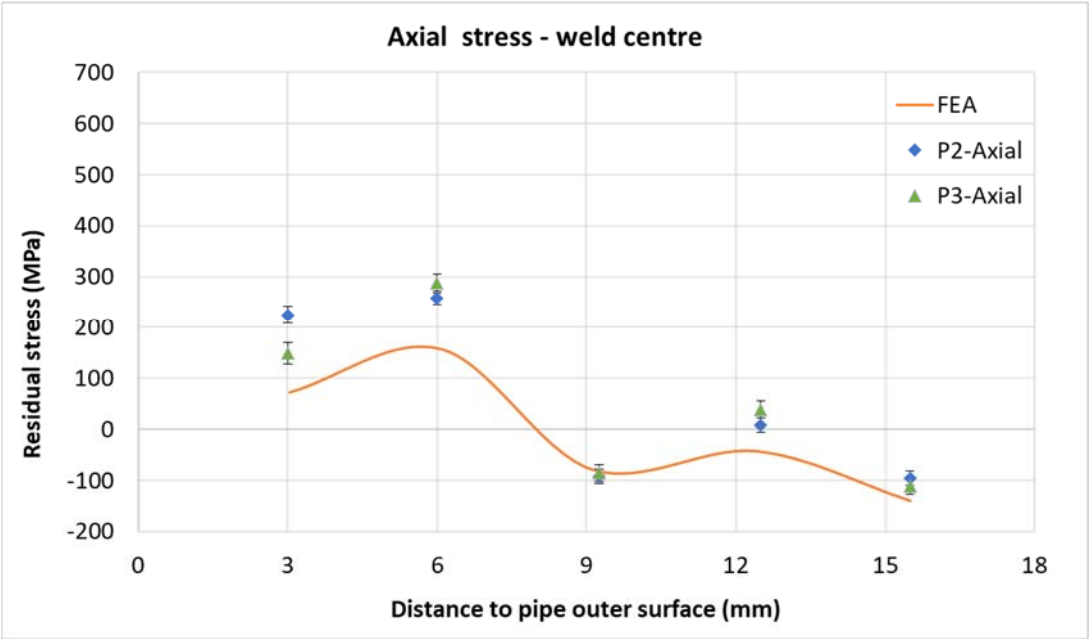

(a)

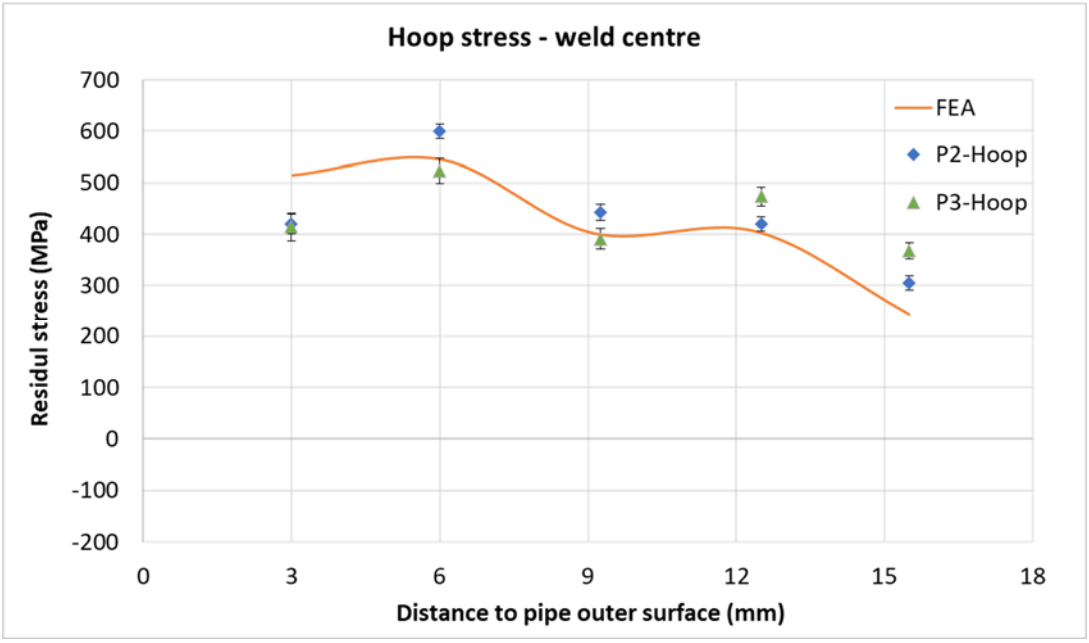

(b)

Figure 7.18 Comparison of residual (a) axial and (b) hoop stresses between FEA and mesurement profiles at weld centre

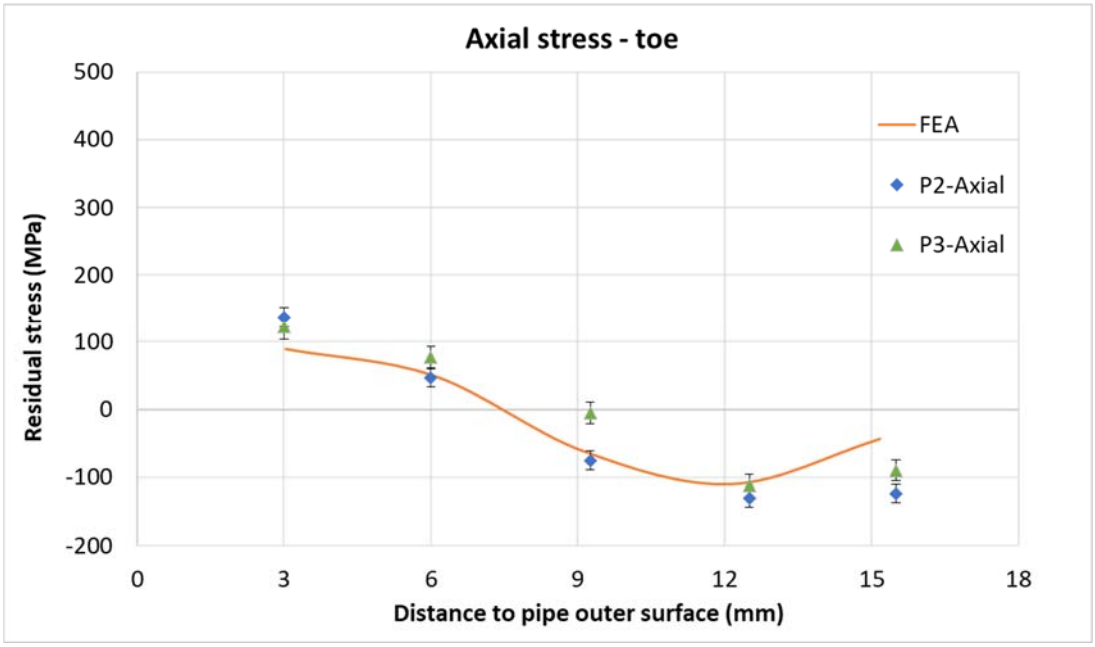

(a)

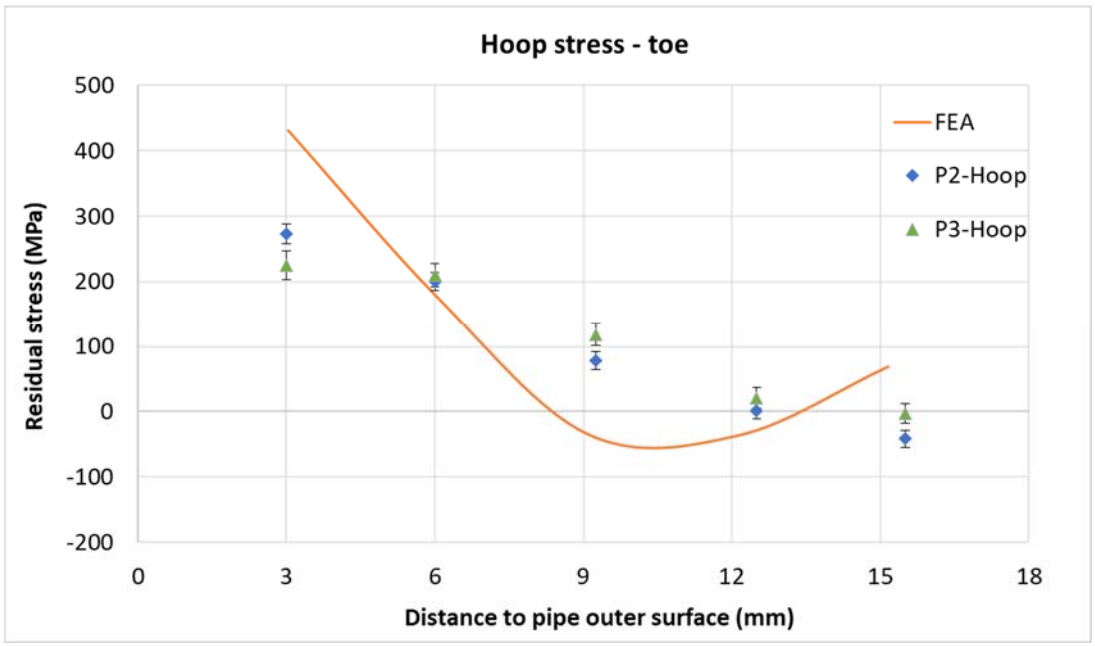

(b)

Figure 7.19 Comparison of residual (a) axial and (b) hoop stresses between FEA and mesurement profiles at weld toe

The trend of stress profiles predicted from FEA model were in good agreement with measured results. Especially for hoop stresses in the axial direction (along pipe length) predicted at near the pipe outer surface and near the mid-thickness, residual stress profiles were either upper bound or just match to the experimental measurement (Figure 7.15b and 7.16b). In comparison, at a region near 3mm to the

pipe inner surface, hoop stresses in weld metal were underestimated with an approximately 150MPa difference (Figure 7.17b).

A poor agreement in the axial residual stresses from FEA and measurement was found in weld zone near the weld cap. Axial stresses at near 3mm to the pipe outer surface (Figure 7.15a and 7.18a) show that, FEA predictions were less than 100Mpa while measured stress were over 200MPa. Another poor agreement was found in the region below the toe. At near 3mm from the pipe outer surface, the region below the toe was predicted with high hoop residual stresses which were over 100MPa than measured results (Figure 7.19b).

7.5 Discussion

7.5.1 Thermal analysis

In order to establish a model which can predict the thermal history of the welding process with a reasonable accuracy, efforts have been taken starting from experiment. Important parameters of the welding process such as the current and voltage of the arc energy, the weld torch travel speed and, inter-pass temperatures were recorded. These values were essential for the determination of the heat input for each weld pass. Installation of thermocouples at various location for temperature measurement enables the validation of the temperature field in the FEA model.

In this work, the thermal cycle predicted from FEA model was in a good agreement with measurement results on pipe's outer surface. However, on the pipe inner surface, FEA results do not match well with those measured near the weld grove edge. It was found that the R-type thermocouples were not well installed. At locations 10mm and further away from the weld, there are better agreements between results of measurement and simulation.

Temperatures at the weld pool are not measurable. Valuable information for predicting temperature domains at the welding zone is the macrograph of the weld cross section. Revealed fusion lines as well as the HAZ area could demonstrate the rough thickness of each weld pass and define the temperature ranges the material had experienced. For a low carbon ferritic steel, the melting point and phase transformation temperature were approximately around 1500°C and 900°C, respectively. In the multi-pass weld model in FEA, input heat flux was revised in

order to achieve an effective melting region which matches weld fusion zone.Once done, reasonable temperature cycles could then be generated for the weld metal.

Although there was a good approximation for defined quantity of energy input and heat distribution in time and space with the assistance of sufficient data from welding parameters and record, it was still challenging to achieve accurate FEA model without sufficient temperature dependent material properties for subsequent stress analysis.

7.5.2 Stress analysis

In this FE simulation, high temperature material properties used for both weld and parent materials were not entirely accurate. The temperature-dependent material properties of the parent material were obtained from literatures, except the tensile properties which were obtained from test at room temperature, in which the material used was in the same grade as in this study but had higher room temperature yield strength and tensile strength. These high-temperature material properties were also applied to the weld metal in FEA model.

When modelling a welding process, the straining hardening effect is an importance factor to be taken into account. Materials experience a series of repeated heating and cooling during the multi-pass welding process. This thermal cycle act as cyclic tensile and compressive loading to the material and induce stress-strain behaviour with plastic deformation hence straining hardening. In this study, a linear kinematic hardening model was employed with the consideration of Bauschinger effect which reduced elastic region (reverse yield) in a reverse loading, thereby reducing the level of residual stress.

Isotropic hardening was employed in preliminary FE models however the results were not reported in this thesis. It was found that without considering the reverse yield which is always maintained the same as the prior yield in the opposite direction, isotropic hardening model has the tendency to overestimate residual stresses[1], [14]–[17]. It is suggested that a combined isotropic-kinematic strain hardening model is more applicable for the actual hardening behaviour of the material [17]. However, because of lack of material data, this hardening behaviour was not modelled.

It is known that creep could occur in metals when the temperature has reached to approximately a third of the melting point [18]. This could affect their mechanical behaviour significantly and lead to difficulties in estimating their values close to the melting temperature.

It is suggested that the material behaviour in the weld are also affected by the associated temperature history which in turn is a result of interaction between microstructure and material properties [19]. For a ferritic steel such as the X65 steel studied in this work, the residual stress field, especially the hoop stress component would be strongly influenced due to volumes changes, as well as the transformation plasticity effects during the final phase transformation from austenite to bainite/martensite [20]. It appears in this case that the, hoop stresses predicted from FE model were in good agreement with measurement results. Only the axial stress in the weld metal near the pipe outer surface was under estimated. Although a number of research work indicates a significant effect of the phase transformation on welding residual stresses [21]–[25], studies could well predict residual stresses without considering martensitic phase transformation if thermal history could be validated.

7.6 Concluding remarks

In this work, a 2D axisymmetric model was created to simulate welding residual stresses in pipe girth welds. Predicted stress components were compared with measurement results obtained using neutron diffraction technique. The following conclusions can be drawn:

1. Thermal model which applied a volume heat flux to the cross section of the weld was used to simulate the thermal history of the welding process well. In this FEA model, with the predicted effective heat input and heating time, temperatures at certain locations in the parent metal was in good agreement with the measurement results recorded from thermocouples.

2. The lack of temperature information in the weld metal, which was not measurable, could be compensated by using a macrograph of the weld cross section to reveal weld fusion lines and even predict overlapped inter-pass areas. The heat input,

therefore, could be adjusted accordingly to obtain an output temperature cycle reasonably matching the experimental measurements.

3. Predicted transient hoop and axial strains on pipe surfaces was validated from the mechanical strain measurements with the assistance of pre-installed and calibrated strain gauges. Well agreed transient strain profiles prove that the employed material properties from literature could represent material high temperature mechanical behaviour for this study.

4. Residual stress profiles obtained from FEA model show similar trend as well as magnitudes, at most studied areas, to that from neutron diffraction measurement. Poor agreement occurred in the weld metal near the weld cap. Factors such as accurate material mechanical properties and material final stage phase transformation were the reasons resulted in the inaccurate prediction. Further studies should be recommended to look into these aspects.

References

[1] J. K. H. Authors, Pingsha Dong, "Recommendations for Determining Residual Stresses in Fitness-For-Service Assessment," *Weld. Res. Counc. Bull.*, vol. 476, 2002.

[2] "British Energy. Assessment of the Integrity of Structures Containing Defects. Procedure R6 Revision 4. British Energy Generation Ltd; 2014." .

[3] D. Rosenthal, "The theory of moving sources of heat and its application to metal treatments," *Trans. AIME*, vol. 68, pp. 849–865, 1946.

[4] V. Pavelic, O. Tanbakuchi, A. Uyehara, and P. S. Myers, "Experimental and computed temperature histories in gas tungsten arc welding of thin plates," *Weld. J. Res. Suppl.*, vol. 48, pp. 295–305, 1969.

[5] R. R. Rykalin, "Energy sources for welding," *Weld. World,* vol. Vol. 12, no. No. 9/10, pp. 227–248, 1974.

[6] J. Goldak, A. Chakravarti, and M. Bibby, "A finite element model for welding heat sources," *Metall. Trans. B*, vol. 15, no. 2, pp. 299–305, 1984.

[7] G. Fu, J. Gu, M. I. Lourenco, M. Duan, and S. F. Estefen, "Parameter determination of double-ellipsoidal heat source model and its application in the multi-pass welding process," *Ships Offshore Struct.*, vol. 10, no. 2, pp. 204–217, 2015.

[8] B. Brickstad and B. Josefson, "A parametric study of residual stresses in multi-pass butt-welded stainless steel pipes," *... J. Press. Vessel. Pip.*, vol. 75, 1998.

[9] B. L. Wei and W. He, "Comparison of Measured and Calculated Residual Stresses in Steel Girth and Butt Welds," vol. 44, no. 0, 2010.

[10] W.-S. Kim, Y.-P. Kim, and K. H. Oh, "The Effects of Heat Input and Gas Flow Rate on Weld Integrity for Sleeve Repair Welding of In-Service Gas Pipelines," *4th Int. Pipeline Conf. Parts A B*, vol. B, pp. 1483–1492, 2002.

[11] D. Deng, H. Murakawa, and W. Liang, "Numerical and experimental investigations on welding residual stress in multi-pass butt-welded austenitic stainless steel pipe," *Comput. Mater. Sci.*, vol. 42, no. 2, pp. 234–244, Apr. 2008.

[12] P. Michaleris and T. Division, "RESIDUAL STRESS DISTRIBUTIONS FOR MULTI-PASS WELDS IN PRESSURE," 1995.

[13] A. Yaghi, T. H. Hyde, A. A. Becker, W. Sun, and J. A. Williams, "Residual stress simulation in thin and thick-walled stainless steel pipe welds including pipe diameter effects," *Int. J. Press. Vessel. Pip.*, vol. 83, no. 11–12, pp. 864–874, Nov. 2006.

[14] J. W. Morris, S. J. Hardy, A. W. Lees, and J. T. Thomas, "Formation of residual stresses owing to tension levelling of cold rolled strip," *Ironnmaking Steelmak.*, vol. 28, no. 1, pp. 44–52, 2001.

[15] A. H. Yaghi *et al.*, "A Comparison Between Measured and Modeled Residual Stresses in a Circumferentially Butt-Welded P91 Steel Pipe," *J. Press. Vessel Technol.*, vol. 132, no. 1, p. 011206, 2010.

[16] J. W. Morris, S. J. Hardy, A. W. Lees, and J. T. Thomas, "Cyclic behaviour concerning the response of material subjected to tension levelling," *Int. J. Fatigue*, vol. 22, no. 2, pp. 93–100, 2000.

[17] L. Wei and M. Gallegillo, "Methods for Measurement and Prediction of Residual Stresses in Pipe Girth Welds in Clad Pipes, TWI core research project report," 2012.

[18] J. Choi and J. Mazumder, “Numerical and experimental analysis for solidification and residual stress in the GMAW process for AISI 304 stainless steel,” vol. 7, pp. 2143–2158, 2002.
[19] L.-E. Lindgren, “The use of simulations and the need of experiments in material processing,” in *Proceedings of The Sixth Cairo University International MDP Conference*, 1995, pp. 149–161.
[20] M. Jonsson and B. L. Josefson, “Experimentally determined transient and residual stresses in a butt-welded pipe,” *J. Strain Anal. Eng. Des.*, vol. 23, no. 1, pp. 25–31, 2007.
[21] D. Deng and H. Murakawa, “Prediction of welding residual stress in multi-pass butt-welded modified 9Cr–1Mo steel pipe considering phase transformation effects,” *Comput. Mater. Sci.*, vol. 37, no. 3, pp. 209–219, Sep. 2006.
[22] A. H. Yaghi, T. H. Hyde, A. A. Becker, and W. Sun, “Numerical simulation of P91 pipe welding including the effects of solid-state phase transformation on residual stresses,” *Proc. Inst. Mech. Eng. Part L J. Mater. Des. Appl.*, vol. 221, no. 4, pp. 213–224, Jan. 2007.
[23] A. H. Yaghi, T. H. Hyde, A. A. Becker, and W. Sun, “Finite element simulation of welding and residual stresses in a P91 steel pipe incorporating solid-state phase transformation and post-weld heat treatment,” *J. Strain Anal. Eng. Des.*, vol. 43, no. 5, pp. 275–293, May 2008.
[24] D. Z. L. Hodgson, C. M. Gill, B. M. E. Pellereau, P. R. Hurrell, and J. Francis, “Finite Element Modelling of 5- and 8-Pass Ferritic Steel Welds Using Phase Transformation Material Models,” *ASME 2011 Press. Vessel. Pip. Conf. Vol. 6, Parts A B*, pp. 1589–1597, 2011.
[25] C. J. Hamelin, V. Luzin, and P. Bendeich, “PVP2011-57426 ACCOUNTING FOR PHASE TRANSFORMATIONS DURING WELDING OF FERRITIC,” pp. 1–9, 2011.

8 Discussion

8.1 On experimental design

Narrow-gap welding is attractive to fabricators of thick-walled pipes and vessels that thick sections can be joint together more efficiently and economically. It is also called narrow-gap welding and employs a joint design with small groove width and large depth with a bevel angle typically in the range of 2-20°. The reduction in groove volume requires less filler material, therefore lower heat input, which results in smaller HAZ and reduces both hoop shrinkage and residual stresses than those typical observed in conventional V-seams.

A component made of thick section often requires heat treatment to relieve the welding residual stresses in the effort to minimize the likelihood of cracking. However, PWHT can be an expensive operation for large metallic assemblies. Some structures with large thickness could be exempted from PWHT if it could be demonstrated that as-welded residual stresses will not contribute to component failure. For common commercial C-Mn steels (P-No.1, Group No.2) in ASME B31.1 and B31.3 such as API 5L X65, it is recommended to conduct post weld heat treatment at 600°C to 650 °C for one hour per 25mm of thickness when the section thickness exceeds 19mm [1].

Neutron diffraction technique is an non-destructive technique to measure through-thickness residual stress in thick sections of which require greater penetration depth. The residual stresses at or near surface can be determined using X-ray diffraction or Synchrotron X-ray diffraction [2]. Alternatively, destructive measurement methods could be employed [3]but they were not selected for this project as it was necessary to keep the pipes intact for measurements after PWHT.

Measuring residual stress using neutron diffraction was achieved using monochromatic neutron sources. Fe (110) and Fe (211) planes give the most refraction among all the available lattice planes in a ferritic steel. These two planes were used to determine the strain-free lattice parameter [4], [5]. The Fe (211) plane was reported to offer this advantage [6] due to the larger scattering angle.

Measurement of the lattice spacing was repeated on the designated locations in the selected pipes PWHT so that the extent of stress relief and impact of various heating band widths could be examined. The use of Scanning Simulation Software (SScanSS) had greatly improved accuracy for sample positioning and alignment as well as instrument control [7], [8], especially for a large scale and thick sample.

8.2 Study of strain-free lattice spacing

By measuring the strain components in the principle stress directions allowed the determination of residual stress[9]. The relationship between the strain and stress are based on continuum mechanics and interpreted Hooke's law.

The estimation of residual strains, hence the subsequent residual stress in a component can be achieved by knowing un-strained condition of the material. A reference sample is often prepared using mechanical processing and its associated lattice spacing is assumed to be in a strain-free condition. Any error introduced in estimation of this strain-free parameter (d_0) will result in an over-or under-estimation of residual stress, which could affect the acceptability of flaw in a given component. It is important to accurately determine and evaluate the value of d_0 in the principal directions in a reference sample.

This research has examined three types of refence samples: 1) thin slice, 2) comb and 3) cuboids. Thin slice sample was extracted from the pipe weld and manufactured to create plane-stress condition. Comb sample was initially machined in a thin slice configuration while with addition cuttings which allowed more macro stress to be relieved. Cuboids were manufactured by destructively cutting smaller pieces from a comb sample. Such sample preparation procedures were designed to systematically investigate the effect of mechanical cutting on extent of stress relief in various reference samples which have not been studied in any previous study [10]–[14], [4], [15], [16]. Similar comparison was repeated after samples were heat treated.

Values of measured lattice spacing were assessed using pseudo micro-strain (relative strain) of the reference samples, which represented the relative changes in the strain, instead of real strains [12]. This effectively demonstrated the difference in the

change in lattice spacing in various reference samples, and/or in different measurement directions in each sample.

Previous study has found in α-Fe matrix, lattice spacing did not change across the comb sample in the HAZ, parent and weld meta[12], therefore averaged value of strain-free d_0 obtained from weld metal, HAZ and parent metal were used for stress evaluation. However, in this research, the pseudo micro-strain (relative change in strain variations) in three principle directions, in weld and parent metals, in the thin-slice, comb and cuboid samples were investigated.

In this research work, it was extremely difficult to study the all the possible configurations of strain-free reference samples, especially in a polycrystalline material of which only the plane of interest could be focused. Experimental efforts doubled in volume when a thorough comparison before and after PWHT was required.

The accuracy of predicted d_0 value and therefore the subsequent strain and stress evaluation should be examined, specified and decided based on practicability and application requirements.

8.3 Residual stress and its relief in narrow-gap weld

The application of an established welding procedure to fabricate narrow-gap girth welds has demonstrated good consistency in terms of residual stress distribution and magnitude in weldments. When comparing against the recommendations given in BS 7910 [17] and R6 [18], hoop residual stresses in weld metal at approximately 3mm beneath pipe outer surface reached approximately 75% of material yield strength and at similar depth beneath the inner surface it was found to be less than 60% of material yield strength. The predicted yield zones were much smaller than those given in R6 procedures.

Across the section thickness, the hoop residual stresses were estimated to be equal to material yield strength at pipe outer surface and gradually decreased closer to inner surface (Equation 4.12 and 4.13). This means for the pipe studied in this research, the upper bound value for hoop residual stress at pipe inner surface would be approximately 94% of weld metal yield.

The residual stress work in this project showed the highest hoop stress of the weld did reach approximately the upper bound limit (ie yield magnitude) but the magnitude decreased to approximately 40% to 60% as the depth increased.

The through-thickness axial residual stress distribution recommended in Annex Q of BS7910 and R6 is non-linear requires the users to take into consideration the welding heat input. The recommendation assumes the axial stress at pipe inner surface is equal to parent metal yield strength regardless of heat input. However, at pipe outer surface, the residual stress generated from low heat input process is postulated to have the yield magnitude of parent metal while under a high heat input process, it is assumed to be 40% magnitude but compressive. Medium heat input will introduce residual stress equivalent to 20% of yield magnitude at outer surface.

It is worth noting the given upper bound limit for low heat input welding implies the axial residual stresses at weld centre are always tensile, which is different from the reported finding in this work. Experimental measurements in this research demonstrates that the axial residual stresses could vary across the thickness with stress changing from tensile near the weld cap to compressive when approaching root. Similar results have been obtained from FEA modelling which will be discussed later.

There is no standard guidance for predicting the residual stress distribution profiles across the parent metals and weldment along pipe length. Typical approach would be to conduct measurement. A concept of yield zone has been defined to describe the hoop residual stress distribution on the surface of thick sections. Due to finite material restraints in the axial direction, the hoop residual stress redistributes leaving tensile stress within but compressive stress outside the yield zone [18]. For axial stress in this girth weld, an upper bound stress magnitude was assumed conservatively to be 0.2% proof yield strength of parent material.

The near surface residual stress profiles along pipe length measured using neutron diffraction measurement have shown the predicted yield zone as well as the recommended highest stress magnitude in R6 procedure are over conservative when assessing a narrow-gap welded joint.

The post-PWHT residual stresses have been evaluated using the guidance given in Annex Q of BS 7910. It was found that the reduction in stress has been successfully achieved to a similar extent using either local or furnace heat treating method. Due to the limited availability of material, equipment and cost, the study on local PWHT only examined the effect of (heating) band width. However, other physical parameters including the widths of soaking bands and gradient control band as well as conditions of thermal cycles, i.e. heating rate, cooling rate, soaking temperature and time, should also be considered for a more thorough investigation.

With regard to narrow-gap multi-pass welds, it is suggested that the residual stresses may be relieved effectively by local PWHT using a band width smaller than the recommended standard size. Further studies are recommended to investigate the effect of other parameters on stress relief in narrow-gap multi-pass welds using experimental and/or FEA approaches according to the availability of the resources.

8.4 Residual stress in FEA modelling

As discussed in previous sections, FE method is often applied to predict residual stresses in welded structures. The accuracy and reliability of the solution is variable because this approach involves various assumptions and approximations for stress analyses [19]. Factors which might affect the accuracy of a numerical simulation are discussed in this section.

It is important to collect as many as possible input data in order to reduce excessive assumptions and approximations. In this research, the information about the grove profile, welding processes, weld arc energy (current, voltage and weld speed), welding pass sequence, preheat condition and inter-pass temperature were collected. They provided crucial details about how the weld was made, and used for the construction of the thermal model. Transient temperature data was also recorded during welding process to support temperature history simulation.

Some approximation and assumption in terms of temperature-dependent material mechanical properties have been made in this study. Material data of API 5L X65 steel (both parent and filler metals) available from literature [20] was used. It was known from tensile and hardness tests that filler metal was overmatching parent material (grade API 5L X65), therefore assignment of literature material properties

to the weld region could be one of the reasons that the predicted residual stresses in weld region showed lower accuracy than that of parent metal.

Tensile material properties have the greatest influence on residual stress in weldments because the availability of the stress-strains properties will determine plastic strain hardening behavior in the model, which has influence on the degree of conservatism of the predicted stress field [21]–[23].

Applying an isotropic hardening model for the prediction of the residual stress was carried out however it was not reported. As it has been demonstrated an isotropic hardening model could overestimate the residual stresses[24]–[27], [20], especially for the hoop component of which the stress magnitude was above the material yield strength. The welding residual stress magnitude which accordingly to BS 7910 cannot exceed yield level. Therefore, it is always A good practice to collect sufficient material stress-strain data from either existing literature and/or specifically recorded using logging equipment. Another option will be to employ more complex hardening models such as in non-linear kinematic behaviour or even a combined isotropic-kinematic strain hardening model such that more accurate stress prediction could be achieved.

As recommended in the R6 procedure, in order to obtain representable analyses, it is preferable the material properties up to melting point (T_m) are measured instead of using literature values. Sometimes a very basic and simple analysis can accommodate material data measured up to $0.6T_m$ with the properties extrapolated up to melting point [18]. This can be applicable for both temperature-dependent thermal and mechanical properties. The use average values of elastic moduli in axial, hoop and radial directions is allowed and it is acceptable if these values are not identical as they are affected by directional solidification.

Material creep data from relaxation test can be used for simulating stress relief behaviors, but this was not covered in this research. The evaluation of residual stress using non-destructive measurement method has shown heat input as well as the thermal gradient had great influence on the stress relief in narrow-gap welds. With the assistance of FEA modelling, more factors such as insulation condition, heating

and cooling rate and soaking temperatures can be varied and simulated in a model to predict the post-heat treatment residual stress.

Reference

[1] D. J. Abson, Y. Tkach, I. Hadley, V. S. Wright, and F. M. Burdekin, "A review of postweld heat treatment code exemptions," *Weld. J.*, vol. 85, no. 3, pp. 63–69, 2006.

[2] A. Sugahara, S. Okano, T. Hashimoto, and M. Mochizuki, "Comparison of weld residual stress measurement results in low alloy welds between X-ray diffraction and stress relief methods," *J. Phys.*, vol. 379, p. 7, Aug. 2012.

[3] F. A Kandil, J. D. Lord, A T. Fry, and P. V Grant, "A review of residual stress measurement methods - A guide to technical selection," 2001.

[4] W. Woo, V. T. Em, B. S. Seong, P. Mikula, and G. B. An, "Residual stress determination in a thick ferritic steel weld plate using neutron diffraction," *J. Mater. Sci.*, vol. 47, no. 14, pp. 5617–5623, Apr. 2012.

[5] A. J. Allen, M. T. Hutchings, C. G. Windsor, and C. Andreani, "Neutron diffraction methods for the study of residual stress fields," *Adv. Phys.*, vol. 34, no. 4, pp. 445–473, Jun. 2006.

[6] F. Fernandez-Alonso and D. Price, *Neutron Scattering – Applications in Biology, Chemistry, and Materials Science*, 1st ed. Academic Press, 2017.

[7] J. A. James, J. R. Santisteban, L. Edwards, and M. R. Daymond, "A virtual laboratory for neutron and synchrotron strain scanning," *Phys. B Condens. Matter*, vol. 350, no. 1–3 SUPPL. 1, pp. 743–746, 2004.

[8] J. A. James and L. Edwards, "Application of robot kinematics methods to the simulation and control of neutron beam line positioning systems," *Nucl. Instruments Methods Phys. Res. Sect. A Accel. Spectrometers, Detect. Assoc. Equip.*, vol. 571, no. 3, pp. 709–718, 2007.

[9] P. J. Withers, M. Preuss, A. Steuwer, and J. W. L. Pang, "Methods for obtaining the strain-free lattice parameter when using diffraction to determine residual stress research papers," *J. Appl. Crystallogr.*, vol. 40, pp. 891–904, 2007.

[10] S. Paddea, J. A. Francis, A. M. Paradowska, P. J. Bouchard, and I. A. Shibli, "Residual stress distributions in a P91 steel-pipe girth weld before and after post weld heat treatment," *Mater. Sci. Eng. A*, vol. 534, pp. 663–672, Feb. 2012.

[11] B. Chen *et al.*, "In situ neutron diffraction measurement of residual stress relaxation in a welded steel pipe during heat treatment," *Mater. Sci. Eng. A*, vol. 590, pp. 374–383, Jan. 2014.

[12] A. Paradowska, T. R. Finlayson, J. W. H. Price, R. Ibrahim, A. Steuwer, and M. Ripley, "Investigation of reference samples for residual strain measurements in a welded specimen by neutron and synchrotron X-ray diffraction," *Phys. B Condens. Matter*, vol. 385–386, pp. 904–907, 2006.

[13] P. J. Withers, M. Preuss, A. Steuwer, and J. W. L. Pang, "Methods for obtaining the strain-free lattice parameter when using diffraction to determine residual stress," *J. Appl. Crystallogr.*, vol. 40, no. 5, pp. 891–904, 2007.

[14] S. Ganguly, L. Edwards, and M. E. Fitzpatrick, "Problems in using a comb sample as a stress-free reference for the determination of welding residual stress by diffraction," *Mater. Sci. Eng. A*, vol. 528, no. 3, pp. 1226–1232, 2011.

[15] A. Krawitz and R. Winholtz, "Use of position-dependent stress-free standards for diffraction stress measurements," *Mater. Sci. Eng. A*, vol. 185, no. (1-2), pp. 123–130, 1994.

[16] P. J. Hutchings, M. T., Bouchard, P. J. & Withers, “Characterization of the Residual Stress State in a Double ‘V’ Stainless Steel Cylindrical Weldment Using Neutron Diffraction and Finite Element Simulation,” in *6th International Conference on Residual Stress*, 2000.
[17] “BSI, ‘BS7910:2013 Guide to methods for assessing the acceptability of flaws in metallic structures,’ 2013,” 2013.
[18] I. Milne, R. . Ainsworth, A. Dowling, and A. Stewart, “Assessment of the integrity of structures containing defects,” *Int. J. Press. Vessel. Pip.*, vol. 32, no. 1–4, pp. 3–104, Jan. 1988.
[19] M. C. Smith and A. C. Smith, “NeT bead-on-plate round robin: Comparison of transient thermal predictions and measurements,” *Int. J. Press. Vessel. Pip.*, vol. 86, no. 1, pp. 96–109, 2009.
[20] L. Wei and M. Gallegillo, “Methods for Measurement and Prediction of Residual Stresses in Pipe Girth Welds in Clad Pipes, TWI core research project report,” 2012.
[21] S. K. Bate and P. J. Bouchard, “Measurement and modeling of residual stresses in thick-section Type 316 stainless steel welds,” *Icrs6*, no. August 2015, pp. 1511–1518, 2000.
[22] L. E. Lindgren, “Finite element modeling and simulation of welding. part 2: Improved material modeling,” *J. Therm. Stress.*, vol. 24, no. 3, pp. 195–231, 2001.
[23] M. C. Smith, “Validation of mixed isotropic-kinematic material hardening models for finite element prediction of residual stresses in austenitic steel welds, British Energy Report,” 2007.
[24] J. K. H. Authors, Pingsha Dong, “Recommendations for Determining Residual Stresses in Fitness-For-Service Assessment,” *Weld. Res. Counc. Bull.*, vol. 476, 2002.
[25] J. W. Morris, S. J. Hardy, A. W. Lees, and J. T. Thomas, “Formation of residual stresses owing to tension levelling of cold rolled strip,” *Ironnmaking Steelmak.*, vol. 28, no. 1, pp. 44–52, 2001.
[26] A. H. Yaghi *et al.*, “A Comparison Between Measured and Modeled Residual Stresses in a Circumferentially Butt-Welded P91 Steel Pipe,” *J. Press. Vessel Technol.*, vol. 132, no. 1, p. 11206, 2010.
[27] J. W. Morris, S. J. Hardy, A. W. Lees, and J. T. Thomas, “Cyclic behaviour concerning the response of material subjected to tension levelling,” *Int. J. Fatigue*, vol. 22, no. 2, pp. 93–100, 2000.

9 Conclusions and recommendations

9.1 Conclusions

This research has investigated the residual stress in narrow-gap multi-pass X65 pipe steel girth weld in as welded condition and after global and local post weld heat treatment procedures using neutron diffraction technique. Measured stress results have been compared with recommendations give for Engineering Critical Assessment (ECA) procedures. This work has also characterised the welding residual stresses at weld zone and adjacent parent material using experimental measurement and FEA modelling approaches. Based on the findings, it is concluded that:

1. In terms of the residual stresses generated in narrow-gap multi-pass girth welds, studied in this work, in both as-welded and PWHT conditions, the recommendations given in current procedures and practices are conservative since they were originally established based on conventional wide-grove weld joints.
2. Small temperature differences during preheating had little or no effect on the overall residual stress of pipe spools.
3. Local PWHT has achieved the same magnitude of stress relief as that of global PWHT, following prescribed procedure. Narrow local heating bands were effective in relieving residual stress as the recommended standard sizes are.
4. The accuracy of measured residual stresses using neutron diffraction depends on the determination of the strain-free lattice parameters from reference samples. It is important to prepare a reference samples in a configuration such as a ‘comb’ or ‘cubes’ for stress relieve in three directions.
5. Measurement of the lattice spacing should be made respectively on weld and parent metals, in axial, hoop and radial directions, and in as-welded and after PWHT conditions.
6. A well-designed welding process and followed by a large collection of temperature and strain data were essential in validating a simple 2D numerical model.
7. Temperature history could be accurately and reliably predicted under an assumed value of the melt pool length and hence an effective distributed body heat flux.

The heat input could be adjusted to match the fusion zones to the weld macrograph.

8. Predicted welding residual stresses in a FEA model was in a good agreement with the results obtained from neutron diffraction measurement at most area of interest.
9. Poor agreement of the stress level at near cap region could be attributed to the exclusion of phase transformation effect and/or inaccurate material high temperature mechanical properties.

9.2 Recommendations for future work

The recommendation for future work include the following:

1. Residual stresses are suggested to be measured using an additional destructive or semi-destructive technique such as contour method or deep hole drilling. Such technique would generate through thickness stress profiles or full stress map which could be used to validate the results obtained from a non-destructive technique.

2. Local post weld heat treatment should be reconducted with better control of the temperature gradient and data collection. The width of narrow heating band might be revised in case of over-heating.

3. FEA could be enhanced by taking into account the effect of phase transformation in ferritic X65 steel and various PWHT parameters, such as widths of heating band, insulation band dimension and thermal cycles. The temperature-dependent material properties (mainly the yield strength and modulus of elasticity), plastic deformation and creep behaviour when a component is subject local PWHT should be characterised and quantified.

4. The work can be extended to a wider scope. As only one material configuration was studied in this work, the findings regarding the residual stress distributions and magnitudes in narrow-gapped multi-pass pipe spool before and after furnace/local PWHT weld were not sufficient to be standardized for general (narrow-gapped weld) cases. It is suggested to perform large numbers of residual stress evaluation on girth welds with various thicknesses or R/t ratio values to provide related residual stress profiles in BS7910 and R6.